NASA CR-1582

TRACE CONTAMINANT ADSORPTION AND SORBENT REGENERATION

By A. J. Robell, C. R. Arnold, A. Wheeler,
G. J. Kersels, and R. P. Merrill

Issued by Originator as Report No. L-62-69-1

Prepared under Contract No. NAS 1-5847 by
LOCKHEED MISSILES & SPACE COMPANY
Palo Alto, Calif. 94304

for Langley Research Center

NATIONAL AERONAUTICS AND SPACE ADMINISTRATION

For sale by the Clearinghouse for Federal Scientific and Technical Information
Springfield, Virginia 22151 – CFSTI price $3.00

FOREWORD

This report describes work performed from February 1966 to July 1969 at the Lockheed Palo Alto Research Laboratory, Palo Alto, California 94304.

This effort was performed for NASA-Langley Research Center under Contract NAS 1-5847. Dr. A. J. Robell was the Program Manager, and the program team included Dr. A. Wheeler and Messrs. C. R. Arnold and G. J. Kersels. Professor R. P. Merrill of the University of California, Berkeley, was consultant and made outstanding contributions to this work.

ABSTRACT

The adsorption and desorption characteristics of activated carbon have been experimentally and theoretically investigated with the following overall goal: To determine the applicability of regenerable sorption to the control of airborne trace contaminants within spacecraft cabins for long mission durations. Capacity correlations for pure and mixed contaminants have been established. A theory has been derived and successfully tested for vacuum desorption rates from single particles and beds. Finally, a quantitative design methodology has been developed for the practical design of regenerable systems.

CONTENTS

ILLUSTRATIONS

TABLES

NOMENCLATURE

Symbol	Definition
A	a convenient constant = 22.4 $C_S \Delta H_d$
A	cross-sectional area
A	desorption curve shape parameter
a	desorption interval fraction (e.g., 0.7943)
b	desorption interval integer (1, 2, 3 ...)
b	isotherm shape factor
C_S	heat capacity
c	concentration
$c_e(S)$	gas-phase concentration in equilibrium with S
c_o	initial equilibrium gas-phase concentration
D	diffusivity
D	an inverse time constant
D	adsorption bed diameter
D'_K	an effective diffusivity
D_{pore}	diffusivity of contaminant in sorbent pores
d_p	particle diameter
E_a	activation energy of adsorption
E_d	activation energy of desorption
f	fugacity of adsorbate
F	flow rate (throughput)
F	limiting conductance
F_x	flow rate per unit bed crosssection at x
f_2	Crank-function
H_a	enthalpy of adsorbate in adsorbed phase
H_g	enthalpy of adsorbate in gas phase

Symbol	Definition
h	mass spectrogram peak height
K	a quantity = $p(1 - \theta)/\theta$
K	adsorption isotherm shape constant
K	rate of heat input
K	a constant $\simeq 0.33$
k	a constant defined by Eq. 6.12
k	Boltzmann constant = 1.380×10^{-16} erg/molecule °K
k_A	adsorption rate constant per unit surface area
k_d	desorption rate constant
K_F	Freundlich-plot intercept
k	frequency factor
k'	a constant defined for Eq. 7.1
L	bed length
L_s	bed length required for adsorption of 10 pseudo-components in a given time
M	molecular weight
m	molecular mass
$\dot{m}$	contaminant production rate
N	Avogadro's number = 6.02×10^{23} molecules/mol
$\dot{N}$	instantaneous desorption rate
N_{TU}	number of transfer units
n	desorption rate order
n	Freundlich constant (slope)
n	number of moles adsorbed in one sorbent granule
n_s	number of moles of gas adsorbed
P	total pressure
P_c	critical pressure
P^o	vapor pressure
Pe	Peclet number
p	partial pressure
Q	reversible heat change
Q	throughput (Appendix H)

Symbol	Definition
q	amount adsorbed per unit sorbent weight
q_{diff}	differential heat of adsorption
q_{st}	isosteric heat of adsorption
R	gas constant
r_A	desorption rate per unit area
r_d	desorption rate
S	empirical sensitivity factor, used with subscript to indicate mass-to-charge (M/e) ratio
S	adsorbed concentration
S_a	entropy of adsorbate at actual coverage
S^o_a	standard-state entropy of adsorbate
S_g	entropy of the gas at adsorption partial pressure
S^o_g	standard-state entropy of the gas
S_p	pumping speed
T	temperature, absolute unless otherwise indicated
T_c	critical temperature
t	time
u	linear velocity
V	volume
V_m	liquid molar volume at normal boiling point (1 atm)
V_o	standard-state gas molar volume = 2.24×10^4 ml STP/mol
$\bar{v}$	average molecular velocity
W	weight of sorbent bed
$\dot{w}$	desorption rate (weight per unit time)
X	molar fraction
x	distance from end of sorbent bed
y	quantity = S/S_o defined for Eq. Q.6
Z	quantity = x/L defined for Eq. Q.6
α	sticking coefficient
β	molecular area

Symbol	Definition
Γ	surface excess concentration
γ	tortuosity factor
γ	surface free energy of adsorbed layer per unit area
γ_A	surface free energy per unit area covered by a monolayer
γ_s	clean-surface free energy per unit area
$\Delta c/\Delta x$	concentration gradient
ΔF_a	free energy change for adsorption
ΔH_a	integral molar enthalpy of adsorption
ΔH_d	heat of desorption
ΔH_L	Langmuir enthalpy of adsorbate in adsorbed phase
ΔH_V	Volmet enthalpy of adsorbate in adsorbed phase
ΔS_a	entropy of adsorption
$\Delta \bar{S}_m$	partial molar entropy
$(\Delta T)_{ad}$	adiabatic temperature drop
ϵ	emissivity of sorbent surface
ϵ	void fraction in bed
η	removal efficiency
θ	fraction of surface covered
λ	Stefan-Boltzmann constant = 5.67×10^{-5} erg/cm^{2}sec°K^4
π	ratio of circumference of circle to its diameter
π	spreading pressure
ρ_p	particle density
σ^o	standard-state molecular area
τ	characteristic time as defined by Eq. L.5
τ	response time of mass spectrometer
τ	reduced-time parameter
ϕ	excess free energy per unit volume

Subscript	
1/2	at one-half desorbed
a	adsorbed phase, of adsorption

Symbol	Definition
d	desorbed, of desorption
e	equilibrium
g	gas-phase
i	of the i-th component
m	in gas mixture, monolayer, molar
o	initial
p	particle
r	remaining adsorbed
s	on surface
x	at distance x

Acronym	
MAC	maximum allowable concentration
ID	inside diameter
OD	outside diameter
QRGA	quadrupole residual gas analyzer
STP	standard temperature and pressure (273.2°K, 1 atm)
VTVM	vacuum-tube voltmeter

TRACE CONTAMINANT ADSORPTION AND SORBENT REGENERATION

By A. J. Robell, C. R. Arnold, A. Wheeler, G. J. Kersels,
and R. P. Merrill*
Lockheed Palo Alto Research Laboratory

Section 1
INTRODUCTION

In any closed ecological system the buildup of trace contaminants from both metabolic processes and material degradation must be controlled by a suitable contaminant removal system. If a sorbent is used in such a system for extended manned space missions, unduly large quantities of sorbent will be required unless a regenerative operation is employed.

The overall goal of this work was to acquire sufficient information on adsorption/desorption phenomena to enable design, optimization, and operation of a regenerable system.

Sorption processes on activated carbon were studied with the goal of arriving at quantitative relationships enabling the correlation and estimation of sorbent capacity, interference effects of multiple contaminants (including water vapor), and desorption rates under spacecraft regeneration conditions.

Despite the use of activated carbon as a sorbent for many years, little or no quantitative work had been done in the above areas at the time of inception of this program. In fact, the state-of-the-art was as follows:

- Activated carbon was the prime candidate for use as a general sorbent, and Barnebey-Cheney type BD was found, during performance of Contract NAS 9-3415 (Design and Fabrication of a Trace Contaminant Removal System for Apollo) to be quite suitable for spacecraft use.

---

*Assistant Professor of Chemical Engineering, The University of California, Berkeley (Consultant at Lockheed Palo Alto Research Laboratory).

- The potential theory had been used to correlate adsorption capacities of single contaminants. It had not been extended to mixtures. There was no other general theory applicable to the mixture problem, nor were there mixture data relative to conditions of interest for spacecraft operation.
- Vacuum desorption rates were unknown.
- Concepts for system design were not based on a fundamental understanding of sorption phenomena; design was performed more or less by rule-of-thumb.

A systematic approach was used to fill these gaps in order to arrive at sound design principles. It was felt that an understanding of sorption by a single particle was fundamental to an understanding of how a collection of particles functions in a bed. Thus, a microbalance system was used to study single particles in a parallel effort to a flow system for beds.

Theoretical extention of the potential theory to very low coverages was undertaken to attain a better understanding of the empirical parameters of the correlation and in its extension to estimations of some of the necessary kinetic parameters. This approach was merged with the satisfactory theoretical analysis of mixed adsorption to give a generalized capacity correlation. The mathematics of transport of sorbate from a bed of particles during vacuum desorption was developed. All of these theoretical advances were combined with the empirical data produced during the contract to indicate a rational design procedure.

Section 2
ADSORPTION OF PURE CONTAMINANTS

The length of time that a trace contaminant system will be usable without regeneration is directly related to the capacity of the adsorbent material for the various contaminants to be encountered. In order to gain a better understanding of the relation of this capacity to contaminant levels, it was necessary to determine extensive adsorption isotherms, which show the relation of adsorptivity to contaminant concentration or partial pressure. These were determined for a few selected components which were felt to represent a typical spectrum of contaminants that are amenable to removal by adsorption on activated carbon.

Since the method of choice for trace contaminant removal is a fixed adsorbent bed in a flowing stream of space cabin air (actually a 50/50 mixture of nitrogen and oxygen at one-half of atmospheric pressure), a number of experiments were conducted using a flow system incorporating a fixed bed scaled down to laboratory dimensions. Using this method the performance of the sorbent bed could be determined under conditions similar to those encountered in a spacecabin atmosphere, but using only one contaminant at a time at a concentration near its maximum allowable concentration (MAC) value. It was also necessary to use this experimental approach to obtain sorbent beds saturated with typical contaminants at these concentrations in order that these beds might then be tested for their vacuum desorption characteristics, as described in Section 7.

Due to the time-consuming nature of the flow experiments, a faster method of determining more extensive adsorption isotherms of the pure components was needed. This was accomplished by use of the gravimetric system described below, in which an isotherm that might take weeks to determine by flow methods could be determined in 1 or 2 days. The core of this system was the microbalance unit, which provided instantaneous weight readings as adsorption partial pressure was varied at will. The

weights were then translated directly into adsorptivity or sorbent capacity values. By having these extensive isotherms for pure contaminants, it was then possible to test various theoretical models (Section 4) that would enable prediction of sorbent bed performance under real conditions in which one or more contaminants would be present at one time. These isotherms were also of value in correlating desorption (regeneration) data in Sections 6 and 7.

2.1 EXPERIMENTAL TECHNIQUES

2.1.1 Flow System

This system was designed so that a stream of gas contaminated with a known concentration of adsorbate or adsorbates could be passed through a cylindrical packed bed of sorbent at subatmospheric pressure while effluent from the bed was monitored for the contaminant. A schematic diagram of the system is shown in Fig. 2-1.

The sorbent bed consisted of a 60-cm stainless steel tube, of 1/4-, 3/8-, or 3/4-in. OD, with stainless steel screen spacers used to hold both ends of the sorbent bed in place. (A slightly different bed design was used in early runs in the F2- and F3-series.) That portion of the tube upstream from (below) the sorbent bed was filled with quartz chips 1 to 2 mm in diameter in order to preheat the gases entering the sorbent bed in experiments at elevated temperatures. In flow run F13 and thereafter, the quartz chips were eliminated because it was of interest to obtain the upstream and downstream pressure of the bed during vacuum desorption. The quartz chip packing would result in misleading upstream pressure readings. A drawing of the flow bed is shown in Fig. 2-2.

Those portions of the flow system upstream from the sorbent bed were constructed from 1/4-in. OD copper and stainless steel tubing, in order to minimize dead volume, and were connected with Swagelok fittings. Portions downstream were made of 1-in. OD copper tubing with sweat soldered fittings in order to provide high conductance for vacuum desorption of the bed.

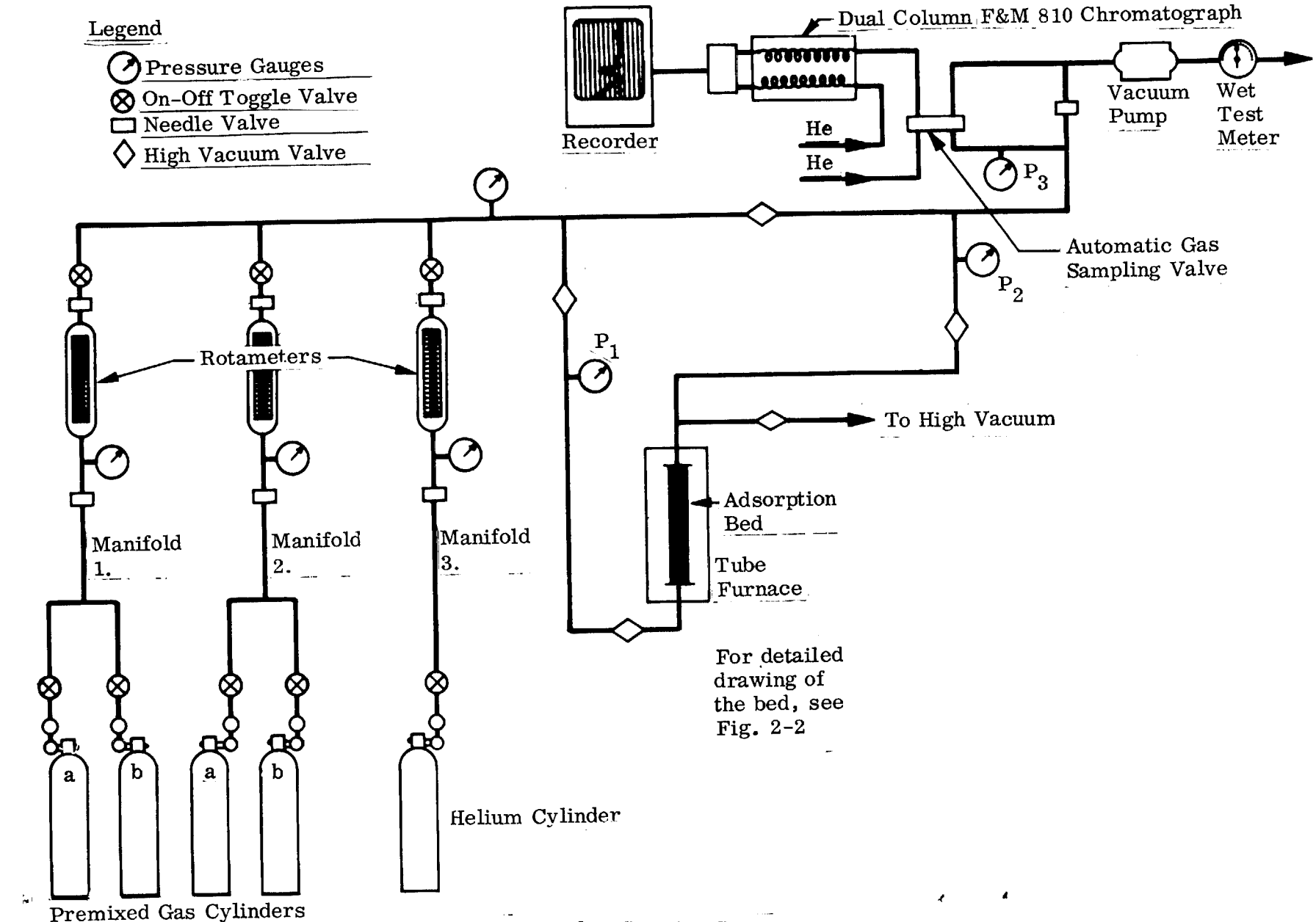

Fig. 2-1 Flow Sorption System

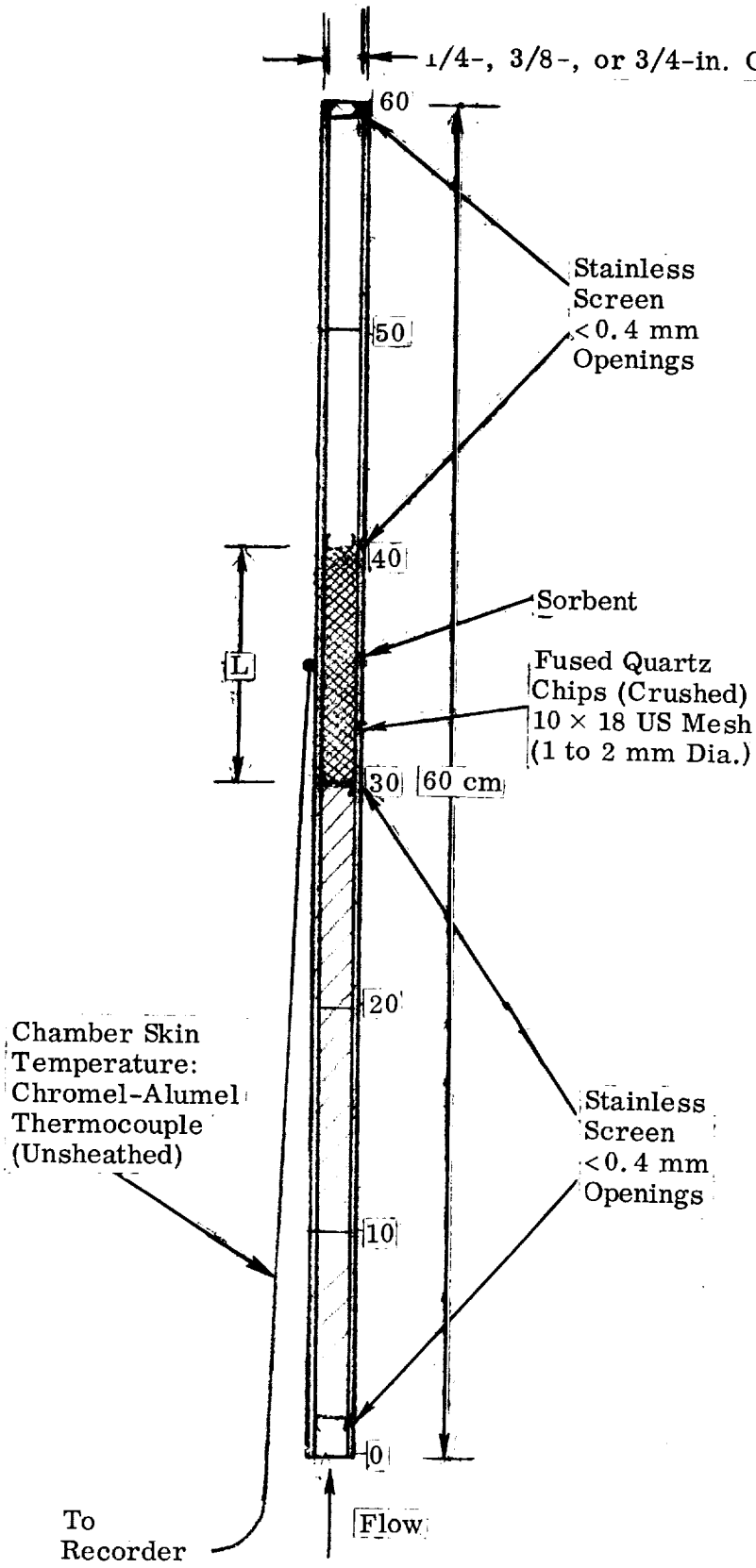

Fig. 2-2 Adsorbent Chamber

Gases were introduced into the system through manifolds, as illustrated in Fig. 2-1. Manifolds 1 and 2 allowed a premixed carrier gas without contaminant to be instantaneously substituted for a similar gas with contaminant, without any significant change in flow rate. Manifold 3 provided for addition of carrier gas components in order to adjust their concentrations or those of the contaminants. The gas cylinders were equipped with standard pressure regulators and, except for those cylinders containing premixed contaminated gases, with molecular sieve 13X traps for removal of traces of extraneous contaminants.

Effluent gas samples were taken automatically, on a preset time cycle, with a gas sampling valve. Such valves have the advantage of giving very reproducible injection volumes, and they have low maintenance needs.

A vacuum pump placed downstream from the gas sampling valve allowed the system to be operated at subatmospheric pressure. This pressure was maintained at approximately 0.5 atm by judicious adjustment of the needle valves located on each inlet manifold and at the outlet to this system vacuum pump.

Valves used in the system were of three types: toggle valves for on-off control of upstream gas flows; needle valves for precise control of flow rates; and screw-type bellows valves for bypass and vacuum portions of the system. Specific locations of these valves are shown in Fig. 2-1.

Since it was found early in this work that rotameters provide marginal measurement reproducibility, total system flow was monitored with a wet test meter located on the exhaust of the system pump. Average flow rates were determined by dividing the difference in wet test meter readings by elapsed time.

The sorbent bed was heated by a Hevi-Duty tube furnace in which it was vertically mounted. Furnace temperature was kept constant by two West JP controllers, while the skin temperature of the bed was measured with a chromel-alumel thermocouple attached near the midpoint of the bed. This thermocouple was connected to a temperature recorder, which provided graphic temperature records. (See Fig. 2-2.)

Total system pressure was measured with Wallace and Tiernan model FA145 Bourdon-tube differential pressure gages. A model FA129 gage, or in later experiments a Barocel capacitance manometer, was used to measure the pressure immediately upstream from the sample injection valve to determine the pressure of the standard volume of gas injected into the chromatograph.

Gas chromatographic analysis of the effluent gases was provided by an F&M model 700 or 810 gas chromatograph equipped with a flame ionization detector. Current output of this detector was converted by an electrometer to a voltage that was displayed on a strip chart recorder. This recorder was equipped with a disc chart integrator for evaluation of the total ionization charge generated by contaminant fractions coming out of the chromatographic columns. Separation of effluent gas components for analysis by the detector was effected by the use of appropriate columns, flow rates, and temperatures.

Raw sorbent materials obtained from outside sources were crushed and sieved to sizes differing by a factor of two. Specifications for these sorbents are given in Table 2-1. Locksorb-2A is a Lockheed proprietary sorbent prepared by impregnating 30 × 40 BD with a Group 1 metal.

Table 2-1

SORBENTS STUDIED

Manufacturer	Type	Sieve Size (U.S. No.)	Approx. Diam. (cm)	Surface Area (m^2/g)	Textual Designation
Barnebey-Cheney	BD, activated coconut shell charcoal	8 × 12	0.20	1100	8 × 12 BD
		16 × 20	0.10	1100	16 × 20 BD
		30 × 40	0.05	1100	30 × 40 BD
		50 × 70	0.025	1100	50 × 70 BD
Union Carbide, Linde Division	Molecular Sieve 13X (Zeolite)	16 × 20	0.10	725 ± 75	16 × 20 LMS 13X
Lockheed	Locksorb-2A	30 × 40	0.05	–	LS-2A

A mixture of 50% oxygen and 50% nitrogen was used as the carrier gas in flow experiments. Contaminants to be studied were obtained premixed in the above carrier or in

oxygen. These premixed gases were supplied by the Matheson Company with their analyses of the contents.

For initial sorbent outgassing, samples were weighed out in air and placed in the 60-cm tube described above. The tube was then inserted into the system and subjected to a flow of helium. Bed temperature was then raised to 400−450° C, while system pressure was maintained at approximately 0.5 atm. After 4 hr the temperature was allowed to come to ambient or to the temperature at which the experiment was to be run. In a few cases it was found that after the heat pretreament small air leaks developed around the O-ring fittings which hold the bed in place. (See Fig. 2-2.) To assure that no leaks were present after the pretreatment, the bed was evacuated to a few microns and isolated. The increase in pressure in the bed tube was measured as a function of time and the leak rate, if any, was determined.

In some cases this pretreatment was performed at a system pressure of 1 atm, but this did not appear to affect the results as demonstrated in subsequent flow runs.

Adsorption experiments on the flow system consisted of five steps:

(1) Calibration of the chromatograph detector for each contaminant to be studied in that experiment
(2) Determination of the inlet concentration of each contaminant, by allowing the flow to bypass the sorbent chamber
(3) The actual adsorption, during which effluent from the bed was monitored for each contaminant
(4) Redetermination of inlet concentration by again bypassing the sorbent bed
(5) Recalibration of the detector for each contaminant

Vacuum desorptions, if any, were next performed. Finally, flow desorption was performed by following steps (1), (3), and (5) of the above procedure.

Calibration was performed by measuring detector response to a known volume of premixed gas of known concentration. After calibration for each contaminant, all premixed gases were then allowed to flow, along with nitrogen or oxygen-nitrogen mix needed to adjust contaminant concentrations and keep the oxygen-nitrogen ratio

at or near unity. The adsorption step was performed by merely diverting the flow through the sorbent chamber and observing chromatograph detector response to the contaminant in question until the effluent concentration appeared to have risen back to the inlet concentration.

Flow desorption was performed, after calibration of the detector, by passing the oxygen-nitrogen mixture through the sorbent bed and monitoring the effluent as in the adsorption step. Strongly adsorbed contaminants were sometimes removed in a similar manner at higher temperatures, using helium instead of oxygen-nitrogen.

Bed effluent contaminant concentrations were determined by measuring the area of peaks on strip chart recordings corresponding to detector output for each contaminant. Since holdup time for each contaminant under study had been determined before beginning the experiment, location of the peak on the recording time axis was relatively simple. Peak area was determined simultaneously by means of an integrator built into the recorder. Records were kept of peak area, electrometer range and attenuation settings, injection pressure, wet test meter readings, and time. A sample calculation of the amount adsorbed appears in Appendix A.

Since detector response to the contaminant varied slightly during the course of each experiment, it was evaluated at two times, as indicated by steps (1) and (5) on page 9 Average response values before and after the run were then interpolated in a linear fashion and used to determine effluent concentrations during the course of the experiment. Sample calculations of electrometer response and of effluent concentration also appear in Appendix A.

Linearity of detector response to contaminants in the concentration range of interest was determined by injecting premixed propylene (50 ppm) in oxygen-nitrogen into the chromatograph and observing detector output. Variation of the amount injected from one-tenth to ten times the volume of interest resulted in a log-log plot with slope equal to unity, as shown in Fig. 2-3, thus indicating completely linear response over this range. Injection of larger volumes of gas tended to blow the detector flame out, while injection of smaller volumes led to poor reproducibility.

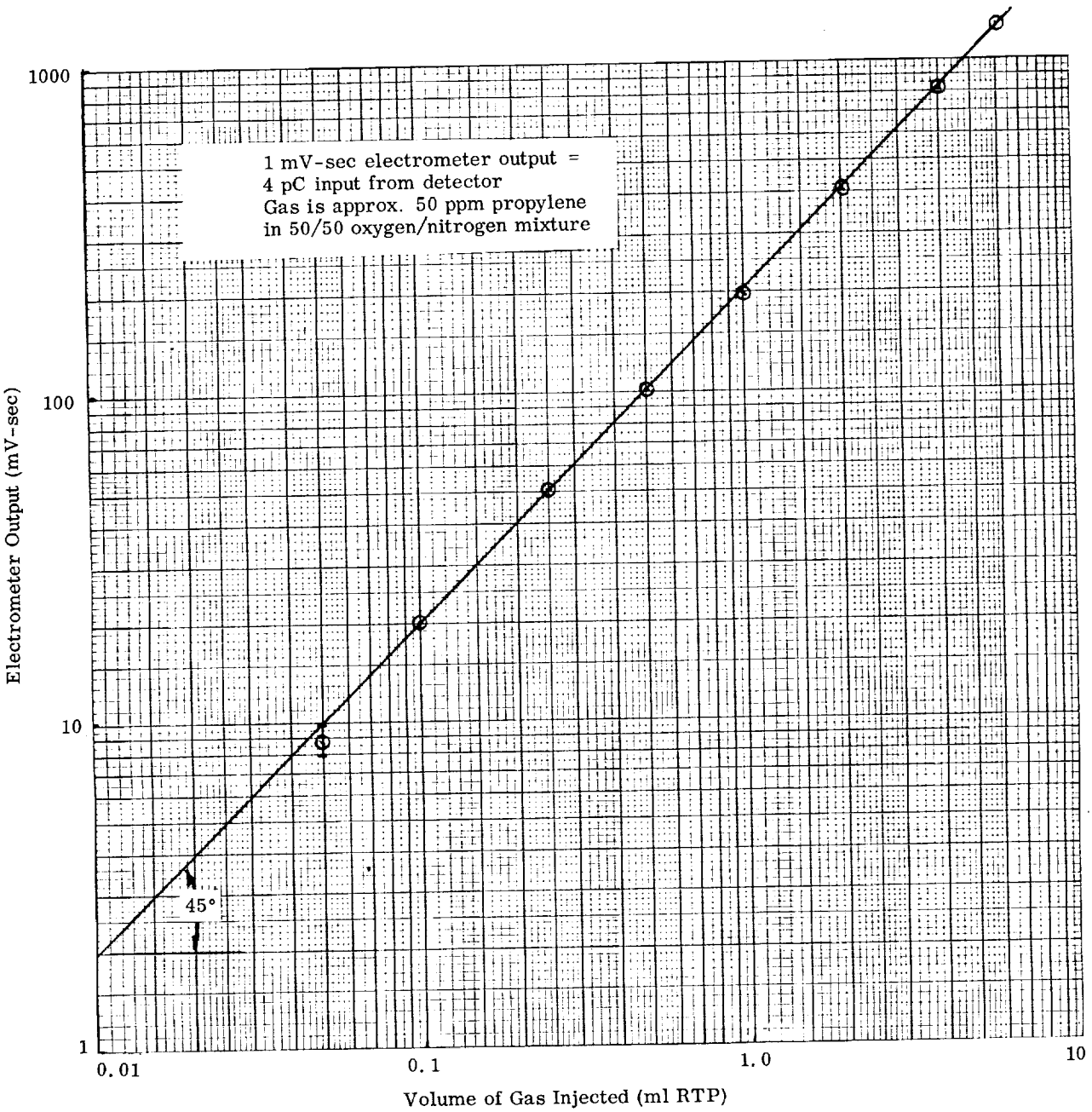

Fig. 2-3 Calibration Curve for Propylene in F&M 700 Flame Ionization Detector

2.1.2 Gravimetric System

The sorbent materials used were the same as those described in section 2.1.1. Gravimetric experiments were performed with a Cahn model RG microbalance. This microbalance has an ultimate sensitivity of 0.2 μg and can measure weight changes as large as 200 mg on its most sensitive beam position. Its sensitivity is 1 μg per chart division while measuring weight changes as large as 10 mg. A vacuum chamber accommodating the microbalance was constructed, as shown in Fig. 2-4.

This gravimetric system consisted of a number of functional parts, most of which are typical of any vacuum system. The jar in which the weighing mechanism was mounted was equipped with provision for three hangdown tubes, one for each beam position. In the present work, only the more sensitive position was used, leaving the hangdown tube port for the less sensitive position available for attachment of a Barocel capacitance-manometer pressure-transducer system, which was used to obtain the pressure data. In earlier experiments this port was used for attachment of a McLeod gage, which was used to calibrate a Pirani gage used for pressure data. This calibration appears in Fig. 2-5.

An ionization gage was provided for checking ultimate vacuum during desorption steps, and for determining apparent system leak rates, which were generally of the order of 10^{-4} to 10^{-5} torr per minute for a system volume estimated at 5 liters. Pumping was provided by a 4-in. water-cooled oil diffusion pump with a baffled liquid nitrogen trap which was connected to the system by a 4-in. Viton-sealed gate valve. Adjustment of range and sensitivity was provided by the microbalance control unit, which was connected to the balance mechanism by electronic cables and appropriate vacuum-type connectors. Readout was provided by a strip chart recorder attached to the output of the control unit.

Introduction of vapors into the leak valve was effected by connection of a manifold, which is shown schematically in the system line drawing in Fig. 2-6. This manifold had provision for introduction of both liquid and gaseous adsorbates. Connections

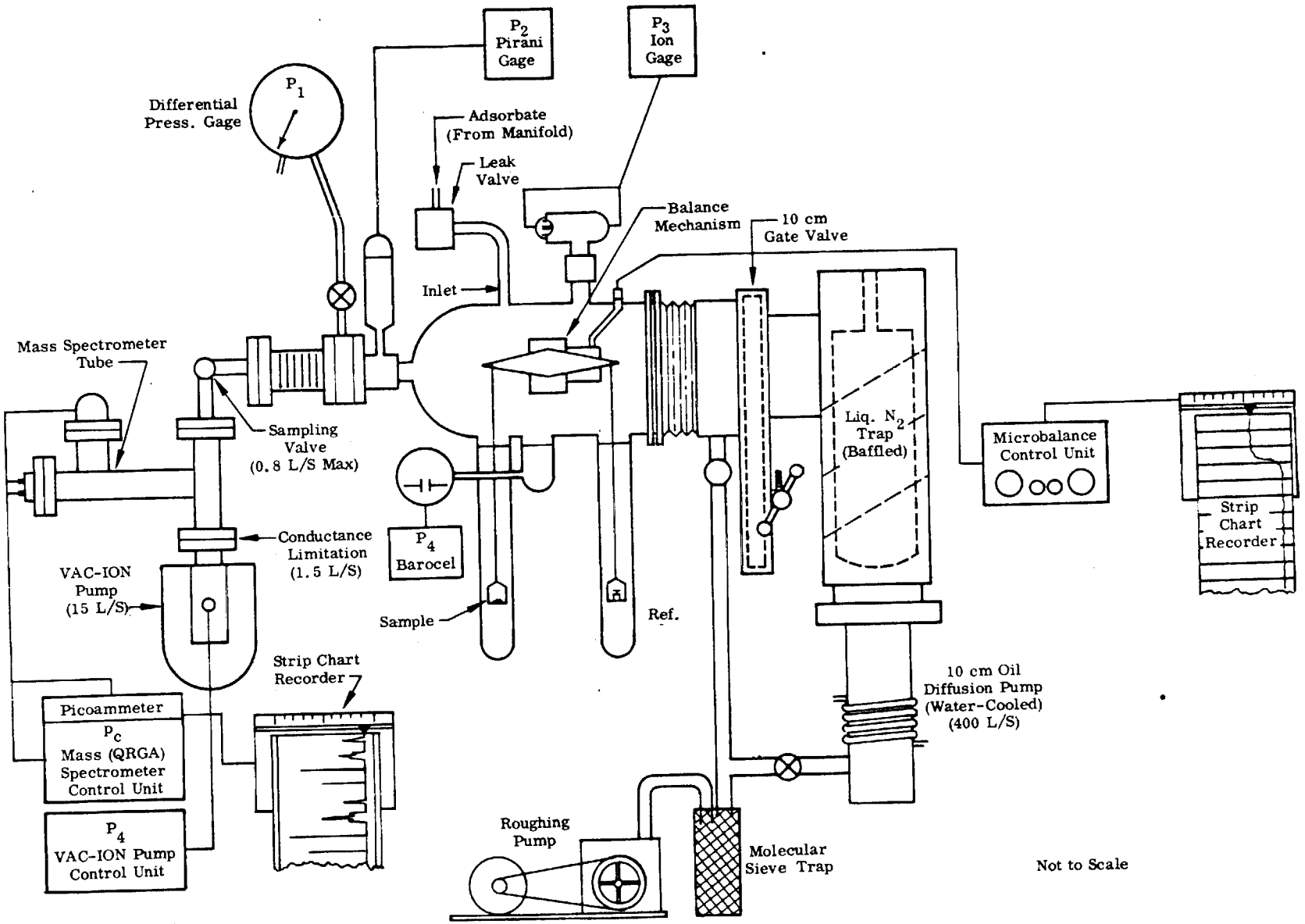

Fig. 2-4 Gravimetric Adsorption System

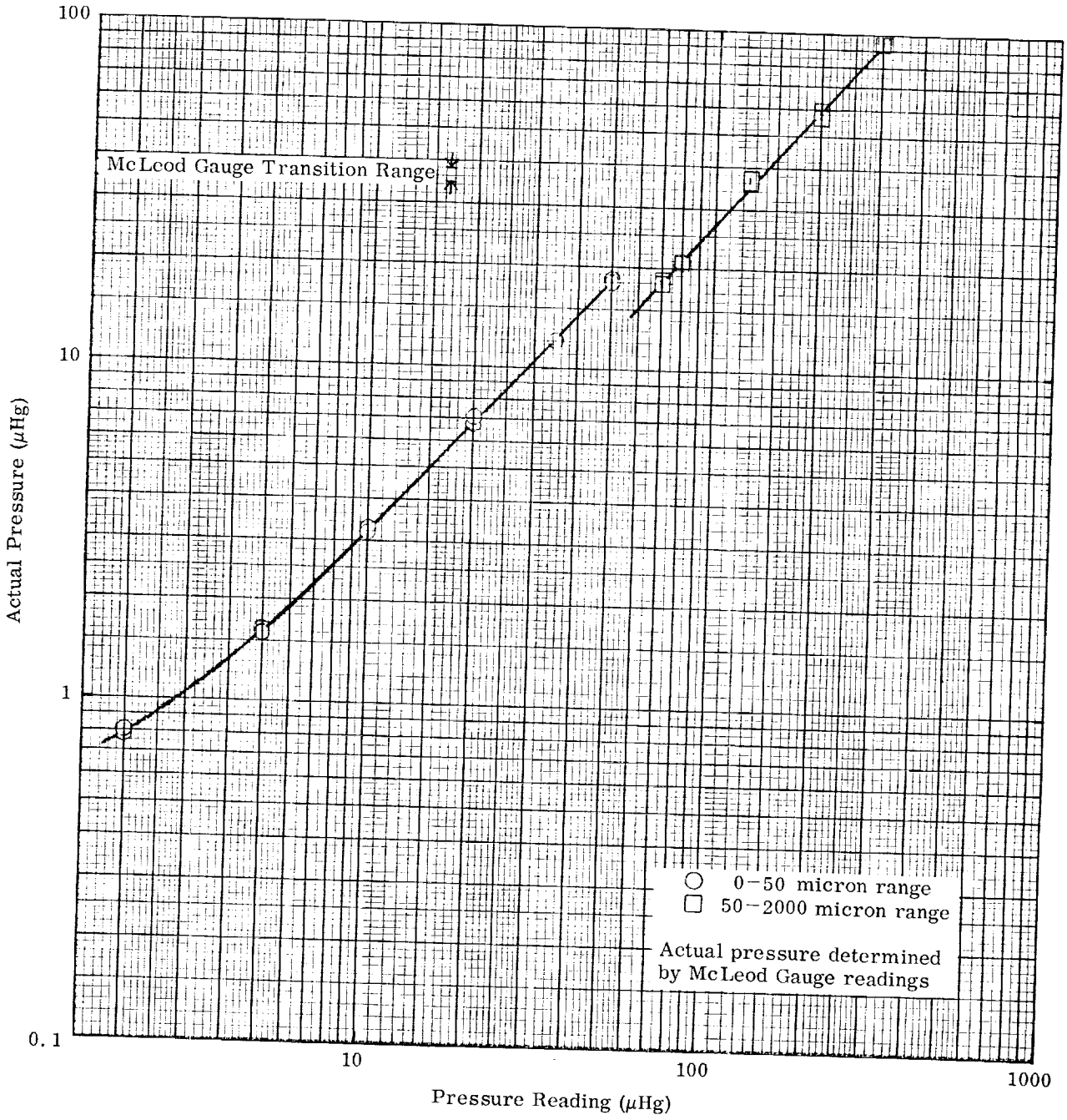

Fig. 2-5 Calibration of Pirani Gage in n-Butane

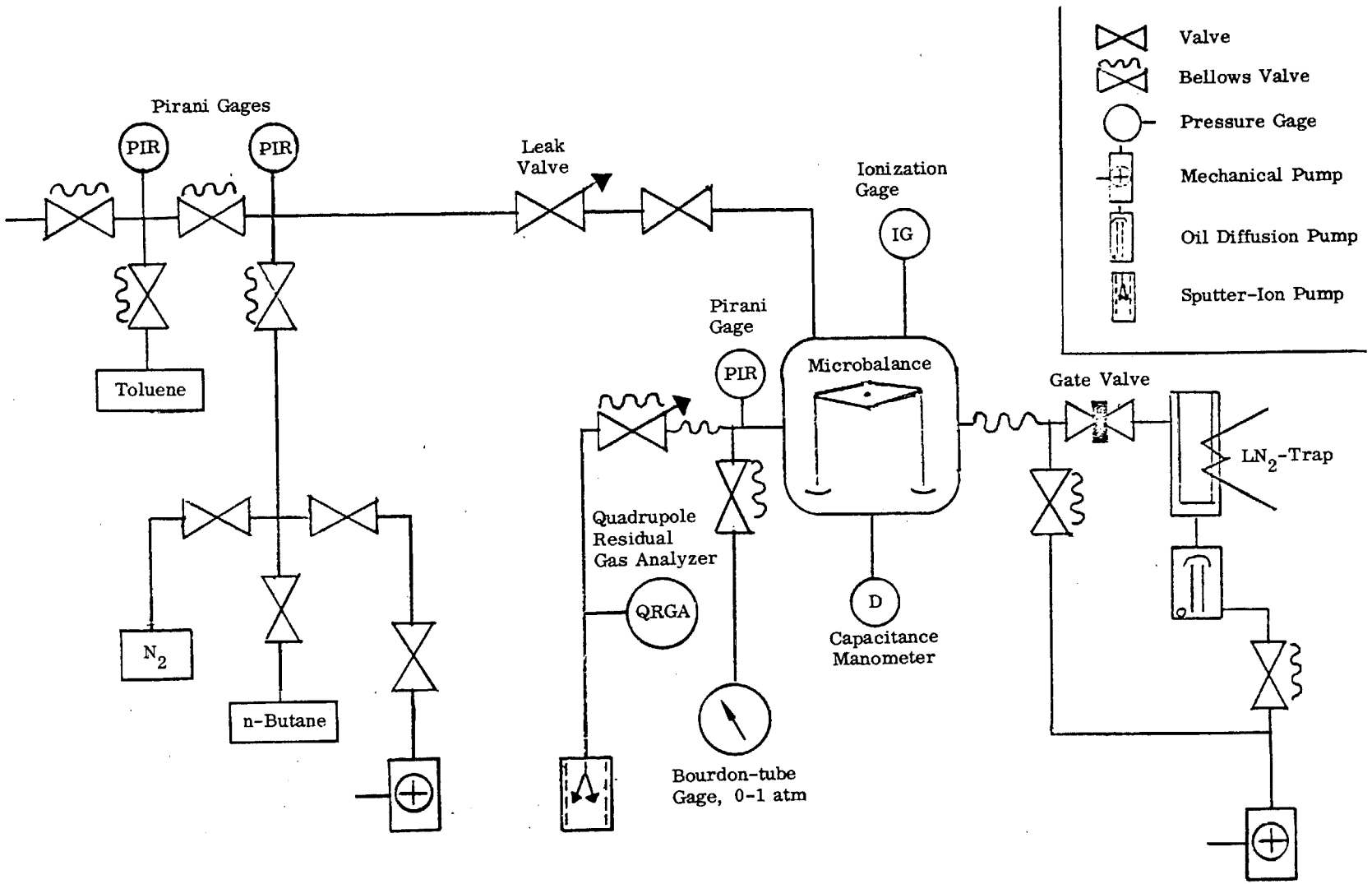

Fig. 2-6 Gravimetric System Line Drawing

to a vacuum pump were provided so that the manifold could be quickly flushed with different vapors. Pirani-gage tubes were provided in each section of the manifold so that leak rates could be estimated.

Heating was provided by two identical cylindrical tube furnaces, which were located by means of adjustable clamps around each hangdown tube in the vicinity of the sample and counterweight pans, as shown in Fig. 2-7. Temperature control was provided by a West JP temperature controller on the sample furnace and by Powerstat autotransformers in series with windings of both furnaces. The temperature controller sensor was an iron-constantan thermocouple placed in the sample tube furnace. Temperature readout was provided by another iron-constantan thermocouple located directly opposite the sample pan at the hangdown-tube surface, and connected to an accurate dc vacuum-tube voltmeter (VTVM).

The microbalance was calibrated periodically to read from 45 to 55 mg with $\pm$ 1 μg precision. Charcoal sample weights were kept as close to 50 mg as possible. Since adsorbed atmospheric contaminants were generally about 5 percent by weight, initial sample weights of about 52.5 mg were weighed out in air with the hangdown tube off. After replacing the hangdown tube and putting the furnaces in place around each tube, the system was rough-pumped for 5 to 10 min and then opened to the oil diffusion pump through the gate valve. After the sample weight rate of decrease was sufficiently low (10$-$20 μg/hr), both hangdown tube furnaces were turned on, first to low heat, which was gradually increased to about 400° C, where it was maintained for a few hours to get constant weight. The furnaces were turned off and allowed to cool for at least an hour before adjusting the temperature to the desired value.

To determine isotherms, first, the introduction manifold (Fig. 2-6) was flushed two or three times with the vapor to be used by first admitting the vapor and then pumping it out with the auxiliary pump. Next, the system gate valve (Fig. 2-4) was closed and the ionization gage (P_3) filament turned off, after noting that the system leak rate was reasonable (less than 10^{-5} torr/min). Then the vapor was admitted to the system by again admitting vapor to the manifold and opening the leak valve

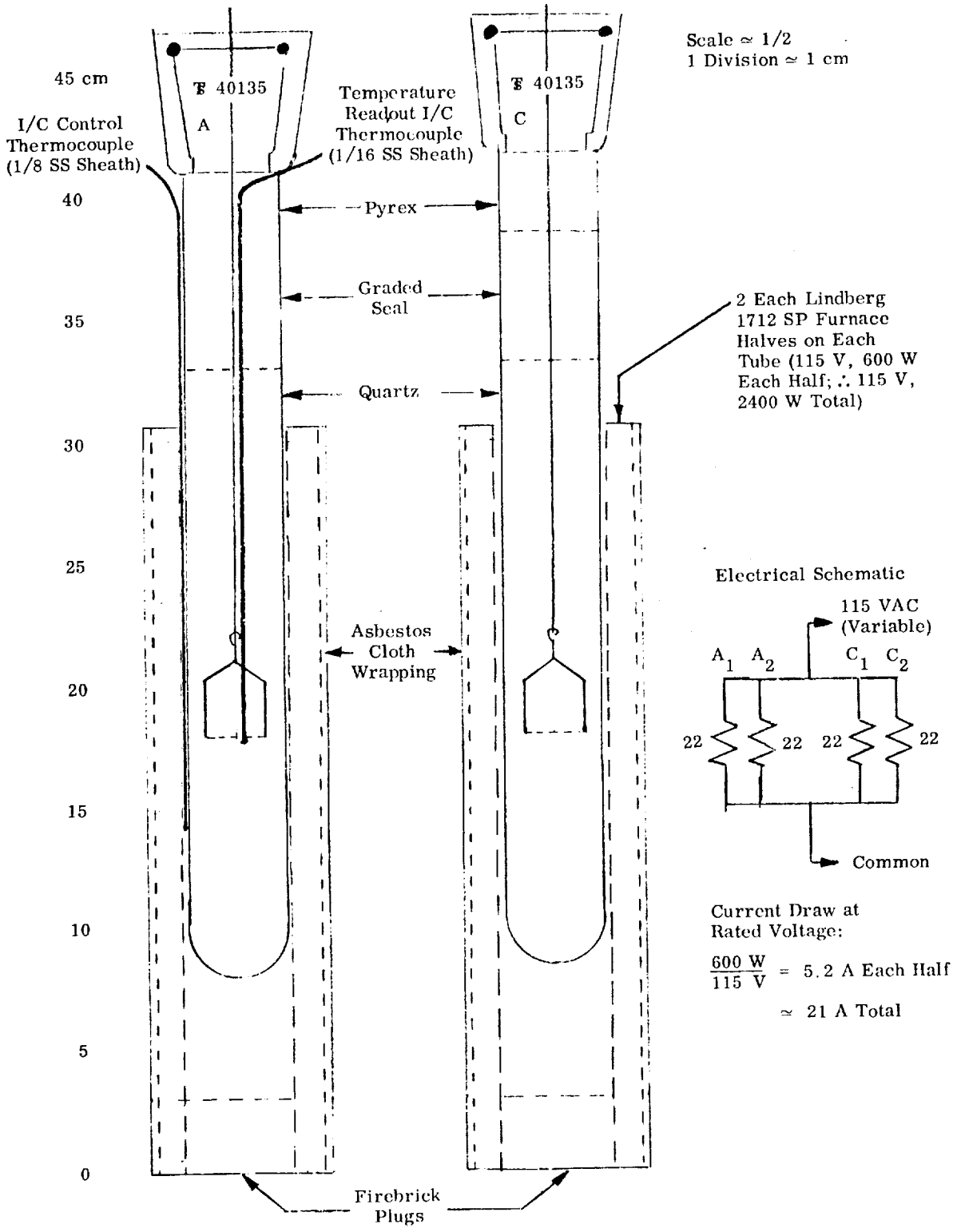

Fig. 2-7 Furnaces for Gravimetric System

sufficiently to allow system pressure to be increased to the lowest desired value for an isotherm point. After equilibrium had been obtained, as evidenced by constant weight and pressure (see strip-chart records in Appendix B), the weight and pressure values were noted and pressure was increased to the next desired value. In some cases, pressures were approached in the opposite direction by cracking the gate valve slightly in order to pump out only a part of the vapor.

Temperature was maintained by judicious adjustment of the temperature controller. In experiments at 27°C, the furnace wrapping was kept damp with water to provide a "wet-bulb" cooling effect, which was then counteracted by heating at very low voltage settings, which were judiciously changed to maintain temperature within ± 0.2°C.

After sufficient points had been obtained to determine an isotherm, the system was pumped out completely by opening the gate valve fully. In cases where more than one point was obtained at a given pressure, a slight weight increase was noted at lower temperatures and with lighter contaminants, such as n-butane and propane. This was assumed to be due to a background of "heavy" contaminants, and was extrapolated over the period of the isotherm experiment as a corrective addition to the initial weight used in calculating the amount adsorbed. In most cases this correction was very minor.

2.2 RESULTS

Isotherm data were obtained for a number of contaminants on the various sizes of BD charcoal listed in Table 2-1. These data were obtained on both the flow system and the gravimetric system. Summaries of data obtained on these systems appear in Appendixes C and D, respectively.

Selected gravimetric data for n-butane and toluene were plotted according to the Freundlich relation,

$$q_a = k_F p^{1/n} \qquad (2\text{-}1)$$

where

q_a	=	amount adsorbed	(ml STP/g)
k_F	=	a constant	[g/ml STP $(torr)^{-n}$]
p	=	partial pressure of contaminant	(torr)
n	=	a constant	

An advantage to plotting the data according to the Freundlich isotherm is that increased accuracy is obtained in reading low pressure and amount of adsorbed values. Such accuracy is required for calculation of thermodynamic state functions.

Early data from gravimetric experiments with n-butane on 0.5-mm charcoal particles based on Pirani-gage readings at various temperatures are plotted in Fig. 2-8. Later data based on Barocel readings for 2.0-mm particles at 27 and 67°C and for 0.5- and 1.0-mm particles at 27 and 107°C are shown in Fig. 2-9.

Data for toluene on 1.0-mm charcoal particles at 27, 67, and 107°C and on 0.5- and 1.0-mm particles at 27°C are shown in Fig. 2-10. Some additional isotherm data were determined for various contaminants in the course of desorption experiments described in section 5.1.1 and are tabulated in Appendix E.

Selected isotherm data, which were obtained in the flow adsorption experiments described in section 2.1.1 and summarized in Appendix C, are also tabulated separately in Appendix F. In addition, some adsorption data for n-butane at much higher pressures which were obtained in other work are tabulated in Appendix G.

The data in Appendixes E and F that were obtained under conditions similar to those of the isotherms in Figs. 2-9 (n-butane) and 2-10 (toluene) are plotted along with these isotherms. Open symbols are used to indicate gravimetric data, while flow data are shown as solid symbols.

Isotherm data were obtained for water on 30 × 40 BD at pressures near the vapor pressure of water at 25°C: 5, 10, 15, and 20 torr. These data are plotted on linear coordinates in Fig. 2-11.

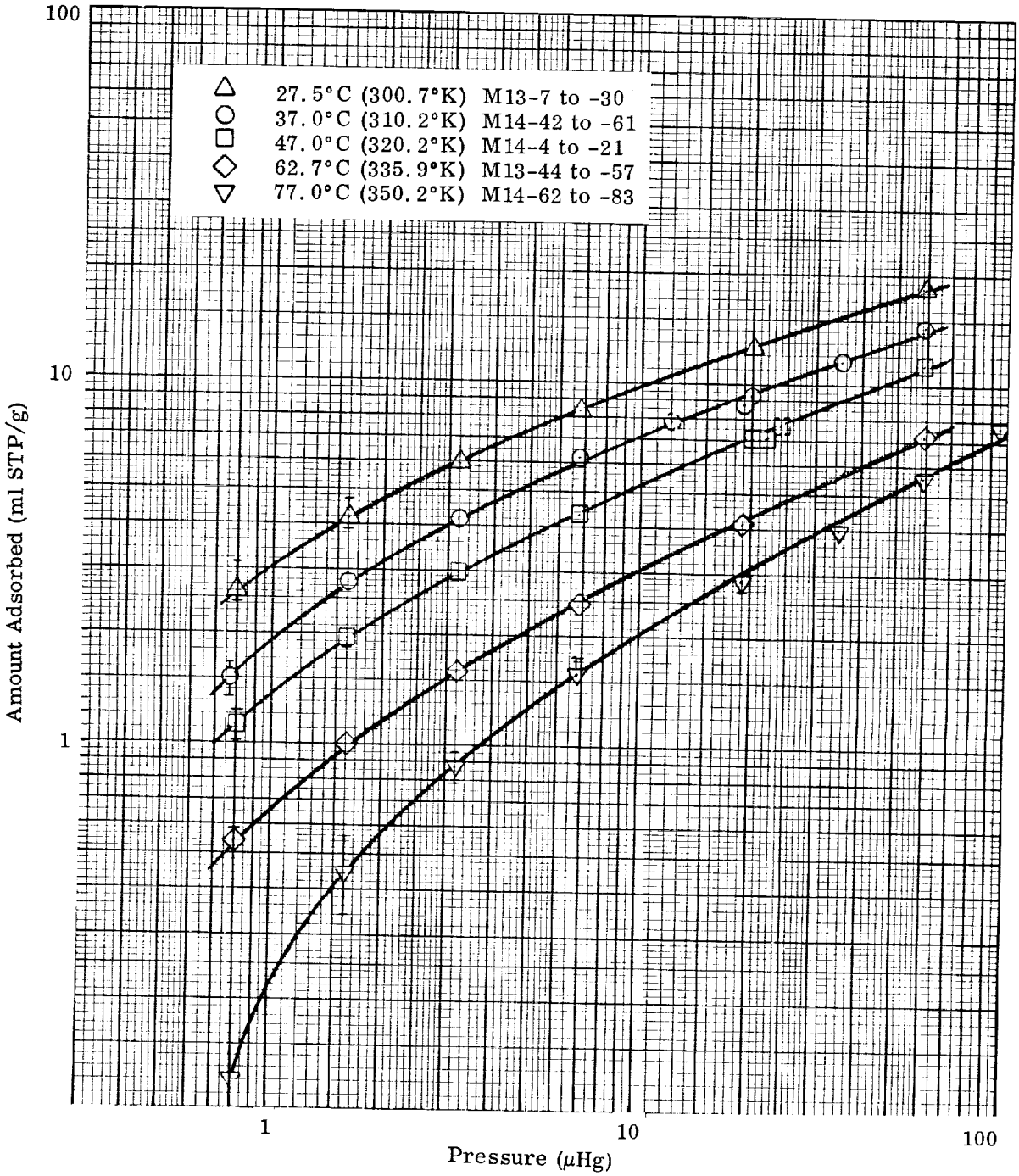

Fig. 2-8 Isotherms of n-Butane on 30 × 40 BD Activated Carbon (d_p = 0.05 cm). Pressure data taken with "calibrated" Pirani gage

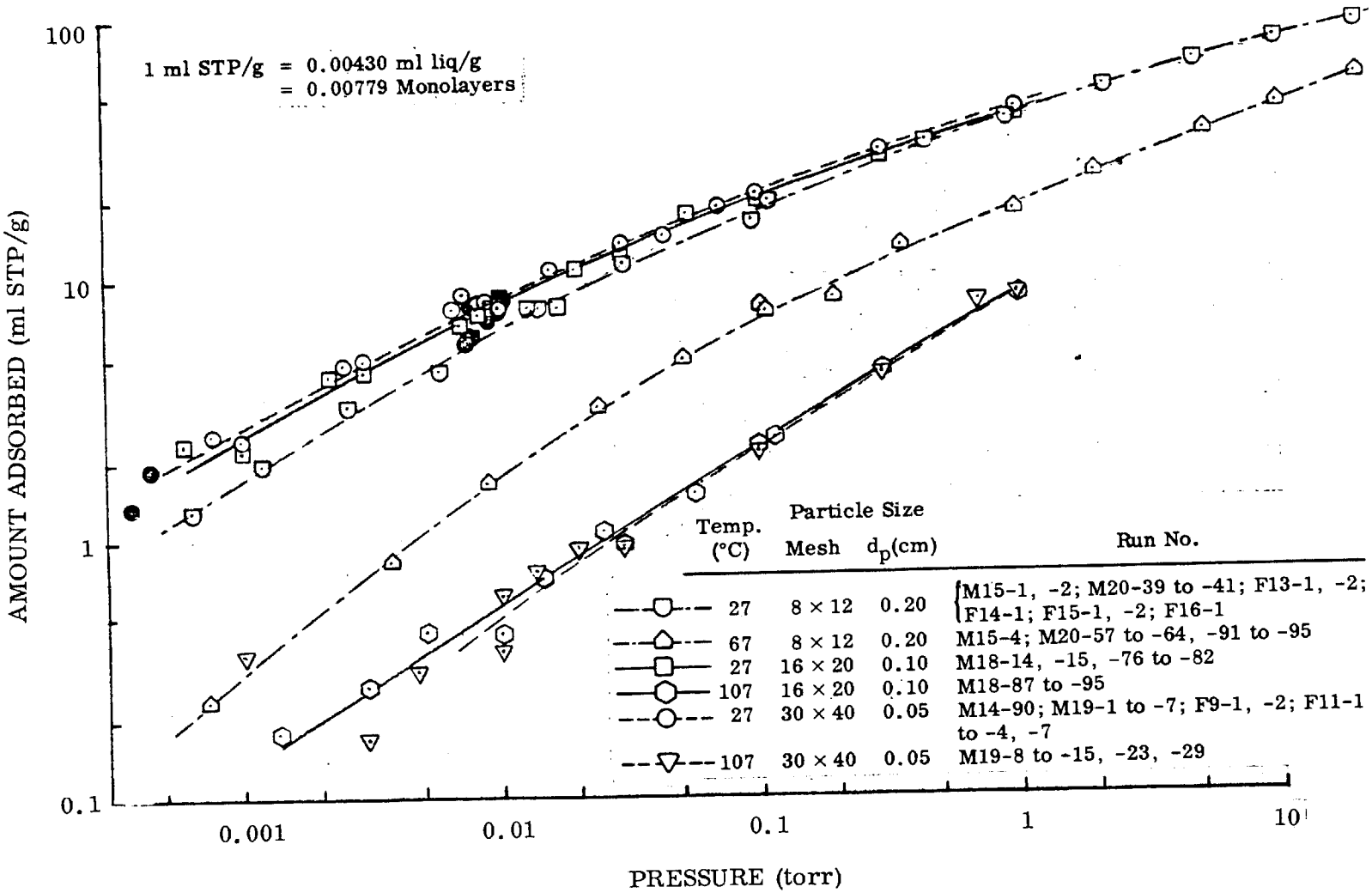

Fig. 2-9 Isotherms of n-Butane on BD Activated Carbon

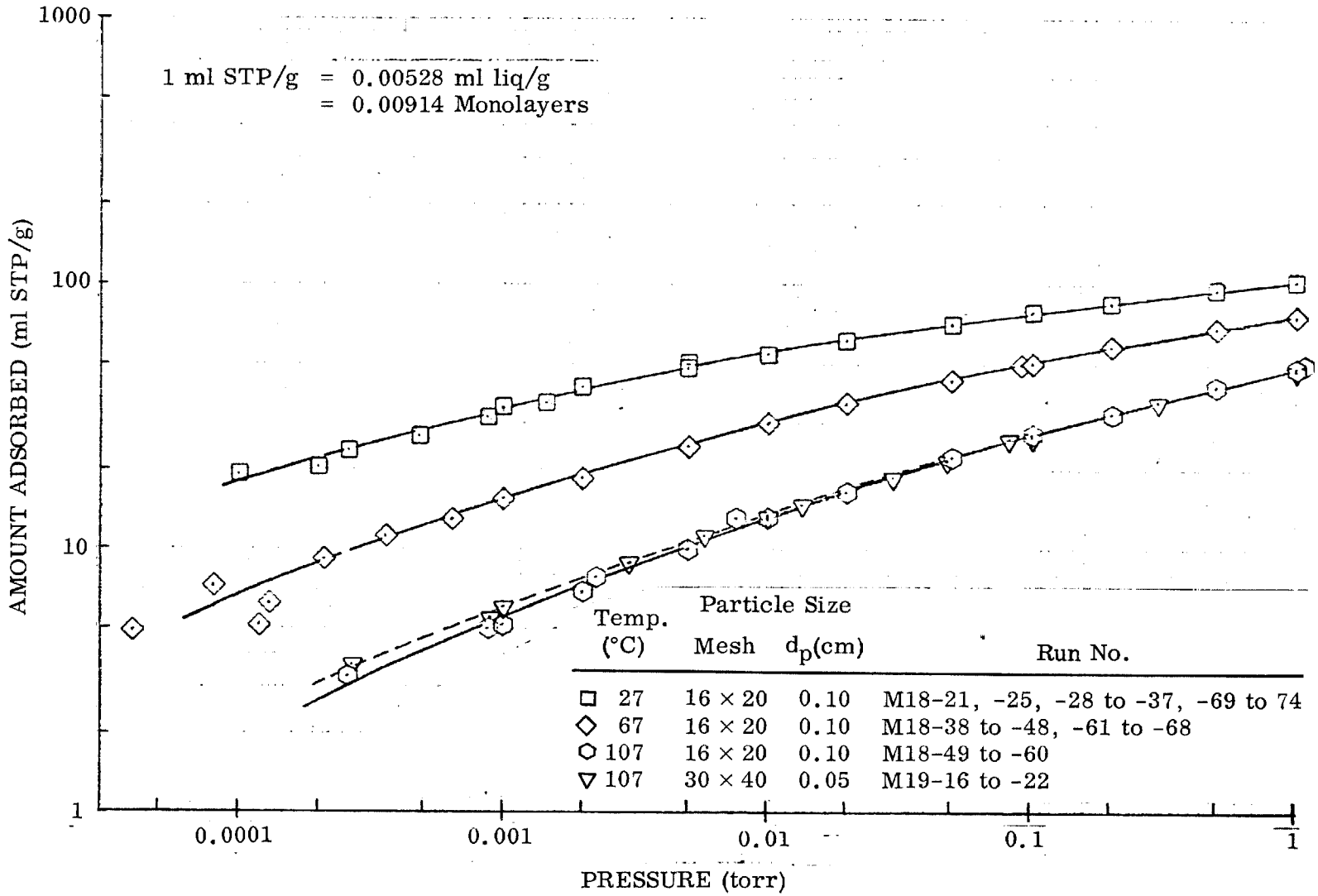

Fig. 2-10 Isotherms of Toluene on BD Activated Carbon

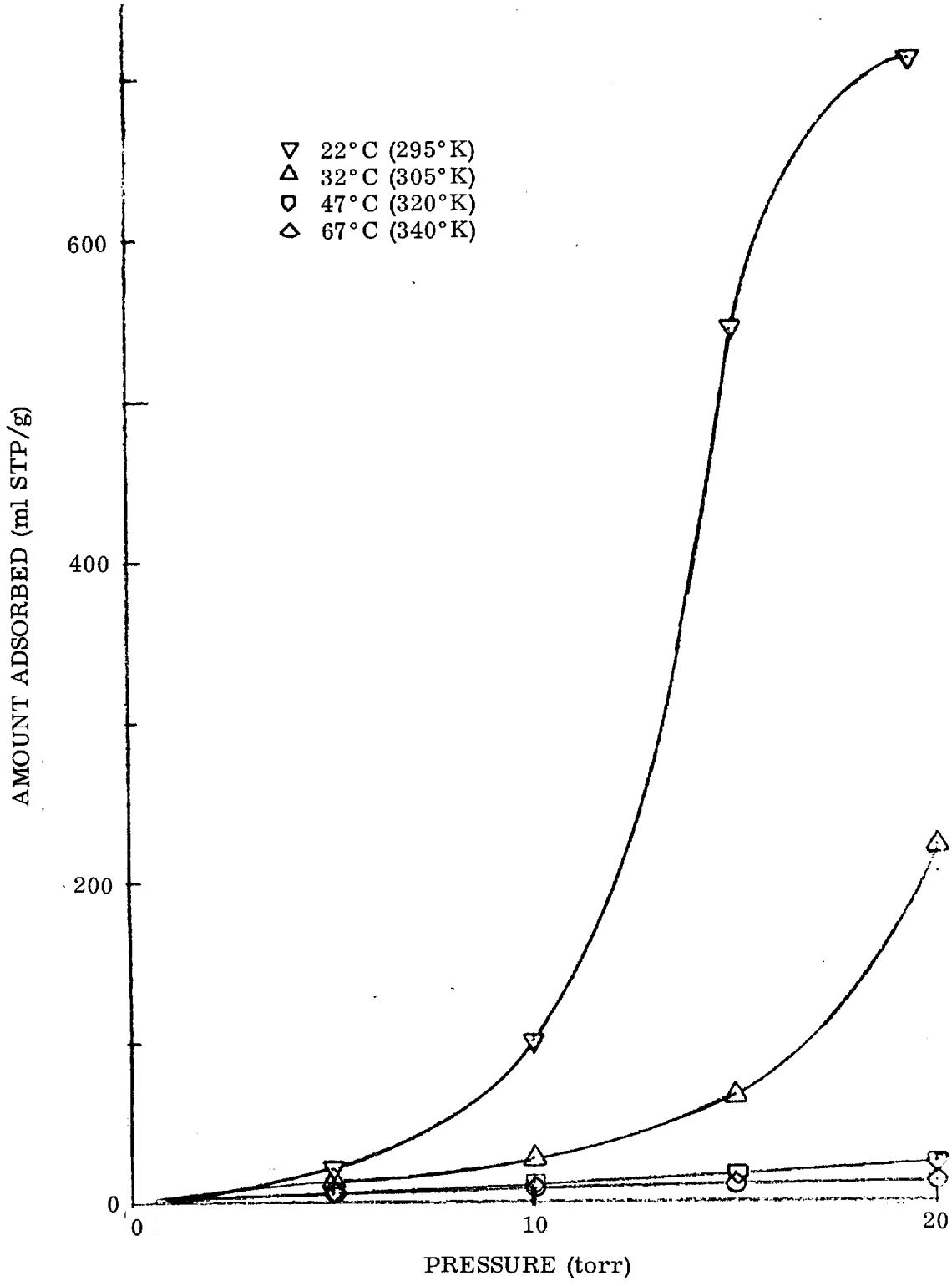

Fig. 2-11 Isotherms of Water on 30 × 40 BD Charcoal (d_p = 0.050 cm)

Section 3
ADSORPTION OF MIXED CONTAMINANTS

While adsorption isotherms such as those determined in Section 2 give one an excellent feeling for the performance of sorbent beds under conditions in which only one contaminant is present in the air, they do not necessarily present sufficient information as to how the presence of other contaminants will affect adsorptivity. The next logical extension of the experimental work then was to perform experiments in which there were two contaminants present. To this end, and also with thought to the vacuum desorption experiments on fixed beds described in Section 7, a number of flow experiments, similar to those described in Section 2 but with two and in one case three contaminants, were performed. Pairs of contaminants with both similar and widely different adsorptivities were selected for these experiments. Since water is not normally considered a contaminant, experiments incorporating it as the second component are described separately in a later section (Section 9).

Due to the time-consuming nature of the flow experiments, which were exaggerated greatly by using two contaminants of widely varying adsorptivities, a faster method was needed to get extensive data on adsorptivity of two contaminants at one time. The microbalance apparatus described in Section 2, this time modified by inclusion of a mass spectrometer for determination of partial pressures of multiple component vapors, was again found to provide adsorption isotherm data in much shorter experiments. Two typical contaminants of quite different adsorptivities in the pure state were chosen for these experiments. These experiments provided valuable data for testing a general theory for prediction of sorbent performance in the presence of more than one adsorbing component, as described in Section 4.

3.1 EXPERIMENTAL TECHNIQUE

3.1.1 Flow System

The same system and procedures were used in multicontaminant flow adsorption as in single contaminant work. There is only one variation in the experimental procedure. In blockage and displacement experiments, the inlet concentration of one contaminant was kept at zero until the other contaminant had been adsorbed on the bed. Oxygen or oxygen-nitrogen was substituted for that contaminant from just prior to the beginning of the adsorption step until some convenient time after adsorption of the first contaminant was complete. In flow experiment F17-3 (see Table 3-1), simultaneous adsorption of n-butane and toluene was studied; therefore, the oxygen-nitrogen mode described above was not used.

3.1.2 Gravimetric System

The apparatus used to determine mixed-contaminant adsorption isotherms was the same as that described in section 2.1.2 for single-contaminant isotherms with the addition of a mass spectrometer section, as shown in Fig. 2-4. This mass spectrometer, a Varian Quadrupole Residual Gas Analyzer (QRGA), was included in a sampling manifold with a 15-liter/sec getter-ion pump at the outlet and with molecular-flow conductance limitations at both the inlet and outlet so that the relative concentrations of each species were the same in the mass spectrometer as in the microbalance jar. (See Appendix H.) Mass spectrometer readout was obtained by connecting a strip-chart recorder to the picoammeter (electrometer) used to amplify ion currents that were detected as various mass-to-charge ratios were electronically swept over the range of interest. The strip-chart recorder, dual-pen version, was also connected to the pressure transducer readout to obtain total adsorbate pressure as a function of time.

Vapor introduction procedures were the same as those described in section 2.1.2, except that in no case was the microbalance system pumped by cracking the gate valve. This limitation was necessary in order to make certain that all the first species

Table 3-1

SUMMARY OF FLOW SYSTEM MIXED ADSORPTION DATA – BLOCKAGE EFFECTS

Run No.	Contaminant	Temperature (°C)	Concentration (ppm)	Blockage (%)
F9-1	n-Butane Propylene	25	20.4 0.54	86 ± 2
F9-2	n-Butane Propylene	25	1.08 13.2	29 ± 7
F11-4	n-Butane Propylene	27	0.9 1580	15 ± 8
F11-7	n-Butane Propylene	25	19.5 13.4	69 ± 3
F11-6	Propylene n-Butane	25	13.2 20.2	0
F6-1	Propylene Vinylidene Chloride	25	21.0 18.3	0
F6-2	Propylene Vinylidene Chloride	46	20.2 25.8	0
F7-2	Vinylidene Chloride Toluene	102	25.1 29.5	6 ± 9
F7-3	Toluene Vinylidene Chloride	102	24.8 25.2	91
F7-7	Toluene Vinlyidene Chloride	102	6.1 23.5	93
F12-1	Propylene Ethylene	25	13.8 27.2	0
F17-3	n-Butane Toluene	107	26.9 26.8	30
F17-4	Toluene n-Butane Freon-12	67	26.5 46.0 38.5	96

introduced was still in the system, except for an insignificant amount that was pumped out for analysis through the mass spectrometer section.

In determining these mixed-adsorption isotherms, the more strongly adsorbed contaminant was admitted first until the weight gain of the charcoal corresponded to a predetermined amount adsorbed, usually 1, 2, 5, 10, or 20 ml STP/g. As equilibrium was being attained, both adsorbate pressure and characteristic mass spectral peak height were noted. Next, the less strongly adsorbed species was admitted, after flushing and pumping the vapor admission manifold with the new vapor. After each admission of the less strongly adsorbed contaminant, total pressure and the mass spectral peak heights of both species were noted.

The peak heights corresponding to the first, more strongly adsorbed contaminant were checked to see if they were remaining constant in order to assure that this contaminant was not being displaced by the less strongly adsorbed one. Partial pressure of the second, less strongly adsorbed contaminant was obtained by subtracting the initial pressure of the first, more strongly adsorbed one from the total at each point in the isotherm determination, while weight gain corresponding to the second contaminant was obtained by subtracting the weight after adsorption of the first one. Both calculations were based on the assumption of no displacement as determined above.

Examples of mass spectra and pressure records and of weight records for n-butane on charcoal with preadsorbed toluene are given in Appendix B.

3.2 RESULTS

3.2.1 Flow System

Results of multiple-component flow adsorption experiments are included in the experimental summary in Appendix C and are summarized in Table 3-1. This table is broken into five sections corresponding to the five contaminant pairs studied: n-butane-propylene; propylene-vinylidene chloride; vinylidene chloride-toluene; propylene-ethylene; and n-butane-toluene. The last group also includes an experiment in which toluene was preadsorbed, followed by concurrent adsorption of both n-butane and Freon-12.

3.2.2 Gravimetric System

Isotherm plots showing adsorption of n-butane at 27° and 67°C with various amounts of preadsorbed toluene are presented in Figs. 3-1 and 3-2, respectively. Data are for 5, 10, and 50 ml STP/g of preadsorbed toluene. In the 50 ml STP/g cases, some displacement of toluene was evidenced by increases in mass spectral peak intensities as n-butane pressure was increased; thus, the butane adsorption shown in these isotherms may be misleadingly low. Virtually no displacement of toluene was experienced at 5 or 10 ml STP/g toluene preadsorbed at either temperature.

In Table 3-2 blockage of n-butane by toluene when n-butane is at MAC pressure (0.02 torr) is shown as a function of amount of preadsorbed toluene. Also shown is the partial pressure of toluene needed to obtain this amount adsorbed. As can be seen, the equilibrium pressures of toluene are far below the MAC value, 0.02 torr, for blockages of n-butane of well over 50 percent. At room temperature (27°C), adsorption of 50 ml STP/g of toluene at only one-third of MAC partial pressure results in 93 percent blockage of n-butane. Thus, a sorbent bed would have to be approximately 14 times as large as predicted for MAC n-butane if toluene were also present, even at this reduced level.

Table 3-2

DATA FOR BLOCKAGE OF n-BUTANE BY TOLUENE ON 8 × 12 BD CHARCOAL

Amount of Toluene Preadsorbed (ml STP/g)	Toluene Equilibrium Pressure		Blockage of n-Butane at MAC (0.02 torr)	
	27°C (torr)	67°C (torr)	27°C (%)	67°C (%)
5	$< 1 \times 10^{-5}$	$\sim 8 \times 10^{-5}$	29	47
10	$< 1 \times 10^{-4}$	5.6×10^{-4}	51	65
50	7.2×10^{-3}	9.1×10^{-2}	93[a]	100[a]

(a) Possibly somewhat less, due to displacement of toluene by n-butane.

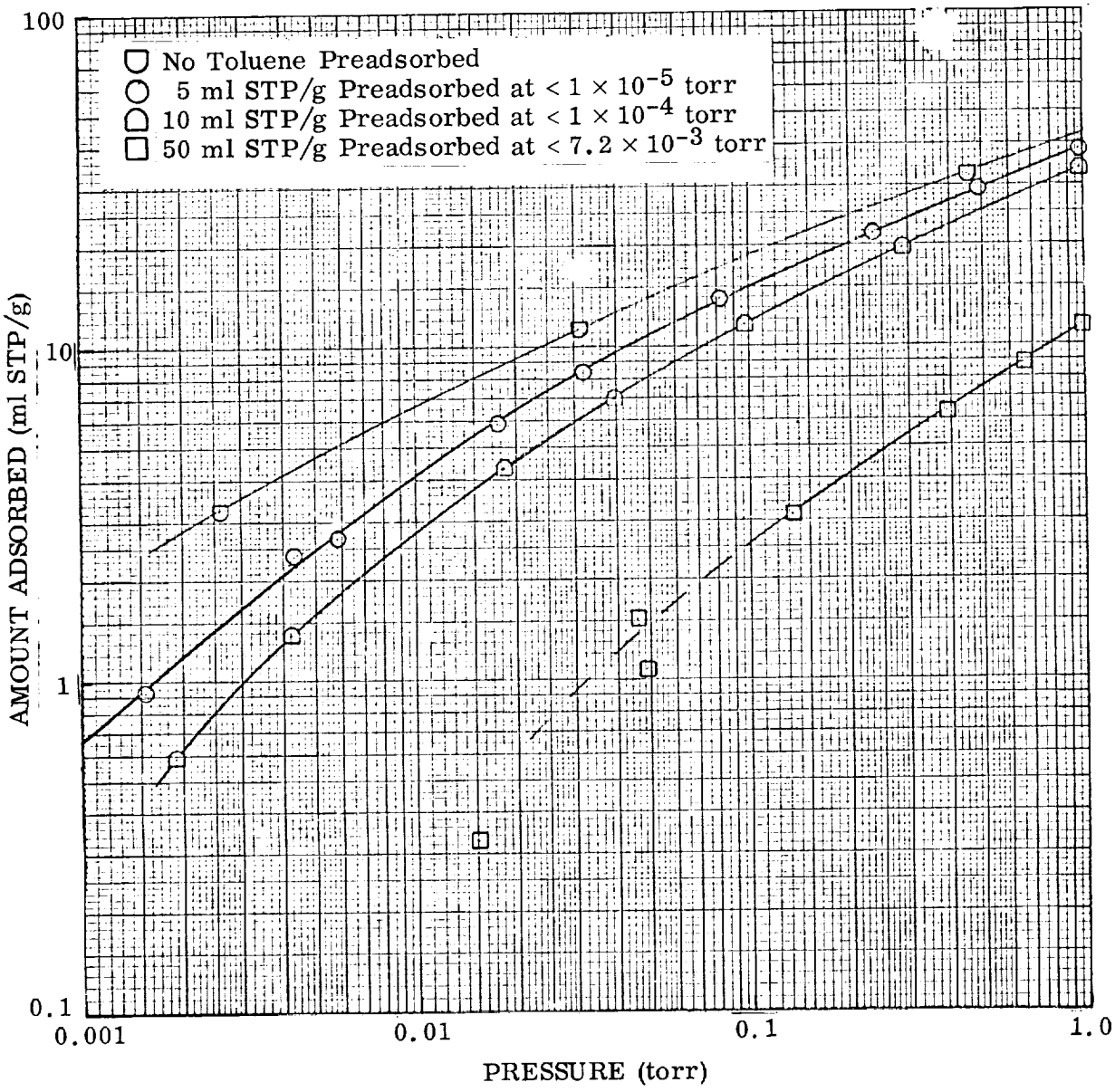

Fig. 3-1 Isotherms of n-Butane on 8 × 12 BD Charcoal at 27°C: Blockage by Toluene at Various Amounts Preadsorbed

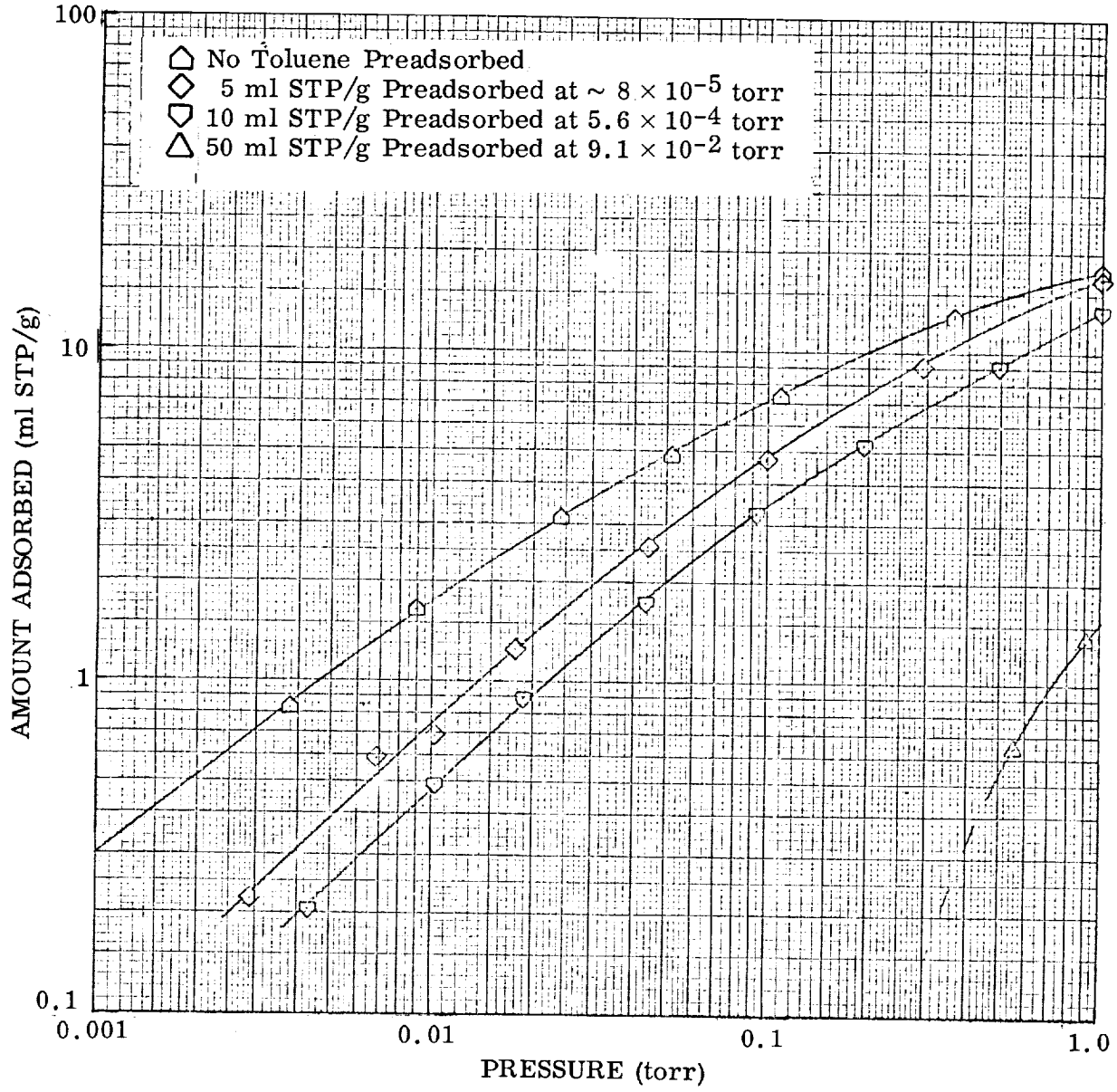

Fig. 3-2 Isotherms of n-Butane on 8 × 12 BD Charcoal at 67°C: Blockage by Toluene at Various Amounts Preadsorbed

In order to compare these gravimetric data with the flow system data in Table 3-1, blockage effects at n-butane partial pressures equivalent to 26.3 ppm at 0.5 atm total pressure are listed in Table 3-3. Thus, these are the blockage effects that would be expected in a flow experiment in which toluene and n-butane were present in the concentrations indicated.

Table 3-3

GRAVIMETRIC SYSTEM MIXED ADSORPTION BLOCKAGE DATA EXPRESSED IN CONCENTRATION TERMS

Run No.	Contaminant	Temperature (°C)	Concentration (ppm)	Blockage (%)
M20-22 to -30	Toluene n-Butane	27	0.01 26.3	39
-74 to -81	Toluene n-Butane	27	0.1 26.3	58
-42 to -49	Toluene n-Butane	27	19 26.3	97
-65 to -73	Toluene n-Butane	67	~0.2 26.3	57
-31 to -38	Toluene n-Butane	67	1.5 26.3	73
-50 to -56	Toluene n-Butane	67	240 26.3	>99

Section 4

DISCUSSION AND THEORETICAL TREATMENT OF ADSORPTION DATA

It is essential, because of the wide variety of compounds known even now to be present as trace contaminants in spacecraft environments, to provide some rational basis for the estimation of expected levels of sorbent loading. While it may not be possible to produce a correlation that is quantitatively accurate and of high precision over the five or six orders of magnitude that are of interest, it is necessary that the correlation be quantitative enough for design purposes and that the physical-chemical data required to apply the correlation be readily available. The so-called "potential theory" of adsorption seems to meet these rather stringent requirements suprisingly well. In this section it is demonstrated that the amount adsorbed as a function of pressure and temperature may be estimated within engineering accuracy merely from molar volume of the liquid at its boiling point and vapor pressure of the pure liquid. The theory is also generalized to the case of multicomponent adsorption.

4.1 POTENTIAL PLOT CORRELATION

The potential theory of adsorption was originally proposed by Polányi (Refs. 1, 2, 3) and later modified by others (Refs. 4 and 5). It was first used to correlate adsorption data collected under spacecraft conditions by Robell et al. (Ref. 6). The correlation, called a potential plot, enables estimation of q, the amount adsorbed, from the adsorption potential:

$$A = \frac{T}{V_m} \log_{10} \frac{P^\circ}{p} \tag{4.1}$$

where

A = adsorption potential (mol °K/ml liq)

T = temperature (°K)

V_m = contaminant molar volume at normal boiling point (ml liq/mol)

P° = contaminant vapor pressure (atm)

p = contaminant partial pressure (atm)

The adsorption potential can be calculated from two basic physical properties – molar volume and vapor pressure. These properties are listed, for a few selected trace contaminants considered in this work, along with estimated values for molecular area and monolayer coverage, in Table 4-1.

Table 4-1

SELECTED PHYSICAL PROPERTIES OF TRACE CONTAMINANTS

Contaminant	Molar Volume V_m (ml liq/mol)	Vapor Pressure at 27°C P° (atm)	Molecular Area β ($\AA^2$/molecule)	Monolayer Coverage q_m	
				(ml STP/g)	(ml liq/g)
Toluene	118.2	0.042	37.4	109.4	0.578
n-Butane	96.4	2.55	31.9	128.3	.552
Vinylidene Chloride	79.7	.84	28.6	143.1	.510
Ethanol	62.1	.084	25.7	159.2	.441
Propane	74.5	9.8	27.1	151.0	.502
Propylene	66.6	12.0	25.4	161.1	.479
Ethylene	49.4	42.5	20.2	203.0	.447
Dichlorodi-fluoromethane (Freon-12)	80.7	6.9	28.9	141.6	.510
Water	18.80	.032	13.1	311	.262

Molecular area, β, has been shown by Hill (Ref. 7) to be equivalent to the two-dimensional van der Waals constant, which can be evaluated by the equation:

$$b = 6.354 \times 10^{-16} (T_c/P_c)^{2/3} \qquad (4.2)$$

where

b = two-dimensional van der Waals constant (cm^2/molecule)
T_c = critical temperature (°K)
P_c = critical pressure (atm)

Values of b were calculated from critical temperature and pressure data of Robell (Ref. 8). These values are to be used only as approximations in surface coverage calculations, since they are quite possibly smaller than actual effective molecular areas. For instance, Davis (Ref. 9) and Emmett (Ref. 10) have shown that n-butane molecular area ranges from 43 to 52 $\mathring{A}^2$/molecule depending on the sorbent. Since similar values for other contaminants studied are not readily available, the b-values provide a consistent means of estimating relative coverages of these contaminants. Values of q_m were calculated from the equation

$$q_m = S_s V_o / N\beta = S_s V_m / N\beta \qquad (4.3)$$

where

q_m = monolayer coverage (ml liq/g)
S_s = sorbent surface area, assumed = 1.1×10^7 (cm^2/g)
V_o = standard state molar volume (ml STP/mol)
N = Avogadro's number = 6.02×10^{23} (molecules/mol)

The derivation of the potential plot correlation is semiempirical and has previously been discussed thoroughly (Ref. 5, 6, 11).

A wealth of adsorption data on Barnebey-Cheney type BD activated carbon have been obtained in this and other programs.

Some of these data are plotted in Fig. 4-1 as a potential plot. The correlation is quite good and extends over four orders of magnitude in amounts adsorbed. It is striking how consistent the results are, even though the data were obtained on the three

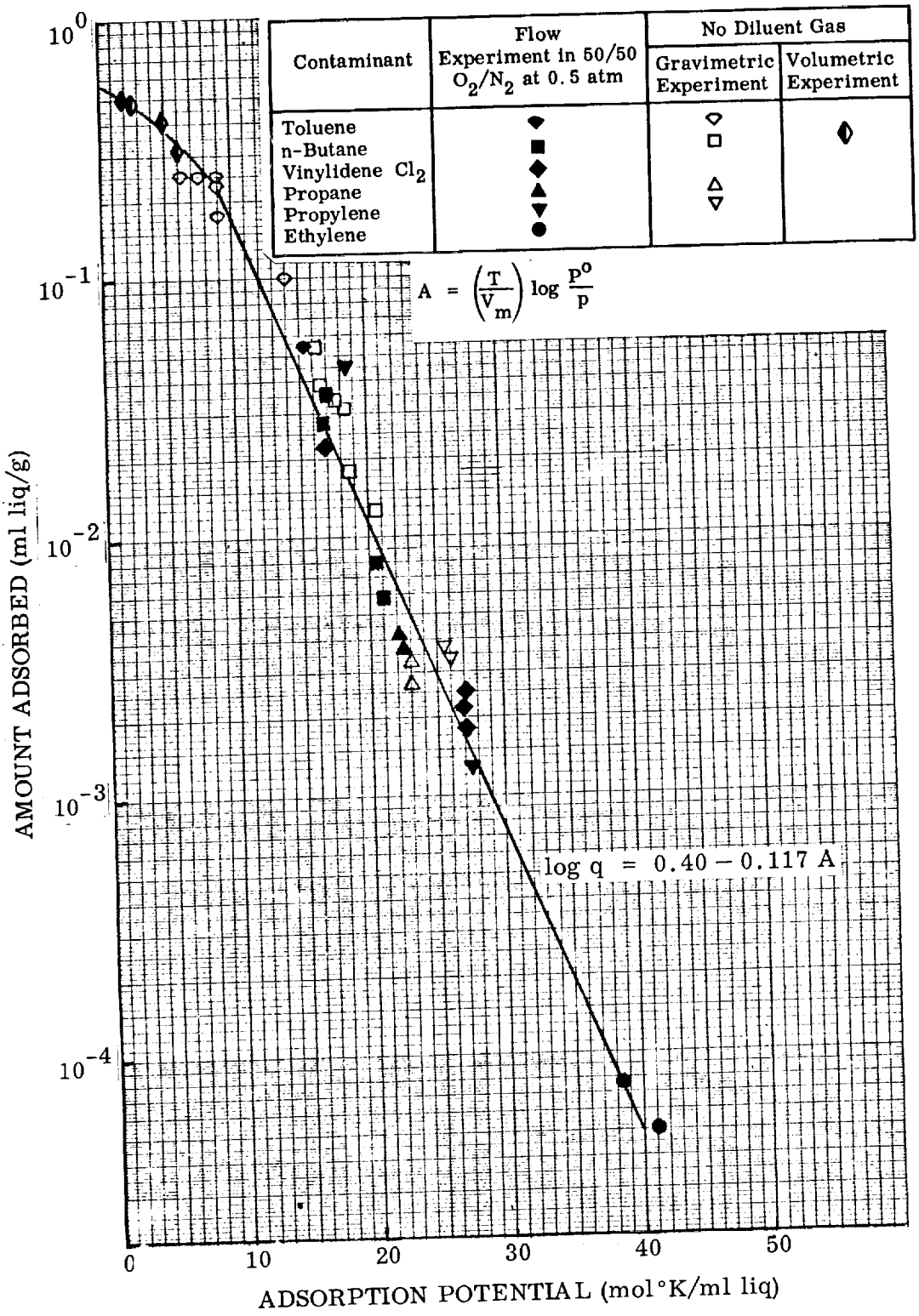

Fig. 4-1 Potential Theory Plot for BD Activated Carbon

separate experimental systems indicated in the figure legend. The correlation is by no means perfect; there are deviations of the order of 30%. However, the potential plot is still the best correlation found to date. It is recommended that Fig. 4-1 be used for design purposes.

The equation shown in Fig. 4-1 delineates the straight-line portion of the plot which, for this work, is the region of interest. All potential plots appearing elsewhere in this report include the line from Fig. 4-1 for reference purposes.

A more detailed exposition of the potential plot correlation for one adsorbate is shown in Fig. 4-2 and 4-3. The dotted line represents the potential plot as determined in Fig. 4-1. The n-butane data shown in Fig. 4-2 fit the correlation admirably, especially considering the temperature range studied and the fact that the data were obtained from three different experimental systems. (Run numbers beginning with M refer to microbalance gravimetric experiments; those beginning with F refer to flow system experiments.)

The toluene data in Fig. 4-3 are quite consistently above the potential plot line. There is no explanation for this variance at present, although the correlation still holds to about 30% as mentioned earlier, and this is adequate for design purposes.

These potential plots were made for single contaminants present in pure form (microbalance runs) and in nitrogen-oxygen mixtures (flow runs). There is no apparent difference in adsorptive capacity between these two cases. However, in the case of mixtures or when humidity is present, adsorptive capacity is drastically affected, as discussed later (Section 9).

A new derivation of the Polányi potential plot is presented in the following paragraphs. This derivation starts from fundamental principles and goes through to the convenient calculation of thermodynamic quantities, such as heat of adsorption, and of kinetics quantities, such as desorption rate order.

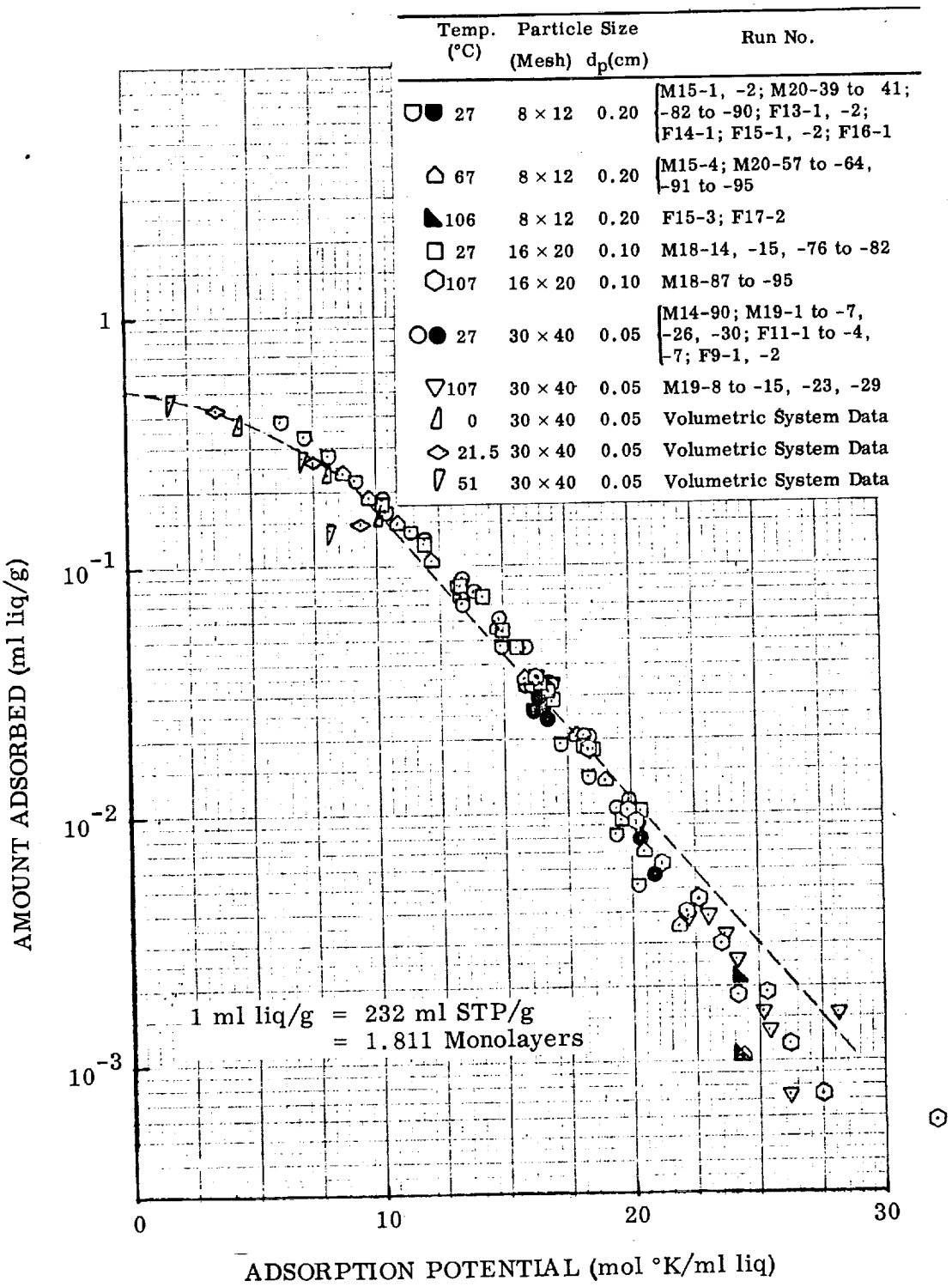

Fig. 4-2 Potential Plot for Adsorption of n-Butane on BD Activated Carbon

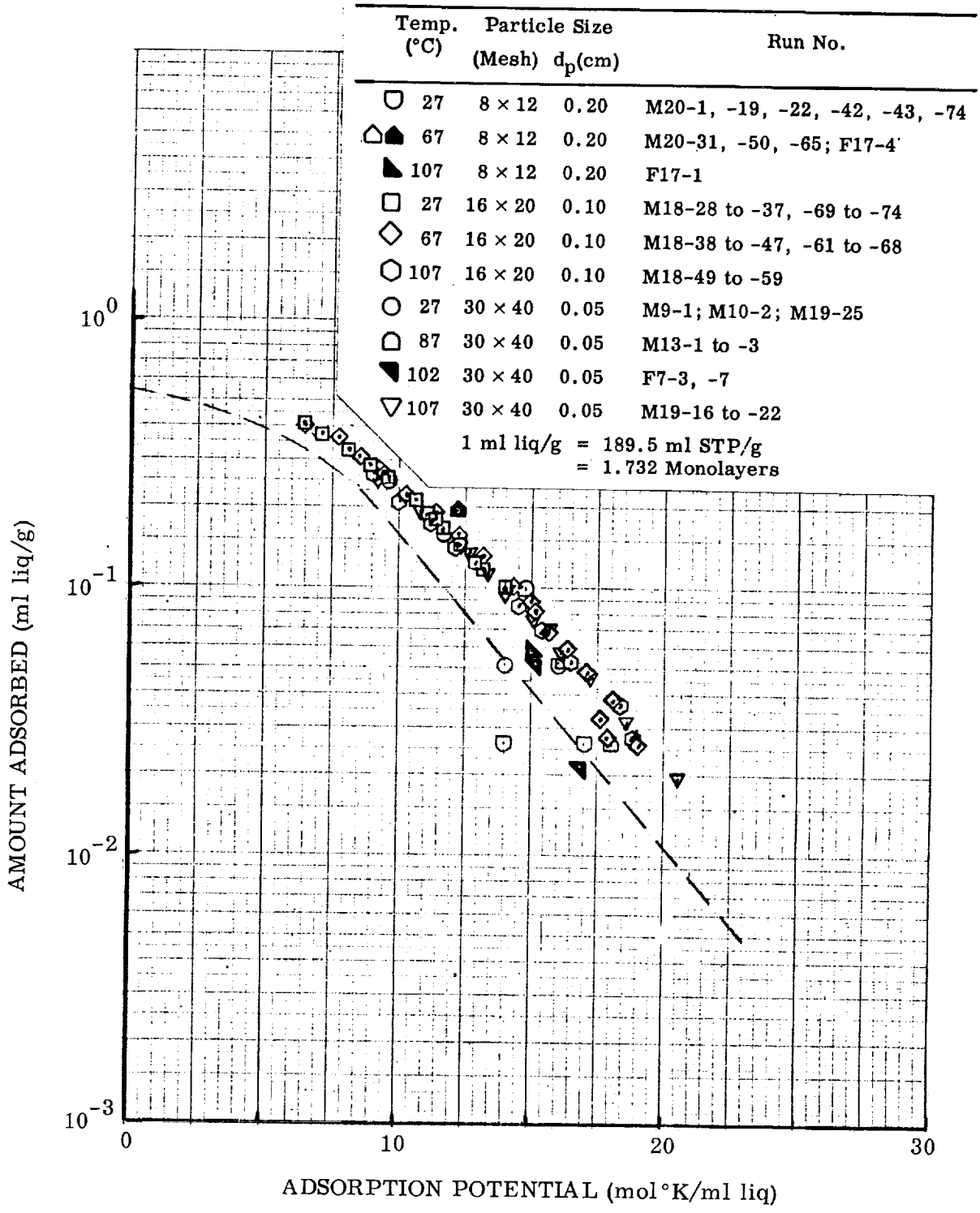

Fig. 4-3 Potential Plot for Adsorption of Toluene on BD Activated Carbon

The general form of the Polányi isotherm can be derived from the Gibbs equation:

$$\pi = (\gamma - \gamma_s) = RT \int_0^p \Gamma d \ln f \qquad (4.4)$$

where

π = spreading pressure (cal/cm^2)
γ = surface free energy of adsorbed layer per unit area (cal/cm^2)
γ_s = clean surface free energy per unit area (cal/cm^2)
R = gas constant (cal/mol °K)
p = pressure (cal/cm^2)
Γ = surface excess concentration (mol/cm^2)
f = fugacity of adsorbate (cal/cm^3)

and two assumptions that are quite reasonable for very low coverages. When this is done the derivation gives exactly the linear form of the isotherm, which is so often observed at very low coverages. Firstly, it is presumed that the surface is composed of portions that are essentially bare and portions covered with absorbate. Secondly, it is assumed that the bare portion has a surface free energy per unit area identical to the clean surface free energy, γ_s, and that the surface free energy per unit area of the portion of the surface covered with adsorbate is a constant, γ_A, independent of coverage for portions of the surface covered only by a monolayer of adsorbate. The surface free energy of the adsorbed phase, γ, may then be written:

$$\gamma = \theta \gamma_A + (1 - \theta) \gamma_s \qquad (4.5)$$

where θ = fractional coverage. Thus,

$$\pi = \theta (\gamma_A - \gamma_s) \qquad (4.6)$$

Equation 4.4 may now be differentiated to give:

$$d\pi = (\gamma_A - \gamma_s) d\theta = \Gamma RT d \ln f \qquad (4.7)$$

but

$$\theta = \beta\Gamma \tag{4.8}$$

where β = monolayer area in cm^2/molecule.

Equation 4.7 may be rearranged to give:

$$d \ln \Gamma = \frac{RT}{\beta(\gamma_A - \gamma_s)} d \ln f \tag{4.9}$$

The quantity $(\gamma_A - \gamma_s)$ in Eq. 4.9 is the excess surface free energy per unit area associated with the adsorbate. There is no a priori reason to expect $(\gamma_A - \gamma_s)$ to be constant in the multilayer region; nevertheless, Eq. 4.8 may be, in principle, integrated even for multilayer adsorption to give the isotherm:

$$\ln \Gamma/\Gamma^\circ = RT \int_{f^\circ}^{f} \frac{d \ln f}{\beta(\gamma_A - \gamma_s)} \tag{4.10}$$

where Γ° and f° are limits suitably chosen for the integration.

At low coverages, as mentioned earlier, it is assumed that γ_A and γ_s are constant and independent of coverage. Then the denominator in Eq. 4.10 is constant, and integration is straightforward.

Following the original idea of Polányi (Ref. 1) or taking guidance from the success of regular solution theory, it is more likely that the surface free energy per unit volume would be independent of the adsorbate on a particular adsorbent than the free energy per molecule. Thus, it might be reasonable to expect that, for a given class of adsorbates (say a homologous series of hydrocarbons), the quantity $(\gamma_A - \gamma_s)/\delta_m$,

where δ_m is the molecular diameter, should be relatively constant. Thus, Eq. 4.9 may be rewritten:

$$\ln \Gamma/\Gamma^\circ = RT \int_{f^\circ}^{f} \frac{\delta_m d \ln f}{V_m(\gamma_A - \gamma_s)} \tag{4.11}$$

and may be integrated to give:

$$\ln \frac{\Gamma}{\Gamma^\circ} = - \frac{RT}{V_m} \cdot \frac{\delta_m}{(\gamma_A - \gamma_s)} \ln f^\circ/f \tag{4.12}$$

which is identical to the empirical low-coverage limit of the Polányi isotherm if f° is taken as the fugacity of saturated adsorbate liquid at the temperature of the adsorption. Of course, Γ° has no real physical significance under such circumstances, and Eq. 4.11 departs from the empirical isotherm as soon as γ_A begins to change with coverage. Nevertheless, a rather simple physical interpretation results from the slope of the linear portion of the Polányi isotherm. It is the reciprocal of the excess surface free energy per unit volume of adsorbate.

A number of thermodynamic properties can be derived simply from Eq. 4.12. The isosteric heat, q_{st}, is given by

$$q_{st} = - R \left(\frac{\partial \ln p}{\partial \frac{1}{T}} \right)_\theta \tag{4.13}$$

but the fugacity usually can be approximated by the pressure at low coverages where Eq. 4.12 is appropriate. Thus:

$$q_{st} = \Delta H_v - \frac{V_m}{\delta_m} (\gamma_A - \gamma_s) \ln \Gamma/\Gamma^\circ \tag{4.14}$$

This has the same functional form as the relation that Halsey and Taylor (Ref. 12) have derived for the Freundlich isotherm and, indeed, Eq. 4.11 can be rearranged in the Freundlich form:

$$\Gamma = k_f p^{1/n} \tag{4.15}$$

if we set:

$$k_f = \Gamma^\circ \, [P^\circ]^{-1/n} \tag{4.16}$$

and

$$n = \frac{V_m(\gamma_A - \gamma_s)}{\delta_m RT} \tag{4.17}$$

While Halsey and Taylor (Ref. 12) derived their results for a heterogeneous surface, this development shows that the Freundlich isotherm and the logarithmic dependence of the isosteric heat (Eq. 4.14) can come as well from a homogeneous surface.

The integral enthalpy of adsorption, ΔH_a, is given (Ref. 13) as:

$$\Delta H_a = H_a - H_g = q_{st} + \frac{T}{\Gamma}\left(\frac{\partial \pi}{\partial t}\right)_\Gamma \tag{4.18}$$

where

H_a = adsorbed-phase enthalpy (cal/mol °K)
H_g = gas-phase (cal/mol °K)

using Eq. 4.6 and 4.14

$$\Delta H_a = - q_{st} + T\beta \left[\frac{\partial}{\partial t}(\gamma_A - \gamma_s)\right]_\Gamma \tag{4.19}$$

and under the assumptions consistent with Eq. 4.12, Eq. 4.19 becomes:

$$\Delta H_a = - q_{st} + TV_m \left(\frac{\partial \phi}{\partial t}\right)_\Gamma \tag{4.20}$$

Where

$\frac{R}{\phi}$ = negative slope of Polányi plot (ml liq/mol °K)

$\phi = \frac{\gamma_A - \gamma_s}{\delta_m}$, excess free energy per unit volume (cal/ml liq)

The integral entropy change is $\Delta H_a/T$. In fact, the isotherm results in a very simple equation of state for the adsorbed layer:

$$\pi = V_m \phi \Gamma \tag{4.21}$$

from which any of the desired thermodynamic properties may be calculated by well-known methods.

Usually ϕ is independent of temperature or nearly so in which case

$$q_{st} \approx \Delta H_a = T\Delta S_a \tag{4.22}$$

Where ΔS_s = entropy of adsorption in cal/mol °K.

The temperature dependence of ϕ is always quite small when Eq. 4.12 is appropriate at all, and reducing experimental data according to Eq. 4.12, and/or Eq. 4.21 substantially facilitates the extraction of thermodynamic properties in contrast to other approaches. These ideas can be applied to the nonlinear portion of the isotherm if it is recognized that outside the linear range one may use for ϕ:

$$\phi = \frac{R\Gamma}{V_m}\left(\frac{\partial \ln \Gamma}{\partial \ln f}\right)^{-1} = -\left(\frac{\partial \ln \Gamma}{\partial A}\right)^{-1} \tag{4.23}$$

Where

A = Polányi adsorption potential (ml liq/mol (°K)

$$A = \frac{RT}{V_m} \ln f°/f \tag{4.23a}$$

4.2 CALCULATION OF HEAT AND ENTROPY OF ADSORPTION FOR BUTANE AND TOLUENE

A good deal of information about the thermodynamics of an adsorbed gas can be obtained from a set of isotherms such as those shown in section 2.2. These thermodynamic properties can then be compared with those calculated for pertinent idealized models of the adsorbed layer. It is shown in the following paragraphs that the picture which emerges is consistent with the desorption mechanism deduced from desorption rate data. For example, it is shown how entropy data as a function of coverage establish the relative surface mobility of adsorbates and how enthalpy data contribute to characterizing surface heterogeneity. In this section these methods are applied in detail to the adsorption of n-butane and toluene on BD charcoal.

Several heats of adsorption may be defined, but the one most easily identified with the adsorption isotherm is the isosteric heat of adsorption, q_{st}, which may be defined (Ref. 14) as the heat released in a constant temperature calorimeter when a differential amount of gas is adsorbed at constant pressure.

$$q_{st} \equiv (\partial Q/\partial n_s)_{T,p} \tag{4.30}$$

where

q_{st} = isosteric heat of adsorption (cal/mol)
Q = reversible heat change of the system (cal)
n_s = number of moles of gas adsorbed (mol)
T = absolute temperature (°K)
p = partial pressure of the adsorbate in the gas phase (cal/cm^3)

The isosteric heat may be calculated from the adsorption isotherms by applying the following equation (Ref. 14):

$$q_{st} = - R [\partial \ln p/\partial (1/T)]_\theta \tag{4.31}$$

where

R = gas constant = 1.98 (cal/mol °K)

θ = fraction of the surface covered with adsorbed molecules

In Fig. 4-4 logarithm of the partial pressure of n-butane is plotted as a function of reciprocal temperature for several values of the amount adsorbed on 0.5-mm carbon. In Fig. 4-5 data for more recent experiments with 0.5-mm carbon are plotted similarly, while data for 1- and 2-mm carbon appear in Fig. 4-6 and 4-7, respectively. The slope of these isosteres is q_{st}/R. The values of q_{st} as deduced from Fig. 4-4 to 4-7 are tabulated in Table 4-2.

A similar plot for toluene adsorption on 1-mm particles appears in Fig. 4-8 and values of q_{st} are tabulated in Table 4-3.

The isosteric heat can be shown (Ref. 13) to be related to the integral molar enthalpy by the following equation:

$$\Delta H_a \equiv H_a - H_g = - q_{st} + (T\beta/\theta)(\partial\pi/\partial T)_\theta \qquad (4.32)$$

where

ΔH_a = integral molar enthalpy of adsorption (cal/mol)

H_g = enthalpy of the adsorbate in the gas phase (cal/mol)

H_a = enthalpy of the adsorbate in the adsorbed phase (cal/mol)

β = molecular area (cm^2)

π = spreading pressure (cal/cm^2)

It is shown in the previous section that systems which follow the Polányi potential theory have a very simple equation of state; i.e.,

$$\Pi = \frac{V_m \phi \theta}{\beta} \qquad (4.33)$$

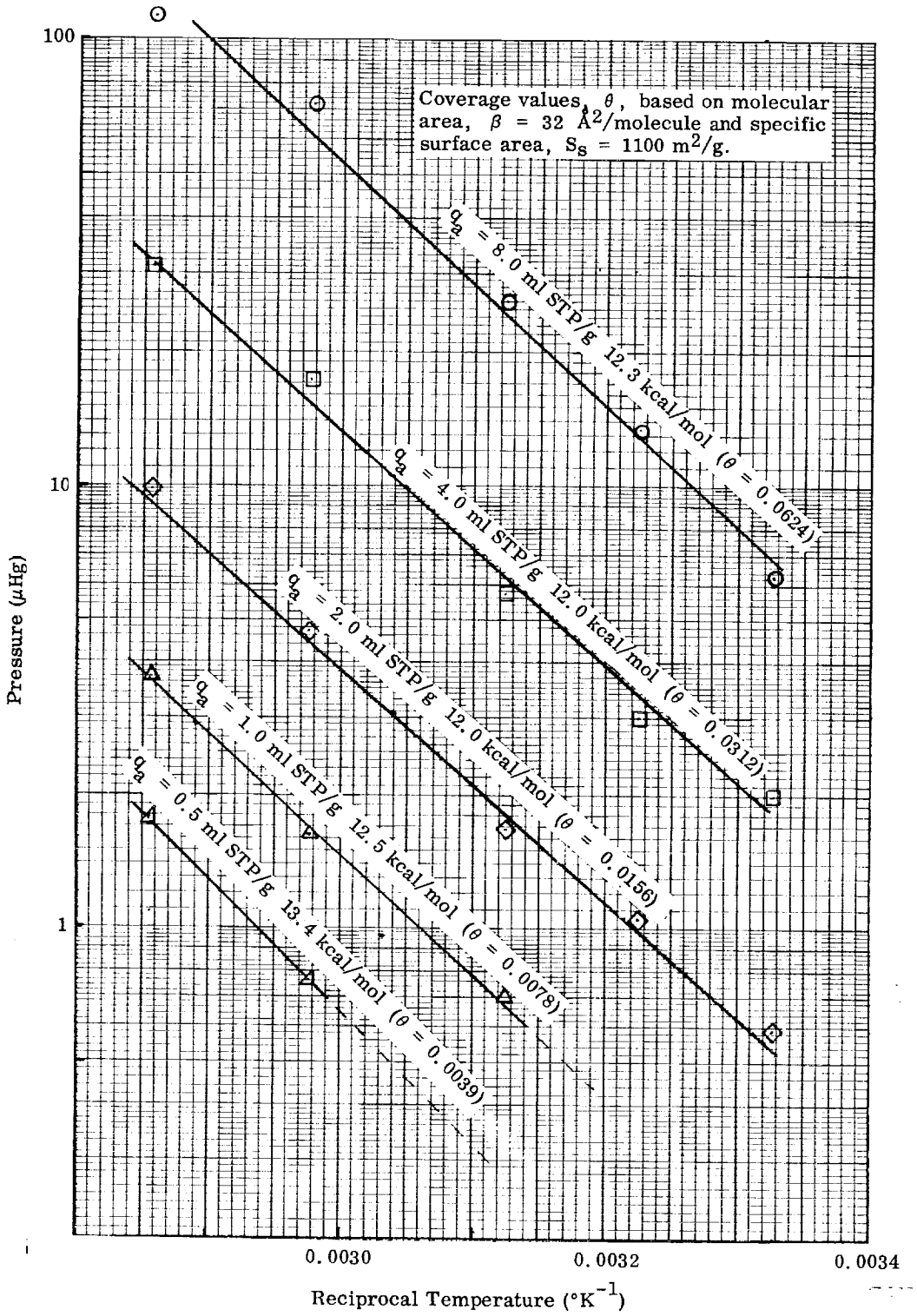

Fig. 4-4 Estimation of Isosteric Heat of Adsorption for n-Butane on BD Charcoal at Various Coverages

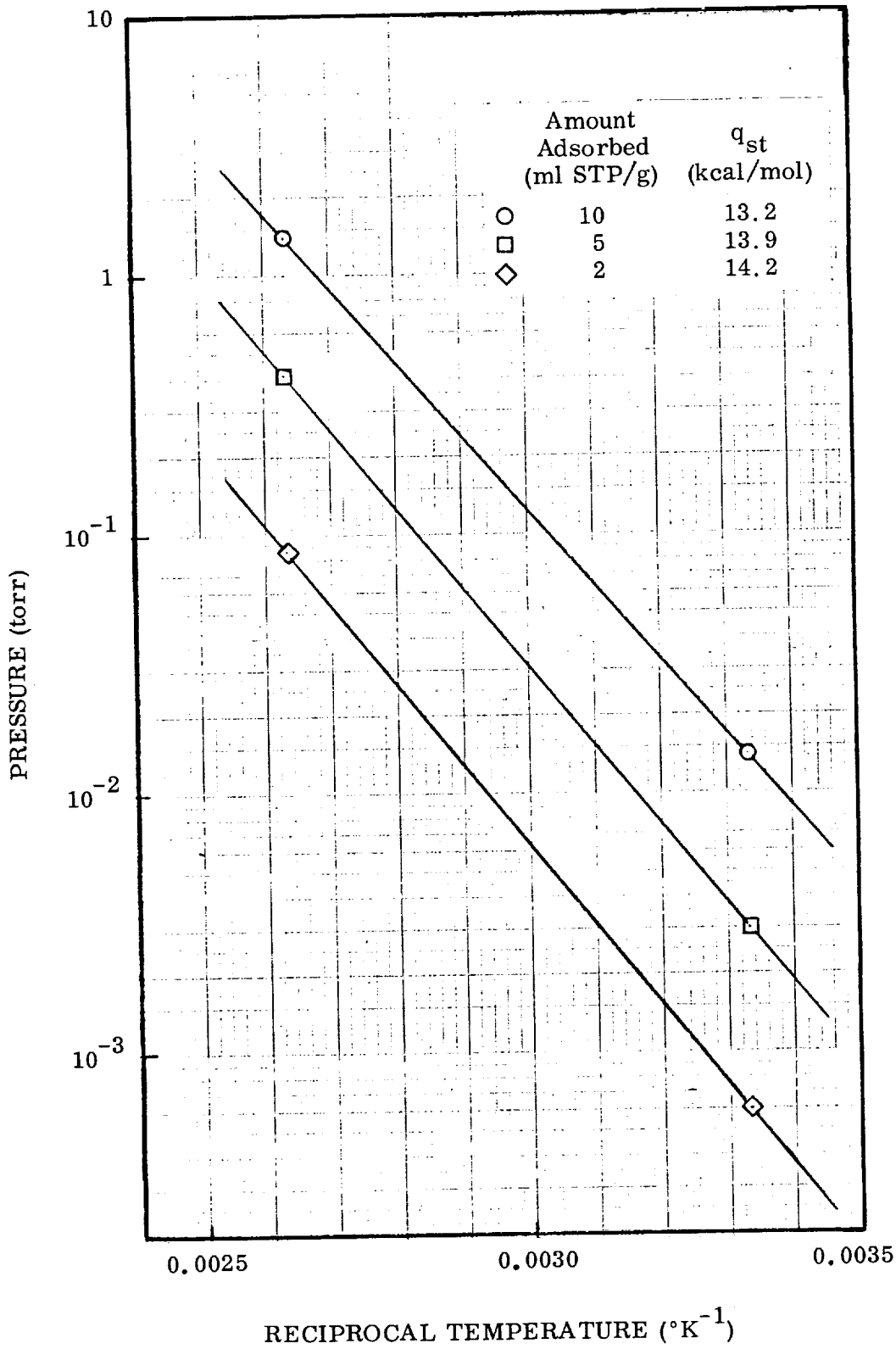

Fig. 4-5 Estimation of Isosteric Heat of Adsorption of n-Butane on 30 × 40 BD Activated Carbon (d_p = 0.05 cm) at Various Amounts Adsorbed

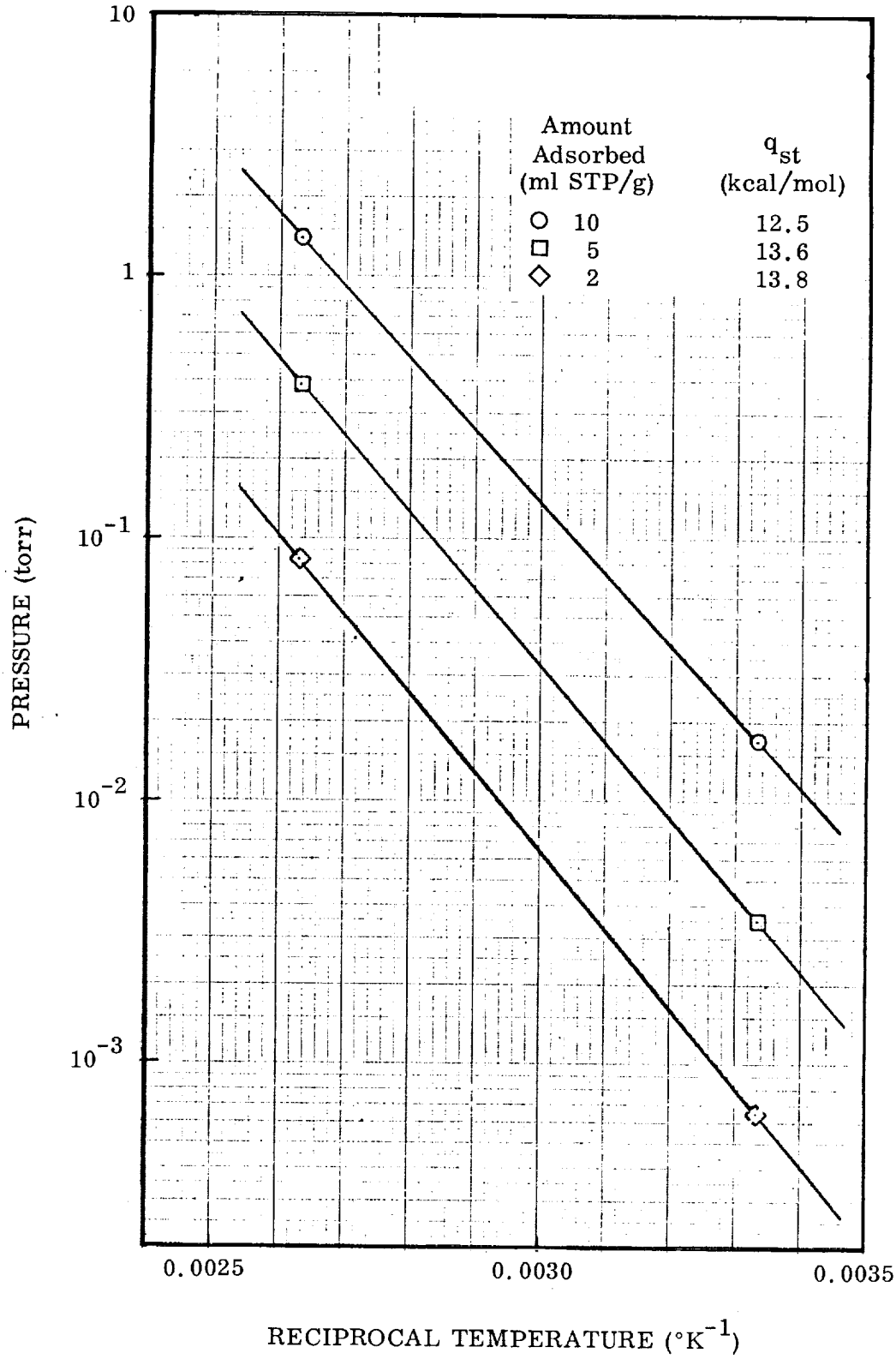

Fig. 4-6 Estimation of Isosteric Heat of Adsorption of n-Butane on 16 × 20 BD Activated Carbon (d_p = 0.10 cm) at Various Amounts Adsorbed

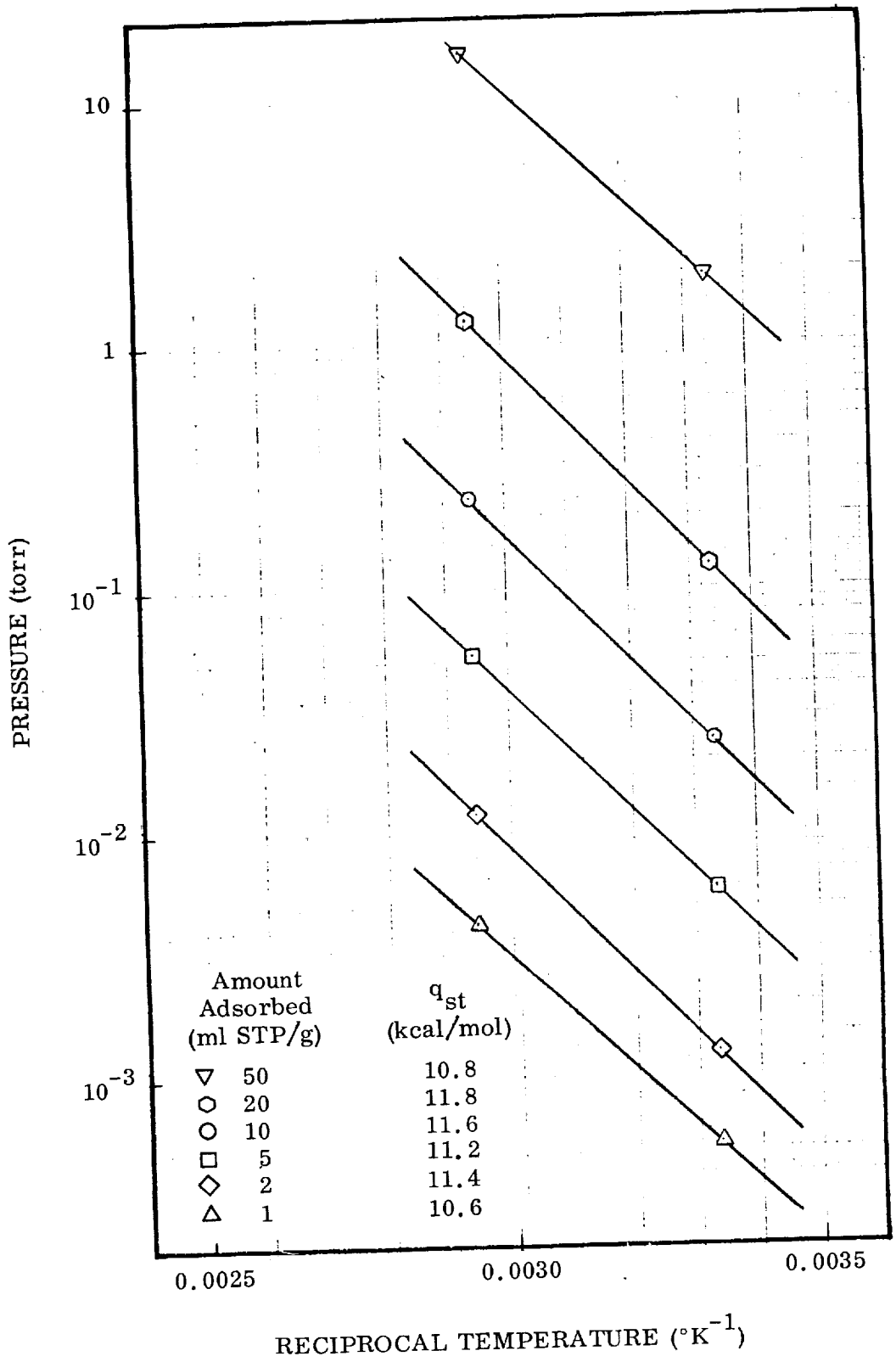

Fig. 4-7 Estimation of Isosteric Heat of Adsorption of n-Butane on 8 × 12 BD Activated Carbon (d_p = 0.20 cm) at Various Amounts Adsorbed

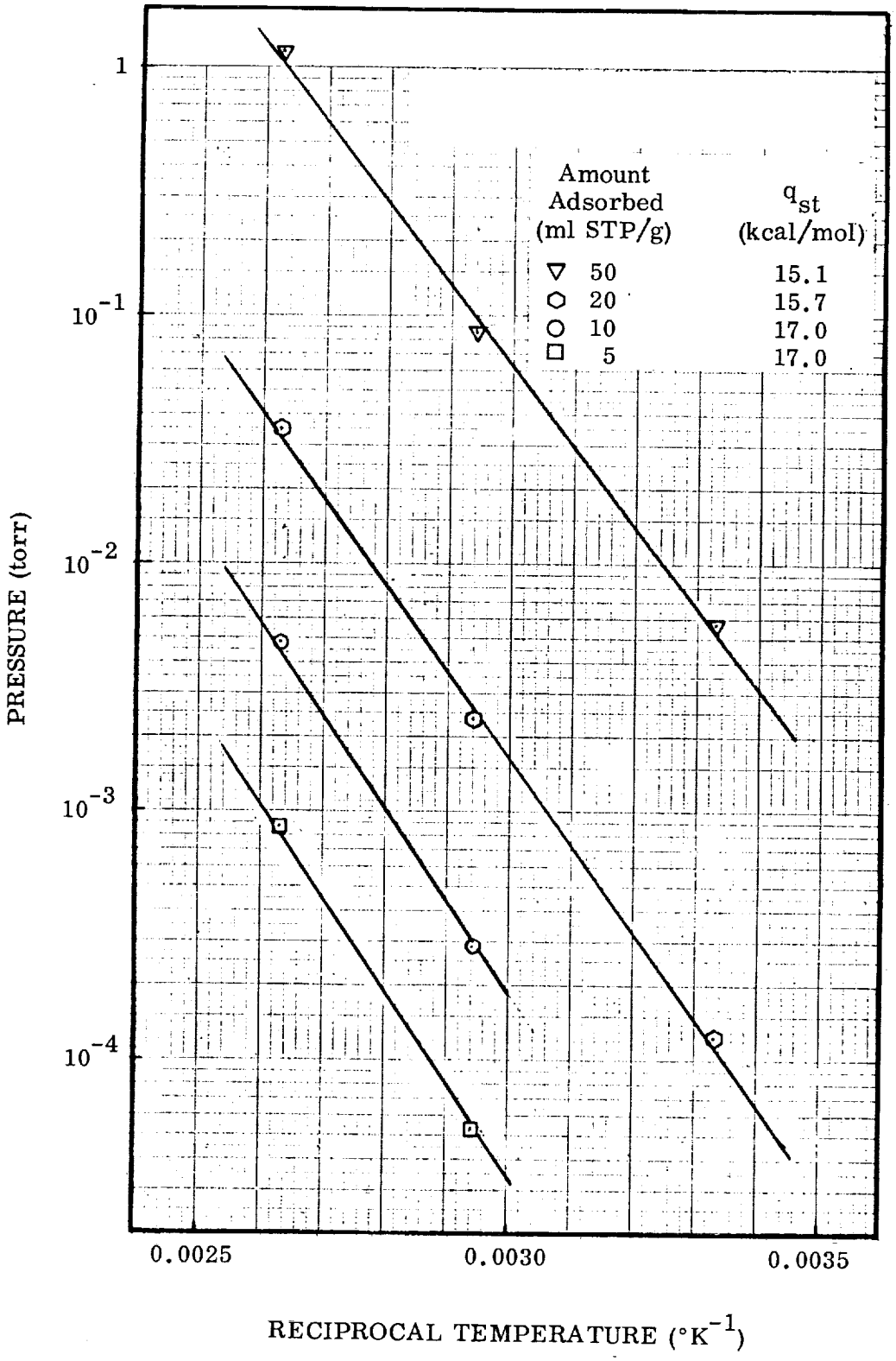

Fig. 4-8 Estimation of Isosteric Heat of Adsorption of Toluene on 16 × 20 BD Activated Carbon (d_p = 0.10 cm) at Various Amounts Adsorbed

Table 4-2

HEAT OF ADSORPTION OF n-BUTANE ON BD ACTIVATED CARBON

Particle Size d_p (cm)	Amount Adsorbed q_a (ml STP/g)	Fractional Coverage θ	Isosteric Heat of Adsorption q_{st} (kcal/mol)
0.05[(a)]	8.0	0.0624	12.3[(a)]
	4.0	.0312	12.0[(a)]
	2.0	.0156	12.0[(a)]
	1.0	.0078	12.5[(a)]
	0.5	.0039	13.4[(a)]
0.05	10.0	0.078	13.2
	5.0	.039	13.9
	2.0	.0156	14.2
0.1	10.0	0.078	12.5
	5.0	.039	13.6
	2.0	.0156	13.8
0.2	50.0	0.39	10.8
	20.0	.156	11.8
	10.0	.078	11.6
	5.0	.039	11.2
	2.0	.0156	11.4
	1.0	.0078	10.6

(a) Early data based on Pirani-gage pressure readings

Table 4-3

THERMODYNAMIC PROPERTIES OF TOLUENE ADSORBED ON 1.0-mm BD ACTIVATED CARBON (16 × 20 MESH) AT 27 °C (300 °K)

Amount Adsorbed q (ml STP/g)	Fractional Coverage θ	Isosteric Heat of Adsorption q_{st} (kcal/mol)
50	0.457	15.1
20	.183	15.7
10	.0914	17
5	.0457	17

where ϕ is the excess free energy per unit volume of adsorbate. This excess free energy is given by:

$$\phi = R\left(\frac{d \log q}{dA}\right)^{-1} \tag{4.34}$$

When the potential plot is linear, ϕ is a constant. Even when ϕ varies with coverage, it is usually nearly independent of coverage so that

$$\left(\frac{\partial \Pi}{\partial T}\right)_{\theta} \approx 0$$

and then

$$q_{st} \approx \Delta H_a = T\Delta S_a \tag{4.35}$$

For the n-butane and toluene adsorption, however, there is some curvature in the potential plot (see Fig. 4-2 and 4-3). The temperature dependence of ϕ is small enough to permit the use of Eq. 4.35.

In Fig. 4-9 the values of ΔH_a for butane are plotted as a function of coverage along with data reported by de Boer and Kruyer (Ref. 15). Although there is a good deal of scatter in the data, it is clear that the isosteric heats decrease more or less linearly with coverage, and that the data obtained for the very low coverage of interest for contaminant control are in essential agreement with previously reported data at much higher coverages. The decrease in the value of q_{st} results from the energetic heterogeneity of the carbon surface.

When a system obeys the Polányi equation (Eq. 4.1), Eq. 4.31 has a very simple form:

$$q_{st} = \Delta H_v - V_m \phi \ln \frac{q}{q_o} \approx \Delta H_a \tag{4.36}$$

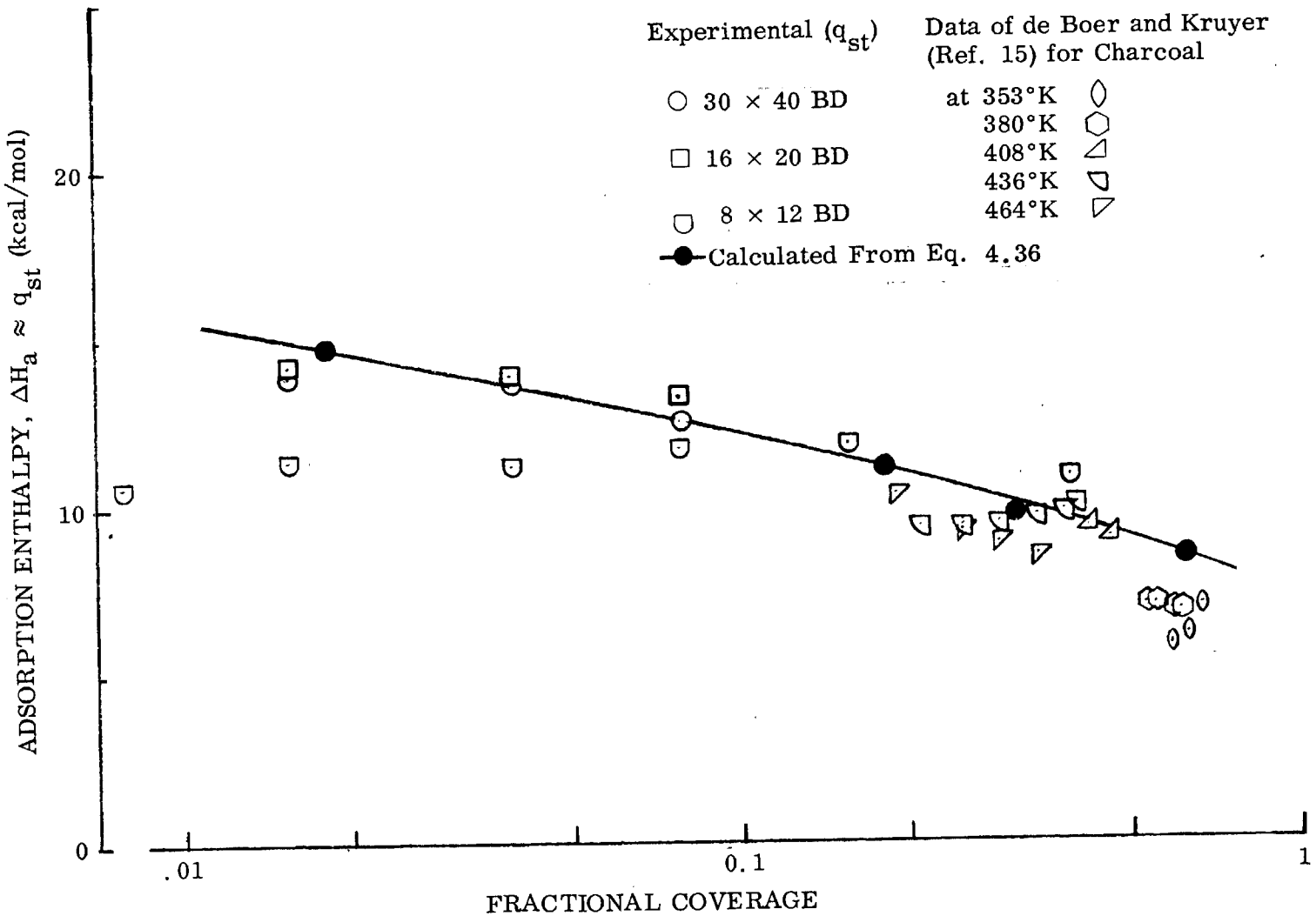

Fig. 4-9 Comparison of Experimental n-Butane Adsorption Enthalpy With Literature Values and With Values Calculated From a Smoothed Potential-Plot Correlation of Data for BD Activated Carbon

The solid line in Fig. 4-9 is the adsorption enthalpy calculated from Eq. 4.36 and the potential plot of the n-butane data. It fits the scattered data rather well and is consistent with the de Boer and Kruyer data. This method for deriving the thermodyanmic properties of adsorbed layers seems to be much preferred over the direct application of Eq. 4.31 on the individual isotherms.

The entropies of adsorption consistent with the solid line in Fig. 4-9 are plotted in Fig. 4-10. It is instructive to compare theoretical entropies for idealized models with these experimentally derived values. From such a comparison it is often possible to infer something about the state of the adsorbed molecules on the surface.

DeBoer and Kruyer (Ref. 16) have outlined the calculation of standard-state adsorptive entropies for both mobile and immobile adsorbed layers. In the case of mobile layers, they select the following for standard states: one atmosphere in the gas phase and an adsorbed layer with an average molecular separation equal to that in the gas-phase standard state. Thus, if only the entropy associated with translation is considered, then

$$S_g = S_g^o - R \ln p \tag{4.37}$$

where

S_g = entropy of the gas at adsorption partial pressure (cal/mol °K)
S_g^o = standard-state entropy of the gas (cal/mol °K)
p = adsorption partial pressure (atm)

and

$$S_a = S_a^o - R \ln \frac{\sigma_o}{\beta\theta} \tag{4.38}$$

where

S_a = entropy of adsorbate at actual coverage (cal/mol °K)
S_a^o = standard-state entropy of adsorbate (cal/mol °K)

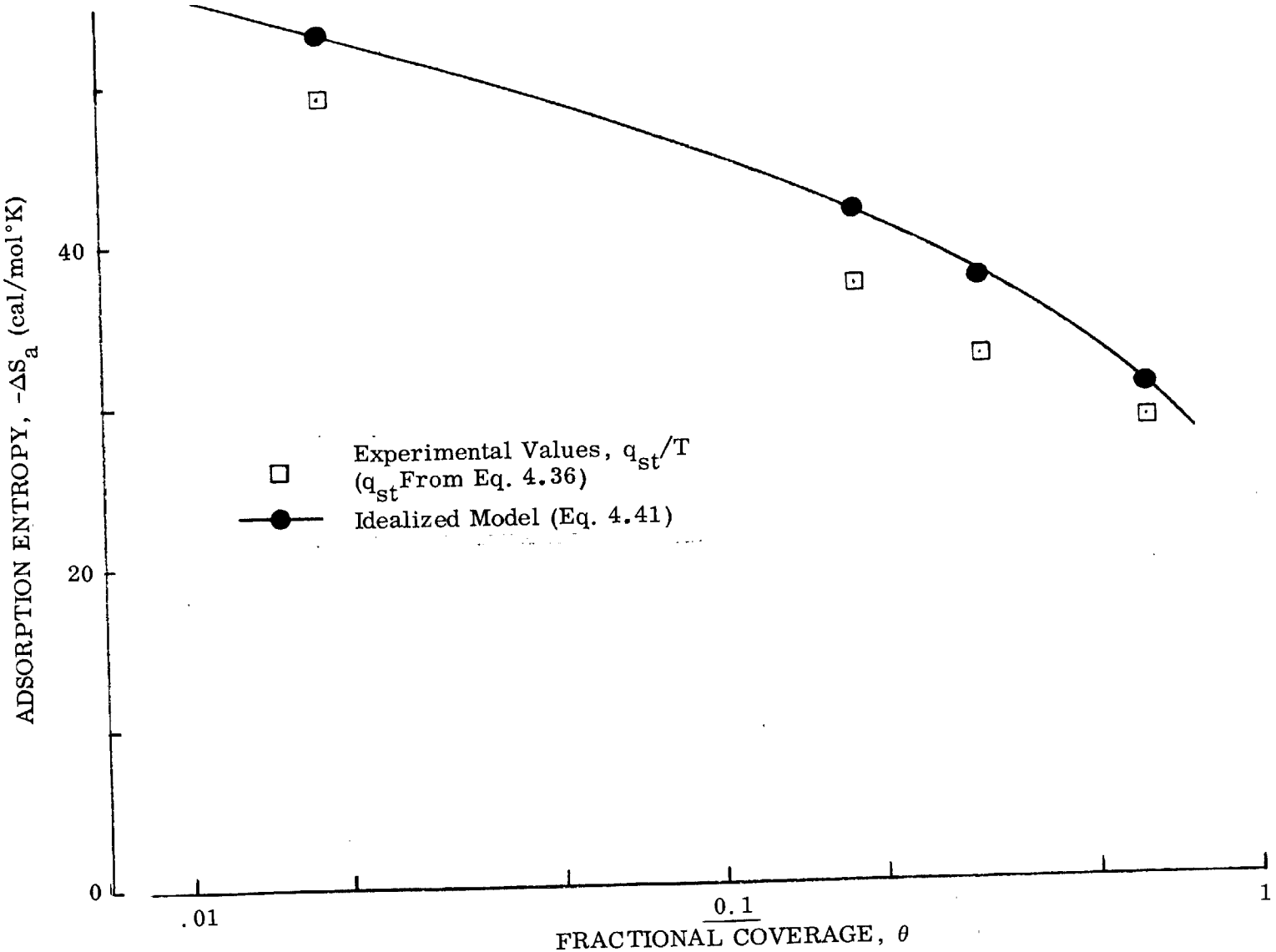

Fig. 4-10 Comparison of n-Butane Adsorption Entropy Derived From a Smoothed Potential-Plot Correlation of Data With an Idealized Model for the Adsorbed Layer at 300°K

σ_o = standard-state molecular area
= $4.08\,T \times 10^{-16}$ (cm^2/molecule)
β = monolayer molecular area (see Table 4-1) (cm^2/molecule)
θ = fractional coverage

Expressions for S_a^o and S_g^o are given in Ref. 16 as:

$$S_g^o = R \ln (M^{3/2} T^{5/2}) - 2.30 \tag{4.39}$$

and

$$S_a^o = \frac{2}{3} S_g^o + \frac{1}{3} R + \frac{1}{3} R \ln \frac{T}{273.15} \tag{4.40}$$

Thus, the adsorption entropy may be calculated by

$$\Delta S_a = S_a - S_g = -\frac{1}{3} R \ln (M^{3/2} T^{5/2}) - 2.28 + 0.662 \ln T - R \ln \frac{\sigma_o}{\beta} + R \ln P + R \ln \theta \tag{4.41}$$

The theoretical entropies for a completely mobile adsorbed layer of n-butane calculated from Eq. 4.41 are plotted as the solid line in Fig. 4-10. These calculations are given in Appendix I. They compare quite well with the measured values, suggesting that the absorbed layer is indeed very mobile. It will be shown later that this result is in agreement with the kinetics of desorption from single particles.

The toluene adsorption data may be treated in an analogous manner. The isosteric heats (integral enthalpies) are plotted in Fig. 4-11. These calculations are also given in Appendix I. Again the heats drop with coverage, and the values derived from the potential plot shown by the solid line in Fig. 4-11 are in agreement with the values obtained directly from the isotherms.

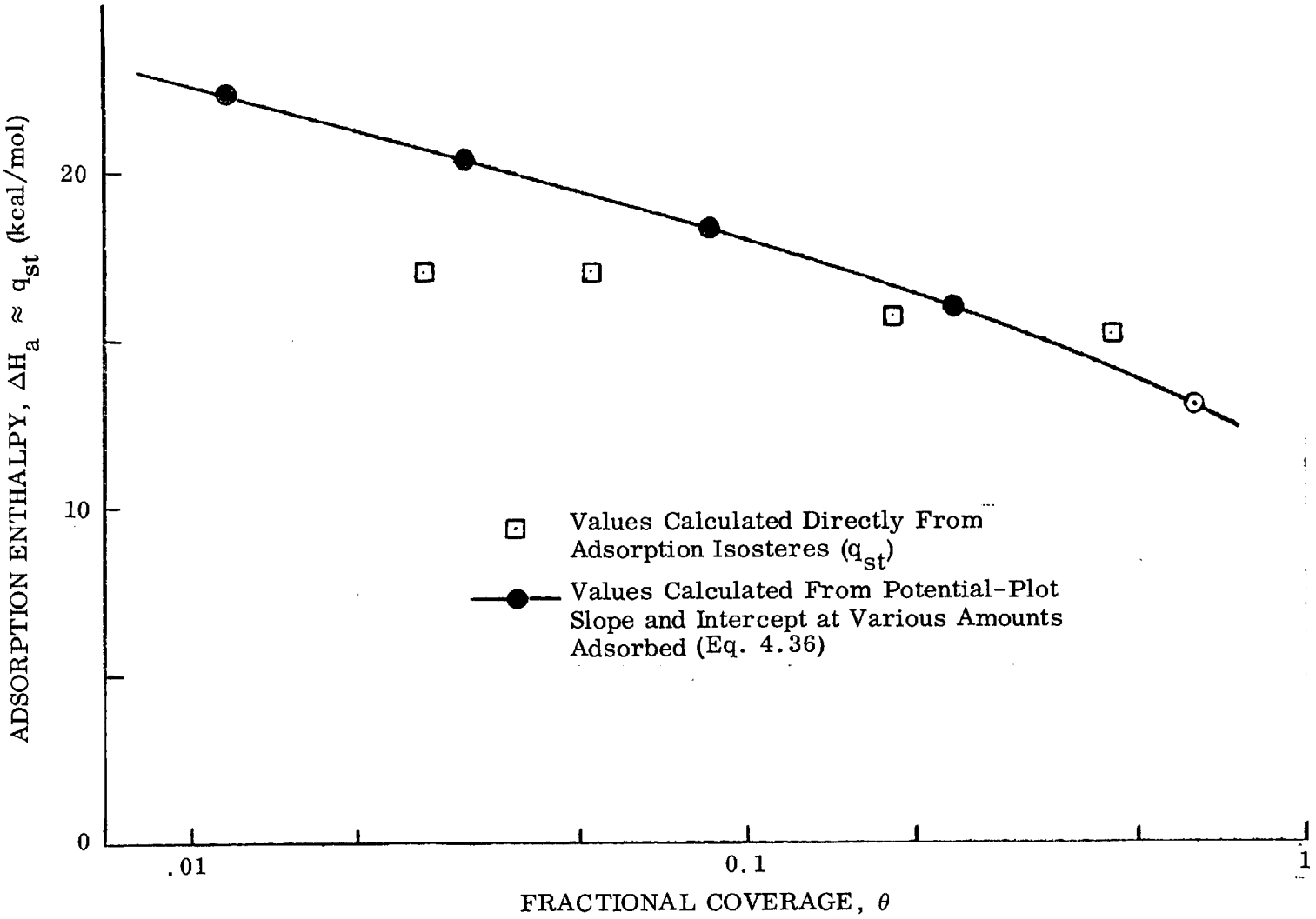

Fig. 4-11 Comparison of Experimental Toluene Adsorption Enthalpy With Values Calculated From a Smooth Potential-Plot Correlation of Data for 8 × 12 BD Activated Carbon (d_p = 0.20 cm)

In Fig. 4-12 the entropies are plotted and compared with Eq. 4.41. Again the agreement is nearly quantitative and it may also be concluded that absorbed toluene, like n-butane, is mobile. It is difficult to say with certainty whether all contaminants will be mobile, but it is certainly not unreasonable to assume that all components lighter than n-butane and toluene are mobile except perhaps for materials which are highly polar, exhibit marked hydrogen bonding, or for other reasons have very strong molecule-molecule interactions.

4.3 FIT OF TOLUENE AND BUTANE ISOTHERMS TO EMPIRICAL EQUATIONS

It is of some interest to fit the adsorption isotherms of toluene and of butane obtained under this contract on BD activated carbon to empirical equations. The toluene isotherms of Fig. 2-10 are fitted by the equation

$$\log_{10} p = - \frac{16\,300 - 57.6\, q_a}{2.303\, RT} + 5.81 + \log_{10} q_a \qquad (4.42)$$

where

p = partial pressure of adsorbate (torr)
R = gas constant = 1.987 (cal/mol°K)
q_a = amount adsorbed (ml STP/g)

The above fit was obtained from the empirical observation that the isotherms when plotted as RT log p/q_a versus q_a gave reasonably straight lines, and the plots for different temperatures were roughly parallel. The quantity

$$16\,300 - 57.6\, q_a \qquad (4.43)$$

is the isosteric heat of adsorption derived from the above plots by the Clausius-Clapeyron equation, and this value agrees well with the values derived in section 4.2.

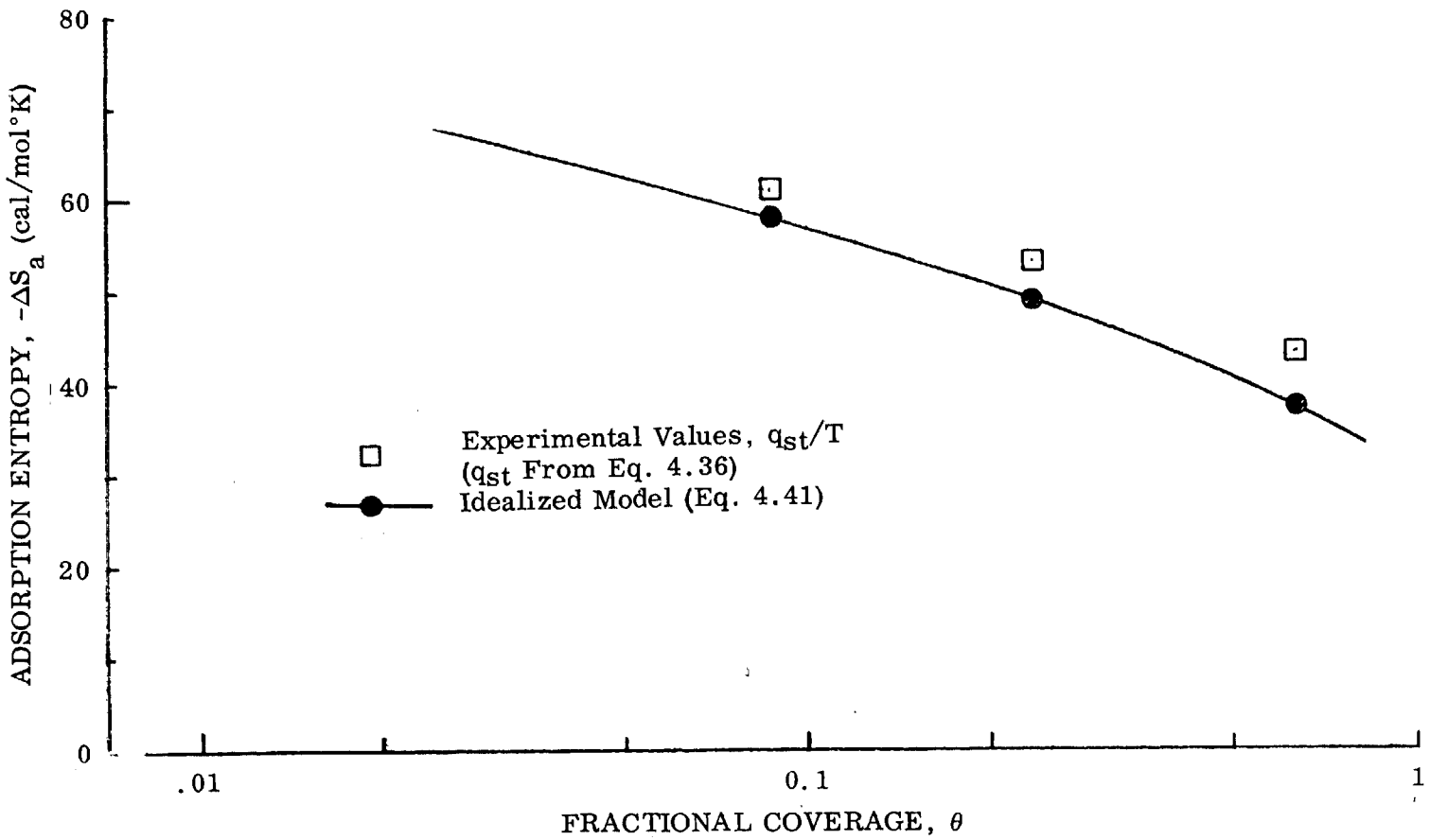

Fig. 4-12 Comparison of Toluene Adsorption Entropy Derived From a Smoothed Potential-Plot Correlation of Data With an Idealized Model for the Adsorbed Layer at 300°K

The older butane isotherms shown in Fig. 2-8 are fitted by:

$$\log_{10} p = -\frac{12\,500 - 100\,q_a}{2.303\,RT} + 8.0 - 2.6\,q_a^{-1/5} \qquad (4.44)$$

Here $12\,500 - 100\,q_a$ is the isosteric heat of adsorption (cal/mol), which is a smoothed fit to the data given in section 4.2. The entropy term $8.0 - 2.6\,q_a^{-1/5}$ was then derived to give a good fit to the isotherm data.

4.4 CORRELATION AND PREDICTION OF MIXED ISOTHERM DATA

An important factor in the proper design of a space-cabin contaminant adsorption bed is the prediction and correlation of adsorber performance in the presence of many contaminants. In Section 3 the experimental adsorption isotherms for several contaminant mixtures have been presented. In this section it is shown how these may be predicted and/or correlated with some accuracy.

Various theories of mixed adsorption have been proposed and the work up to 1962 has been summarized by Young and Crowell (Ref. 14, pp. 371-91). More recent work includes that of Myers and Prausnitz (Ref. 17), Grant and Manes (Ref. 18), and Loven (Ref. 19).

The main objective of a theory of mixed adsorption is to predict the adsorption isotherms of the mixture from the isotherms of the pure components. The equation which appears to be most general and empirically accurate is that proposed by Grant and Manes and by Loven:

$$p_{m1} = X_1\,p_{o1}\,(q_t) \qquad (4.45)$$

where

p_{m1} = equilibrium partial pressure of component 1 in the gas mixture (torr)
X_1 = mole fraction of component 1 in the adsorbed phase

$p_{o1}(q_t)$ = pressure of pure component 1 (at the same temperature as the mixture) which would be in equilibrium with a quantity of adsorbed gas q_T equal to the sum total of all the adsorbed gases in the mixture (torr)

Equation 4.45 sufficies to compute the adsorption isotherm for a mixture of many components. Thus, if the composition of the adsorbed phase is fixed at an amount q_1 of component 1, an amount q_2 of component 2, etc., then these are summed to give q_T, and the mole fraction X_1 of component 1 in the adsorbed phase is computed as the ratio of q_1 to the sum of the q's (q in ml STP/g).

From the isotherm of pure component 1, the pressure $p_{o1}(q_t)$ in equilibrium with an amount q_t of component 1 is read off. Then from Eq. 4.45 the pressure of component 1, p_{m1}, in equilibrium with this presumed adsorbed mixture (q_1, q_2, etc.) is calculated.

In this manner the dashed curves of Fig. 4-13 and 4-14 were computed. The agreement between theory and experiment is almost within the experimental error. To further clarify the method of calculation using Eq. 4.45, we estimate the circled point in Fig. 4-13 at 27° in which, with 5 ml STP/g of toluene preadsorbed, 5.8 ml STP/g of butane is adsorbed at a butane pressure of 1.78×10^{-2} torr. To compute this point, the assumption is that q_1 (amount of butane adsorbed) is 5.8 ml STP/g and q_2 (amount of toluene adsorbed) is 5 ml STP/g, so that $q_t = q_1 + q_2 = 5.8 + 5.0 =$ 10.8 ml STP/g and X_1 = mole fraction of butane in the adsorbed phase = 5.8/10.8 = 0.537. The pressure of pure butane in equilibrium with q_t = 10.8 ml STP/g is now read from the pure butane isotherm as 2.8×10^{-2} torr. Thus, the desired butane pressure in equilibrium with q_1 = 5.8, q_2 = 5.0 ml STP/g can be immediately computed from Eq. 4.45.

$$p_{m1} = 0.537 \times 2.8 \times 10^{-2} = 1.5 \times 10^{-2} \text{ torr}$$

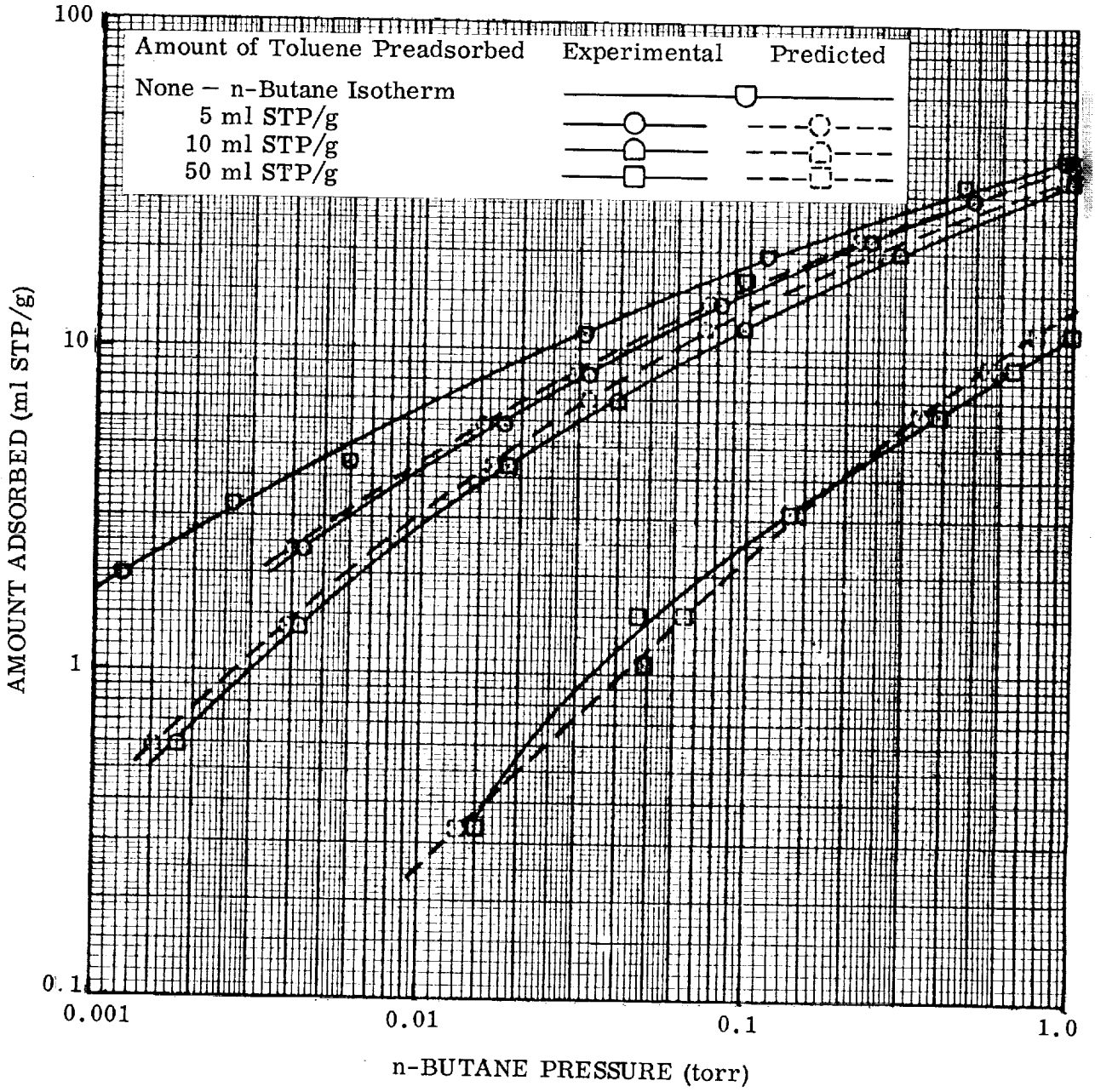

Fig. 4-13 Blockage of n-Butane by Toluene on 8 × 12 BD Charcoal at 27°C: Comparison With Blockage Predicted From n-Butane Isotherm

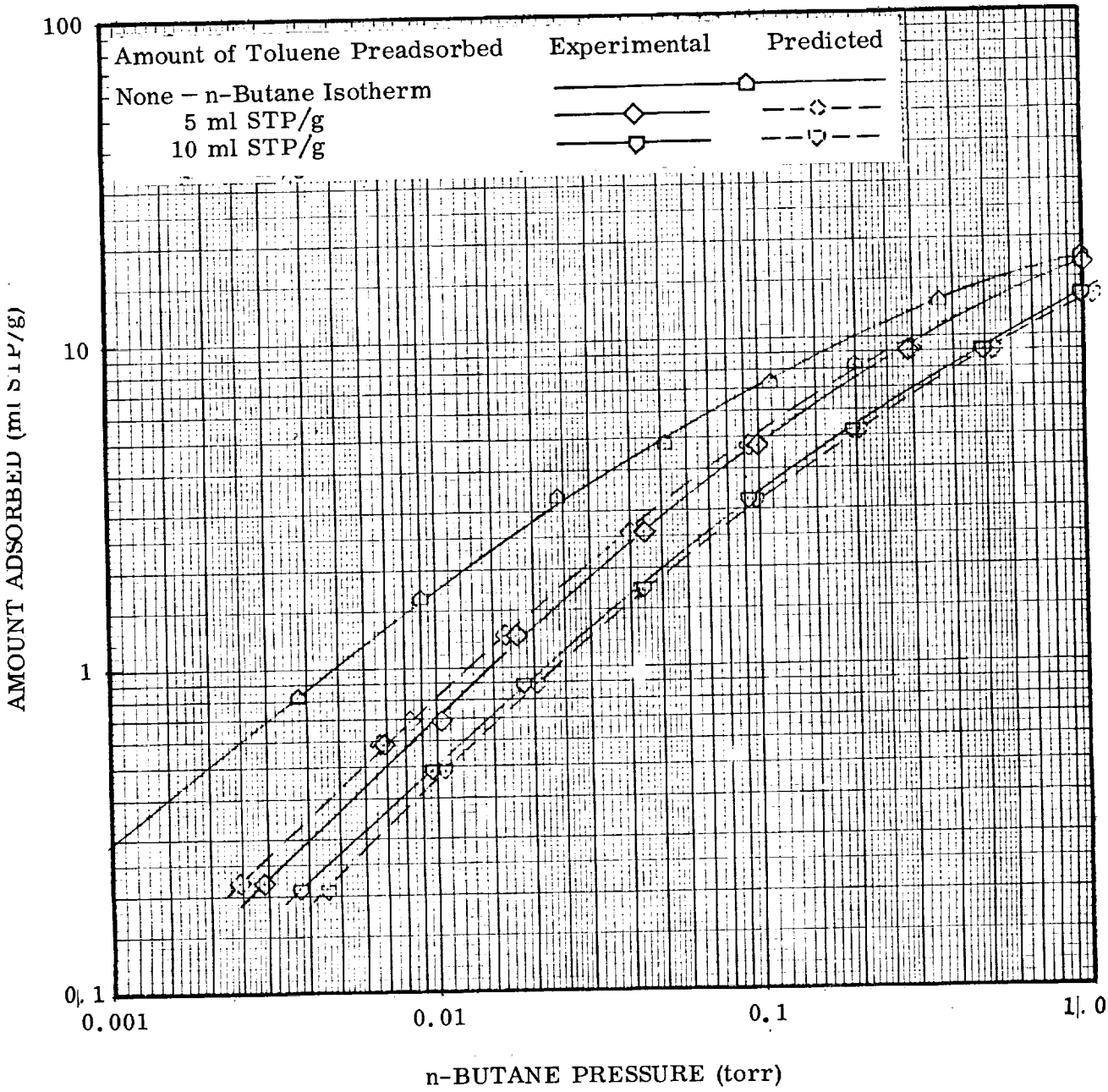

Fig. 4-14 Blockage of n-Butane by Toluene on 8 × 12 BD Charcoal at 67°C: Comparison with Blockage Predicted From n-Butane Isotherm

which thus locates the desired point and is within probable experimental error equal to the measured value, 1.78×10^{-2} torr.

The origin and meaning of Eq. 4.45 are of some interest. Grant and Manes, and Loven appear to have intuitively assumed it as a logical extension of the Polanyi potential theory. In Appendix J, it is shown that

- Equation 4.45 may be derived by a simple kinetic argument.
- The Langmuir theory of mixed adsorption, and an equation due to Glueckauf (Ref. 20) for mixed Freundlich-type adsorption on a more uniform surface are special cases of Eq. 4.45.

The basic assumption of Eq. 4.43 is that the heat of adsorption depends only on the total adsorbed coverage, q_T, and not on the exact composition of this adsorbed layer. This may be shown by differentiating both sides of Eq. 4.43 (after taking logarithms) with respect to temperature to obtain the usual Clausius-Clapeyron-type of equation for q_{st}, the isosteric heat of adsorption. A second assumption implicit in Eq. 4.43 appears to be that the mixed adsorbed layer forms a perfect solution so that the partial molar entropy of mixing for component 1 is

$$\Delta\bar{S}_m = R \ln X_1 \tag{4.46}$$

where

$\Delta\bar{S}_m$ = partial molar entropy (cal/mol °K)
R = gas constant = 1.987 (cal/mol °K)

Whatever its origin, not only this research but also the work of Loven (Ref. 19) and that of Grant and Manes (Ref. 18) show that it predicts and correlates a large number of mixed adsorption data.

As shown above, Eq. 4.45 allows rapid computation of the mixed adsorption isotherms when the composition of the adsorbed phase is assumed known, and the unknowns are

the partial pressures of gases in equilibrium with this adsorbed composition. The converse case, when the partial pressures are known (and the desired quantities are the unknown amounts adsorbed), becomes more unwieldy mathematically. Here there will be an equation of the same type as Eq. 4.45 for each component, and this equation must be solved simultaneously for the unknown q's, after fitting the isotherms for the pure components to a mathematical expression.

Finally, it is easy to show that Eq. 4.45 also predicts the correct blockage of propylene by butane, as shown in Table 3-1. For runs F9-1, F9-2, and F11-4 the adsorbed mole fraction of propylene may be predicted from Eq. 4.45, inverted to read

$$X_1 = \frac{p_{m1}}{p_{o1}(q_t)} \tag{4.47}$$

and these computed values are compared with the experimental ones in Table 4-4.

Table 4-4

PREDICTED BLOCKAGE OF PROPYLENE BY n-BUTANE AT 27° C

Run No.	X_1 (Calculated)	X_1 (Experimental)
F9-1	$\frac{0.54}{1000} = 5.4 \times 10^{-4}$	5.7×10^{-4}
F9-2	$\frac{13}{150} = 8.7 \times 10^{-2}$	1.14×10^{-1}
F11-4	$\frac{1580}{1800} = 8.8 \times 10^{-1}$	8.7×10^{-1}

The agreement is within the experimental error. In computing the predicted values of X_1, an approximate propylene isotherm was derived from the points of Runs F9-3, F11-5, F6-1 (see Table 3-1). This isotherm can be represented by

$$q_a = 2.13 \times 10^{-4} c^{0.72} \tag{4.48}$$

where

q_a = amount adsorbed at 27° C (ml liq/g)
c = propylene gas phase concentration at a total pressure of 0.5 atm (ppm)

The mixed adsorption equation (Eq. 4.43) can be incorporated in adsorption potential theory parameters as follows:

In a mixture, the adsorption potential A_T which correlates with the total amount adsorbed q_T is

$$A_T = \frac{T}{V_m} \log \frac{P^\circ}{p_{o1}(q_t)} \tag{4.49}$$

Substituting Eq. 4.47,

$$A_T = \frac{T}{V_m} \log \frac{P^\circ X_1}{p_{m1}} \tag{4.50}$$

or

$$A_T = A + \frac{T}{V_m} \log X_1 \tag{4.51}$$

where

$$A = \frac{T}{V_m} \log \frac{P^\circ}{p_{m1}} \tag{4.52}$$

Thus, Eq. 4.48 or 4.51 can be used to correlate mixed adsorption capacity data on a potential plot.

This procedure is used to correlate the humid air data (see Section 9) and is also applied to several flow runs involving three different contaminant pairs, propane-n-butane, ethylene-propane, and n-butane-toluene. These data are summarized in Table 3-1 and plotted as suggested by Eq. 4.51 in Fig. 4-15. All the data correlate well with the slope of the generalized potential plot (dotted line in Fig. 4-15) but all are somewhat higher than the generalized correlation. The deviations, however, are not appreciably greater than the scatter in the data used to establish the generalized correlation (see Fig. 4-3), nor are they greater than the consistent deviation exhibited by the extensive toluene adsorption data shown in Fig. 2-10. Within the accuracy and precision of the generalized plot, this simple theory of mixed adsorption seems to be quite adequate and it is thus recommended for design purposes.

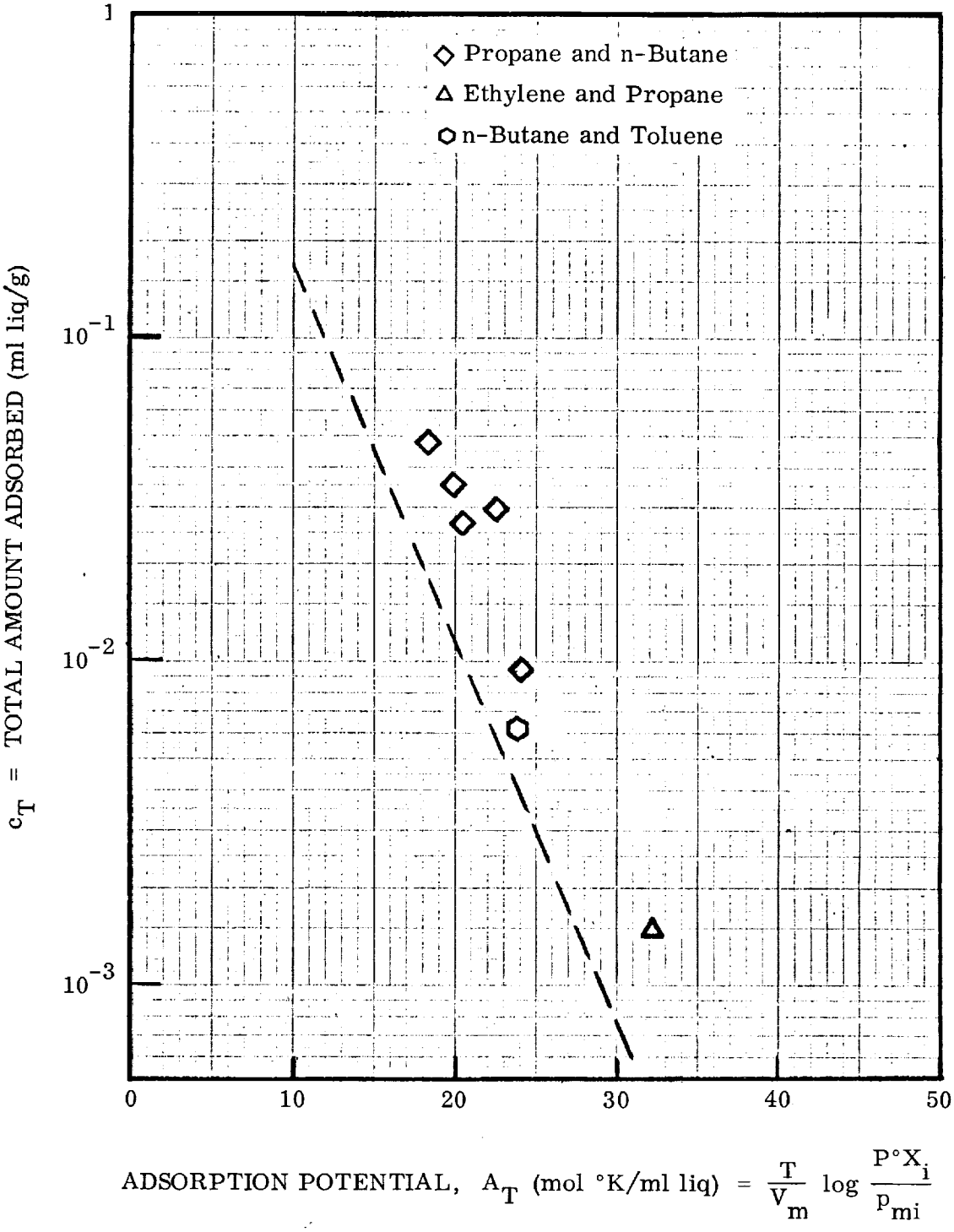

Fig. 4-15 Potential Plot for Mixed Adsorption

Section 5

VACUUM DESORPTION FROM SINGLE PARTICLES – EXPERIMENTAL AND RESULTS

Regeneration of sorbents after saturation with contaminants has been one of the major goals of this effort. In order to be able to make any sort of meaningful attempts at design of a spacecraft sorbent regeneration system involving the use of space vacuum, it is necessary to have extensive information on the effects of vacuum on the individual sorbent particles. Once the effects of temperature, particle size, and contaminant species have been established, it should be possible to relate these to the performance of packed beds under vacuum desorption conditions.

With this end in mind, a series of experiments was performed on the gravimetric system described in Section 2. In this series the above parameters were varied. In addition, experiments were performed, perhaps for the first time, in which more than one contaminant was monitored instantaneously during simultaneous vacuum desorption. This was made possible by using the gravimetric system with mass spectrometer described in Sections 2 and 3. A few experiments were also performed on a volumetric apparatus in order to supplement the gravimetric experiments.

5.1 EXPERIMENTAL TECHNIQUES

5.1.1 Single-Component Experiments

The apparatus used in vacuum desorption experiments consisted of the same vacuum microbalance system as described in section 2.1.2. Extremely high pumping speed was provided by the 400-liter/sec oil diffusion pump and baffled liquid-nitrogen trap located next to the 10-cm gate valve on the microbalance jar.

The procedure for adsorption of contaminants was the same as that described in section 2.1.2, except that the amounts adsorbed were controlled to certain nominal values by allowing weight to increase by a predetermined amount in each experiment. For the desorption portion of the experiments, the strip-chart recorder speed was set sufficiently high (2 or 4 in./min) so that desorption time data could be taken to the nearest 0.5 sec. At time zero, the gate valve was quickly opened, and the ionization gage was turned on after about 5 sec.

5.1.2 Multicomponent Experiments

The apparatus used in multicomponent desorption experiments consisted of the system as described in sections 2.1.2, 3.1.2, and 5.1.1. The adsorption procedure was the same as for the first point on a multicomponent adsorption isotherm, with the equilibrium amount of the second, less strongly adsorbed contaminant somewhat greater than that of the first one. Desorption was initiated in the manner described in section 5.1.1 but with the mass spectrum/pressure strip-chart recorder running at higher speed. The ratio of desorption rates at any given instant was assumed to be equal to the ratio of partial pressures in the mass spectrometer as determined by the mass spectral peak heights corresponding to each species. Since the total amount of each species adsorbed was known, and assuming that only the more strongly adsorbed contaminant remained adsorbed in significant quantity after the desorption was 90 percent complete, it was possible to get instantaneous desorption rates for each species, as explained in section 5.2.2.

5.1.3 Volumetric Method

To supplement the gravimetric method for measuring vacuum desorption rates from single activated carbon granules, a volumetric desorption system was designed. In this method, the desorbed contaminant was caught in a cold trap (which also acted as

the pump) and was measured volumetrically after warming up the cold trap. The method has several advantages over the microbalance technique:

(1) Freedom from thermogravimetric and other spurious effects, such as were encountered when gas was suddenly admitted to or evacuated from the microbalance
(2) Great simplicity, since a large stopcock (or better, a solenoid valve), a suitable vacuum gage, and a vacuum pump are the only equipment needed
(3) The capability of inserting a thermocouple directly into an activated carbon granule, so that adiabatic cooling effects can be directly measured simultaneously with desorption rate
(4) The capability of varying pumping speed by simply lowering the liquid nitrogen level on the cold trap, which acts as the pump

The sensitivities of the two methods are about equal, since a microgram of n-butane in 300 cm^3 volume results in a pressure of about 10^{-3} torr, which is easily detectable. A disadvantage of this method is that only one point on the desorption curve is measured in a given run, since the desorption process is interrupted to measure the amount of butane desorbed. However, each point takes only about 15 min, so that in a few hours the whole curve (amount desorbed versus time) can be established.

The all-glass apparatus that was finally used after a little experimentation is shown in Fig. 5-1. The activated carbon granules were supported on a fine mesh nickel screen in the vertical tube, T_1. The charcoal could be isolated from the rest of the system by the very large hollow-plug, single-hole, high-vacuum-type stopcock, S. The choice of S is critical, as an ordinary stopcock or valve will reduce the pumping speed too severely. Likewise, the diameter of the tube, T_1, must be kept large (about 2 cm) to provide adequate pumping speed to the charcoal. In this apparatus the pumping speed was limited by the 7.0-cm length of 20-mm OD tubing which connected the charcoal to the larger stopcock. The pumping speed of this tube was 10 liters/sec (as read from Fig. 2-1, p. 92, of Ref. 21). When the large stopcock was open, the carbon was connected to a U-tube cold trap, T_2, 20 mm OD and 15 cm long, which

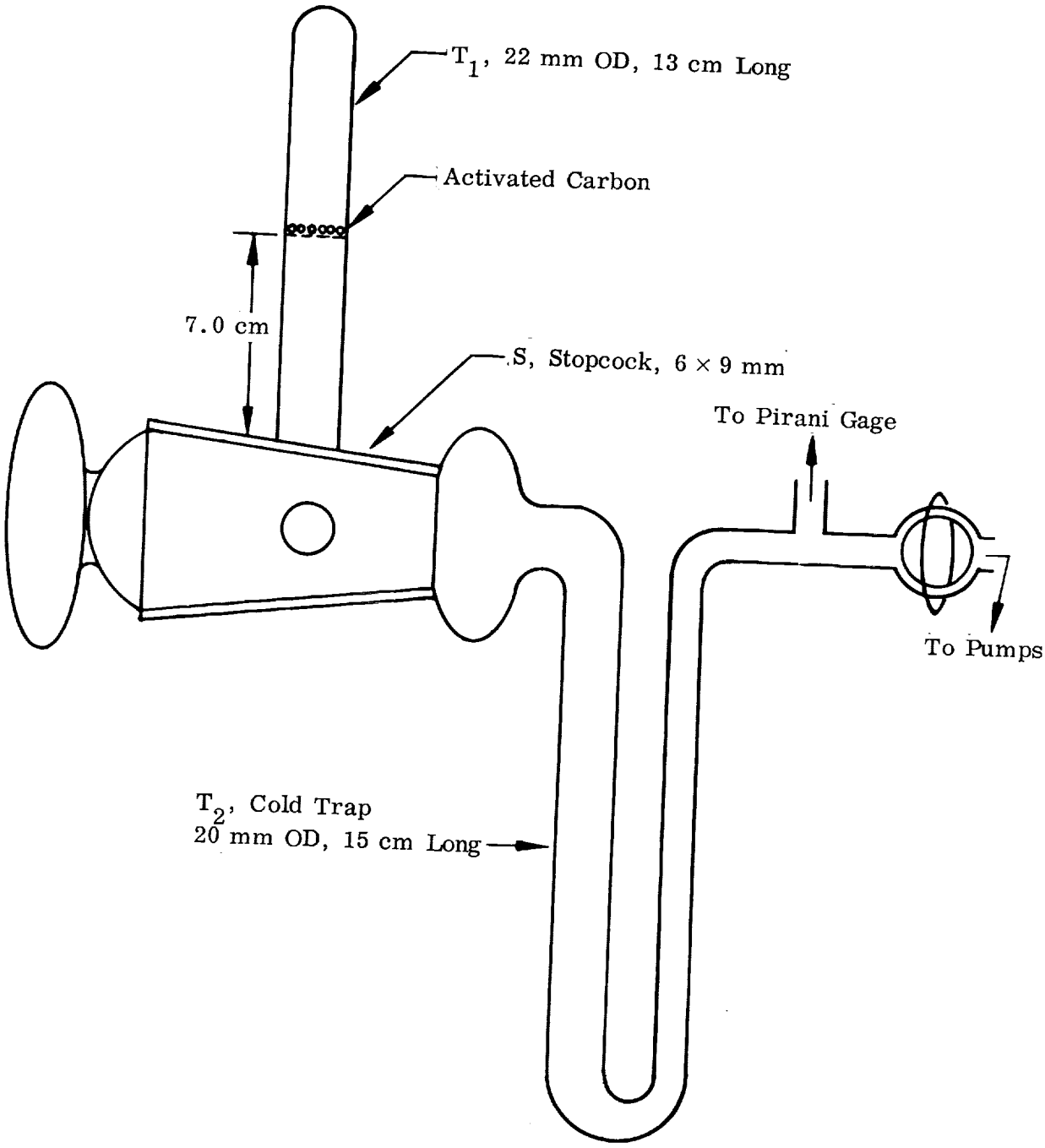

Fig. 5-1 Volumetric Apparatus for Determining Rate of Vacuum Desorption

could be immersed in liquid nitrogen. A Consolidated Vacuum Corporation Pirani gage was connected on a side seal, and a second stopcock isolated the system from the vacuum pumps and from a McLeod gage used to calibrate the Pirani gage. Obvious improvements would be to eliminate stopcock grease by using a metal solenoid valve or bakeable gate valve in place of S , and to use a disphragm-type pressure transducer in place of the Pirani gage.

Carbon granules were introduced into T_1 by blowing a hole in the top of the tube, which was later sealed. The optimum weight of carbon used was a small problem. Too large a weight would cause results to be affected by pumping speed, and too small a weight would cause sampling errors and errors due to contaminants desorbed from the apparatus walls. In these experiments 20-mg samples were used, although 10-mg samples were also tried in initial experiments.

A typical experiment was carried out as follows: The charcoal was first degassed in high vacuum for 4 hr at 300 – 400°C by slipping an electric furnace over the tube, T_1 . During bakeout the large stopcock, S , was turned at frequent intervals to degas the stopcock grease. (Bakeout temperature was varied from 250°C to 400°C with no significant change in desorption rate of butane at room temperature.) The carbon was next cooled to room temperature and the stopcock, S , was closed. A desired pressure of butane was then admitted to the volume containing the Pirani gage and large stopcock. This volume was 366 cm^3 for the case described here. Thus, from the perfect gas law, 0.364 torr in 366 cm^3 gave an initial loading of 8 ml STP/g on a 20 mg sample, corresponding to the initial loading in the microbalance experiments. This pressure of butane was admitted to the carbon at 26°C, and the rate of adsorption was determined by measuring the amount adsorbed as a function of time. This rate was initially too fast to determine, due to time lags in the Pirani-gage system. Within about 10 sec the pressure dropped by a factor of 3 to 10, and adsorption equilibrium was established in 10 – 20 min. (A point on the adsorption isotherm was thus measured in each experiment.) The stopcock, S , was then closed and the cold trap, T_1 , was completely immersed in liquid nitrogen. The desorption rate was then measured by opening the

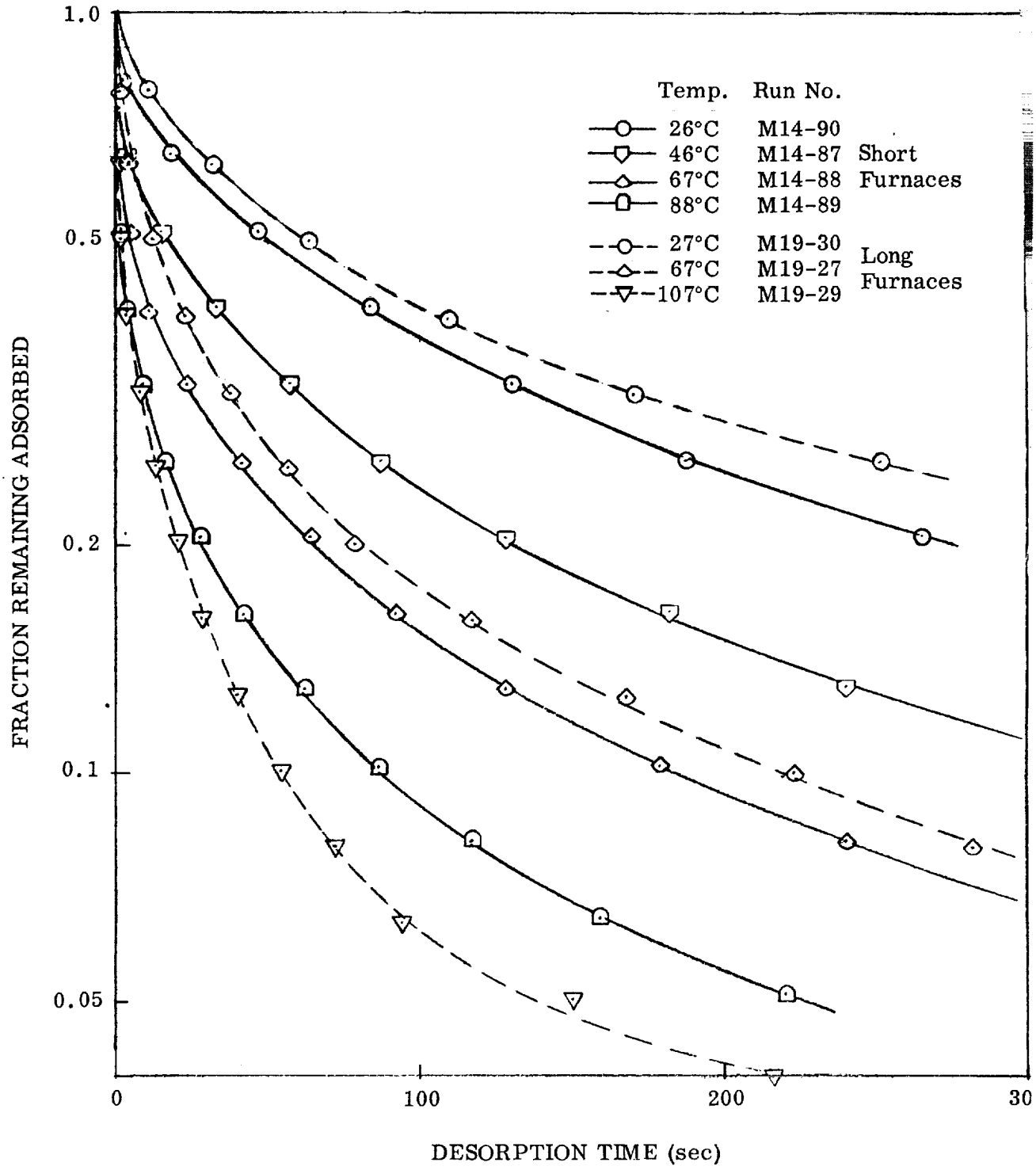

Fig. 5-2 Gravimetric Desorption of n-Butane From 30 × 40 BD Activated Carbon (d_p = 0.05 cm)

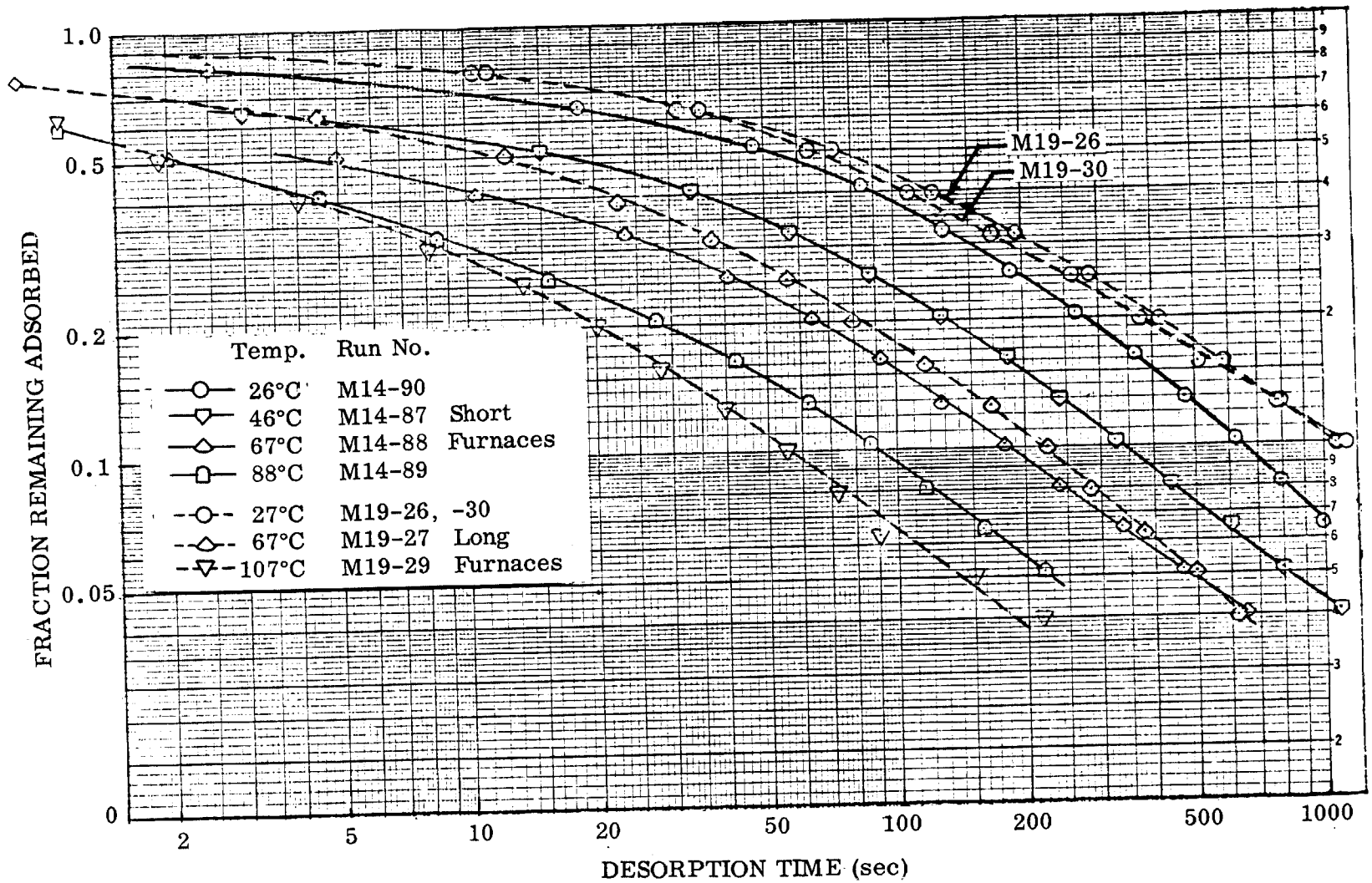

Fig. 5-3 Gravimetric Desorption of n-Butane From 30 × 40 BD Activated Carbon (d_p = 0.05 cm)

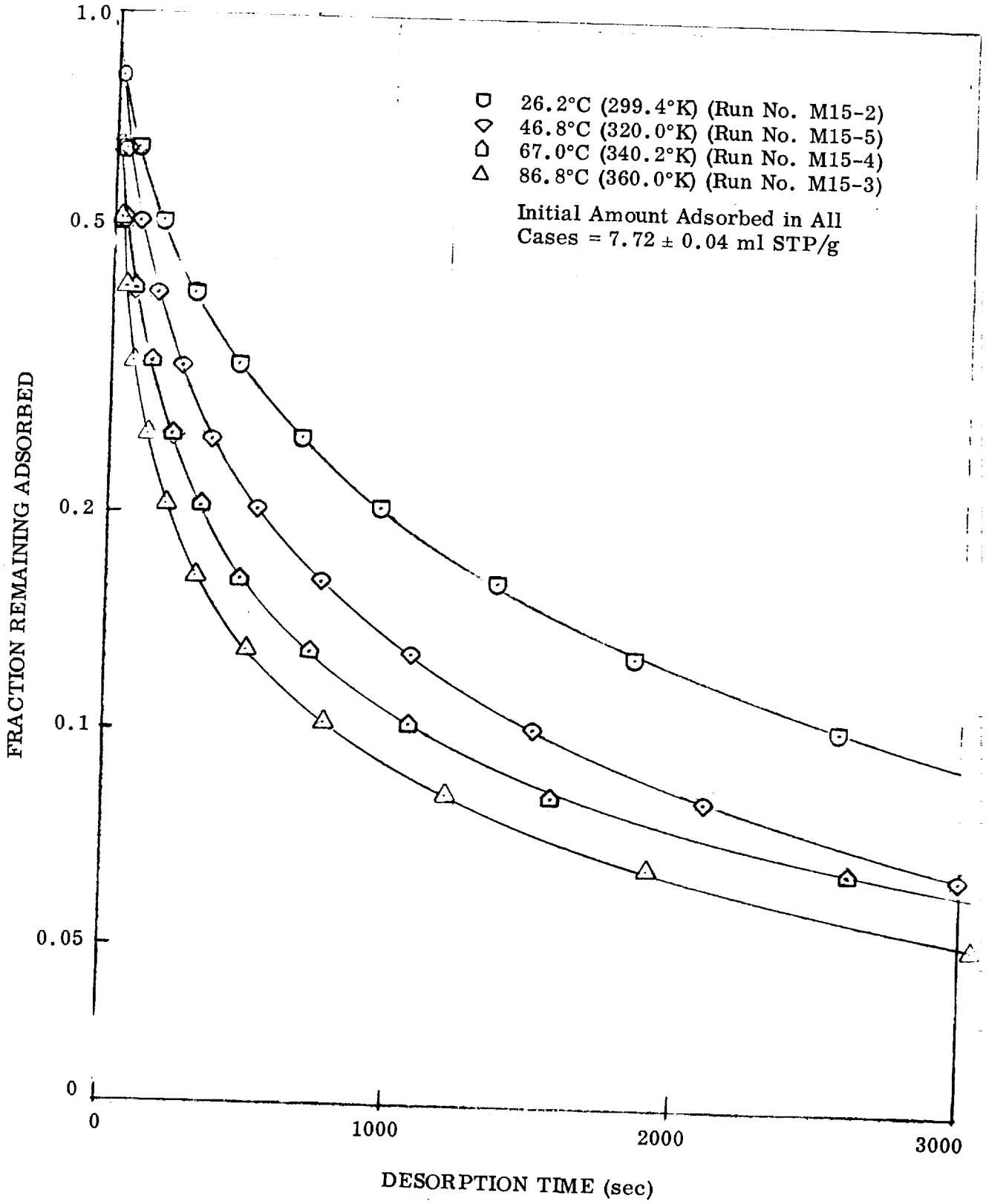

Fig. 5-4 Gravimetric Desorption of n-Butane From 0.2 cm BD Activated Carbon Particles at Various Temperatures

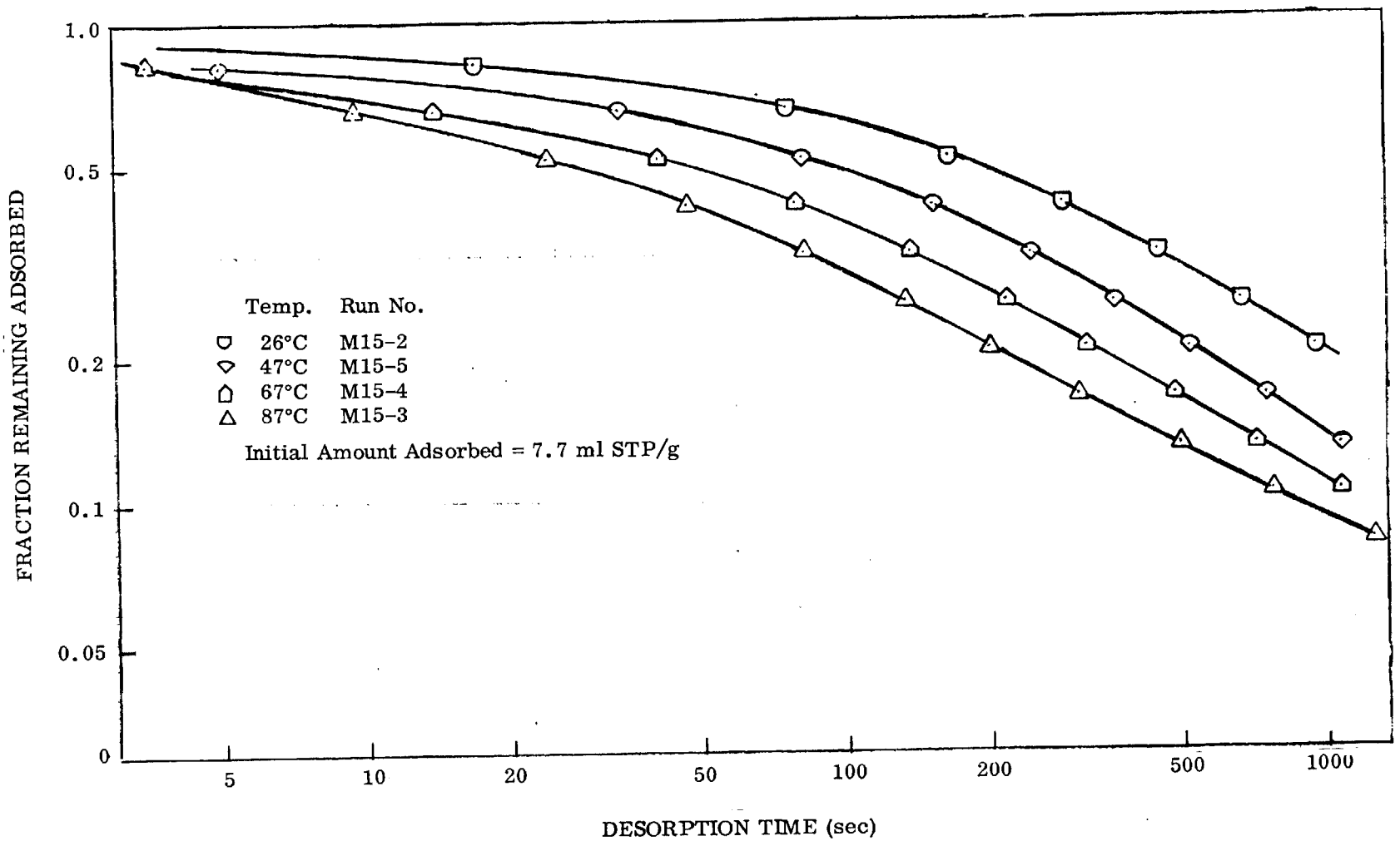

Fig. 5-5 Gravimetric Desorption of n-Butane From 8 × 12 BD Activated Carbon (d_p = 0.20 cm)

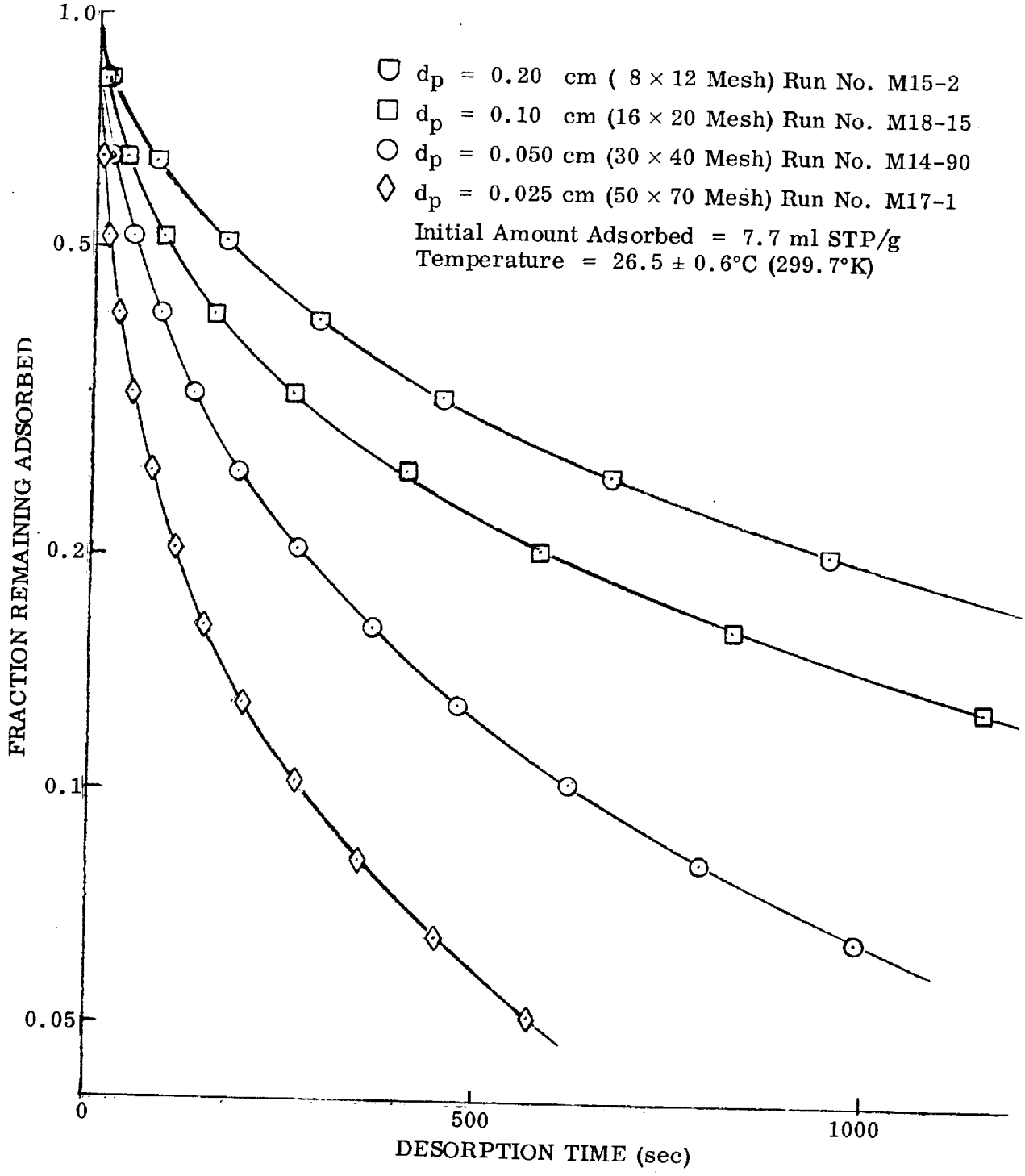

Fig. 5-6 Gravimetric Desorption of n-Butane From BD Activated Carbon: Variation With Particle Size

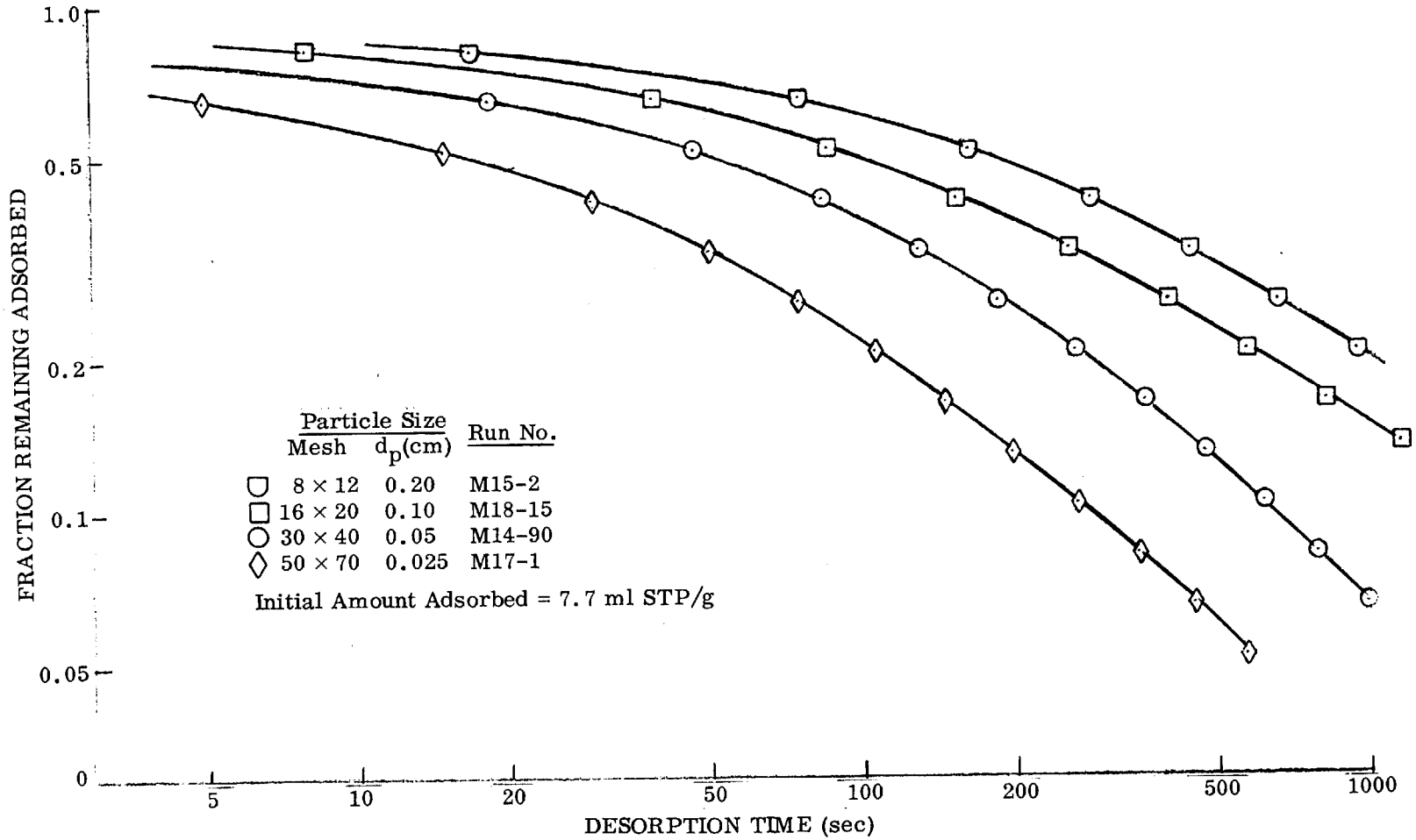

Fig. 5-7 Gravimetric Desorption of n-Butane From BD Activated Carbon at 27°C (300°K)

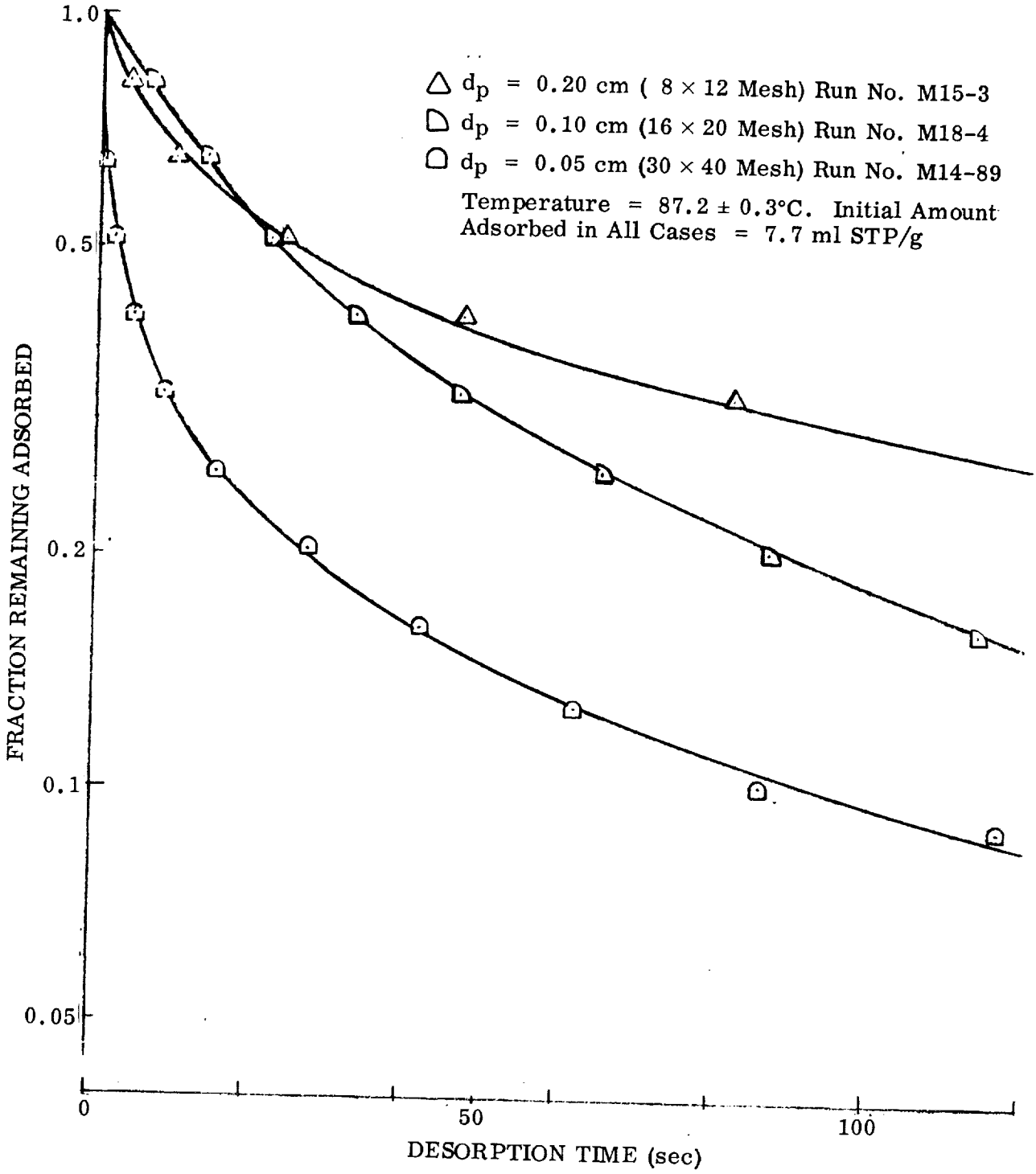

Fig. 5-8 Gravimetric Desorption of n-Butane From BD Activated Carbon: Variation With Particle Size

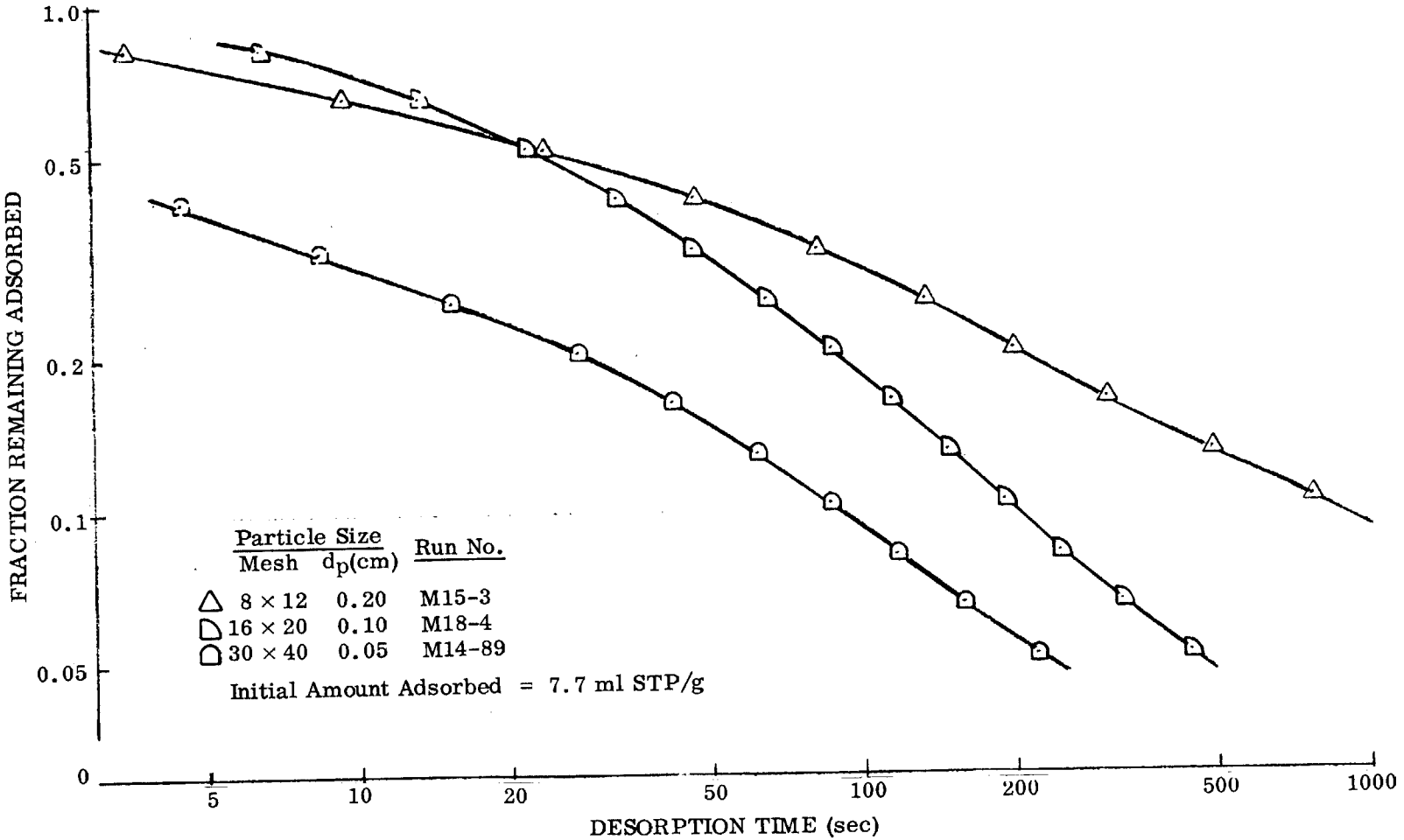

Fig. 5-9 Gravimetric Desorption of n-Butane From BD Activated Carbon at 87°C (360°K)

Data from experiments on 1.0-mm charcoal at 87°C using both the shorter and the longer furnace designs are compared in Fig. 5-10. Initial desorption rates were somewhat higher using the longer furnaces but approached the same rate after about 30 percent of the n-butane had been desorbed. Data are shown from the two sets of longer furnaces, in which only the heater winding material was different. While the furnaces with magnetic windings resulted in very unstable weight readings, desorption rate data do not appear to have been appreciably affected.

Data for an additional set of experiments in which n-butane initial loading was varied are plotted semilogarithmically in Fig. 5-11 and 5-12. In the former plot the actual amount adsorbed is shown as a function of desorption time, while in the latter the amounts adsorbed are normalized by dividing out the initial amount adsorbed.

Data for the desorption of toluene from 1.0-mm particles at various temperatures are shown logarithmically in Fig. 5-13 and 5-14. The initial amount adsorbed was 50 ml STP/g. In addition, the results of some preliminary experiments with toluene on both BD charcoal and sorbent LS2A are shown in Fig. 5-15, which unlike previous plots is on linear coordinates.

Propane desorption data for two particle sizes at 27°C are shown semilogarithmically in Fig. 5-16. The initial amount adsorbed was 1.1 ml STP/g.

5.2.2 Multiple-Component Desorption

The measurement of the desorption rate of two components from charcoal involves a new factor, since the rate of total weight change as read from the microbalance record must be supplemented by analysis of the off-gas, so that the individual rates may be computed. In the present work a quadrupole mass spectrometer was used for the instantaneous gas analyses.

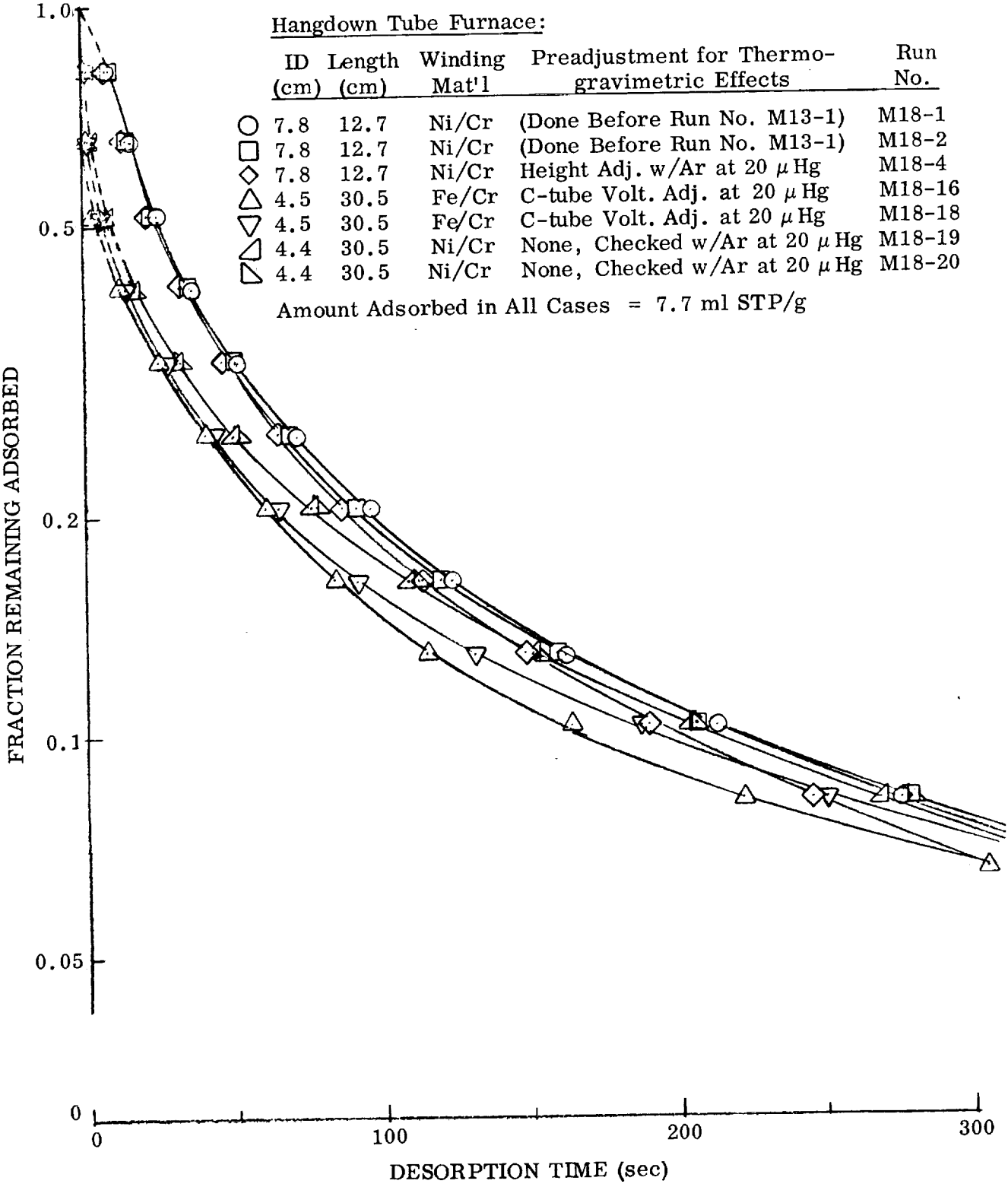

Fig. 5-10 Gravimetric Desorption of n-Butane From 16 × 20 BD Activated Carbon: Effect of Various Heating Arrangements at 87°C

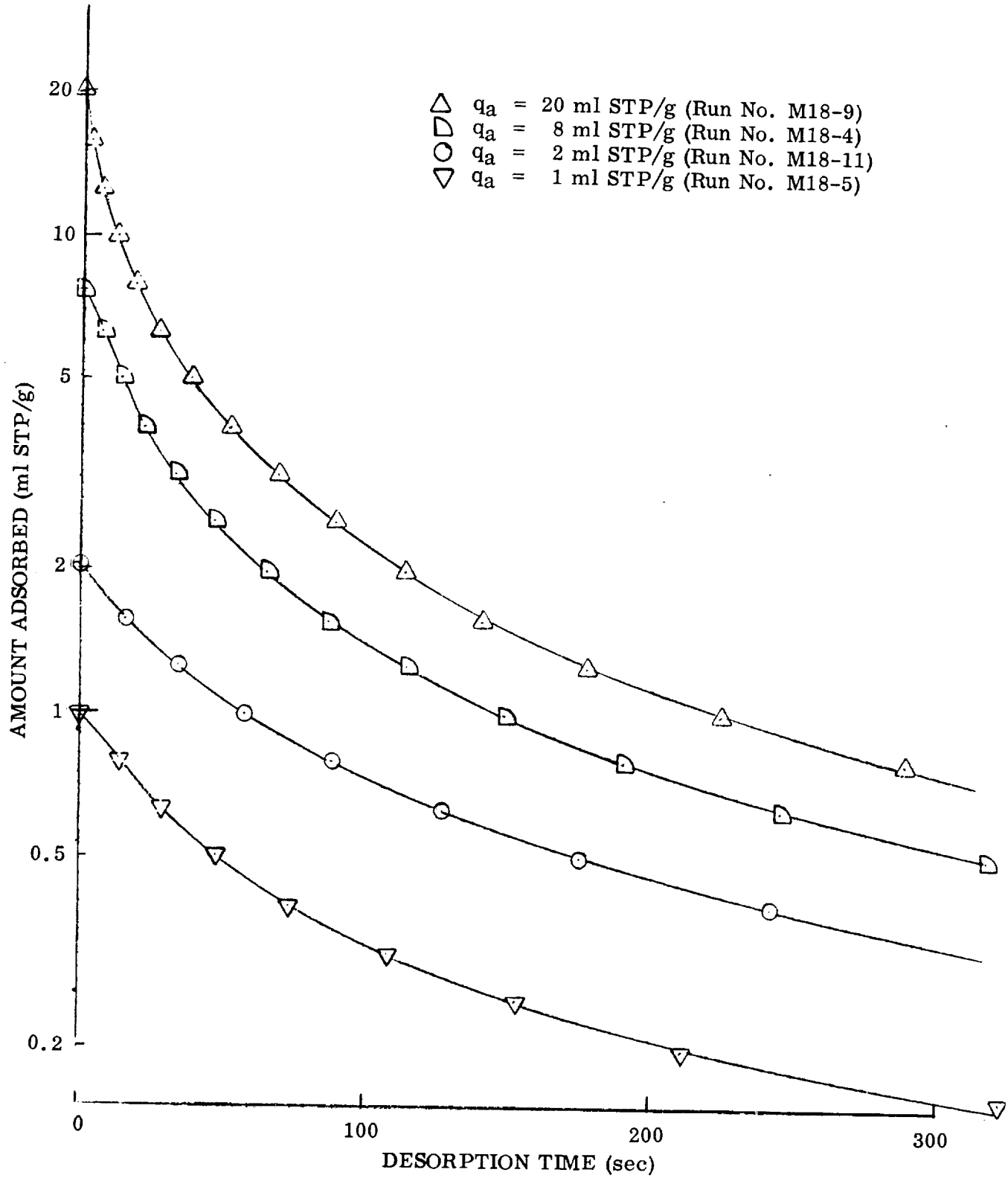

Fig. 5-11 Desorption of n-Butane From 16 × 20 BD Activated Carbon at 87°C and Various Amounts Previously Adsorbed

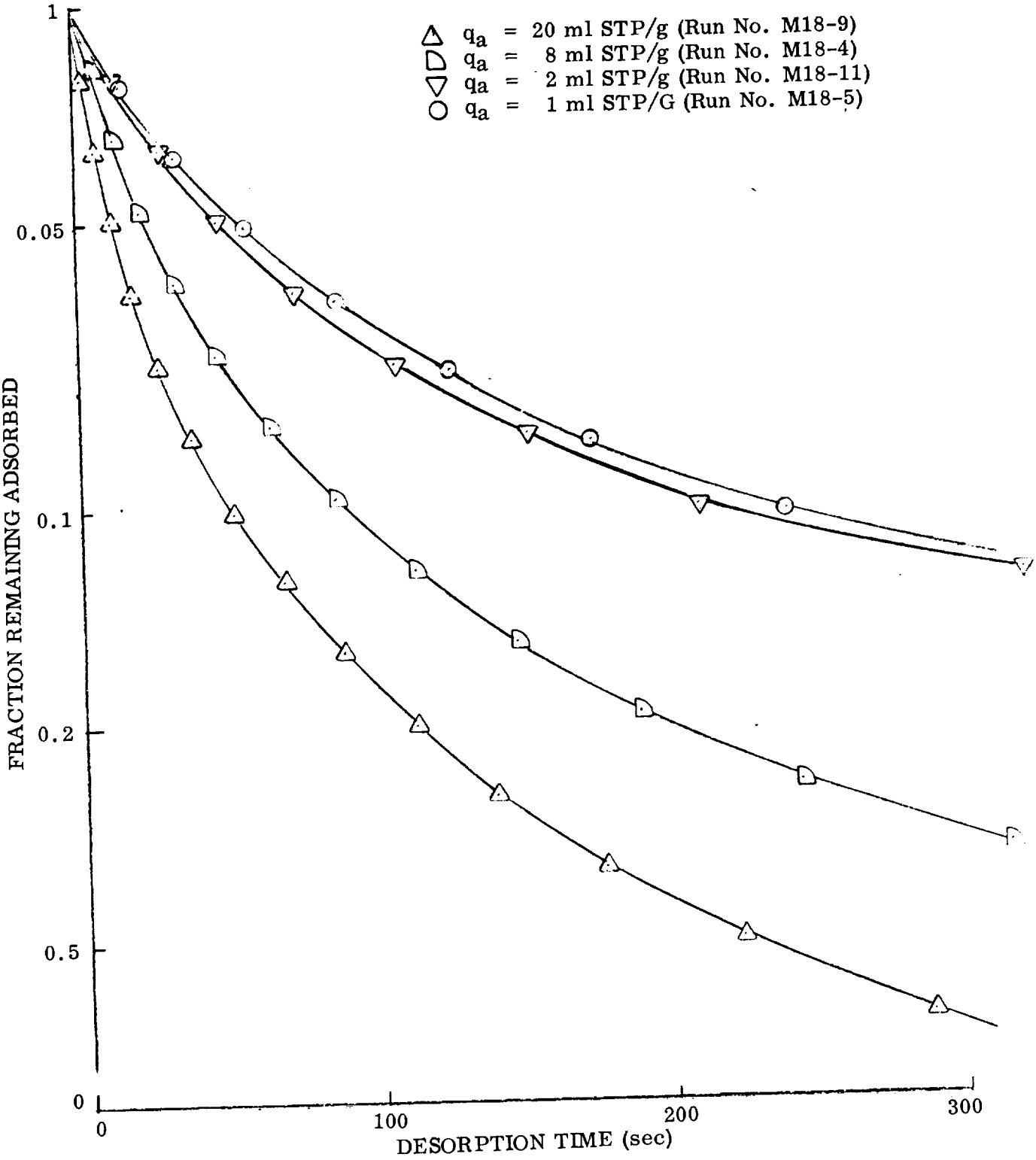

Fig. 5-12 Desorption of n-Butane From 16 × 20 BD Activated Carbon at 87°C and Various Amounts Previously Adsorbed

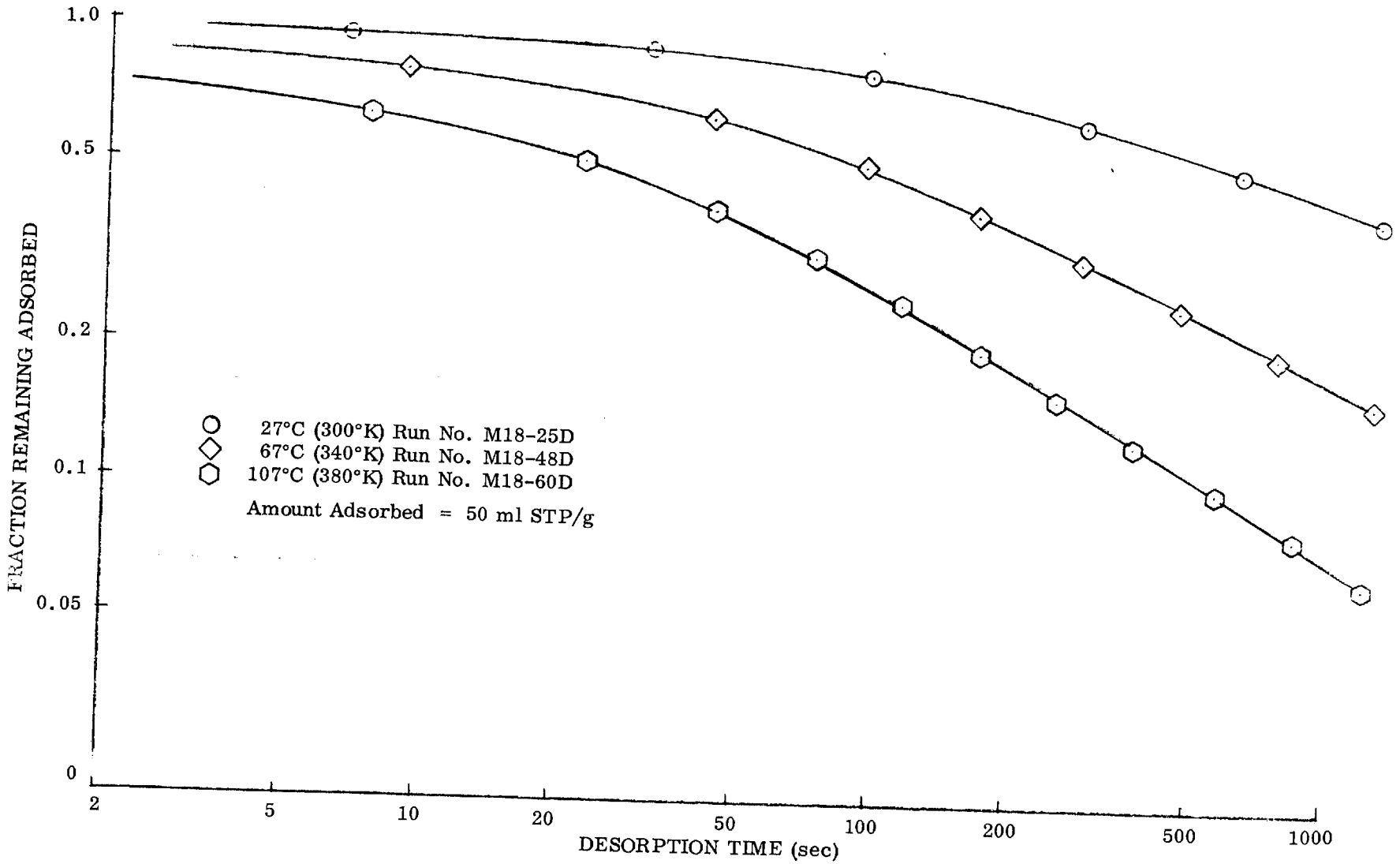

Fig. 5-13 Gravimetric Desorption of Tolune From 16 × 20 BD Activated Carbon

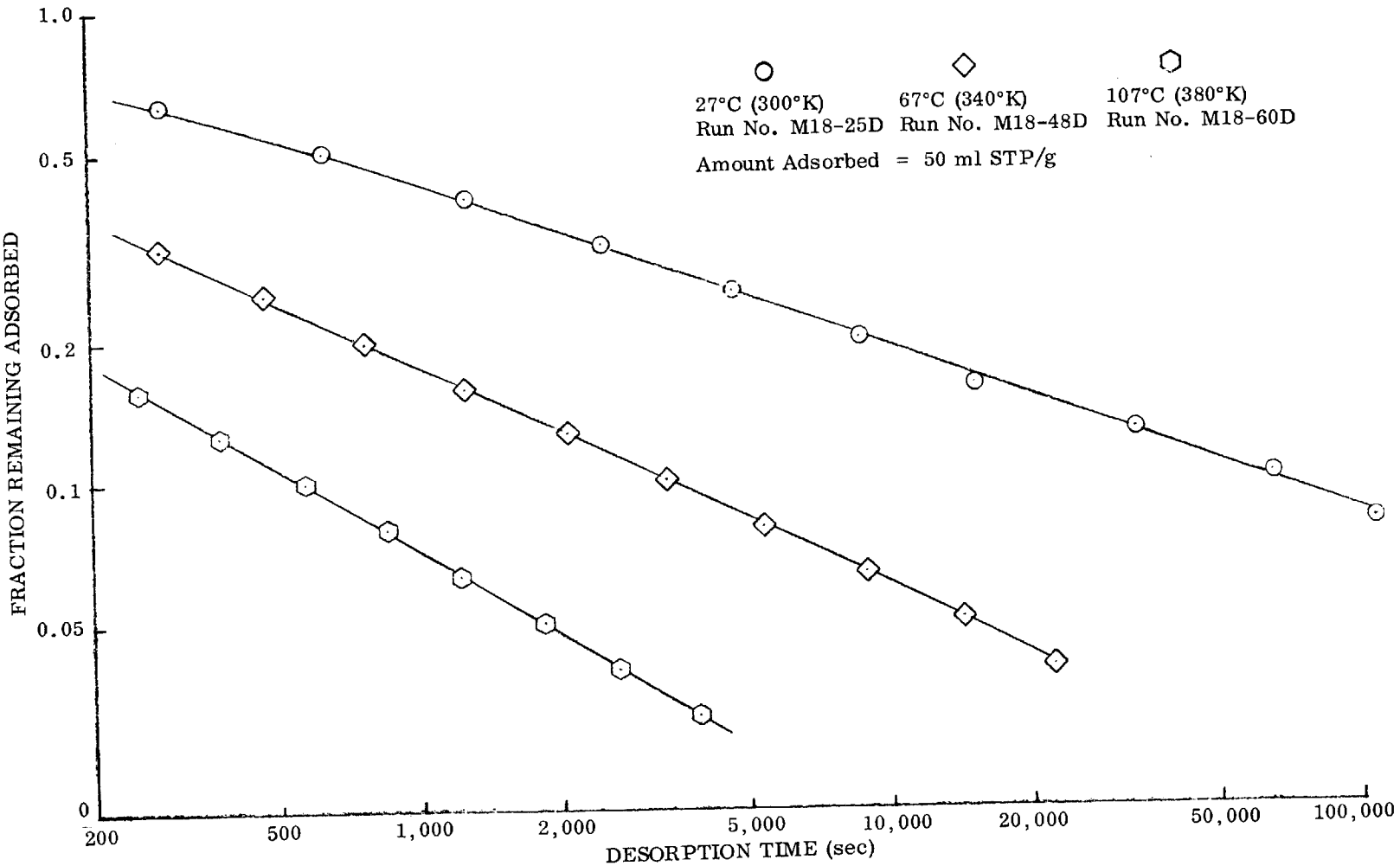

Fig. 5-14 Gravimetric Desorption of Toluene From 16 × 20 BD Activated Carbon

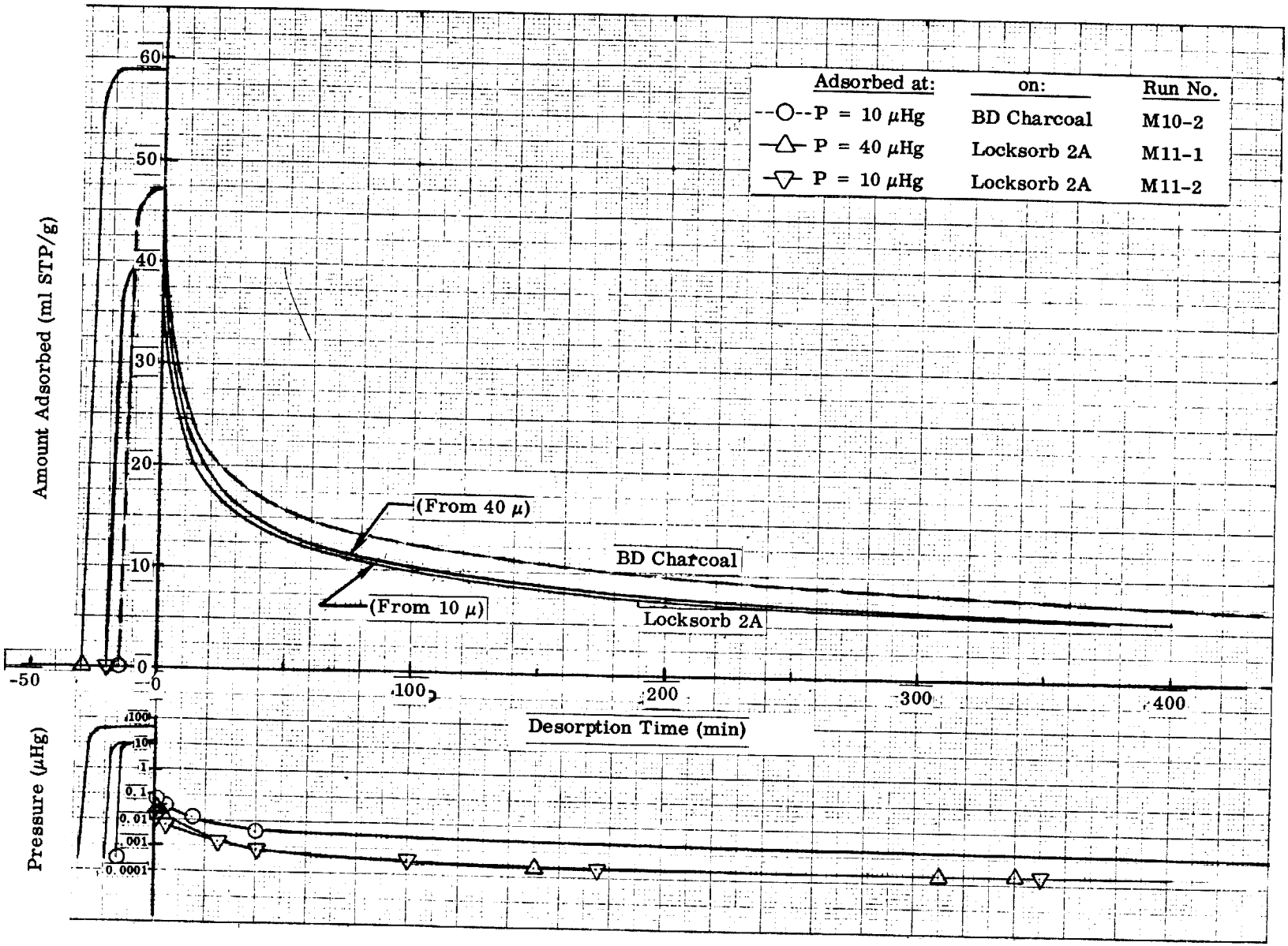

Fig. 5-15 Adsorption and Desorption of Toluene on Two Sorbents

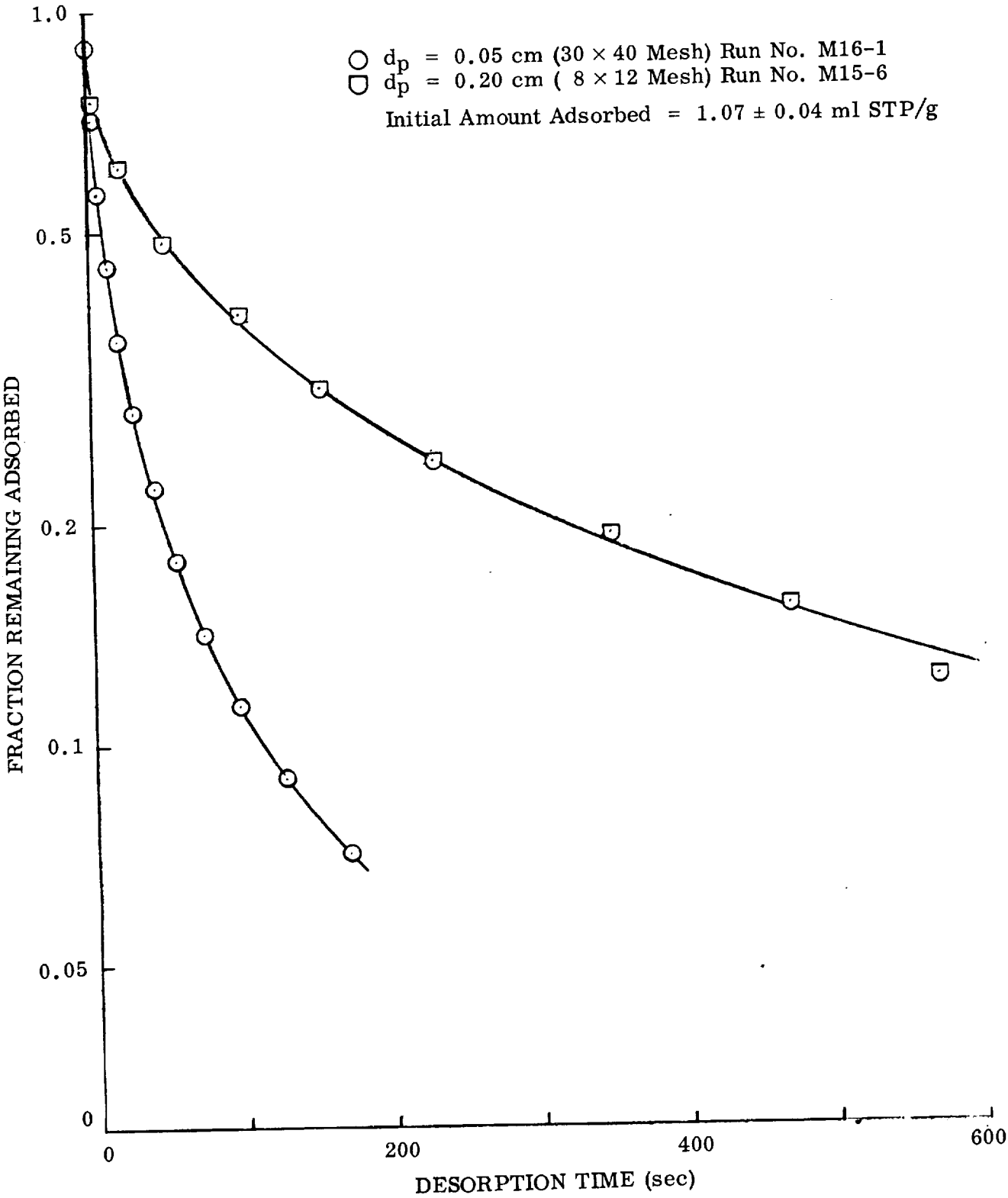

Fig. 5-16 Gravimetric Desorption of Propane From BD Activated Carbon: Variation With Particle Size

It follows that an equation is needed which allows the individual desorption rates to be computed from the total weight change and the instantaneous gas analyses. This equation is

$$\dot{N}_t = \frac{\dot{w}}{M_t + M_b(X_t/X_b)} \tag{5.1}$$

where

$\dot{N}_t$ = instantaneous desorption rate of toluene (mol/sec)
$\dot{w}$ = total desorption rate (g/sec)
M_t, M_b = molecular weight of toluene and butane, respectively (g/mol)
X_t, X_b = mole fraction of toluene and butane, respectively, in the off-gas at that time

Equation 5.1 follows directly from the equation of mass balance:

$$M_t\dot{N}_t + M_b\dot{N}_b = \dot{w} \tag{5.2}$$

plus the equation

$$\frac{\dot{N}_t}{\dot{N}_b} = \frac{X_t}{X_b} \tag{5.3}$$

which expresses the basic fact that the mole ratio in the off-gas at any instant is equal to the relative rates of desorption. An equation exactly the same as Eq. 5.3 with subscripts interchanged holds for butane.

Thus, the total weight of toluene desorbed up to any time can be computed by integrating Eq. 5.1 graphically:

$$N_t = \int_0^t \frac{\dot{w}}{M_t + M_b(X_t/X_b)}\, dt \tag{5.4}$$

where N_t = number of moles of toluene desorbed up to time t.

In determining the off-gas composition, the mass spectrometer peak at M/e = 51 was chosen for toluene and at M/e = 43 for n-butane. If the peak heights at M/e = 51 and 43 are, respectively, h_{51} and h_{43}, then the mole ratio X_t/X_b is computed from

$$\frac{X_t}{X_b} = \frac{S_{43}h_{51}}{S_{51}h_{43}} \tag{5.5}$$

where S_{43} and S_{51} are empirical sensitivity factors, related to ionization probabilities. The sensitivity ratio in Eq. 5.5 can be determined either empirically from a known gas mixture or alternatively from Eq. 5.4 since only the correct ratio will give the correct number of moles of toluene desorbed at infinite time.

For this experiment at 27°C, toluene was first adsorbed at 8×10^{-4} torr equilibrium pressure which gave an adsorption of 31.6 ml STP/g. Butane was then admitted at 0.30 torr pressure which gave an equilibrium adsorption of 1.125 ml STP/g. This relatively high butane pressure was necessary to get a significant adsorption. Evacuation was then started, with recording of both the total weight versus time, and the mass spectrometer peaks versus time.

The total weight versus time is shown in Fig. 5-17, while Fig. 5-18 displays the mole ratio versus time, using a sensitivity ratio $S_{51}/S_{43} = 0.04$. This ratio was determined from the fact that it gave a good mass balance when Eq. 5.4 was, in effect, integrated out to infinite time. The increase in this ratio during later stages of the desorption is probably due to n-butane being gradually reevaporated from the liquid nitrogen trap used in pumping the system. The ratio dropped to a much lower value when the trap was filled at about 1550 sec desorption time.

The rate of toluene desorption versus time is shown in Fig. 5-19 and was computed from Eq. 5.1 using the sensitivity ratio of 0.04.

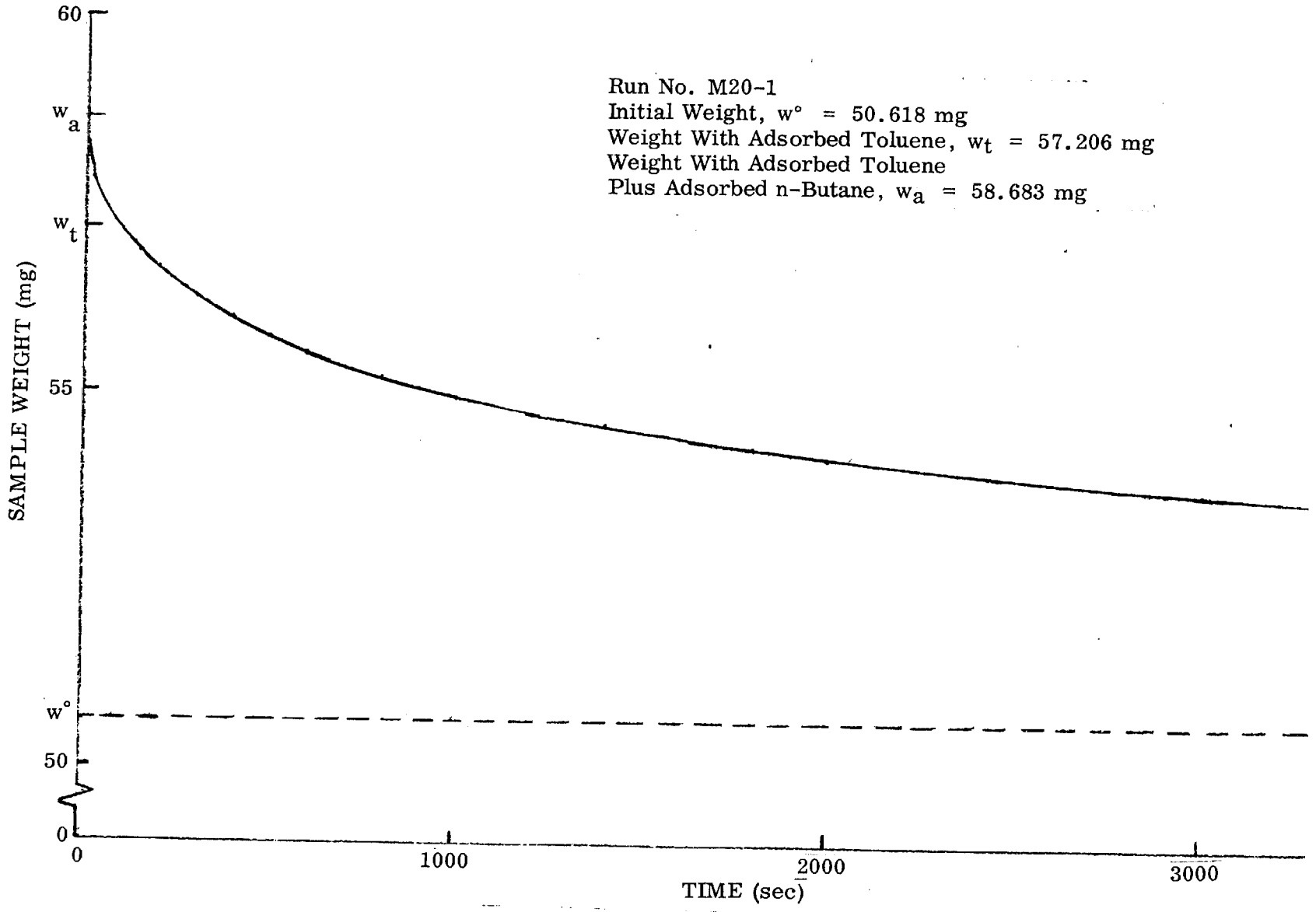

Fig. 5-17 Desorption of n-Butane and Toluene From 8 × 12 BD Activated Carbon at 27°C

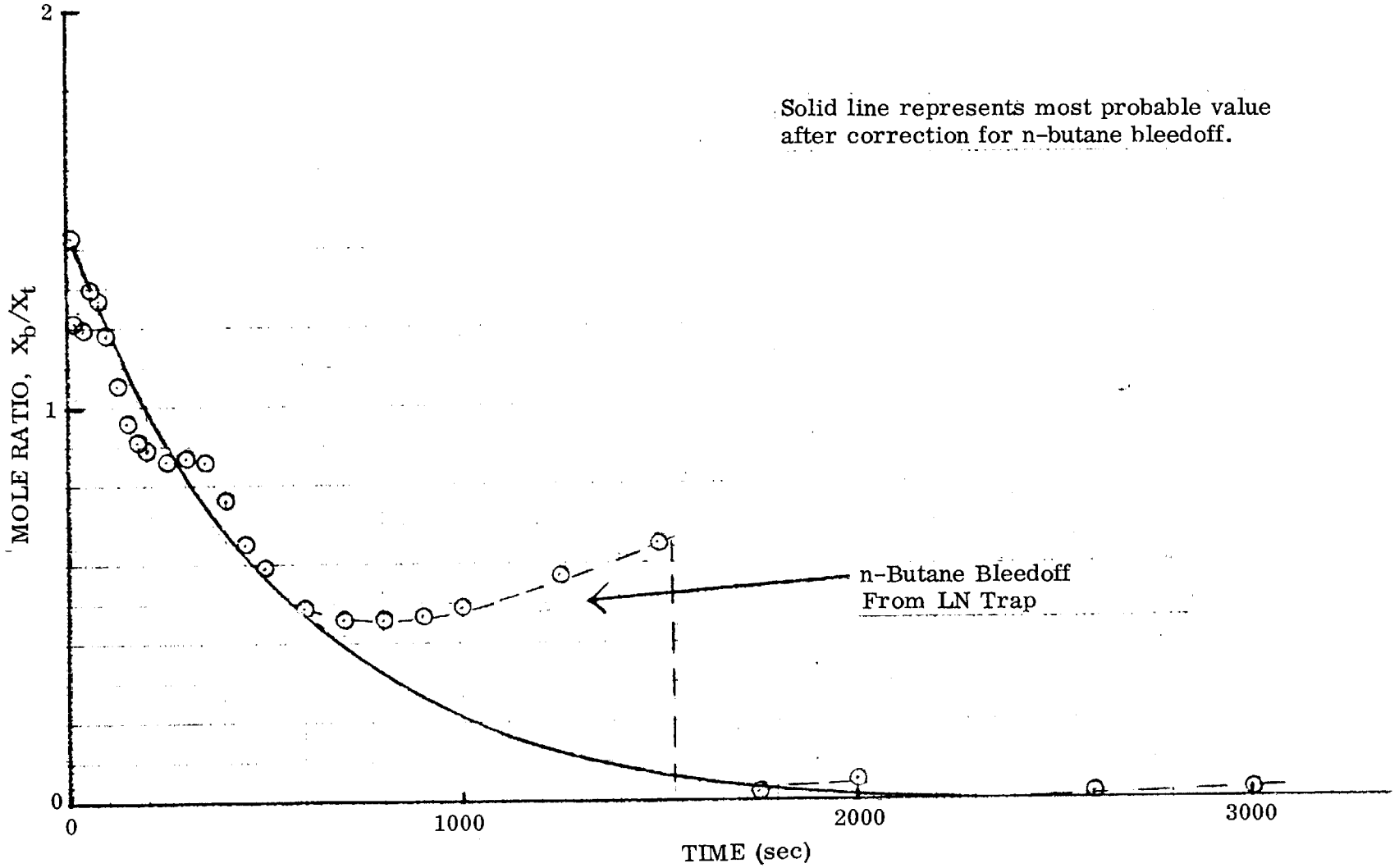

Fig. 5-18 Mole Ratio of n-Butane to Toluene During Vacuum Desorption From 8 × 12 BD Activated Carbon at 27°C as Determined From Mass Spectrometric Analysis of Gases Being Desorbed

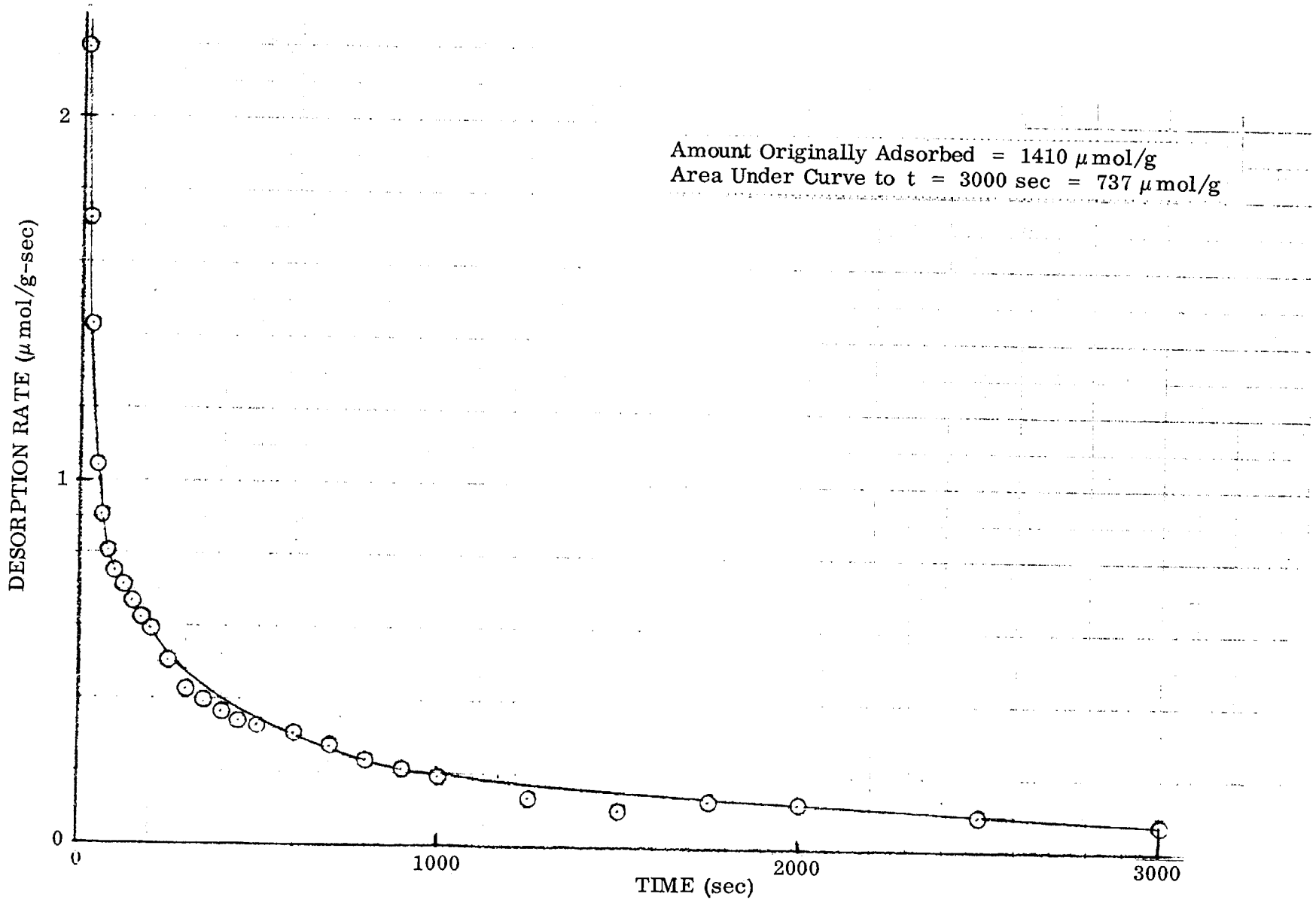

Fig. 5-19 Estimation of Toluene Desorption Rate During Concurrent Desorption of n-Butane From 8 × 12 BD Activated Carbon at 27°C

The integrated version of Fig. 5-17, converted to the fraction remaining adsorbed versus time, is shown in Fig. 5-20. Also shown in Fig. 5-20 is a curve representing previous desorption data for toluene on 0.1-cm particles, one-half the size of the present ones. This curve is from a previous experiment in which somewhat more toluene (50 ml STP/g) was initially adsorbed than in the present experiment (31.6 ml STP/g). This curve has been replotted for comparison purposes with zero time assigned to the point where 31.6 ml STP/g remained adsorbed. It is predicted that desorption time for this smaller particle size would be decreased by a factor of about 1.8, as was experienced with n-butane desorptions on various particle sizes as reported in section 5.2.1. The ratio here is somewhat less—about 1.2; however, it would be best to compare the present data with pure toluene desorption data obtained on the same particles at the very same initial loading, since there is some variation in the charcoal and probably as increased cooling effect in the case of the data from the previous work due to the larger amount initially adsorbed. It thus appears that the desorption rate of toluene is not greatly affected by the presence of n-butane.

5.2.3 Volumetric Apparatus

Experimental data were obtained using the volumetric system for desorption from two particle sizes, 16 × 20 mesh and 8 × 12 mesh (corresponding to average diameters of 0.1 and 0.2 cm, respectively). Experiments were performed at 26°C on two carbon sample weights, 10 and 20 mg. Within the experimental error of reading the Pirani gage (2 to 5 percent), all desorption rates were essentially second order; that is, a plot of the inverse of the fraction remaining versus time was a straight line over the whole range of time.

Data for the experiments with 10-mg samples were not very reproducible, especially in the case of the 0.2-cm particles, 10 mg of which consists of only 2 or 3 particles. In one case a sample of 10 mg of 0.2-cm particles actually desorbed faster than a similar sample of 0.1-cm particles, resulting in an experimental scatter of more than a factor of 2.

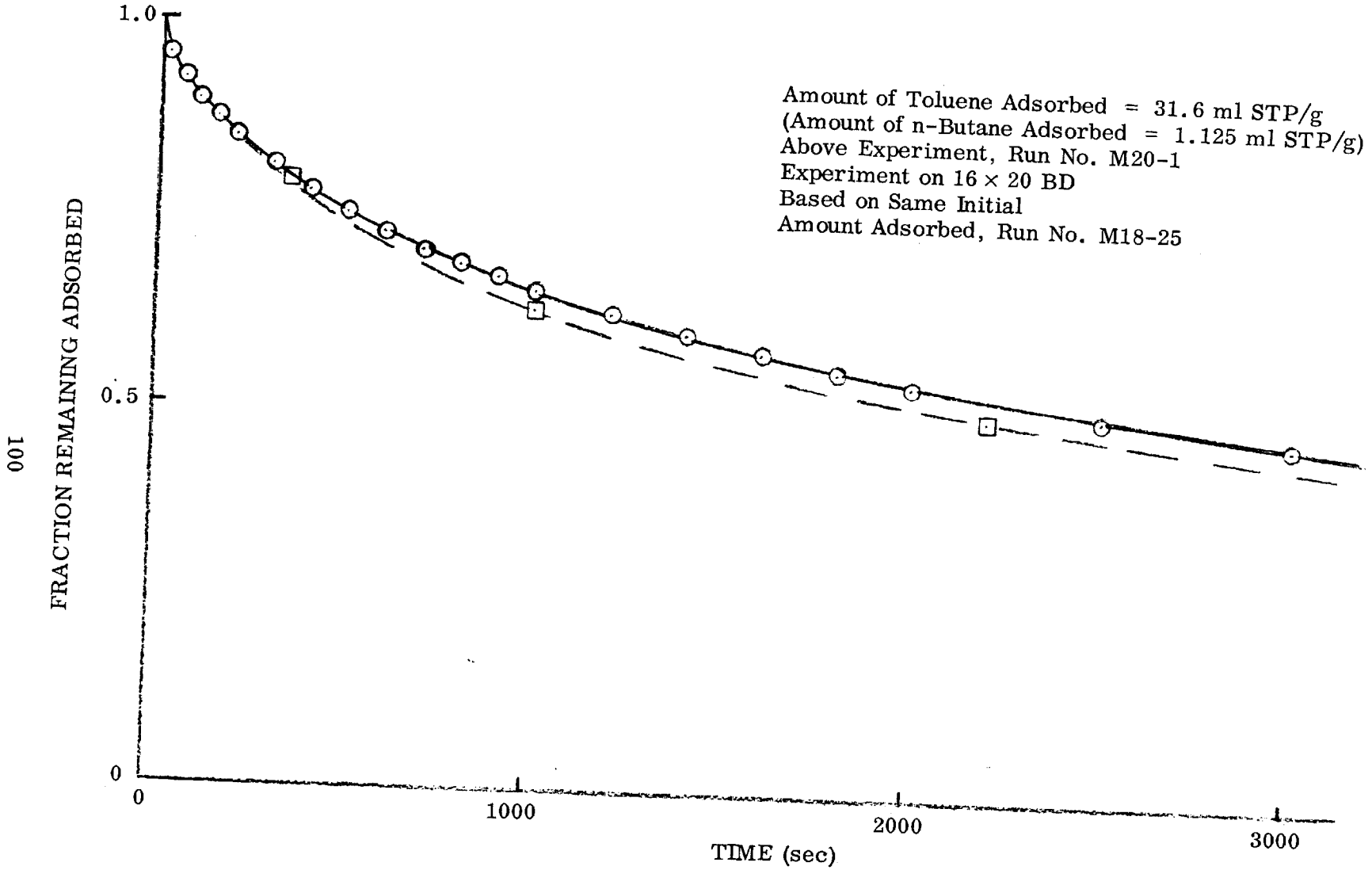

Fig. 5-20 Desorption of Toluene From 8 × 12 BD Activated Carbon at 27°C During Concurrent Desorption of n-Butane

Data for the experiments using 20-mg samples were considerably more reproducible than those using 10 mg. The 20-mg data are given in Fig. 5-21, in which time for half-desorption is plotted against initial loading of n-butane. Straight lines of unit slope have been drawn through the data, since second-order desorption kinetics seem to be well established. Both the upper line for 0.2-cm particles and the lower line for 0.1-cm particles are within 10 – 15 percent of the values obtained in gravimetric experiments. Experiments were reproducible to 5 percent or better for a given set of charcoal granules at a given loading, but changing to a new sample or to a new loading of n-butane introduced a scatter of up to 20 percent.

Some additional details of the volumetric data are presented in Appendix K.

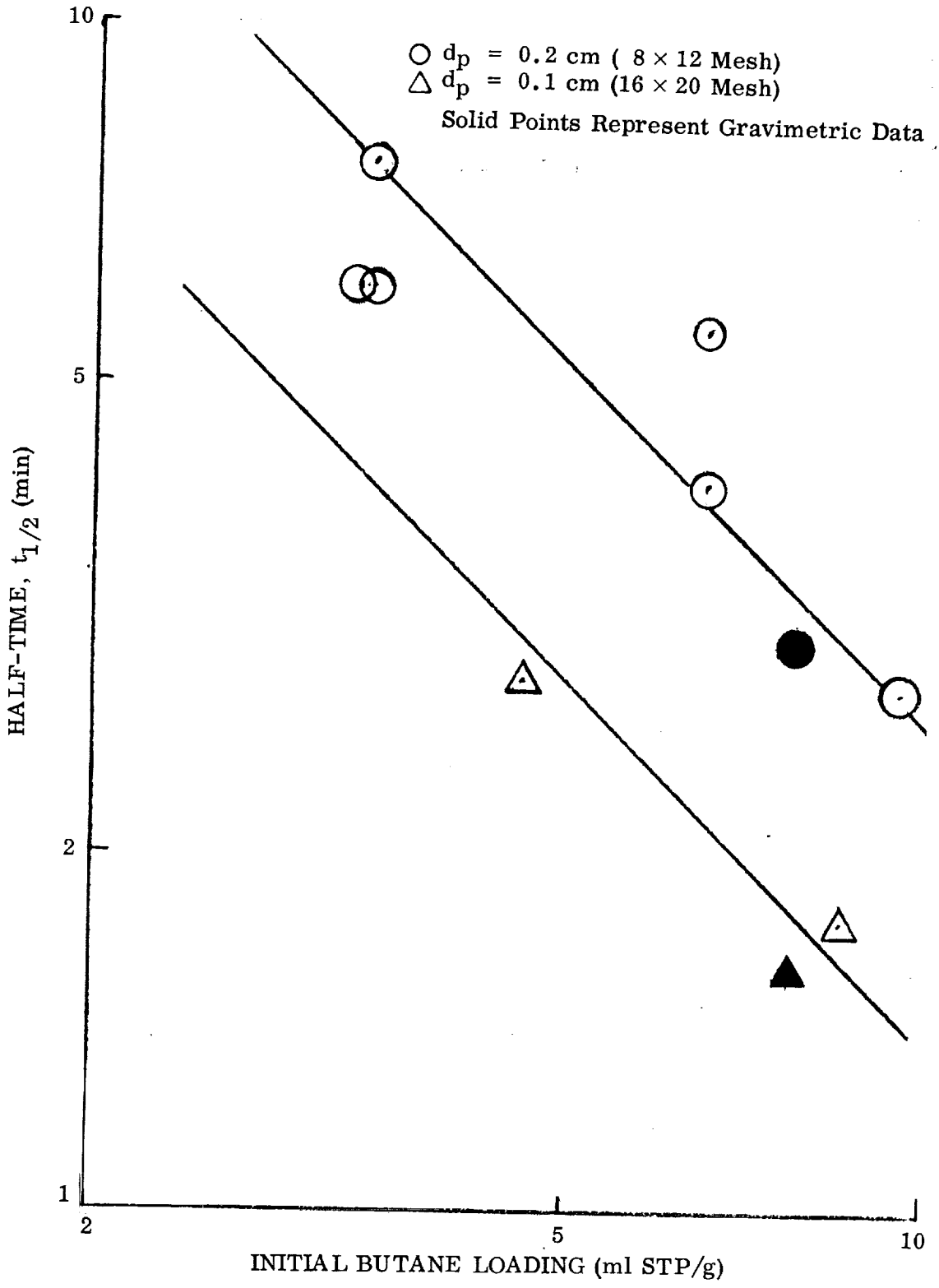

Fig. 5-21 Rate of Desorption of n-Butane From BD Activated Carbon in Volumetric Apparatus

Section 6

VACUUM DESORPTION FROM SINGLE PARTICLES – DISCUSSION

Once extensive vacuum desorption data have been obtained for single activated carbon particles, it should be possible to gain considerable insight into the physical processes that are taking place when such particles are subjected individually to the approximate equivalent of space vacuum. In this section, data from Section 5 are discussed in relation to various physical models for desorption.

The kinetics of desorption (desorption rate, rate order, rate constants, and desorption activation energies) are discussed with respect to variations in temperature and particle size for a few selected contaminants in order to have some basis for predicting the effect of such variations on the performance of packed beds during vacuum regeneration. Various mechanisms for single-particle desorption are examined for similar reasons. Cooling effects are treated in order to determine the magnitude of the cooling which naturally results when single particles with no thermally conductive path to the surroundings are subjected to fast vacuum desorption. This is needed in order to make valid comparisons with vacuum desorption data from packed beds, in which thermal conductivity of closely packed particles is much better than in the single-particle case.

6.1 FIT TO APPARENT RATE ORDER

A means of correlating the gravimetric kinetic data is simply to seek the empirical order of the desorption rate. That is, it is assumed that the desorption rate follows simple power-law kinetics:

$$r_d = k_d q_r^n \tag{6.1}$$

where

r_d	= desorption rate	(ml STP/g-sec)
k_d	= desorption rate constant	[(ml STP/g)$^{n-1}$/sec]
q_r	= amount remaining adsorbed	(ml STP/g)
n	= desorption rate order	

Desorption rates which obey such kinetics give rise to a Freundlich isotherm since the adsorption rate may be defined by

$$r_a = k_a p \tag{6.2}$$

where

r_a	= adsorption rate	(ml STP/g-sec)
k_a	= adsorption rate constant	(torr-ml STP/g-sec)
p	= pressure	(torr)

The net rate of adsorption is

$$r_n = k_a p - k_d q_r^n \tag{6.3}$$

At equilibrium, this net rate is equal to zero, so that

$$q_r = (k_a/k_d)^{1/n} p^{1/n} = k_F p^{1/n} \tag{6.4}$$

where

k_F	= Freundlich constant	[(torr)^{n}ml STP/g]

Furthermore, a linear potential plot (see section 4.1) is consistent with Eq. 6.3, and hence it is expected that the simple power-law kinetics of Eq. 6.1 are appropriate.

The most direct way to determine desorption rate order is by the method outlined in Appendix L. There it is shown that a plot of log q versus log τ (τ being a characteristic time) is linear. The slope at any point during the desorption is equal to 1 - n, where n equals the rate order. Also, the rate constant may be calculated from the intercepts of such a plot, as shown in Appendix L.

Using this method, rate orders and constants were graphically determined for the n-butane desorption results given in section 5.2.1. Rate orders were found to be essentially constant after about half the n-butane had been desorbed. For desorption from 0.5-mm particles, the slopes of the lines thus determined are all only slightly greater than -1, as shown in Fig. 6-1. Rate orders in this case are then equal to slightly more than 2. For 0.20-cm particles, the rate order increases from 2.3 at 26°C to n = 2.8 at 87°C, as shown in Fig. 6-2. Comparisons of rate orders for different particle diameters at 27 and 87°C are given in Fig. 6-3 and 6-4, respectively. Rate orders for 0.025- and 0.05-cm particles are near 2.0, while those for 0.10- and 0.20-cm particles are somewhat higher. Rate orders for desorptions from 0.10-cm particles at 87°C with initial loadings other than the usual 7.7 ml STP/g are shown in Fig. 6-5, and are approximately equal to 2.0 except for very small initial loadings where the value goes as high as 2.5.

In Fig. 6-6, the data from a second set of runs on 0.05-cm particles are treated in the same way as in Fig. 6-1. The temperature range is a bit greater for these data but still the rate order, n , varies between 2.1 and 2.4. If the data of both these runs are taken together, there is no recognizible correlation of the order, n , with temperature. Furthermore, the data depicted in Fig. 6-6 are analyzed for n by graphical differentiation (to be described more completely below) in Fig. 6-7. Here the orders vary from 2.3 to 2.5. From all of this, it may be concluded that the order is known to be between 2.0 and 2.5 or so far the small particles with no easily recognizible trend with temperature. For the longest particles (0.20-cm), there appears to be a slight but significant increase in the order, perhaps up to as high as 2.8. Rate constants for each of these plots determined from the intercepts (see Appendix L) are indicated on the respective rate order curves.

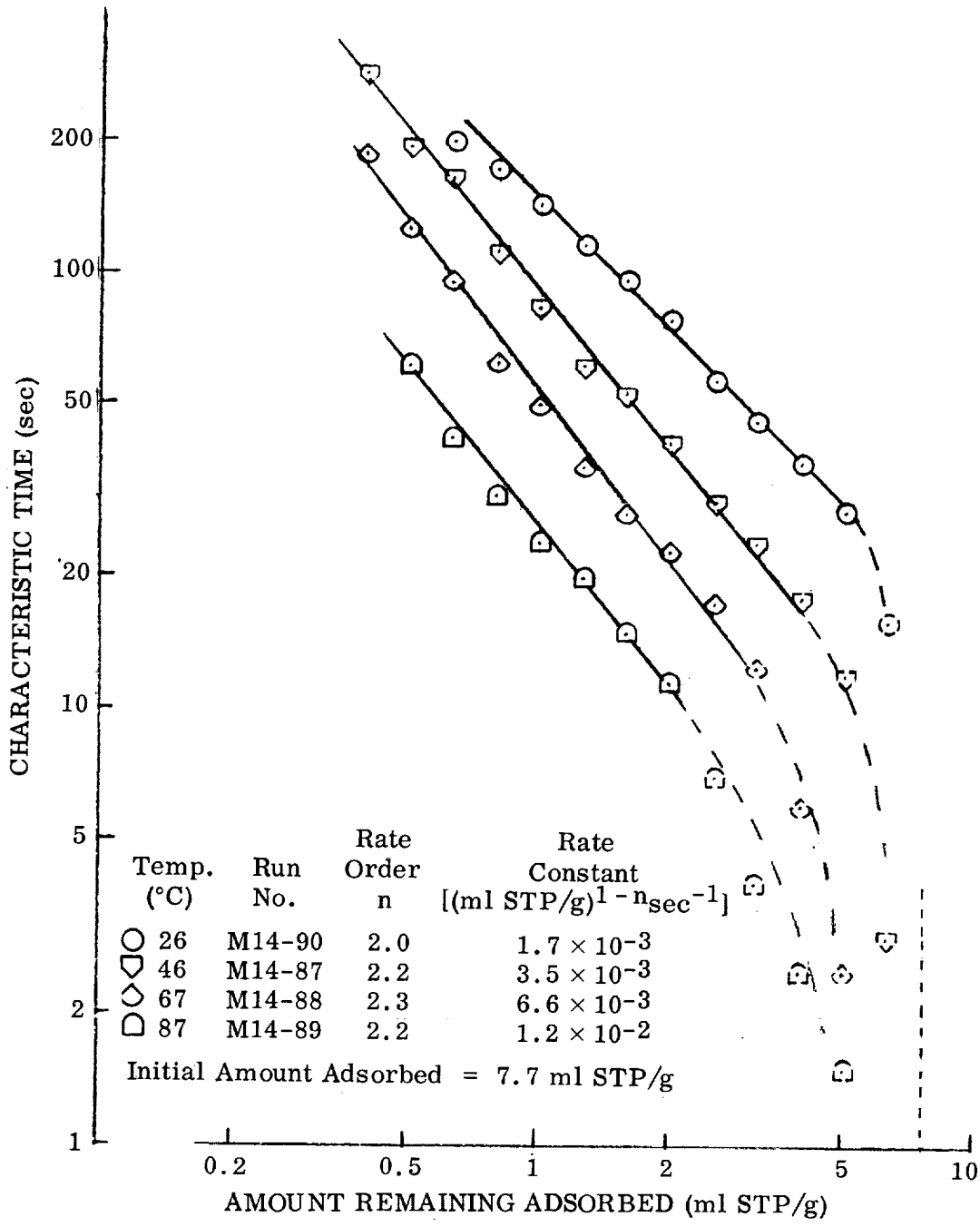

Fig. 6-1 Determination of Rate Order and Constants for Gravimetric Desorption of n-Butane From 30 × 40 BD Activated Carbon (d_p = 0.05 cm)

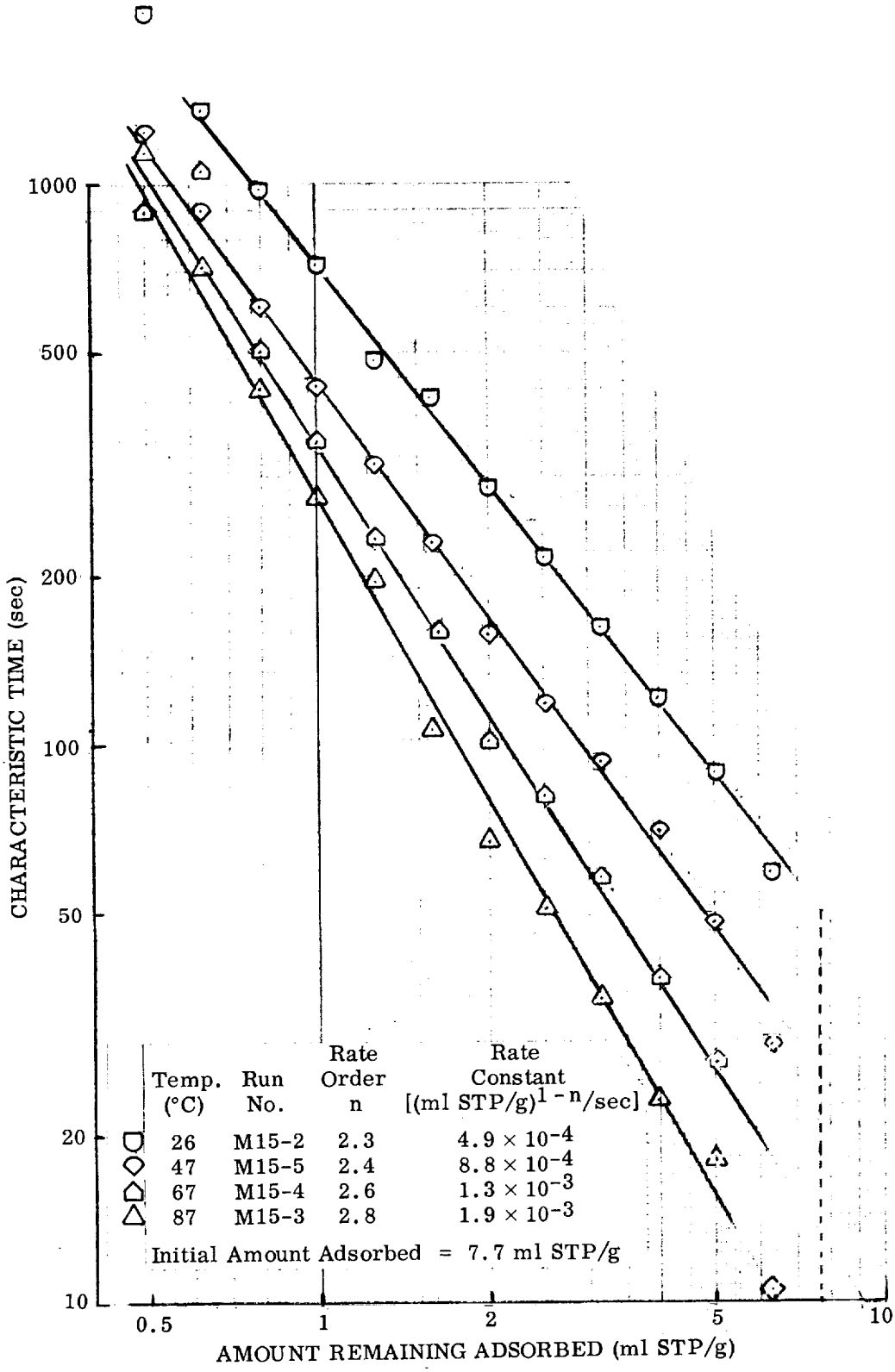

Fig. 6-2 Determination of Rate Order and Constants for Gravimetric Desorption of n-Butane From 8 × 12 BD Activated Carbon (d_p = 0.20 cm)

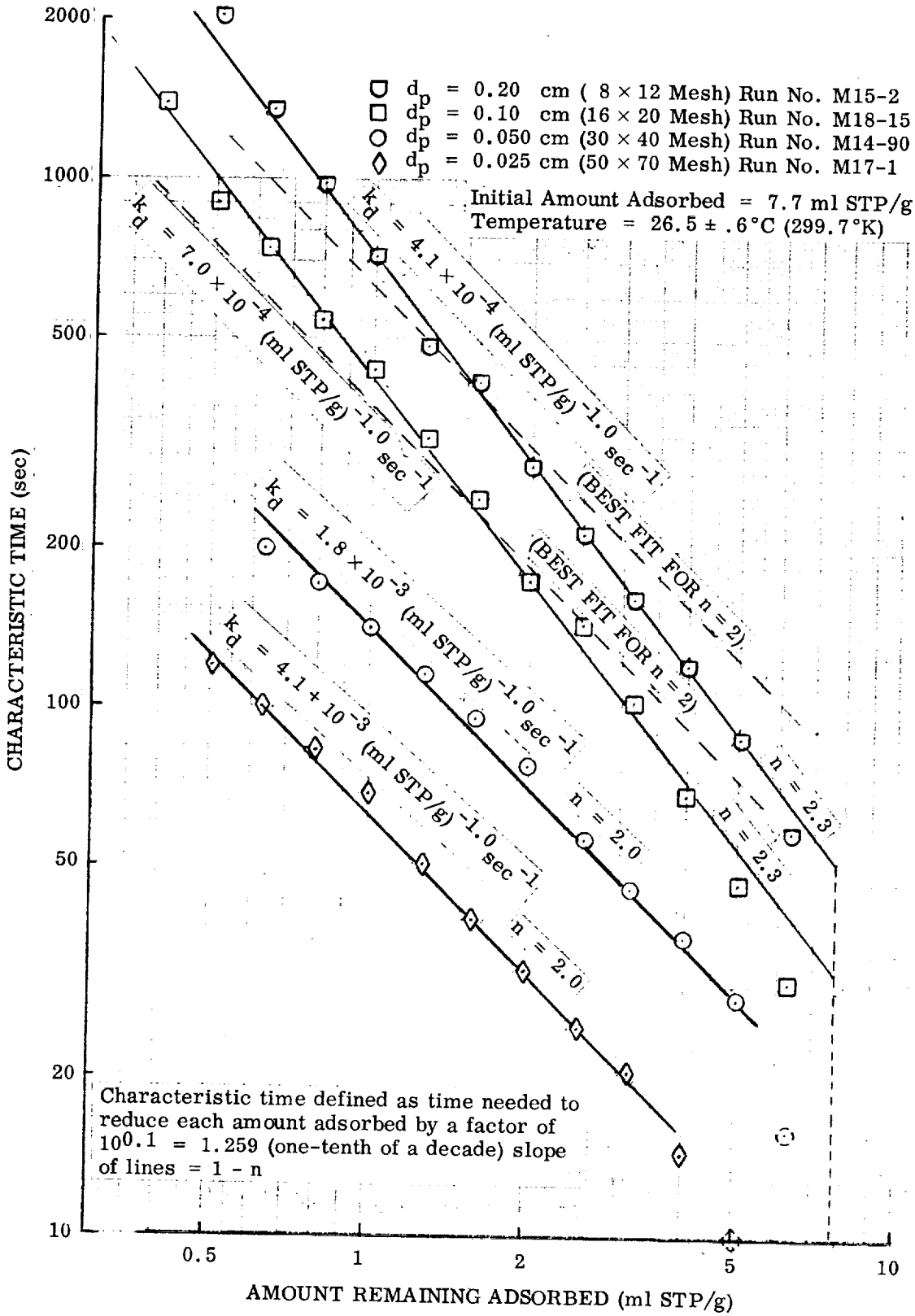

Fig. 6-3 Determination of Rate Order and Constants for Gravimetric Desorption of n-Butane From BD Activated Carbon at 27°C: Variation With Particle Size

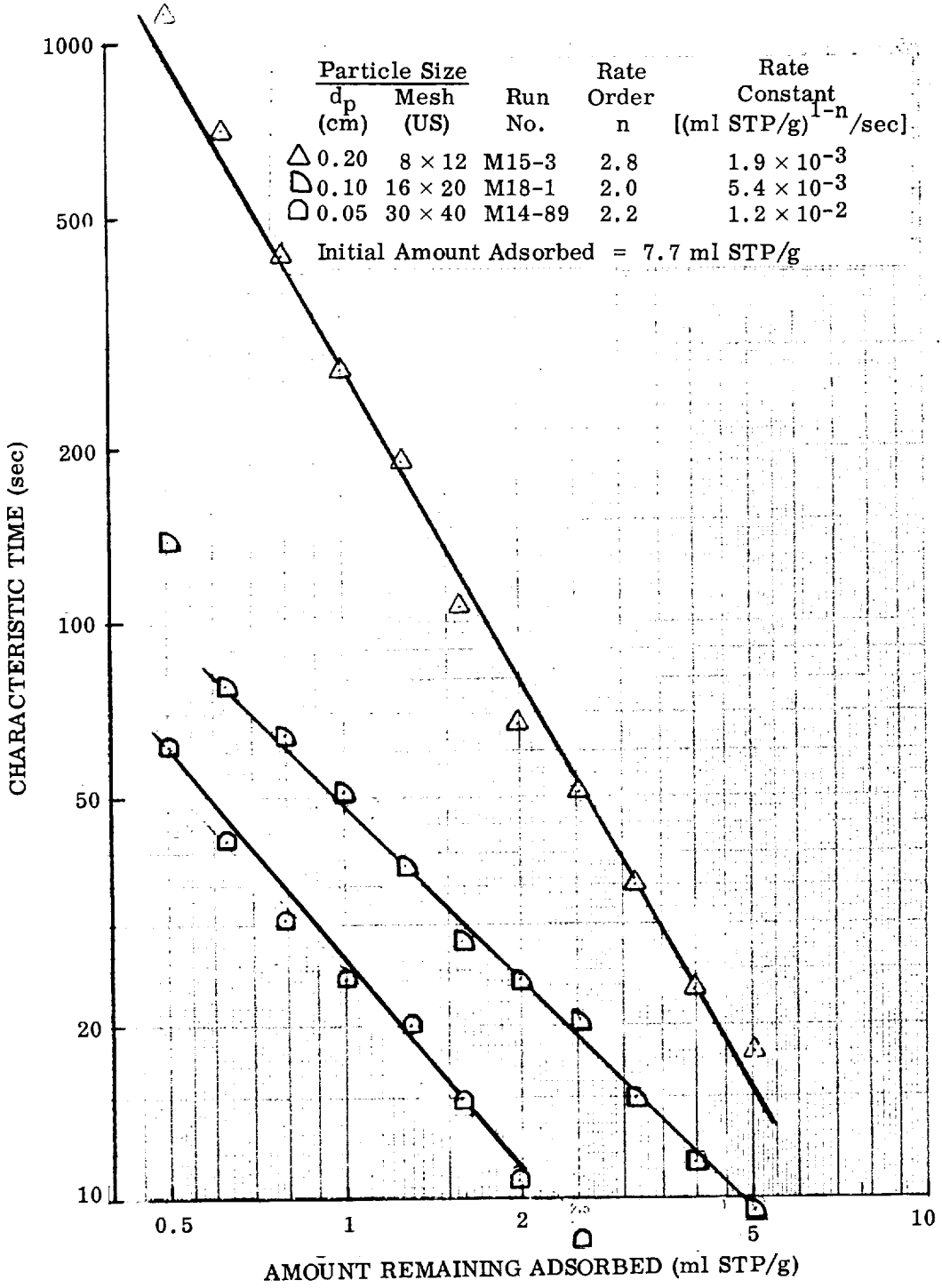

Fig. 6-4 Determination of Rate Order and Constants for Gravimetric Desorption of n-Butane From Various Particle Sizes of BD Activated Carbon at 87°C

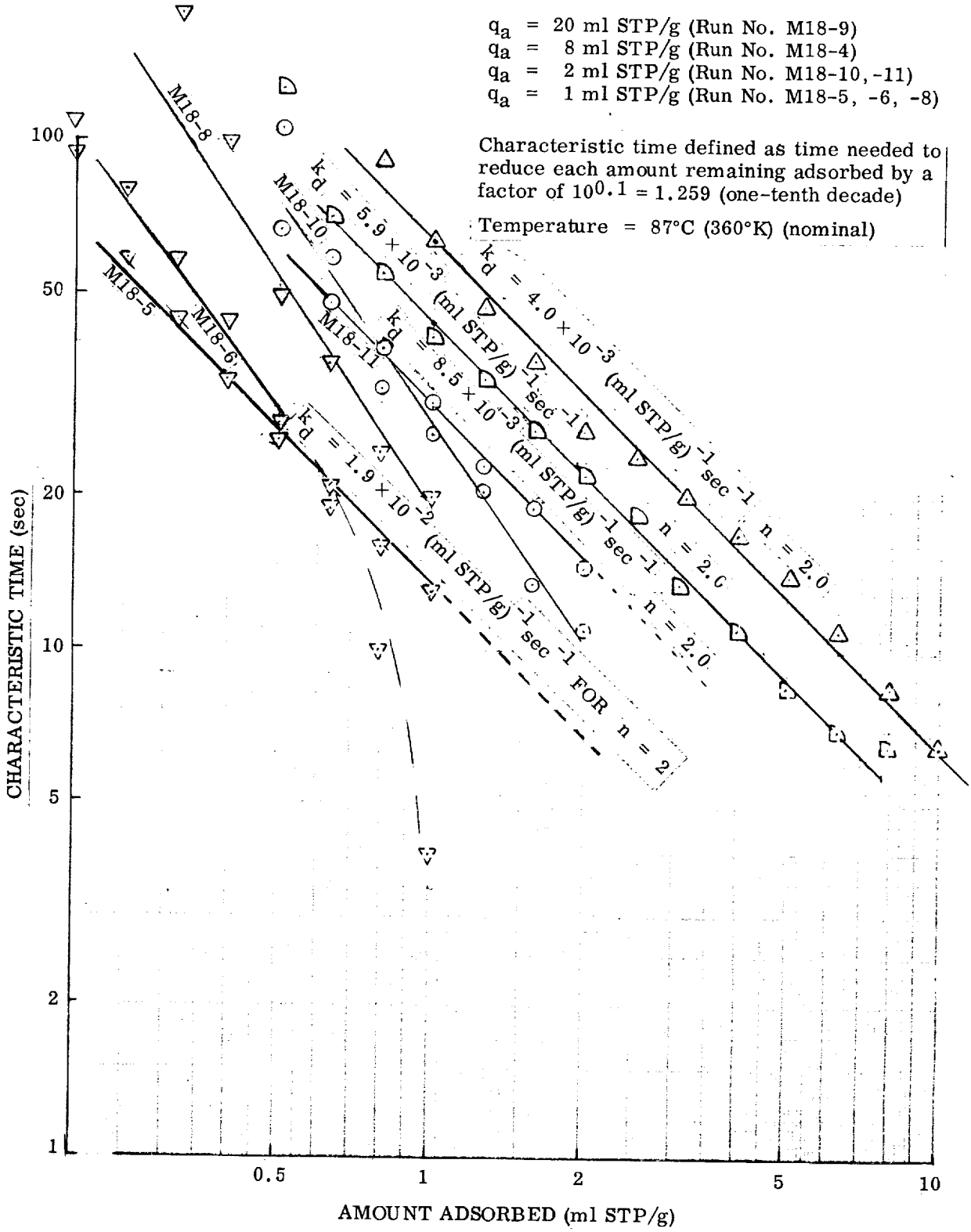

Fig. 6-5 Determination of Rate Order and Constants for Desorption of n-Butane From 16 × 20 BD Activated Carbon: Variation With Amount Previously Adsorbed

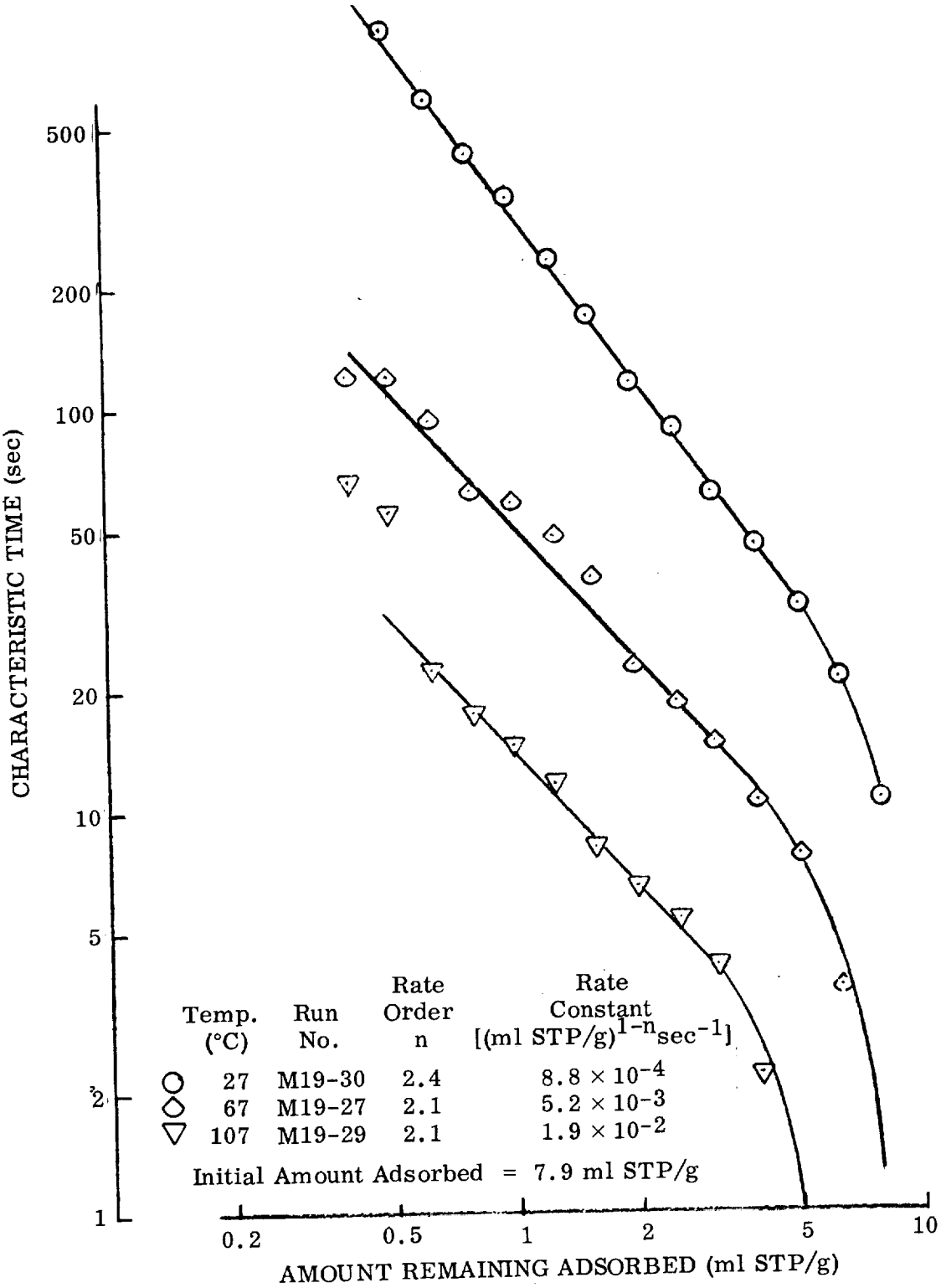

Fig. 6-6 Determination of Rate Order and Constants for Gravimetric Desorption of n-Butane From 30 × 40 BD Activated Carbon (d_p = 0.05 cm)

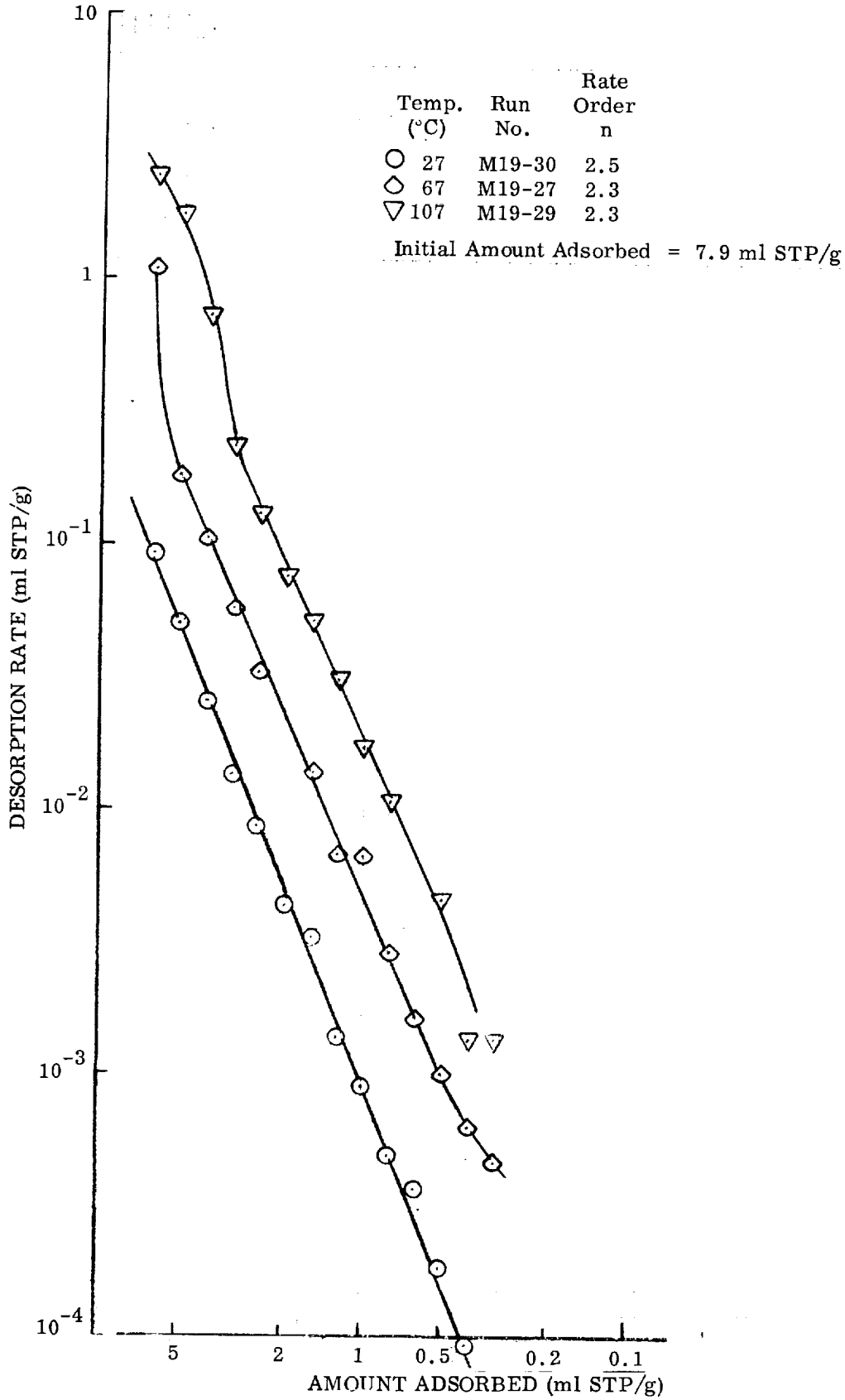

Fig. 6-7 Gravimetric Desorption of n-Butane From 30 × 40 BD Activated Carbon: Desorption Rates at Various Amounts Remaining Adsorbed

n alternate method of determining rate order and constants, the one more commonly sed, requires graphic differentiation of the desorption curves at various points to etermine instantaneous desorption rates. These rates are then plotted against the mount remaining adsorbed on log-log coordinates, as shown in Fig. 6-8 for the same xperiments evaluated in Fig. 6-5 for various amounts initially adsorbed on 0.1-cm arbon. Since the axis for the amount remaining adsorbed in Fig. 6-8 (and also in ig. 6-7) is negative, the rate order is the negative of the slope of the lines. This ıethod is less precise because the slopes obtained are greater by one than those btained in the method of Appendix L. Thus, the deviation of rate order from n = 2 is ess obvious in Fig. 6-7 and 6-8 than in plots similar to Fig. 6-4.

tate constants are somewhat easier to obtain from this type of plot, the value being letermined directly from the intercept with the $q_r = 1$ axis, where q_r = amount emaining adsorbed. Units for the rate constants are (ml STP/g)$^{1-n}$sec^{-1}.

)nce desorption rate order has been established, it is possible to determine rate :onstants by yet another method. Since the rate expression is

$$- dq/dt = k_d q_r^n \tag{6.5}$$

it may be integrated to

$$\frac{1}{n-1} q_r^{1-n} = k_d t \tag{6.6}$$

Thus, a plot of q_r^{1-n} versus t will have a slope of k_d^{n-1}. Such plots for four of the experiments whose rate order was determined in Fig. 6-1 are shown in Fig. 6-9, in which the resulting values of the rate constant are indicated. The rate order was $n = 2$ in all cases. A similar plot for rate orders determined in Fig. 6-2 is given in Fig. 6-10. In this case, rate orders varied from 2.3 to 2.8; thus, it was necessary to calculate q_r^{1-n} for each point and then to divide the slope by $n - 1$ in order to get each rate constant, which is shown next to its respective curve in Fig. 6-10.

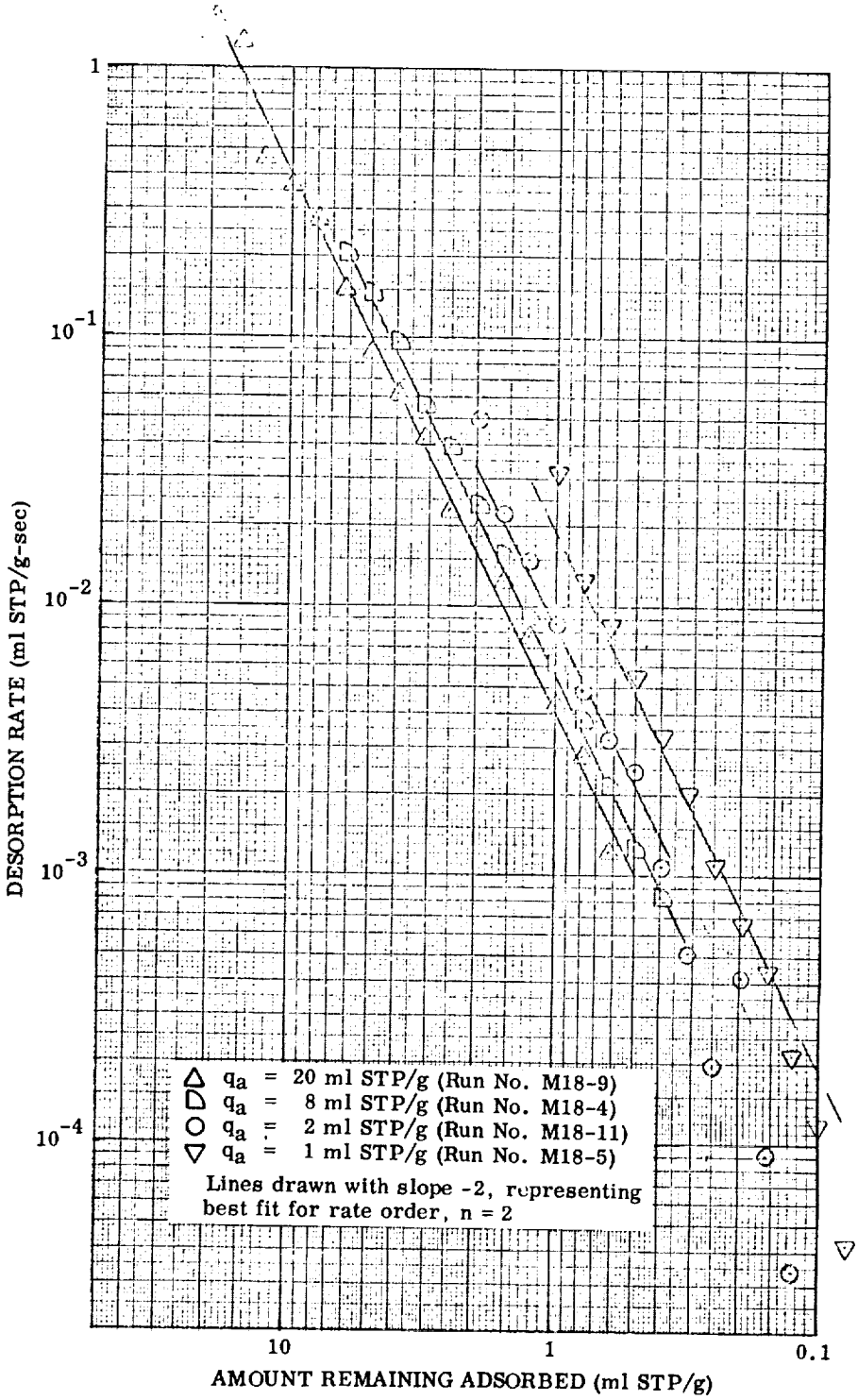

Fig. 6-8 Desorption Rate as a Function of Amount Remaining Adsorbed (Reciprocal) for n-Butane on 16 × 20 BD Activated Carbon at 87°C: Variation With Amount Previously Adsorbed

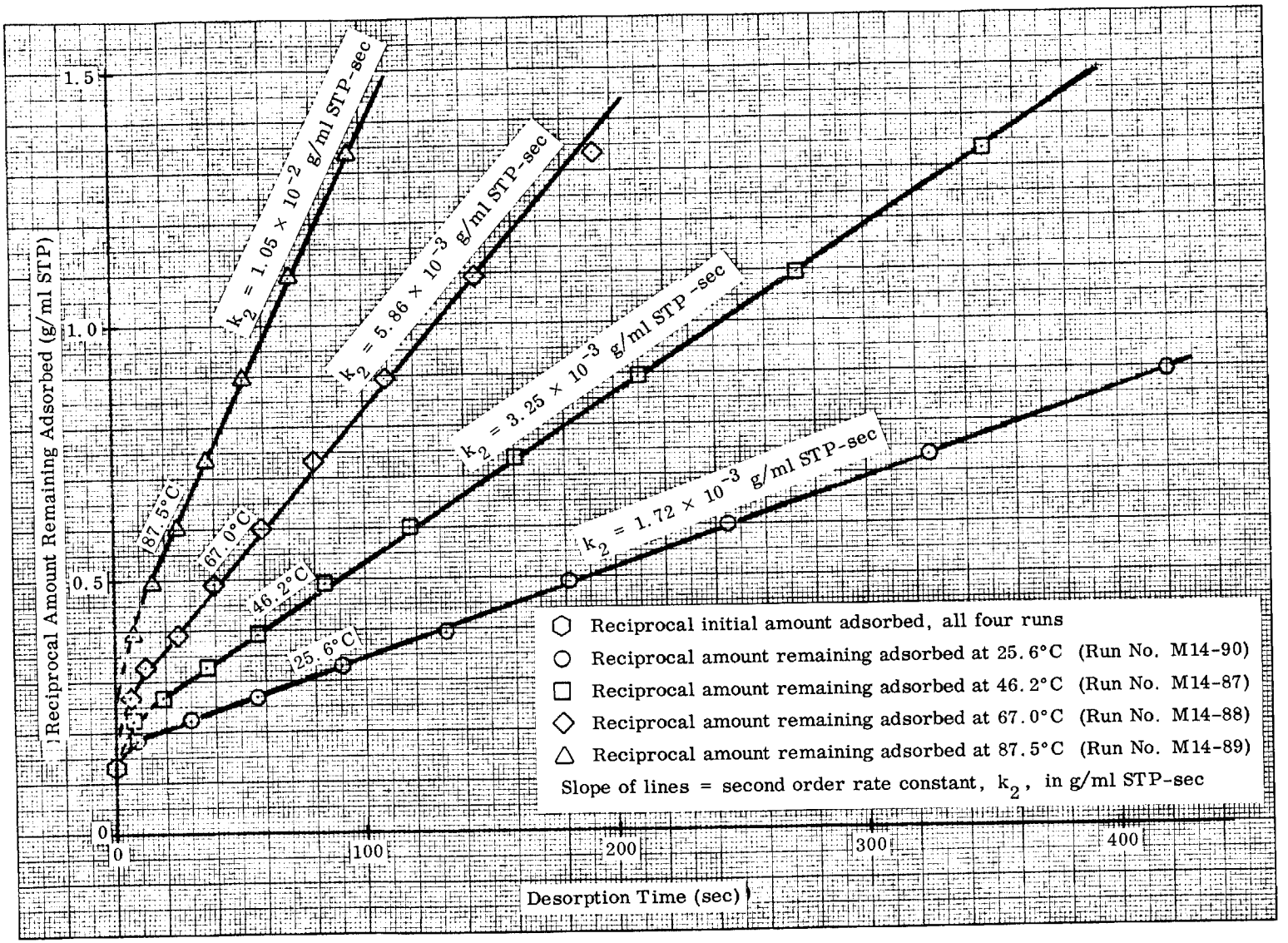

Fig. 6-9 Second-Order Rate Plot for Desorption of n-Butane From BD Activated Carbon

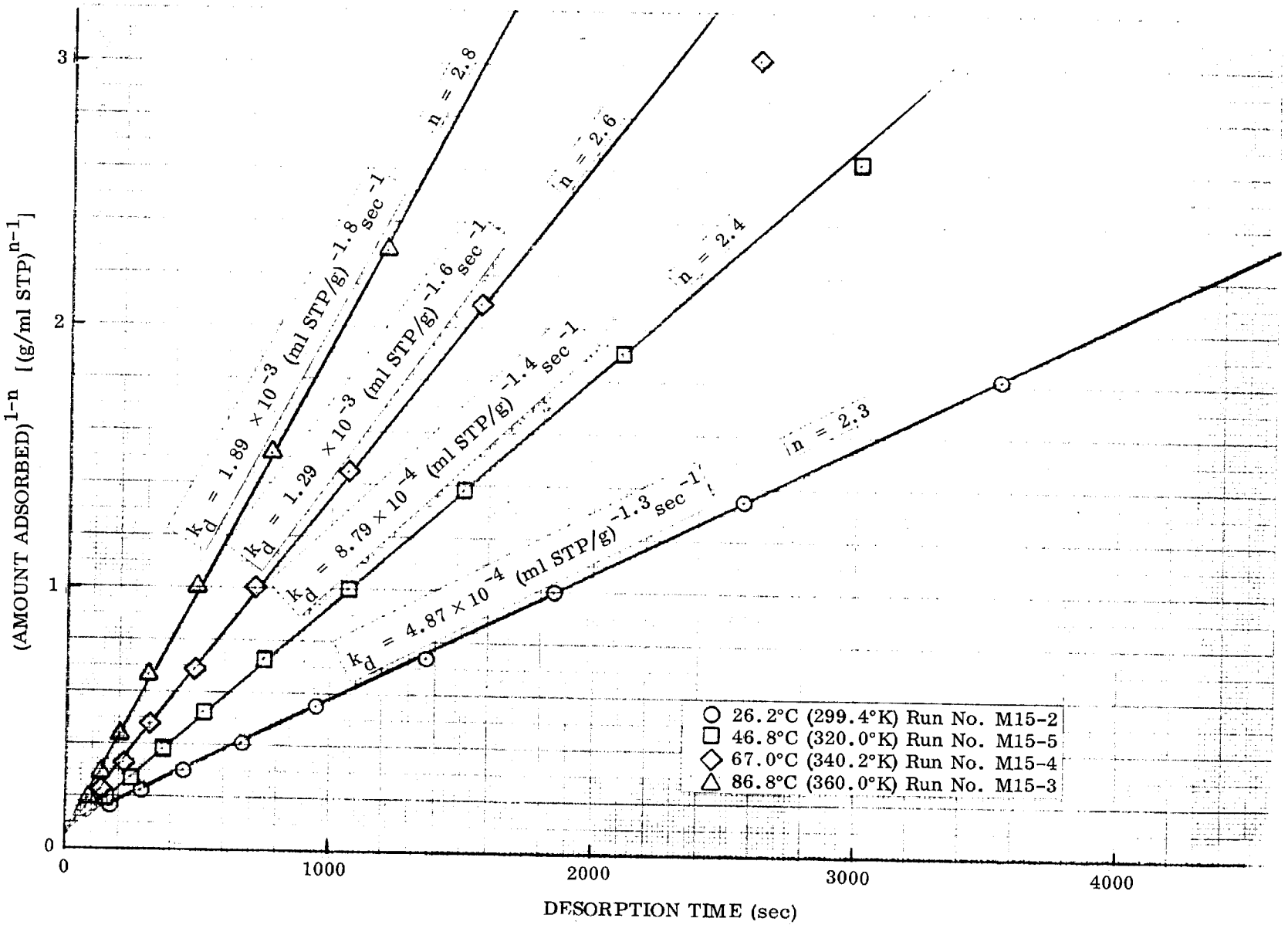

Fig. 6-10 Determination of Rate Constants for Desorption of n-Butane From 0.2 cm BD Activated Carbon Particles

Toluene desorption rate orders were determined for the one set of experiments with 1-mm BD charcoal, in which temperature was varied from 27 to 107°C. Those determined by the method of Appendix L are shown in Fig. 6-11, which is plotted on log-log coordinates with unequal axes in order to bring the slopes of the lines nearer to unity for accuracy. In Fig. 6-12, desorption rates determined from the weight records have been plotted versus the amount remaining adsorbed on log-log coordinates with the latter axis reversed as in Fig. 6-8. In both cases, the rate order varies from 3.5 at 27°C down to 2.6 at 107°C.

The resultant rate orders and rate constants along with the reciprocal slopes of the Freundlich-type isotherms given in section 2.2 are tabulated in Table 6-1 for n-butane and Table 6-2 for toluene.

It has already been shown that the apparent rate order is related to the excess free energy of adsorption, ϕ :

$$n = \frac{V_m \phi}{kT} \tag{4.24}$$

The quantity ϕ may be obtained from the slope of the potential plot (see Fig. 4-3). For toluene, ϕ is constant over a large range of amounts adsorbed and independent of temperature. Thus, Eq. 4.24 gives explicitly the magnitude and temperature dependence of the reaction rate order. In Fig. 6-13 the observed rate orders are plotted as a function of reciprocal temperature and compared to Eq. 4.24 with a value of $\phi = 19.6$ cal/cm^3 calculated from the toluene potential plot. The points are very close to the line, indicating that Eq. 4.24 predicts quantitatively both the value of n and its temperature dependence.

Even though there is no easily recognized temperature dependence in the orders for butane desorption, it is instructive to see how those values compare with the prediction of Eq. 4.24 for n-butane. In this case, there is a slight curvature in the potential plot over the range of interest, but ϕ has been evaluated for the

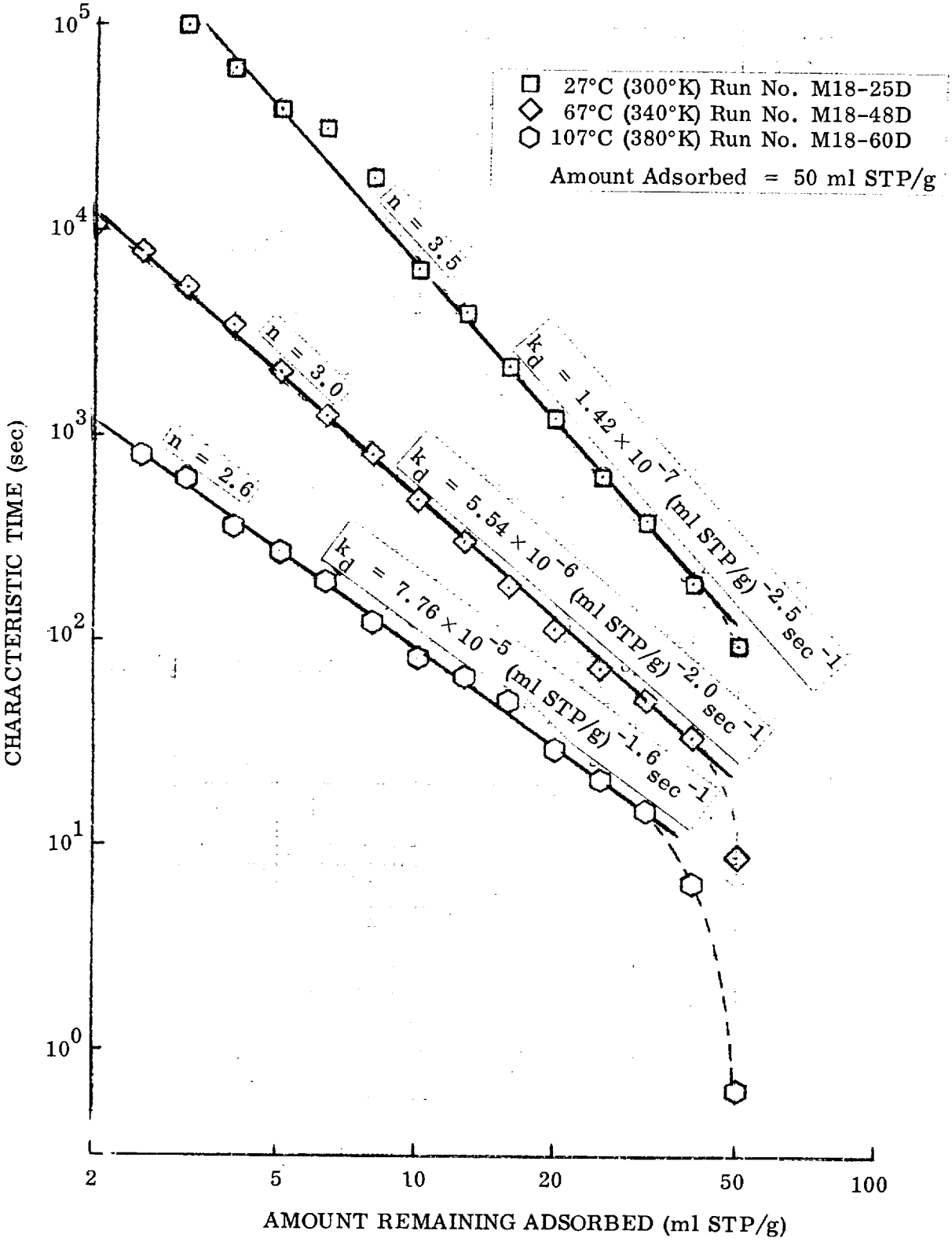

Fig. 6-11 Determination of Rate Order and Constants for Desorption of Toluene From 16 × 20 BD Activated Carbon: Variation With Temperature

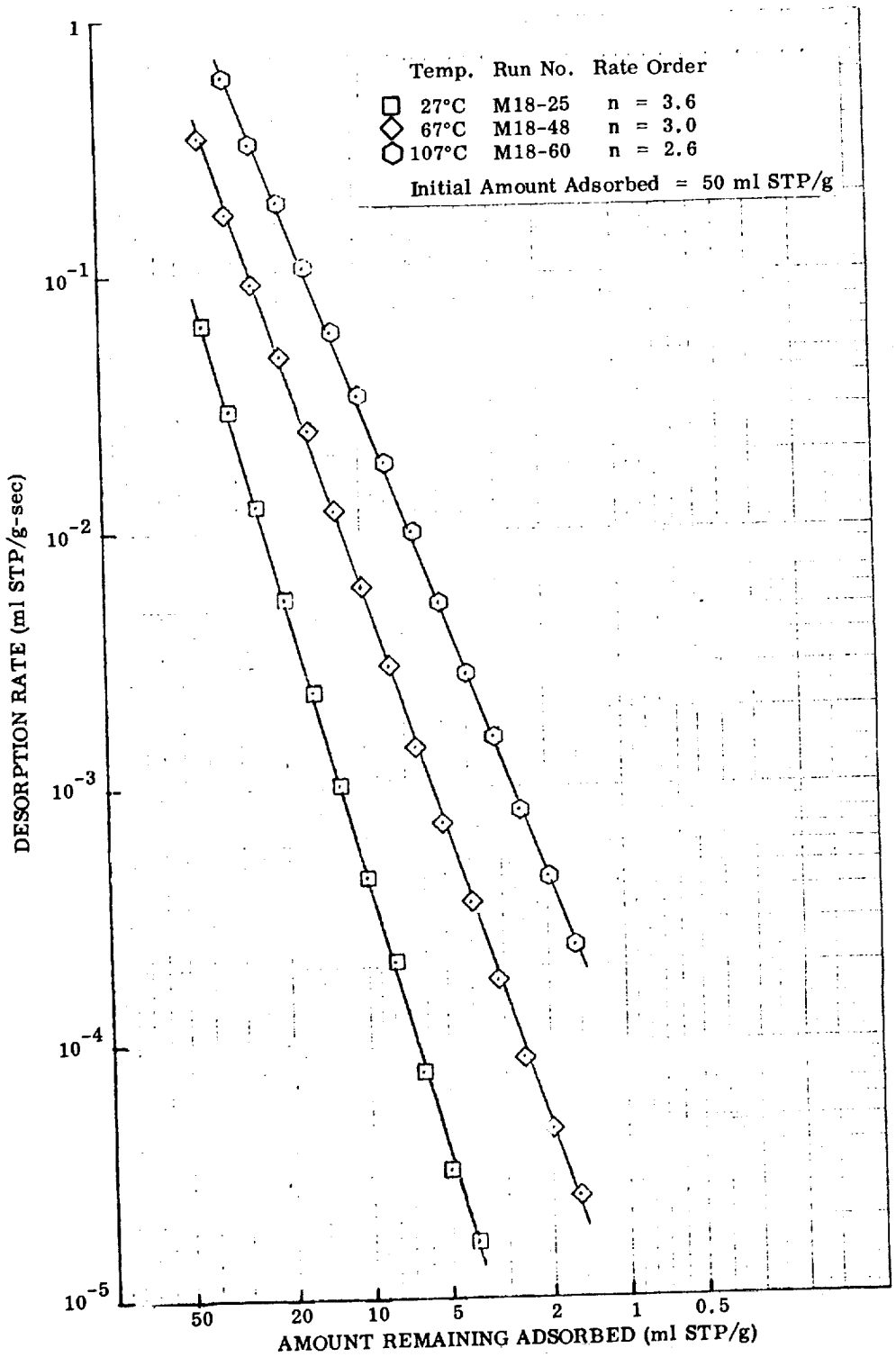

Fig. 6-12 Gravimetric Desorption of Toluene From 16 × 20 BD Activated Carbon: Desorption Rates at Various Amounts Remaining Adsorbed

Table 6-1

SUMMARY OF n-BUTANE DESORPTION RATE EXPERIMENTS
(q_a = 7.7 ml STP/g)

Rate Order (Values of n)					
Nominal Temperature →	27°C	47°C	67°C	87°C	107°C
50 × 70 Mesh, d_p = 0.025 cm	2.0	–	–	–	–
30 × 40 Mesh, d_p = 0.05 cm	2.0 2.5	2.2 –	2.3 2.3	2.2 –	– 2.3
16 × 20 Mesh, d_p = 0.10 cm	2.3	–	–	2.0	–
8 × 12 Mesh, d_p = 0.20 cm	2.3	2.4	2.6	2.8	–

Rate Constants [(ml STP/g)$^{1-n}$/sec]					
Nominal Temperature →	27°C	47°C	67°C	87°C	107°C
50 × 70 Mesh, d_p = 0.025 cm	3.8×10^{-3}	–	–	–	–
30 × 40 Mesh, d_p = 0.050 cm	1.7×10^{-3} 9.0×10^{-4}	3.5×10^{-3} –	6.6×10^{-3} 4.6×10^{-3}	1.2×10^{-2} –	– 1.8×10^{-2}
16 × 20 Mesh, d_p = 0.10 cm	8.5×10^{-4}(a)	–	–	5.4×10^{-3}	–
8 × 12 Mesh, d_p = 0.20 cm	4.9×10^{-4}(b)	8.8×10^{-4}	1.3×10^{-3}	1.9×10^{-3}	–

Reciprocal Slopes of Freundlich-Type Isotherms at q_a = 3.85 ml STP/g (Half-Desorption)					
Nominal Temperature →	27°C	47°C	67°C	87°C	107°C
50 × 70 Mesh, d_p = 0.25 mm	–	–	–	–	–
30 × 40 Mesh, d_p = 0.50 mm	1.84 1.93	2.27			1.59
16 × 20 Mesh, d_p = 1.0 mm	1.93				1.59
8 × 12 Mesh, d_p = 2.0 mm	1.79		1.76		

(a) 4.1×10^{-4} = best fit for n = 2.
(b) 7.0×10^{-4} = best fit for n = 2.

Table 6-2

DATA FOR TOLUENE SORPTION ON 16 × 20 MESH (0.10 cm) BD CHARCOAL

Temperature T (°C)	Freundlich Isotherm Data at 25 ml STP/g*		Overall Desorption Rate Order n	Overall Desorption Rate Constant kd $[(\text{ml STP/g})^{1-n}\text{sec}^{-1}]$	Half Desorption Time $t_{1/2}$ (sec)	Toluene Vapor Pressure P° (torr)	Adsorption Pressure for 50 ml STP/g	
	Slope	1/Slope					Absolute p (torr)	Relative p/P°
27	0.27	3.7	3.5	1.42×10^{-7}	630	32	0.0060	1.87×10^{-4}
67	0.27	3.7	3.0	5.5×10^{-6}	95	177	0.091	5.1×10^{-4}
107	0.27	3.7	2.6	7.8×10^{-5}	23	660	1.070	1.62×10^{-3}

*From Fig. 2-10.

loading equal to one-half the amount initially adsorbed. Also the large particle size (0.20-cm) data have been omitted, since as mentioned earlier there seems to be an increase in the order for these particles relative to the smaller ones. The comparison between these data and values calculated from Eq. 4.24 is also made in Fig. 6-13. Within the experimental scatter of these data, which admittedly is quite large, Eq. 4-24 is again quite adequate using $\phi = 14.6$ cal/cm^3, which was derived as indicated from the appropriate point on the n-butane potential plot.

These quantitative comparisons between rate parameters and equilibrium quantities are confiriming evidence of the generality of the potential-plot correlations and the validity of using them to predict some features of the rate phenomena.

Because of the importance of the effect of particle size on the desorption rate in understanding the details of the desorption mechanism, one series of runs using n-butane was performed specifically to evaluate this dependence. The data for these runs are shown in Fig. 5-6 and 5-7. From these figures, the half-times as a function of particle size can be determined. These are shown in Fig. 6-14. The data included are quite linear with respect to particle size throughout the whole range tested. In section 6.3, it is demonstrated that this implies that the rate-limiting step is desorption from the external surface of the particles, accompanied by rapid surface diffusion within the particles.

6.2 CALCULATION OF APPARENT ACTIVATION ENERGIES

The most direct way to calculate isosteric activation energies for desorption is to plot the logarithm of absolute desorption rate at a given coverage versus reciprocal temperature. The activation energy can then be determined by multiplying the slope of such a plot by the molar gas constant (and by ln 10 to convert the slope to natural logarithms), as shown by a version of the Arrhenius equation

$$E_d = 2.303\, R \left[\frac{d \log r_d}{d\,(1/T)}\right] \qquad (6.7)$$

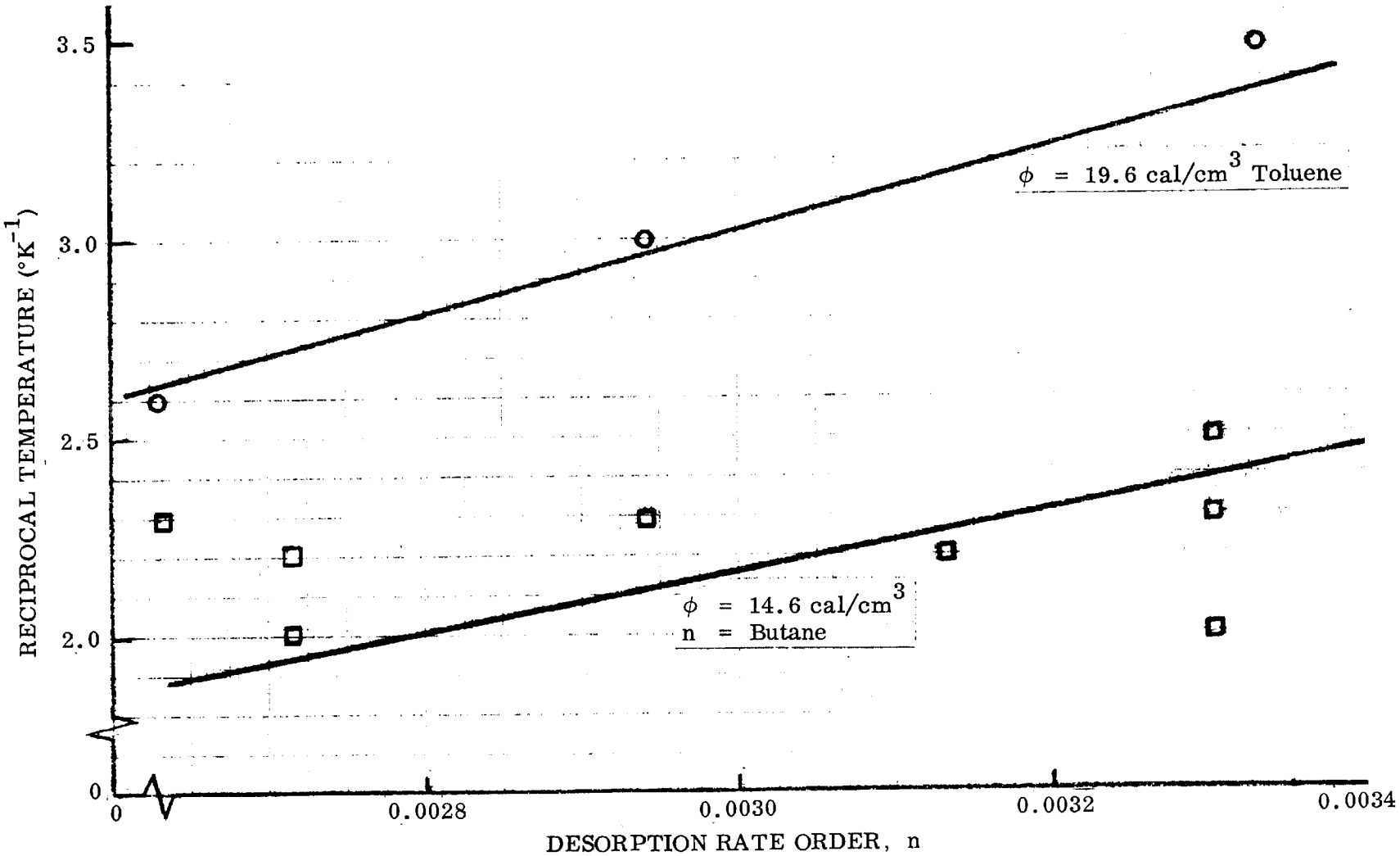

Fig. 6-13 Temperature Dependence of Desorption Rate Order

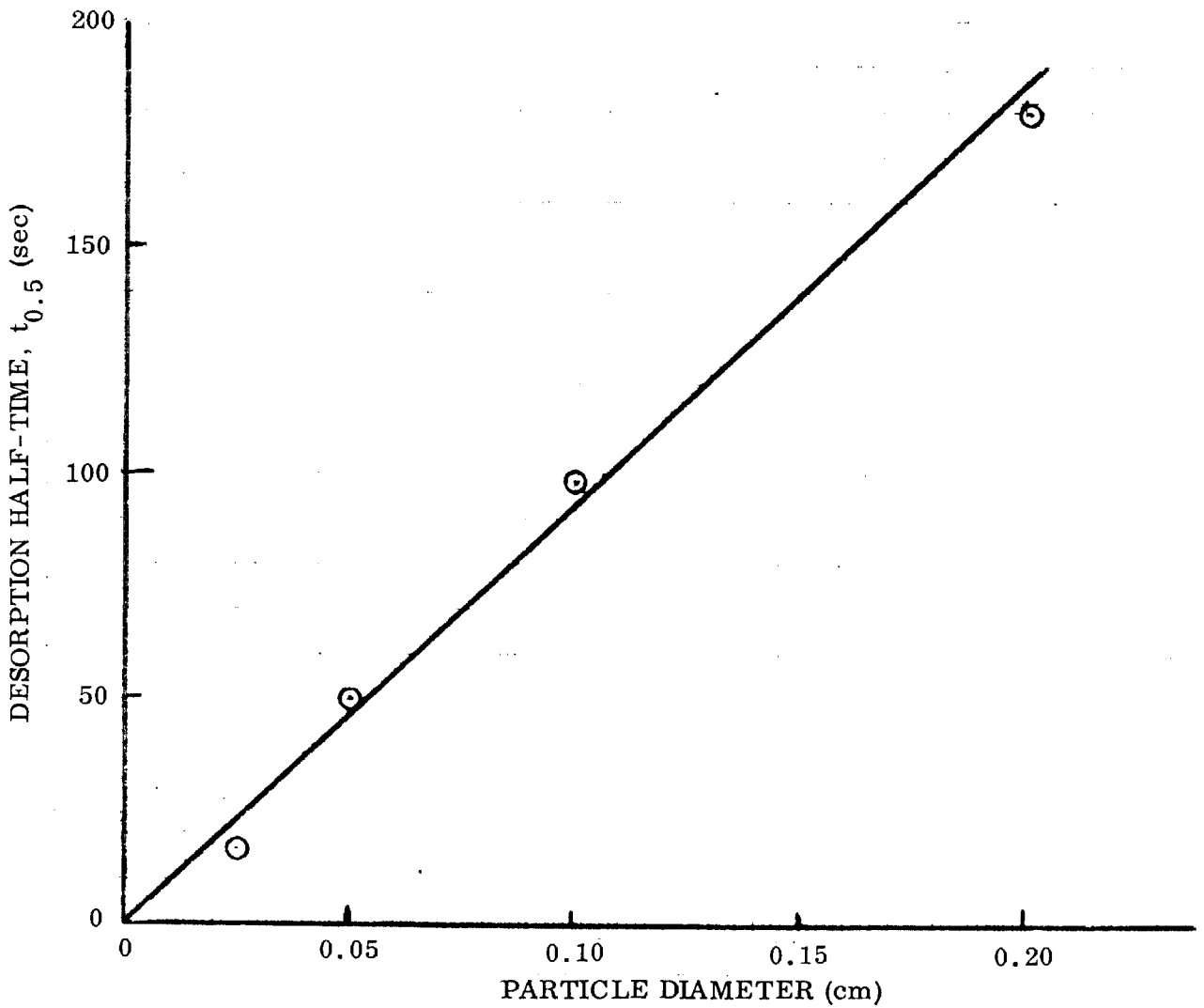

Fig. 6-14 Effect of Particle Size on Desorption Half-Rates of n-Butane on BD Activated Carbon

where

E_d = activation energy of adsorption (cal/mol)
R = gas constant = 1.987 cal/mol°K
r_d = desorption rate (ml STP/g-sec)
t = time (sec)
T = absolute temperature (°K)
q = amount adsorbed (ml STP/g)

This has been done for n-butane on 0.5-mm carbon in Figs. 6-15 and 6-16 for toluene on 1.0-mm carbon in Fig. 6-16. Desorption rate data were taken from Figs. 6-8 and 6-12, respectively.

The apparent activation energies calculated from Figs. 6-15 and 6-16 are tabulated in those figures. The values are only approximate since data for the three temperatures used, 27, 67, and 107°C do not fall exactly in a straight line. These values are somewhat less than the heats of adsorption reported in section 4.2.1 and they increase slightly with decreasing coverage. Adiabatic cooling effects could be responsible for the low apparent activation energies, since at the higher temperatures the individual granules are actually cooled below the nominal furnace temperature in order to supply the energy necessary to desorb the n-butane. Otherwise, it would be expected that the activation energies would always be slightly greater than the isosteric heats, approaching them quantitatively only when the activation energy for adsorption is zero.

6.3 THEORY AND MECHANISMS

In order to interpret the experimental results of the preceding sections, the various possible mechanisms of desorption must be examined. In the desorption of a contaminant from a charcoal granule, there are four possible rate-determining processes:

(1) Pumping speed
(2) Rate of pore diffusion from within the charcoal granule to the external surface

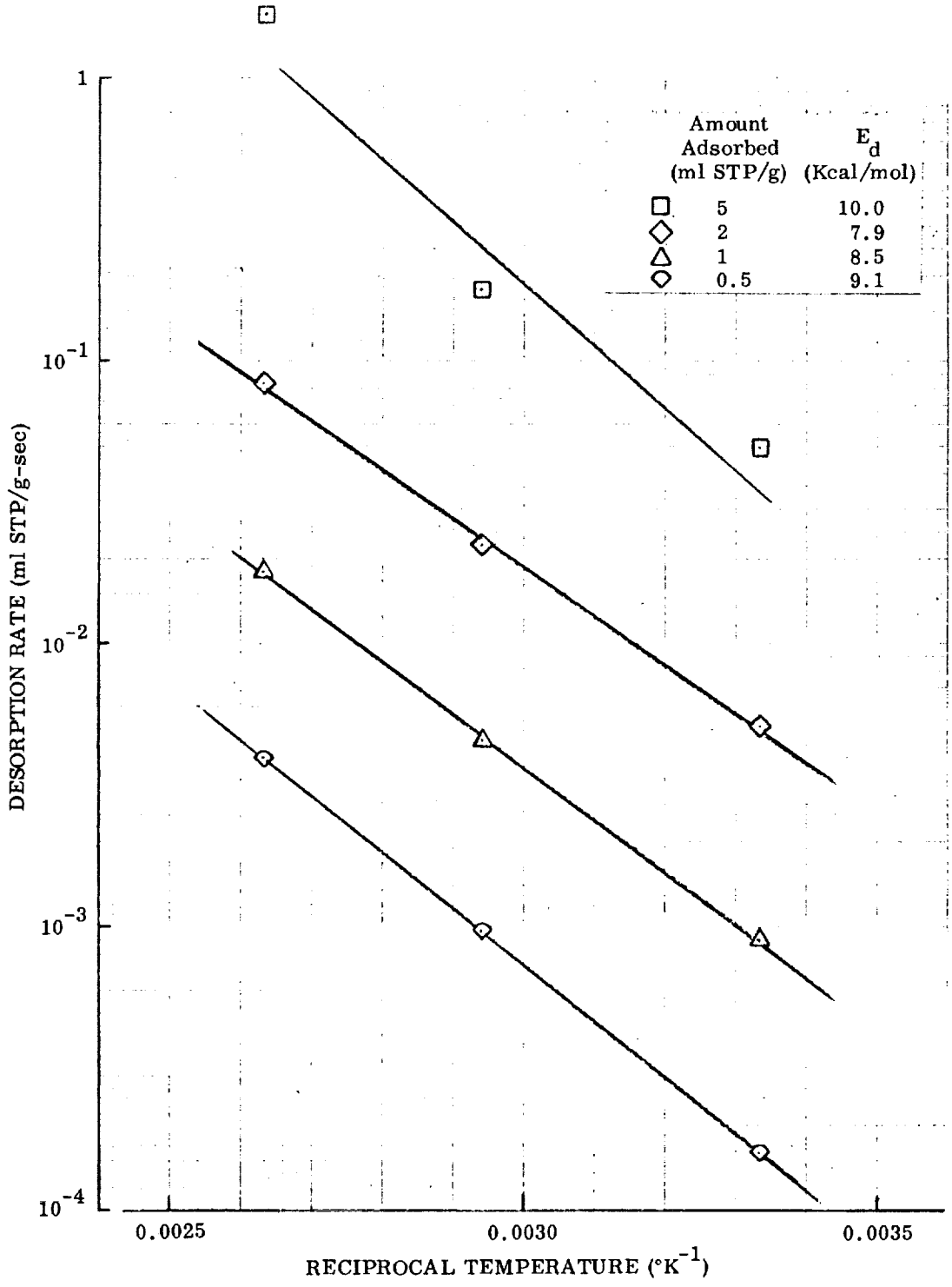

Fig. 6-15 Estimation of Apparent Activation Energy for Desorption of n-Butane From 30 × 40 BD Activated Carbon (d_p = 0.05 cm) at Various Amounts Adsorbed

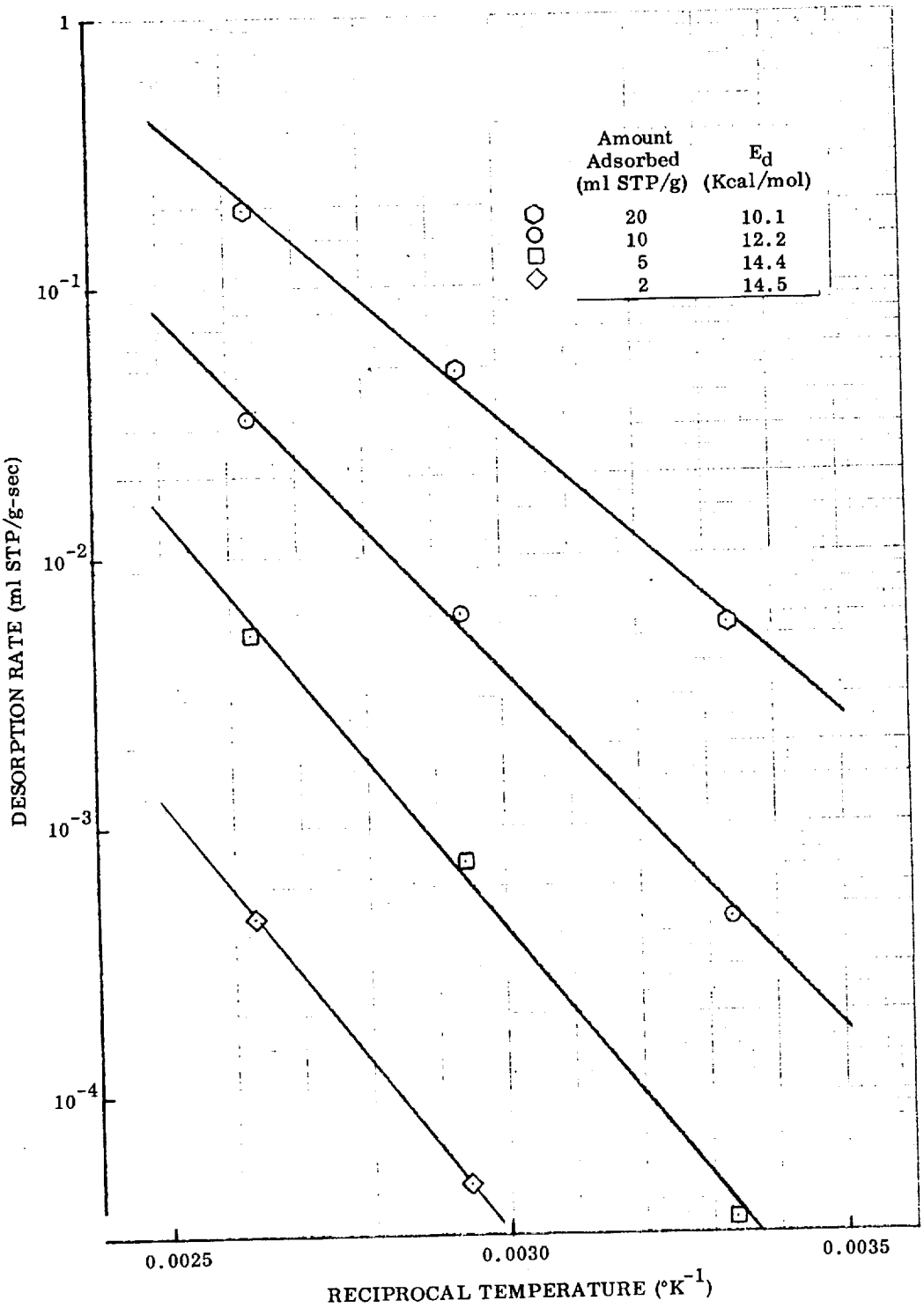

Fig. 6-16 Estimation of Apparent Activation Energy for Desorption of Toluene From 16 × 20 BD Activated Carbon (d_p = 0.10 cm) at Various Amounts Adsorbed

(3) Rapid gas-phase diffusion within the pores, and slower desorption of a molecule from the pore wall into the pore void space

(4) Rate of evaporation from the external granule surface when this is supplied by a very fast surface diffusion along the pore walls

Fortunately, all of these mechanisms but the last one may be eliminated, as described in the following paragraphs.

6.3.1 Pumping Speed Rate-Determining

When pumping speed is controlling, the concentration at the charcoal granule will be related to the equilibrium (isotherm) pressure. Since the total rate of removal equals the pumping speed times the pressure, the rate per unit volume of bed may be expressed as

$$\frac{-dS}{dt} = \frac{\rho_p}{W} S_p c_e(S) \qquad (6.8)$$

where

S =	adsorbent concentration per unit bed volume	(mol/cm^3)
t =	time	(sec)
ρ_p =	particle density	(g/cm^3)
S_p =	pumping speed	(cm^3/sec)
$c_e(S)$ =	gas phase concentration in equilibrium with the adsorbed concentration S	(mol/cm^3)
W =	weight of carbon used	(g)

The above equation shows that the half-time depends on the weight of charcoal used (i.e., on the number of granules used in this particular experiment). Rate will be independent of particle size (for a given weight used) and will depend strongly on temperature, since the equilibrium pressure depends strongly on temperature. The apparent activation energy will be exactly the heat of adsorption. The apparent "order of reaction" will be the order of the Freundlich isotherm. (That is, if the adsorption obeys the Freundlich isotherm with n = 2, desorption will be second order.)

Since in the present work desorption rate depends on particle size (at constant charcoal weight), it appears certain that in the experiments on the microbalance the pumping speed is not rate-determining, and this is checked by experiments in the volumetric system (see section 5.2.3) in which the pumping speed was varied. This possible mechanism can thus be eliminated.

6.3.2 Pore Diffusion Rate-Determining

When diffusion through the pores to the particle surface is controlling, then the time for half desorption can be shown (see Appendix M) to be given by

$$t_{1/2} = K \frac{d_p}{D} \frac{S_o}{c_o} \tag{6.9}$$

where

$t_{1/2}$	=	time for half-desorption	(sec)
d_p	=	granule diameter (presumed spherical)	(cm)
D	=	diffusion coefficient	(cm^2/sec)
S_o	=	initial adsorbed phase concentration	(mol/cm^3)
c_o	=	initial equilibrium gas phase concentration	(mol/cm^3)
K	=	constant which depends on the shape of the adsorption isotherm and which increases as the isotherm becomes more nonlinear (e.g., $K = 0.008$ for the linear isotherm)	

It follows from Eq. 6.9 that for this mechanism the desorption rate is inversely proportional to the square of particle size. The apparent activation energy is exactly equal to the heat of adsorption for the case of gas diffusion through its pores, but for two-dimensional surface migration through the pores the exact activation energy beomces somewhat hazy due to uncertainties in formulating the diffusion equation, although it is certain to be less than the heat of adsorption.

This possible mechanism may be eliminated, since the present work shows the time for half-desorption to be proportional to the first power, not the square, of granule size.

A rate-controlling mechanism of slow surface diffusion in the adsorbed layer to the external particle surface would result in the same dependence on R as above. The expression for $t_{1/2}$ would also be the same, except that D would refer to surface diffusion rather than pore diffusion. The apparent activation energy would be less than ΔH_a. Clearly, this mechanism is ruled out by the same argument as for pore diffusion.

6.3.3 Desorption From Pore Wall Rate-Determining

When the actual surface desorption step from the pore wall into the pore voids is rate-determining, the desorption rate will be independent of granule size, since the charcoal will behave as if its entire surface area were exposed as a plane surface. (That is, by hypothesis, pore diffusion is much faster than desorption.) This mechanism can thus be eliminated since, in the present results, rate depends on granule size.

6.3.4 Desorption From External Granule Surface Rate-Determining

If two-dimensional surface diffusion along the pore wall is very rapid, then a possible rate-determining step is the rate of desorption from the external granule surface, into the gas phase, supported by the very rapid surface diffusion. In Appendix N, it is shown that the rate for this process may be formulated as

$$-\frac{dq}{dt} = (1.98 \times 10^{-3})\frac{273}{T}\frac{\bar{v}}{d_p \rho_p}\,\alpha\, p_e \qquad (6.10)$$

where

q	= adsorbed concentration	(ml STP/g)
T	= temperature	(°K)

$\bar{v}$ = average molecular velocity (cm/sec)

d_p = particle diameter (cm)

ρ_p = bulk density (g/cm^3)

α = sticking coefficient for adsorption (i.e., the probability that a molecule striking the charcoal surface will be adsorbed)

p_e = pressure of adsorbate in equilibrium with the adsorbed concentration q (torr)

The importance of Eq. 6.10 is that it predicts the correct dependence of rate on granule size, and apparently this is the only mechanism that gives the inverse first power of particle size. The only unknown in Eq. 6.10 is α, the sticking coefficient, so that α may be calculated from the experimental rate data. Thus, a severe test of this mechanism is that the absolute value of α must be reasonable (i.e., less than unity but not too small. Sticking coefficients for vapor molecules onto liquid surfaces are known to be in the range 0.02 to 1.0. (See, for example, Wyllie, Ref. 22, p. 389.)

To apply Eq. 6.10 conveniently to the experimental data, if the adsorbate obeys approximately the Freundlich isotherms

$$p_e = k_F q^n \tag{6.11}$$

then the equation may be rewritten

$$-\frac{dq}{dt} = kq^n \tag{6.12}$$

where

$$k = 1.98 \times 10^{-3} \frac{273}{T} \frac{\bar{v}}{d_p \rho_p} \tag{6.13}$$

The time for 50% desorption may then be formulated from standard kinetics as

$$t_{1/2} = \frac{500\,(2^{n-1} - 1)}{(n-1)} \frac{d_p \rho_p q_o}{\bar{v}\,\alpha\, p_e^o} \frac{T}{273} \tag{6.14}$$

where

p_e^o = pressure of adsorbate in equilibrium with the initial amount adsorbed q_o (i.e., the amount adsorbed at zero time) (torr)

From Eq. 6.14, the sticking coefficient α may be calculated for butane at 27°C, using the experimental values for $t_{1/2}$. Since $n = 2$, $\rho_p = 0.86$ g/cm^3, $\bar{v} = 3.3 \times 10^4$ cm/sec, and for the data of Fig. 5-6, $q_o = 7.7$ ml STP/g, $p_e = 9.6 \times 10^{-3}$ torr, $d_p = 0.1$ cm, $t_{1/2} = 96$ sec, α may be computed at 0.0115. Since this is a very reasonable value, this may be taken as confirmatory evidence that the above mechanism is a reasonable one. A similar calculation for toluene desorption at room temperature gives $\alpha = 0.053$, which is also very reasonable.

If similar calculations are made for α at more elevated temperatures, the values turn out lower. For example, at 107°C for toluene the computed value is a factor of almost 10 lower (0.0060). While it is true that energy accommodation is more difficult at higher gas temperatures, it is believed that this decrease in α at the higher temperatures is associated not with energy accommodation but with uncertainties in the temperature brought about by the adiabatic cooling which accompanies the rapid desorption rates observed at higher temperatures.

Further evidence for this particular rate-controlling step is found from the analysis of the entropies of adsorption (see Section 4). The experimentally determined entropies are consistent with a freely mobile adsorbed layer. Such mobility, of course, is necessary for the rapid surface diffusion which the kinetics of desorption suggests.

A summary of factors relating to these various mechanisms for vacuum desorption from single particles is presented in Table 6-3.

6.4 COOLING EFFECTS

All the possible mechanisms discussed in the last section predict an apparent activation energy equal to the heat of adsorption,* essentially because for each mechanism the

*Actually, the last mechanism discussed, desorption from the external surface of the particle, predicts an activation energy somewhat higher than q_{st}, since α is most likely a function of temperature.

Table 6-3

KINETICS OF VACUUM DESORPTION FROM SINGLE GRANULES

Possible rate-determining mechanism[a]	Dependence of rate on particle size, d_p	Time for 50% desorption, $t_{1/2}$
Pumping speed	Independent, but depends on weight of particles used	$\frac{w}{\rho_p}\frac{1}{S_p}\frac{S_o}{c_o}$
Gas diffusion in pores	$1/d_p^2$	$K^*\frac{d_p^2}{D_K}\frac{S_o}{c_o}$ [b]
Evaporation from internal pore wall with very fast gas diffusion in pores	Independent of particle size	$1/k_d$
Evaporation from granule surface fed by fast surface diffusion	$1/d_p$	$\frac{1}{6}\frac{d_p}{k_A}\frac{S_o}{c_o}$

(a) For these mechanisms, apparent activation energy = ΔH_a = enthalpy of adsorption.

(b) K^* is a numerical constant depending on the shape of the adsorption isotherm.

rate is proportional to the equilibrium pressure, at a given loading of adsorbate. Since at constant loading of adsorbate, the change in equilibrium pressure with temperature is given by

$$\frac{d \ln p}{d(1/T)} = -\frac{q_{st}}{R} \tag{6.15}$$

it follows that the desorption rate will also have q_{st} as its apparent activation energy. Here, q_{st} is the isosteric heat of adsorption. Physically, this corresponds to the

fact that the adsorbed molecule must acquire its heat of adsorption before it can desorb, so that the activation energy should be at least this large.

Experimentally, however, the apparent activation energy is much less than the heat of adsorption, e.g., for n-butane the initial apparent activation energy is 10 kcal/mol or less, while the heat of adsorption is 12−14 kcal/mol. (See sections 4.2 and 6.2.)

This dilemma may be resolved if one assumes that at elevated temperatures the granules are not at the furnace temperature but at some lower temperature. Using the furnace temperature to compute activation energies in such cases would result in apparent activation energies somewhat lower than the correct values.

The charcoal granules can be colder than the furnace temperature for either of two reasons: (1) poor furnace design, so that the granules are not completely surrounded by the furnace, and (2) adiabatic cooling during desorption. The former can be eliminated from consideration, since the same furnaces are used to measure the adsorption isotherms, so that too low an isosteric heat of adsorption would also be measured. Also two different sets of furnaces have been used. The most likely explanation is that there exists an adiabatic cooling of the granules due to the loss of the heat of desorption as desorption proceeds. If the charcoal granule were completely thermally isolated from its surroundings, the cooling effect due to evaporation of adsorbate would be, from a simple heat balance,

$$(\Delta T)_{ad} = \frac{(q_{st})\, q_o}{22.4 \times C_s} \tag{6.16}$$

where

$(\Delta T)_{ad}$ = adiabatic temperature drop due to evaporation of adsorbate (°C)
q_{st} = heat of adsorption (kcal/mol)
C_s = heat capacity of the charcoal (cal/g°C)
q_o = initial amount of adsorbate adsorbed (ml STP/g)

For butane with q_o = 7.7 ml STP/g, C_s = 0.17 cal/g°C, q_{st} = 12 kcal/mol, the adiabatic cooling effect is 24°C. For toluene with the larger loading, q_o = 50 ml STP/g, and the larger heat of adsorption (about 16.5 kcal/mol), the adiabatic temperature drop would be 217°C.

In a given experiment, only part of these large adiabatic drops will be realized due to heating of the granule during the desorption by radiation and conduction. If the time constant for desorption (e.g., time for 50% desorption) is much shorter than the time constant for radiative and conductive heating, then most of the adiabatic drop will be observed. Conversely, if the desorption time constant is much longer than the radiative heating time constant, then very little temperature drop will occur.

The equation of heat balance which determines this is

$$-\rho_p(\pi d_p^3/6)C_s(dT/dt) = \rho_p(\pi d_p^3/6)\frac{\Delta H_d}{22.4}(-dq/dt) - (\pi d_p^2)K(T_o - T) \qquad (6.17)$$

where

ρ_p	=	sorbent particle density = 0.86	(g/cm^3)
d_p	=	effective sorbent particle diameter	(cm)
dT/dt	=	cooling rate	(°C/sec)
$-dq/dt$	=	desorption rate	(ml STP/g-sec)
K	=	rate of heat input to sorbent from surroundings per unit area and per unit temperature difference due to radiation and conduction	
T_o	=	temperature of surroundings	(°C)
C_s	=	heat capacity of sorbent	(cal/g°C)
ΔH_d	=	heat of desorption	(kcal/mol)

The left side of Eq. 6.17 is the rate of heat loss from a single granule from the standpointof heat capacity and temperature drop. The right side is the net difference between the energy loss due to evaporation and the energy gain due to radiation and conduction from the surroundings.

At pressures of 10^{-3} torr and lower, which are typical during vacuum desorption, calculation shows that gaseous heat conduction is negligible as compared with radiation, in determining the value of K in the above equation. Thus, K is determined by the relation

$$K(T_o - T) \cong \epsilon\lambda(T_o^4 - T^4) \simeq 4\,\epsilon\lambda\, T_o^3(T_o - T) \tag{6.18}$$

where

ϵ = emissivity of sorbent surface (assume = 1)

λ = Stefan-Boltzmann constant = 5.67×10^{-5} g/cm-sec^3°K^4

K = as above, but in cgs units (erg/cm^2 sec°K)

Equation 6.17 may be rearranged to

$$-\frac{dT}{dt} = A\left(-\frac{dq}{dt}\right) - D(T_o - T) \tag{6.19}$$

where

$$A = \frac{\Delta H_d}{22.4\, C_s} \tag{6.20}$$

$$D = \frac{24}{d_p}\frac{\epsilon\lambda\, T_o^3}{\rho_p C_s} \times 2.39 \times 10^{-8} \tag{6.21}$$

In Eq. 6.21 D is the inverse of the time constant for radiative heating of a sorbent granule. For 0.1-cm particles with the emissivity ϵ taken as 1.0, this time constant works out to be about 33 sec. Since the time for 50% desorption at temperatures above room temperature is of this order or smaller for both butane and toluene, it appears that a significant adiabatic cooling effect can be expected. The full temperature history of a granule during desorption can be obtained by integrating Eq. 6.19. Since this is

linear and of first order, it may be immediately integrated. It is convenient to eliminate time in favor of q by the relation

$$\frac{dT}{dt} = \frac{dT}{dq}\frac{dq}{dt}$$

The solution of Eq. 6.18 then becomes.

$$\frac{T_o - T}{(\Delta T)_{ad}} = \exp\left[D \int - \left(\frac{dq}{dt}\right)^{-1} dq\right] \int_{\frac{q}{q_o}}^{1} \exp\left[- D \int - \left(\frac{dq}{dt}\right)^{-1} dq\right] d\left(\frac{q}{q_o}\right) \quad (6.22)$$

where $(\Delta T)_{ad}$ is the adiabatic temperature drop equal to $A q_o$ which would be observed when $D = 0$ (i.e., for a pellet completely thermally isolated from its surroundings). Numerical integration of Eq. 6.22 can be carried out using the experimental data for $- dq/dt$.

For first-order desorption kinetics, i.e.,

$$- \frac{dq}{dt} = k_d q \quad (6.23)$$

Equation 6.22 may be integrated in closed form to give the simple result

$$\frac{T_o - T}{(\Delta T)_{ad}} = \frac{1}{1 - D/k_d}\left[\left(\frac{q}{q_o}\right)^{D/k_d} - \frac{q}{q_o}\right] \quad (6.24)$$

Equation 6.24 confirms the intuitive guess that the main factor in determining the adiabatic cooling effects is the ratio of time constants, D/k_d. In Fig. 6-17, Eq. 6.24 is plotted, each curve corresponding to a different value of D/k_d.

Figure 6-17 indicates that significant adiabatic cooling effects can be expected even when the radiative time constant is four times larger than the reaction rate time constant. This curve (for $D/k_d = 4$) rises to only about 15% of the full adiabatic cooling effect, but for toluene this amounts to over 30°C of cooling since $(\Delta T)_{ad}$ is over 200°C.

The value of D/k_d has been calculated from the actual data representative of those runs used for evaluation of the activation energy. For n-butane, D/k_d is about 3.5 (Run No. M19-27). This results in a maximum temperature drop of around 4°C. This seems hardly enough to explain the large discrepancy between the desorption activation energy and the isosteric heats. Nevertheless, it is obvious that the adiabatic cooling even for n-butane is not entirely negligible.

In the case of toluene, D/k_d is about 6.3 (Run No. M18-48). The maximum temperature drop in this case, however, is about 20°C, since the adiabatic temperature drop is much higher for toluene (200°C). Such an error in the temperature would most assuredly affect the activation energy. Thus, for toluene the adiabatic cooling is obviously sufficient to account for the low apparent activation energies. Before applying Eq. 6.21 in detail to the experimental data however, it may be apparent to perform a relatively simple experiment in which a thermocouple is inserted directly into a charcoal granule and the cooling effect during desorption is actually measured.

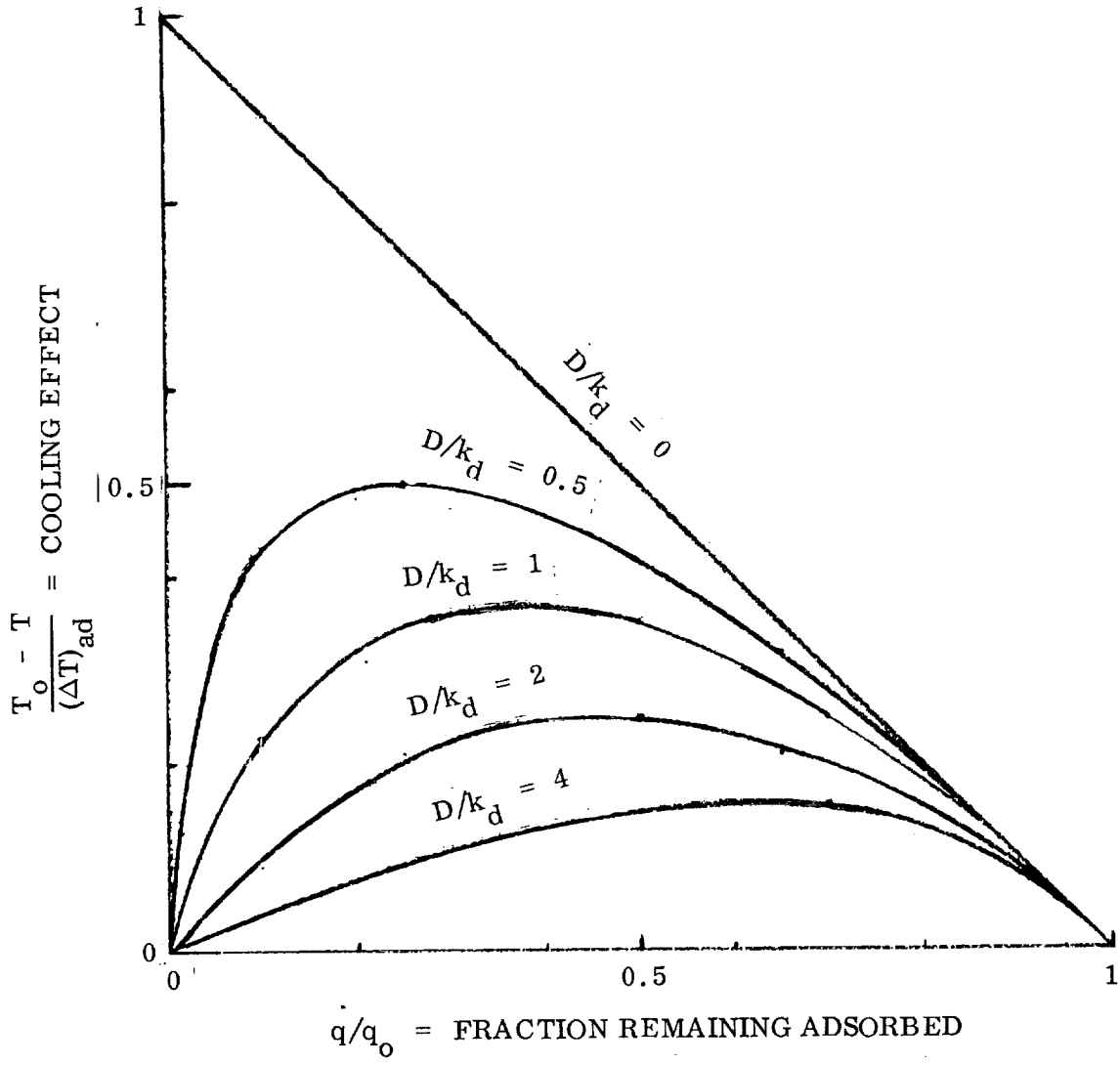

Fig. 6-17 Cooling Effect as a Function of Fraction Remaining Adsorbed for Various Ratios of Radiative Time Constant to First-Order Desorption Rate Constant

Section 7

VACUUM DESORPTION FROM ACTIVATED CARBON BEDS

Sections 5 and 6 dealt with the effects of vacuum upon single particles of activated carbon under various conditions of temperature, particle size, and contaminant species. In order to extrapolate these effects from the single particle case to the packed bed situation, it was necessary to obtain some typical data on desorption from such beds. To this end, a number of experiments were conducted in which, after saturation of the bed with one or more contaminants in a flowing stream of air, the bed was subjected to vacuum for varying lengths of time. In early experiments, the effectiveness of this procedure was measured at only one point, after a given vacuum desorption time, by desorbing the remaining contaminants in a gas stream, usually at elevated temperatures. Later refinements of the experimental method permitted determination of the amount desorbed for more than one contaminant at a number of points in the vacuum desorption, thus condensing the work of many long, tedious experiments into single ones. In addition, a number of experiments on diffusion of gases through such beds were performed in order to have necessary data to test various desorption models suggested below.

Using the data presented in Section 5 and 6 and in this section, it was then possible to formulate a model for desorption of contaminants from packed beds. Using this model, it should then be possible to extrapolate desorption data from a few key experiments to the case of practical-sized packed beds for use in spacecraft contaminant removal systems.

7.1 EXPERIMENTAL TECHNIQUES

The initial vacuum desorption system used in Phase 1 is shown in Fig. 7-1. The system between the bed and diffusion pump was constructed of 5/8-in. OD copper tubing

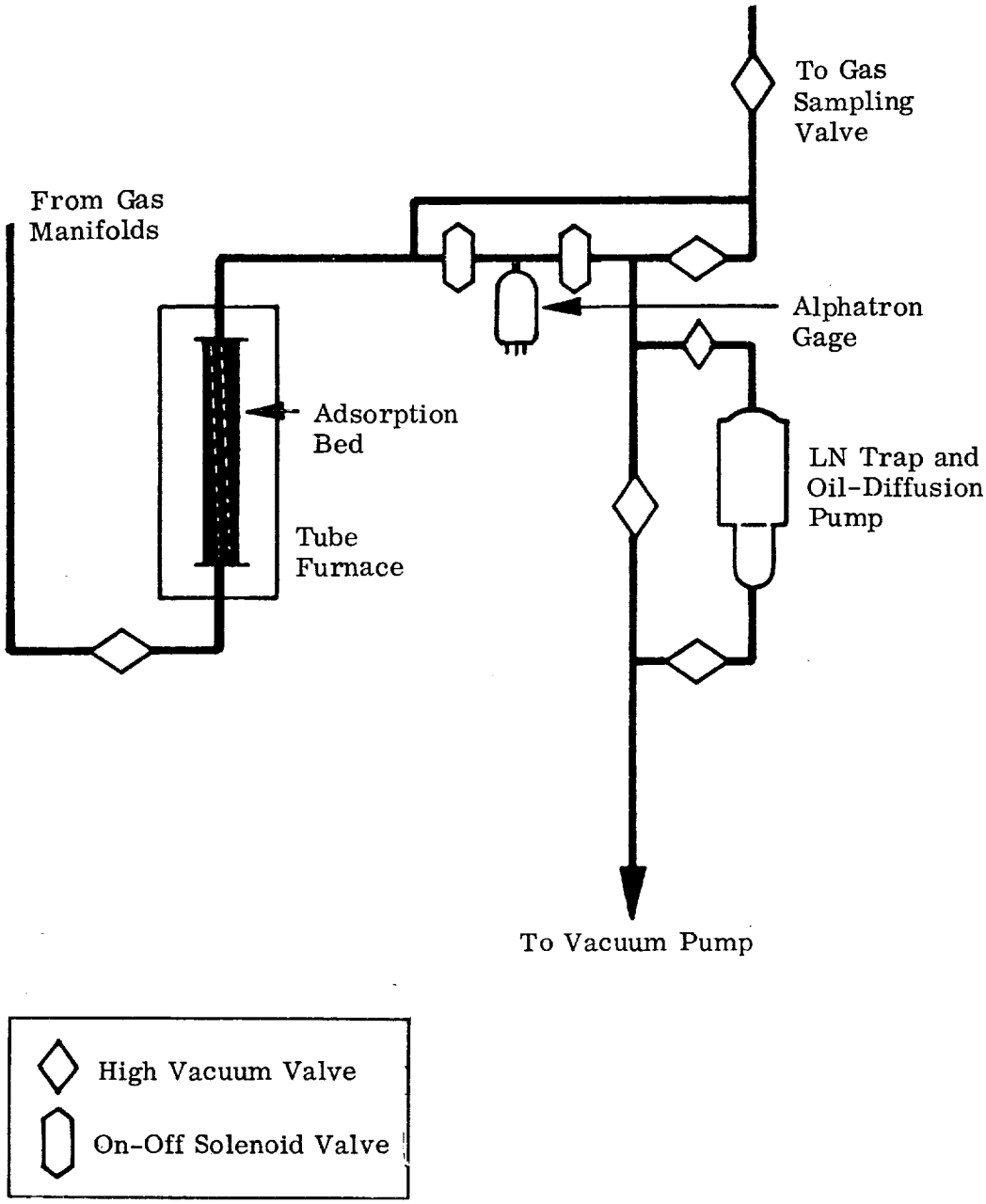

Fig. 7-1 High Vacuum System Used in Phase 1 (see Fig. 2-1)

with sweat-soldered fittings in order to provide high conductance for vacuum desorption of the bed. To simulate space vacuum, the system consisted of a Veeco 2-in. oil-diffusion pump with a liquid nitrogen trap, plus associated valves and roughing pump. Vacuum desorption pressure was monitored with an NRC Model 530 Alphatron gauge, whose minimum pressure sensitivity is 1×10^{-5} torr.

To increase data collection efficiency, the vacuum desorption system was modified in Phase 2 of the present work. The 5/8-in. OD copper tubing and 2-in. Veeco diffusion pump were replaced by 1-in. OD glass tubing and a 4-in. oil diffusion pump (see Fig. 7-2). The system also contained two large glass cold traps, connected in parallel, to allow continuous collection of all desorption products. All the pertinent bed dimensions, such as length, diameter, and particle size, are summarized in Table 7-1.

During a vacuum desorption experiment, pressure at the high vacuum (downstream) end of the bed is measured by a Hastings DV-6 gauge (down to 1 micron) and by a Veeco RG-3 ionization gauge below 1 micron. At the high pressure end of the bed (upstream end), pressure is monitored by a Hastings DV-6 gauge.

7.1.1 Single-Component Desorption

The first step in the experimental procedure, leading to vacuum desorption, is saturation of the bed with some contaminant to a known amount (see section 2.1). At the conclusion of the flow adsorption, the bed is isolated by closing two high-vacuum valves upstream and downstream of the bed.

In Phase 1 of the work, the vacuum desorption was performed by pumping, first with the roughing pump and then with the oil diffusion pump, according to standard vacuum system procedure. Desorption time was measured from the time at which the roughing valve was first opened. The desorption step was terminated by closing the valve to the diffusion pump. To determine the amount of material vacuum desorbed

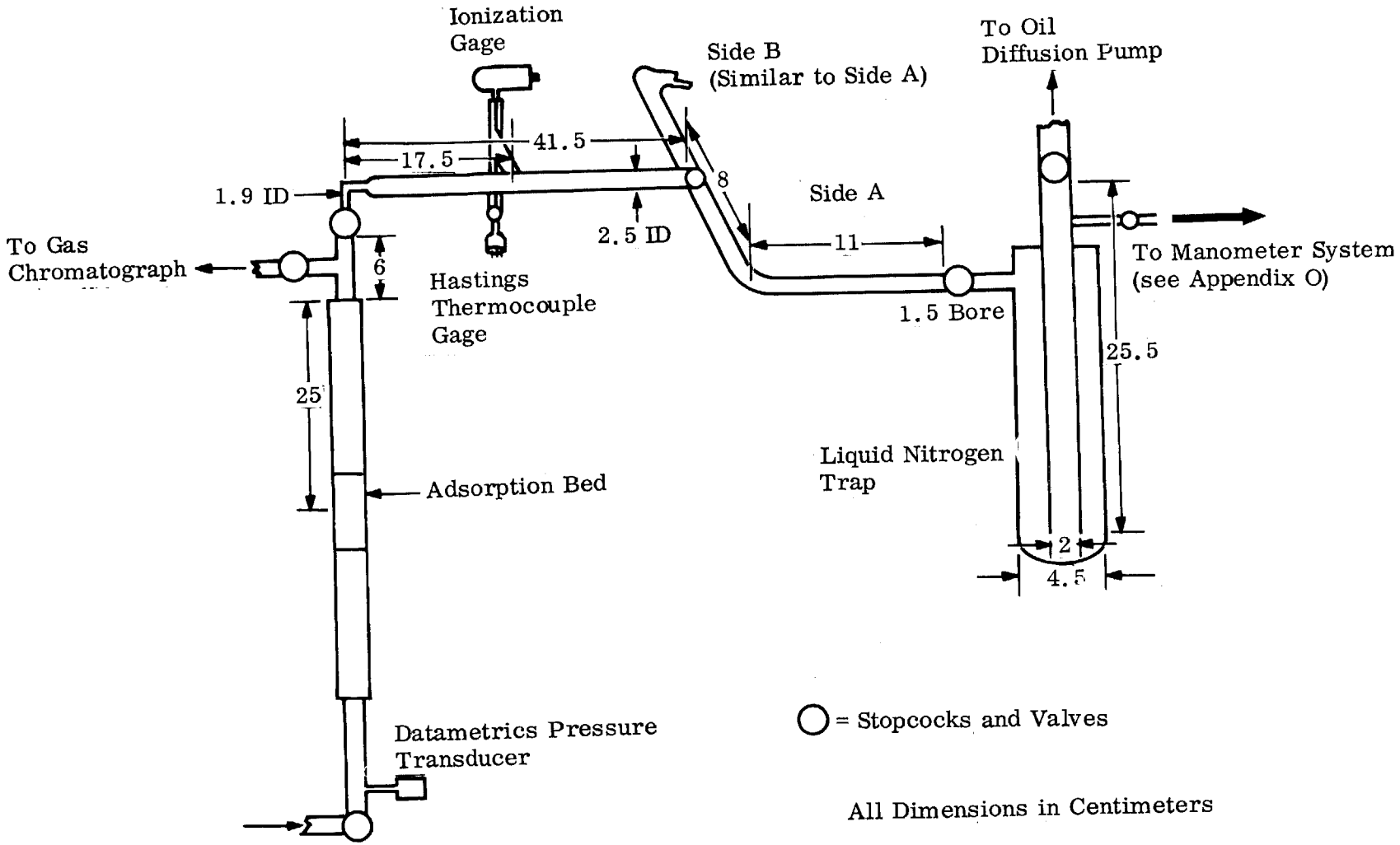

Fig. 7-2 High Vacuum Desorption System

Table 7-1

DESORPTION HALF-TIMES

Run No.	d_p (cm)	T (°K)	L (cm)	Species	$t_{1/2}$ Exp. (min)	$t_{1/2}$ Calc (min)	D (cm)	Remarks
F5-1 to -6	0.05	298	10.9	C_3H_8	575	430	0.493	
F-9-1, F11-1 to -3	.05	298	4.8	$n\text{-}C_4H_{10}$	3150	1170	.493	
F14-1	.2	298	4.6	$n\text{-}C_4H_{10}$	270	226	.493	Quartz Chips
F13-2[a]	.2	298	4.45	$n\text{-}C_4H_{10}$	520	446	1.65	
F15-1[a]	.2	298	4.5	$n\text{-}C_4H_{10}$	520	446	1.65	
F15-2[a]	.2	298	4.5	$n\text{-}C_4H_{10}$	520	446	1.65	
F16-1	.2	298	8.0	$n\text{-}C_4H_{10}$	1650	1435	1.65	Long Bed
F17-1	.2	379	4.4	C_7H_8	1000	1240	1.65	
F17-2	.2	380	4.4	$n\text{-}C_4H_{10}$	32	31.4	1.65	
F17-3	.2	380	4.4	C_7H_8	1060	1240	1.65	
F17-3	.2	380	4.4	$n\text{-}C_4H_{10}$	9	8.5	1.65	
F17-4	.2	340	4.4	$n\text{-}C_4H_{10}$	6	3.5	1.65	
F17-4	.2	340	4.4	C_7H_8	4200	3100	1.65	

(a) All three runs averaged.

some time t , the bed was completely flow desorbed as described in section 2.1.1, and the amount vacuum desorbed was determined by taking the difference between flow adsorption and flow desorption. This same procedure had to be repeated several times, with a different value for time t , to establish a full curve for the amount desorbed with time (see Fig. 7-3). To eliminate this tedious repetition procedure, it was decided to modify the vacuum desorption system for the Phase 2 work, so that one complete desorption curve was obtained with each run. The experimental procedure for preparation of the bed and the amount adsorbed were the same in both cases. The main difference occurred during vacuum desorption. The rate of vacuum desorption was continuously measured by condensing any desorbed contaminant in one of the two liquid-nitrogen traps (see Fig. 7-2). After a measured time interval, the cold trap was isolated by two stopcocks, and the other trap, in parallel, was opened to the vacuum lines. After isolation of the first trap, it was warmed up and any condensed material was transferred into the calibrated volumetric system by use of liquid nitrogen, and isolated (see Appendix O).

If the contaminant was, say, n-butane, the volumetric system was allowed to warm up and the pressure measured by the manometer (see Fig. 7-2). In cases where low vapor pressure gases were used, such as toluene, and the contaminant was a liquid at room temperature, a special small-bore stopcock and associated tube were used. In this procedure, the condensed material was isolated from the system by closing the small stopcock; then the tube and stopcock were removed from the system and weighed on an analytical balance. Since the tare weight was predetermined, the amount of material condensed could be calculated (see Appendix P).

7.1.2 Two-Component Desorption

All the work on mixed desorption from packed beds was done in Phase 2. The versatility of the new desorption system made this possible.

The general procedure for mixed adsorption was similar to that used earlier for single-component, flow-adsorption vacuum desorption. A mixed stream of 26.9 ppm n-butane

and 26.8 ppm toluene in 50% oxygen/50% nitrogen was admitted to the adsorption bed. The average flow rate through the bed was 936 ml RTP/min, and was very close to the flow rate used in previous single adsorption experiments with butane and toluene.

The general procedure for obtaining vacuum desorption data was similar to that used in previous desorptions; namely, the contaminants desorbed from the bed were condensed in a large liquid nitrogen trap. To obtain a desorption point, the trap was isolated from the main desorption stream and warmed up to room temperature. The trap was then opened to a manometer system and all the contaminants were recondensed into a small trap with a stopcock. The trap was slowly warmed up to -22 °C (carbon tetrachloride slush) and held at this temperature until the butane had expanded to its maximum volume (pressure). The above-mentioned temperature was chosen because at that temperature the vapor pressure of n-butane is about 400 torr while that of toluene is less than 10 torr. Thus, a fairly efficient one-stage flash evaporation is achieved. Good mass-balance results obtained with toluene indicated that reasonable separation was achieved by this procedure. Finally, the stopcock on the collecting tube was closed and the tube with the toluene was weighed.

7.1.3 Three-Component Desorption

To analyze for the composition of the vacuum desorbed material, the following procedure was adopted. As before, the sample was collected in a liquid nitrogen-cooled cold trap in the pumping line. This main trap was warmed to room temperature and was then opened to an auxiliary removable cold trap. After condensing in the removal trap, the sample was transferred to a previously evacuated 5-liter calibrated flask. All the condensed gases were expanded in the known volume and the total pressure brought up to 1 atm with helium. After allowing sufficient time for homogeneous mixing of all the gases, 1-ml gas samples were taken and injected into the chromatograph. Using this procedure, it was found that all the Freon-12 was vacuum desorbed in just a few minutes and all the n-butane was desorbed within 30 min.

7.2 RESULTS ON SINGLE CONTAMINANTS

All the data on vacuum desorption are summarized in Table 7-1.

The total desorption curve at 25°C was described by the flow experiments F5-1, -2, -3, -4, -5, and -6, and the data are shown in Fig. 7-3. An initial theoretical model for the desorption process based on Knudsen pore diffusion, which was proposed in the Phase 1 report (Ref. 23),

$$q_r/q_a = \frac{8}{\pi^2} \sum_{n=0}^{\infty} (2n + 1)^{-2} \exp - \left[k't(2n + 1)^2 \right] \qquad (7.1)$$

where

k' = a constant = $D'_K \pi^2/4\tau\ell'^2$
q_r = amount remaining adsorbed
q_a = amount originally adsorbed
n = an integer
t = time (sec)
D'_K = an effective diffusivity (cm^2/sec)
τ = reciprocal of a desorption rate constant (sec)
ℓ' = effective bed length = $\ell(1 - \epsilon)$ (cm)
ϵ = void function

was used to predict a desorption rate curve. A comparison of this curve with experimental data is shown in Fig. 7-4.

An initial set of experiments was conducted on the vacuum desorption of n-butane from a 30 × 40-mesh (0.05 cm) charcoal bed at 25°C. This work was done in Phase 1, and the data are shown in Fig. 7-5. To verify the effect of particle size as predicted by the theory of desorption described in section 7.5, more desorptions were run using n-butane adsorbed on an 8 × 12-mesh (0.2 cm) charcoal bed. The consistency of

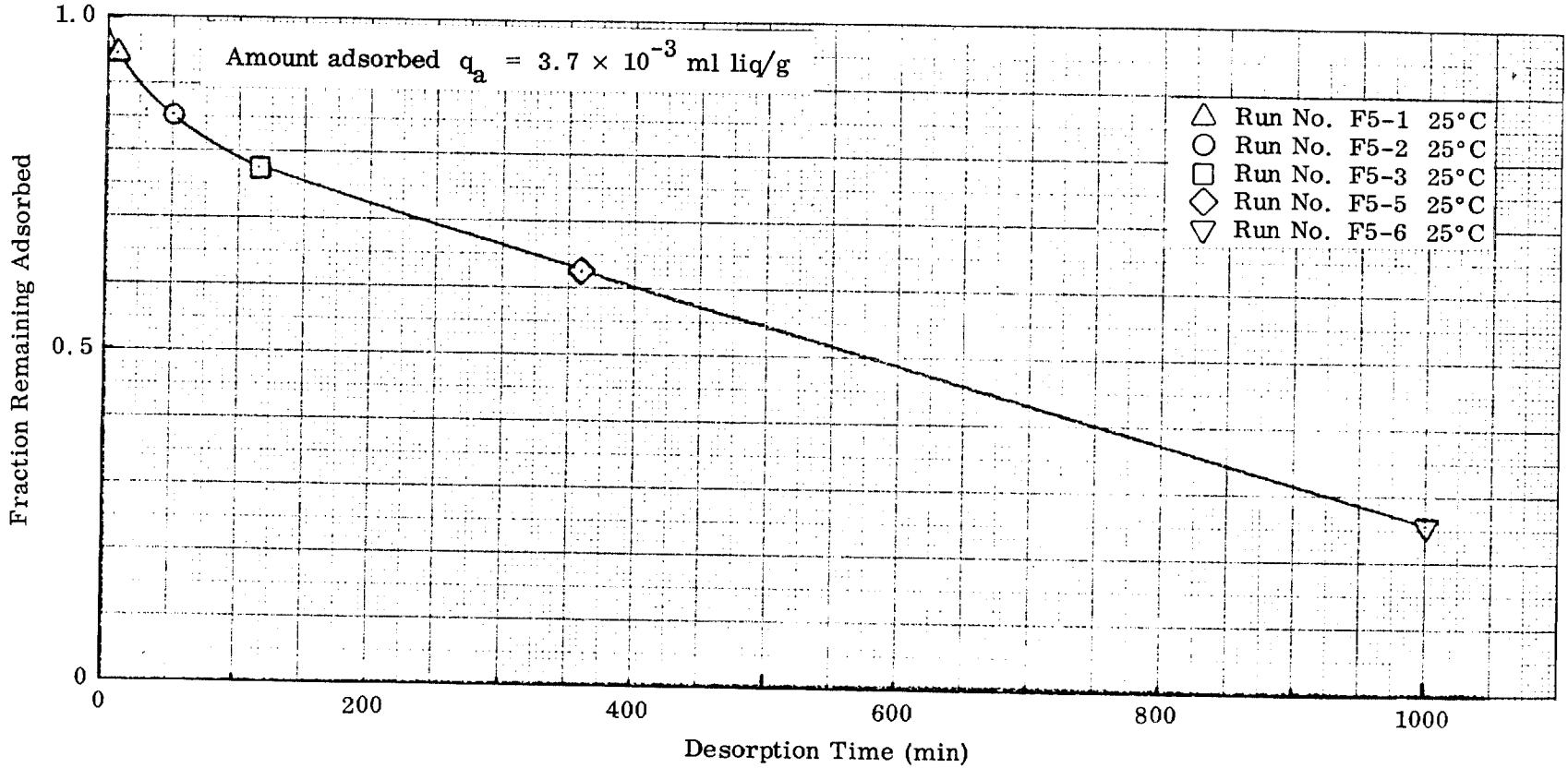

Fig. 7-3 Vacuum Desorption of Propane From Packed Bed of BD Activated Carbon

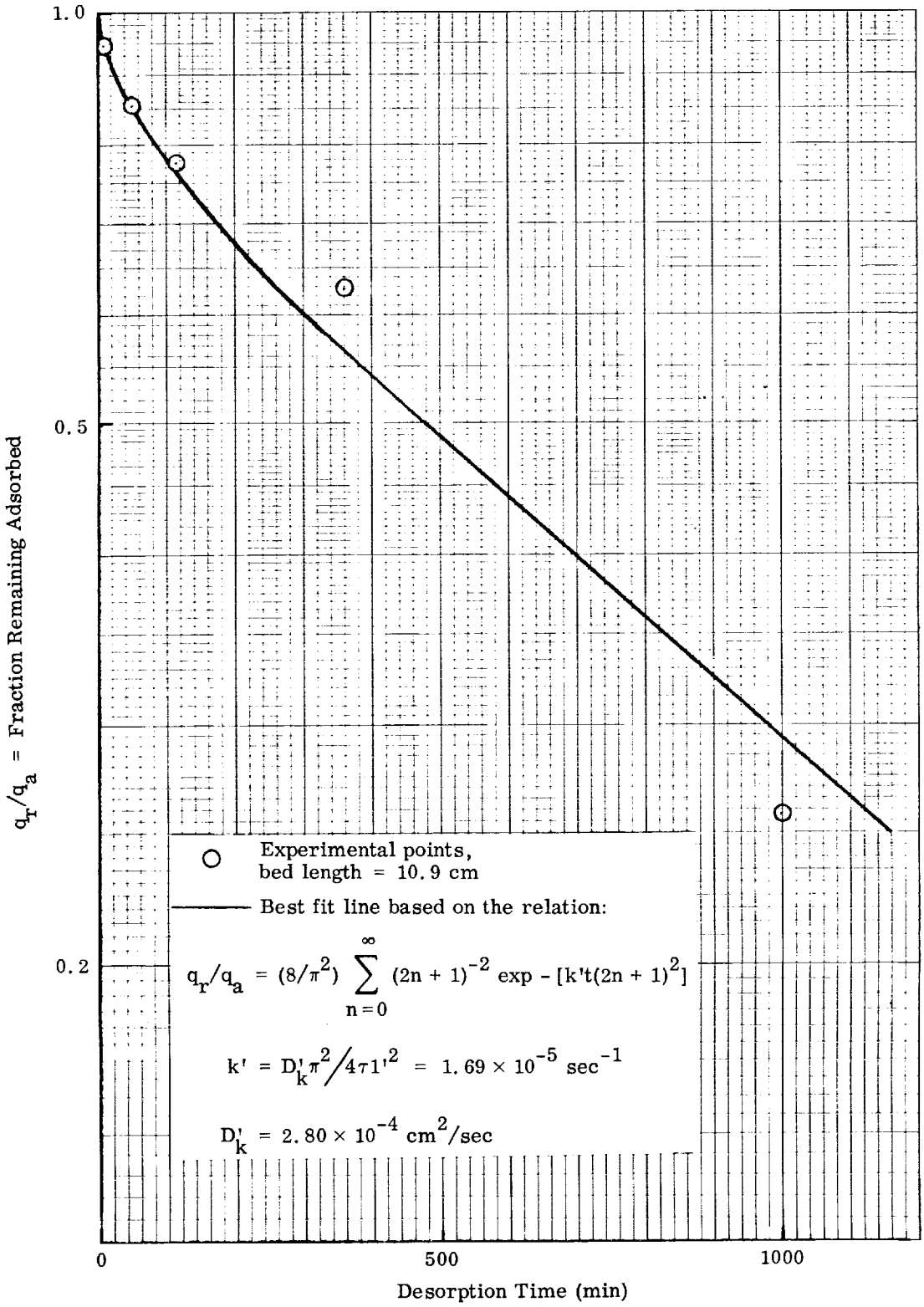

Fig. 7-4 Vacuum Desorption of Propane From Packed Bed of BD Activated Carbon

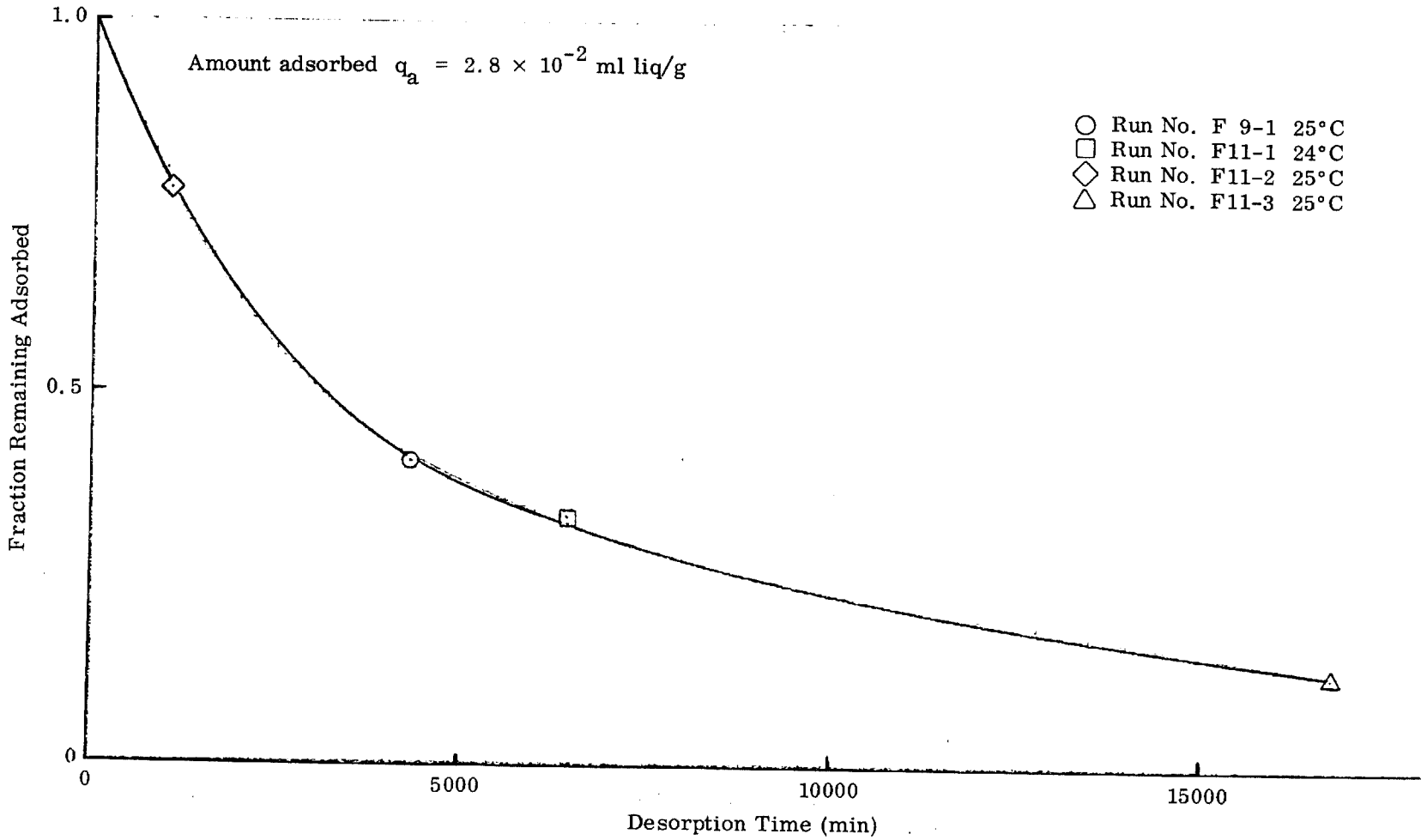

Fig. 7-5 Vacuum Desorption of n-Butane From Packed Bed of BD Activated Carbon

the results was checked by performing the desorption experiment three times. The results are shown in Fig. 7-6, and it can be seen that the results were quite reproducible. In agreement with the theory, the larger particles desorbed more rapidly. Sample calculations are shown in Appendix P.

To test the theory of desorption from packed beds further, other experiments were performed. In run F14-1, the bed was diluted to one-half by volume with nonadsorbing quartz chips. This tested the term S_o in the desorption equation (Eq. 7.8). Since S_o is the amount initially adsorbed per unit volume, if the bed is diluted,the term should decrease by the same factor,and the total half-time for desorption should also decrease. All of this was found to be true quantitatively in experiment F14-1 (see Fig. 7-7).

In another test of the desorption equation, the bed length was increased from 4.5 to 8.0 cm in Run F16-1. This would test the dependence of bed length to desorption. From theory it was predicted that the desorption half-time should increase with the square of the length. This was confirmed by experiment F16-1 (see Fig. 7-8). Furthermore, once a desorption curve is established from experiment, the other curves could be predicted as shown in Fig. 7-8.

Another test of the desorption theory was the variation of bed temperature. In flow run F17-2, the bed temperature was increased to 107°C. Since the diffusion coefficient, D_K, in the desorption equation is a function of the square root of absolute temperature, and the adsorption isotherm for n-butane on charcoal was determined independently on the microbalance, a prediction of desorption half-time could be made. The results and theory are in quite good agreement (see Fig. 7-9 and Table 7-1).

In further investigating the desorption characteristics of packed beds, it was of interest to look at desorption of a heavy contaminant such as toluene. Furthermore, it was decided to do it at 107°C to keep the amount adsorbed to a reasonable value. At

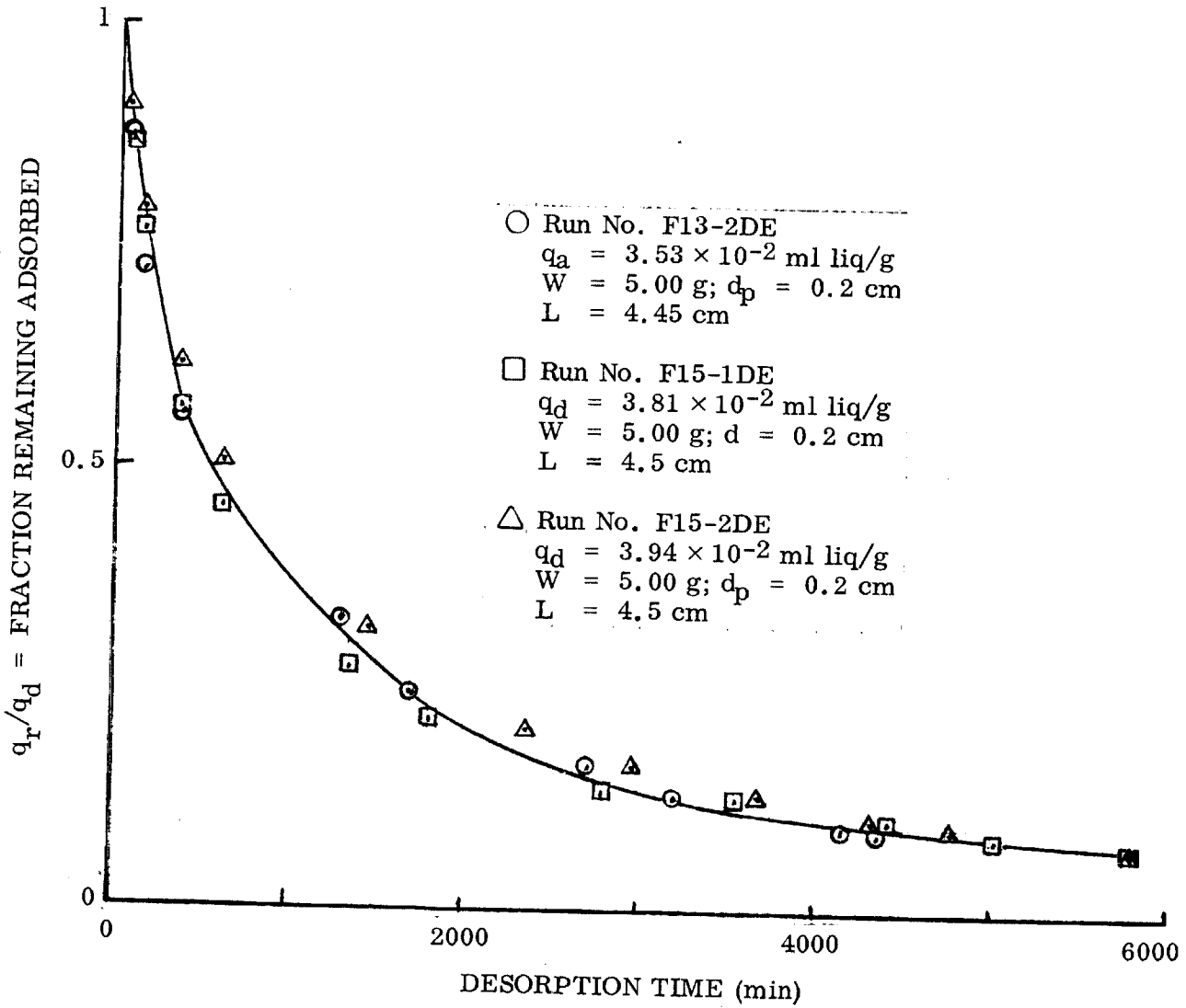

Fig. 7-6 Vacuum Desorption of n-Butane From Packed Beds of BD Activated Carbon

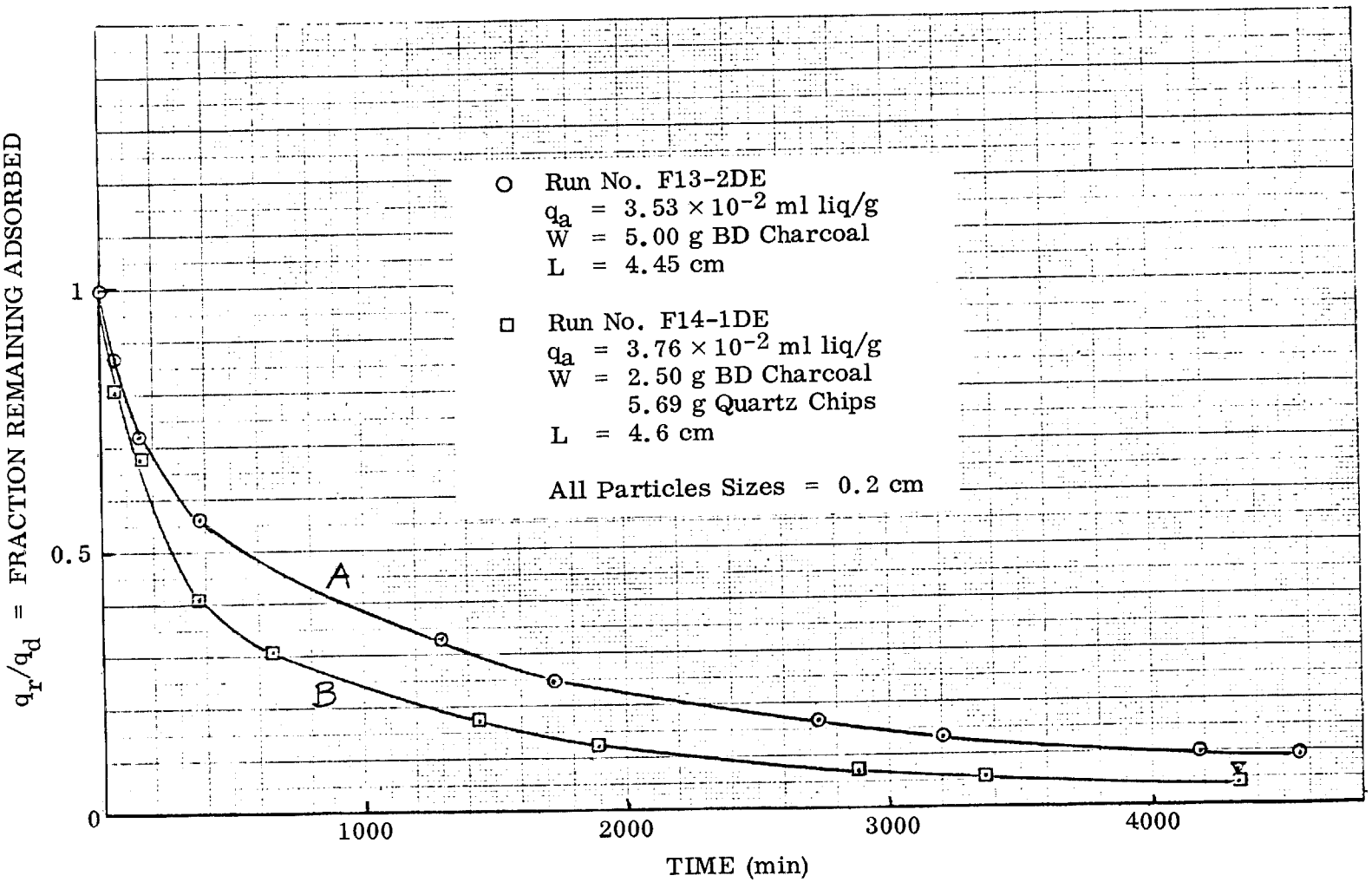

Fig. 7-7 Vacuum Desorption of n-Butane From Packed Beds of BD Activated Carbon

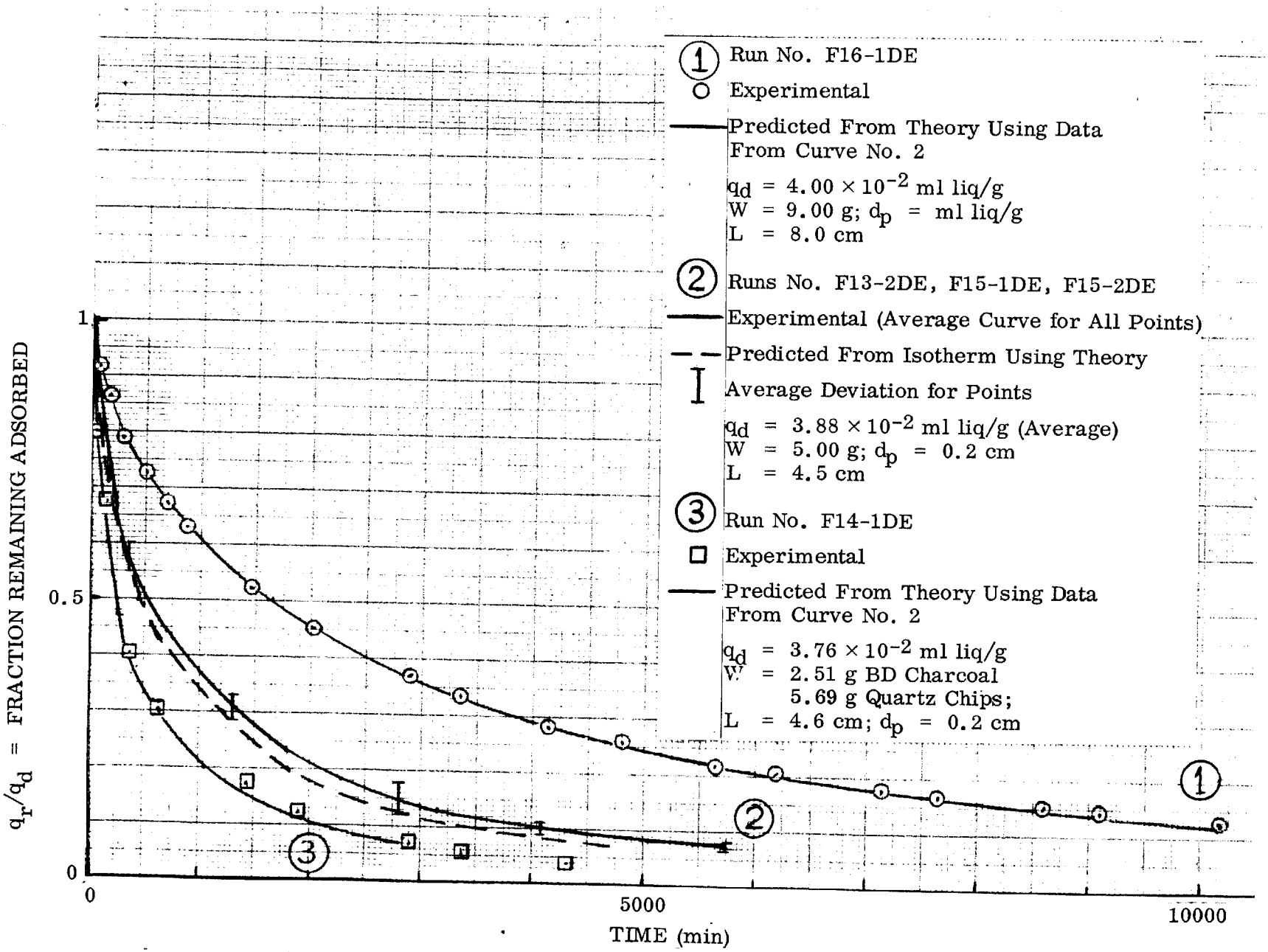

Fig. 7-8 Vacuum Desorption of n-Butane From Packed Beds of BD Activated Carbon

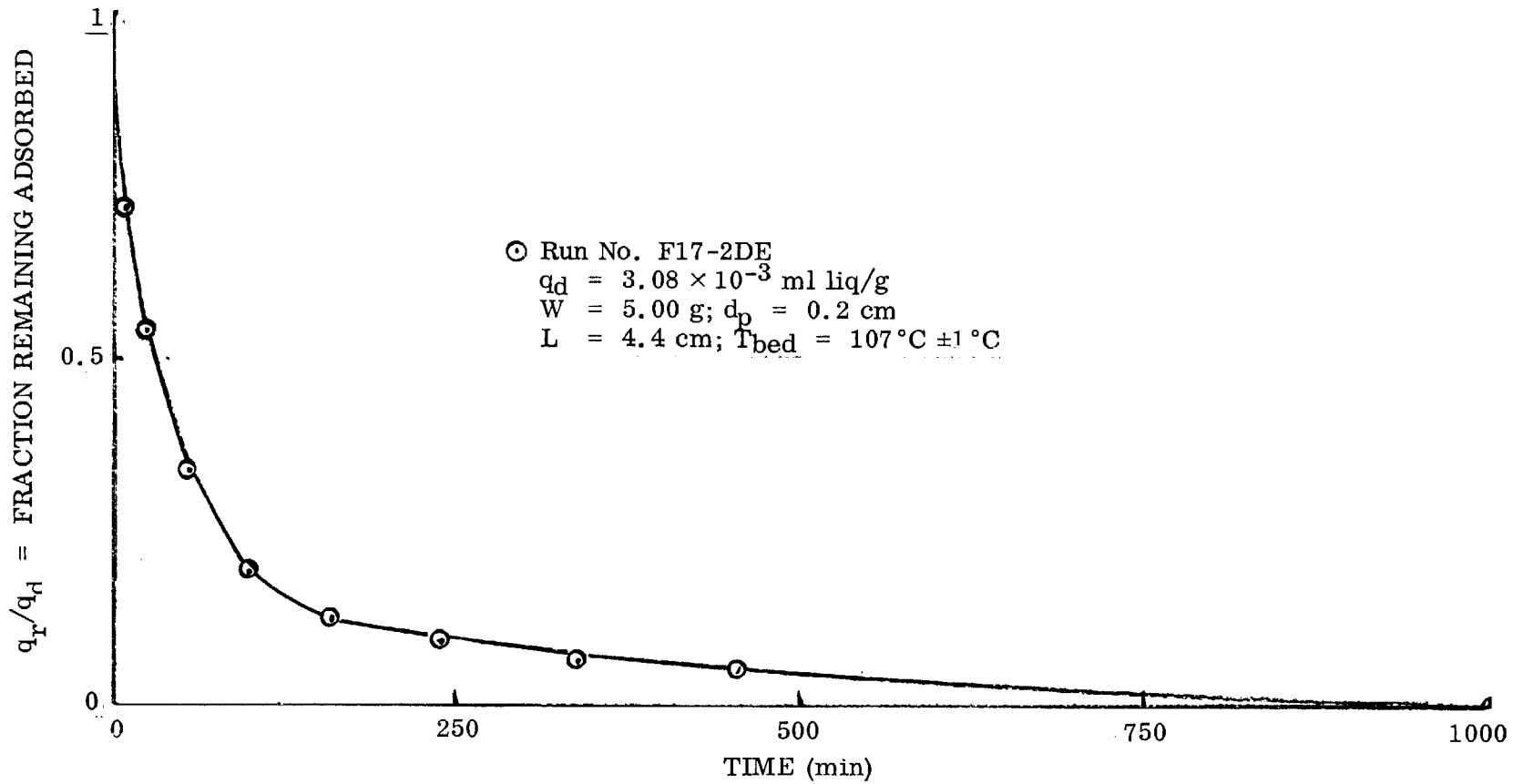

Fig. 7-9 Vacuum Desorption of n-Butane From a Packed Bed of BD Activated Carbon

room temperature, the total adsorption and desorption cycle would have taken weeks. This experiment was used as a control or background data to determine the effects in the following experiments, when the coadsorption of n-butane and toluene was investigated. That was the purpose of flow run F17-1, and the desorption data are given in Fig. 7-10. The desorption was stopped after 2750 min, when only about 30% of the original toluene remained on the bed. There was little point in continuing the experiment because the main objective was to experimentally define the desorption half-time (50% remaining), and this was accomplished.

7.3 RESULTS ON MULTIPLE CONTAMINANTS

7.3.1 Multiple-Contaminant Desorption: Phase 1

The first multiple-contaminant desorption studies were conducted in Phase 1 of the Contract. They were the vacuum desorption of the propylene/vinylidene chloride pair and the vinylidene chloride/toluene pair. The results were inconclusive due to the very fast equilibrium obtained in the case of propylene and due to suspected leaks in the system in the experiments with toluene. In addition, some difficulty was experienced in getting satisfactory analysis of vinylidene chloride using the gas chromatograph. Thus, it was decided to perform similar experiments with other contaminant pairs more amenable to gas chromatographic analysis.

7.3.2 Toluene/n-Butane Desorption at 107°C

The first meaningful results on the simultaneous desorption of coadsorbed species were achieved in run F17-3. The desorption characteristics of each of the individual contaminants were examined at 107°C in flow runs F17-1, -2, and -3. The effects of coadsorption on vacuum desorption were also observed. It was found, as expected, that there was blockage of n-butane by toluene. There was about an 80% decrease in the amount of n-butane adsorbed in run F17-3 compared with run F17-2. The only difference was the presence of toluene at one-half its MAC concentration. Due to the lower initial amount of butane adsorbed, the desorption half-time for n-butane was shorter in F17-3 than in F17-2, but the value was still predictable (see Fig. 7-11 and and Table 7-1).

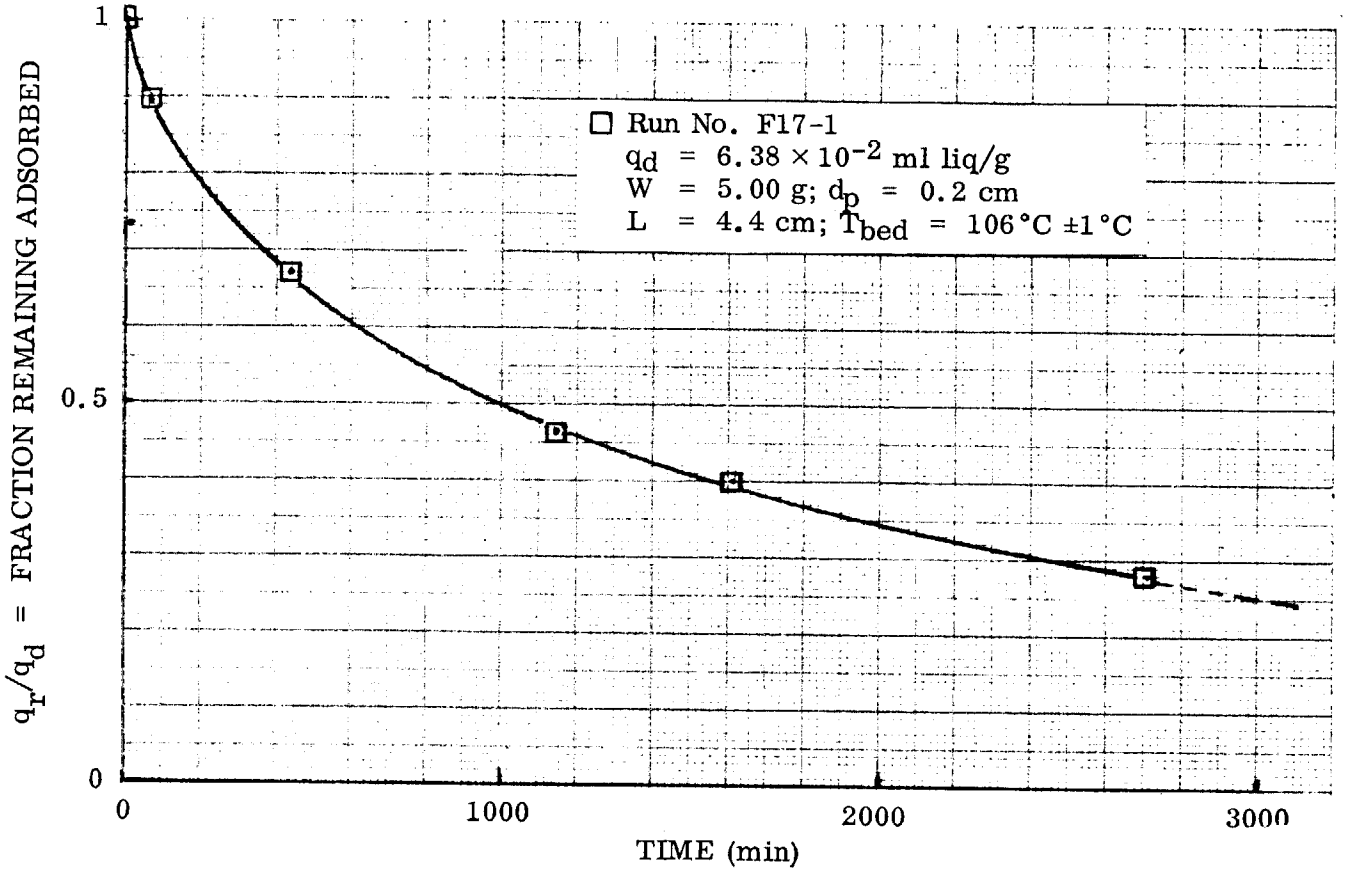

Fig. 7-10 Vacuum Desorption of Toluene From a Packed Bed of BD Activated Carbon

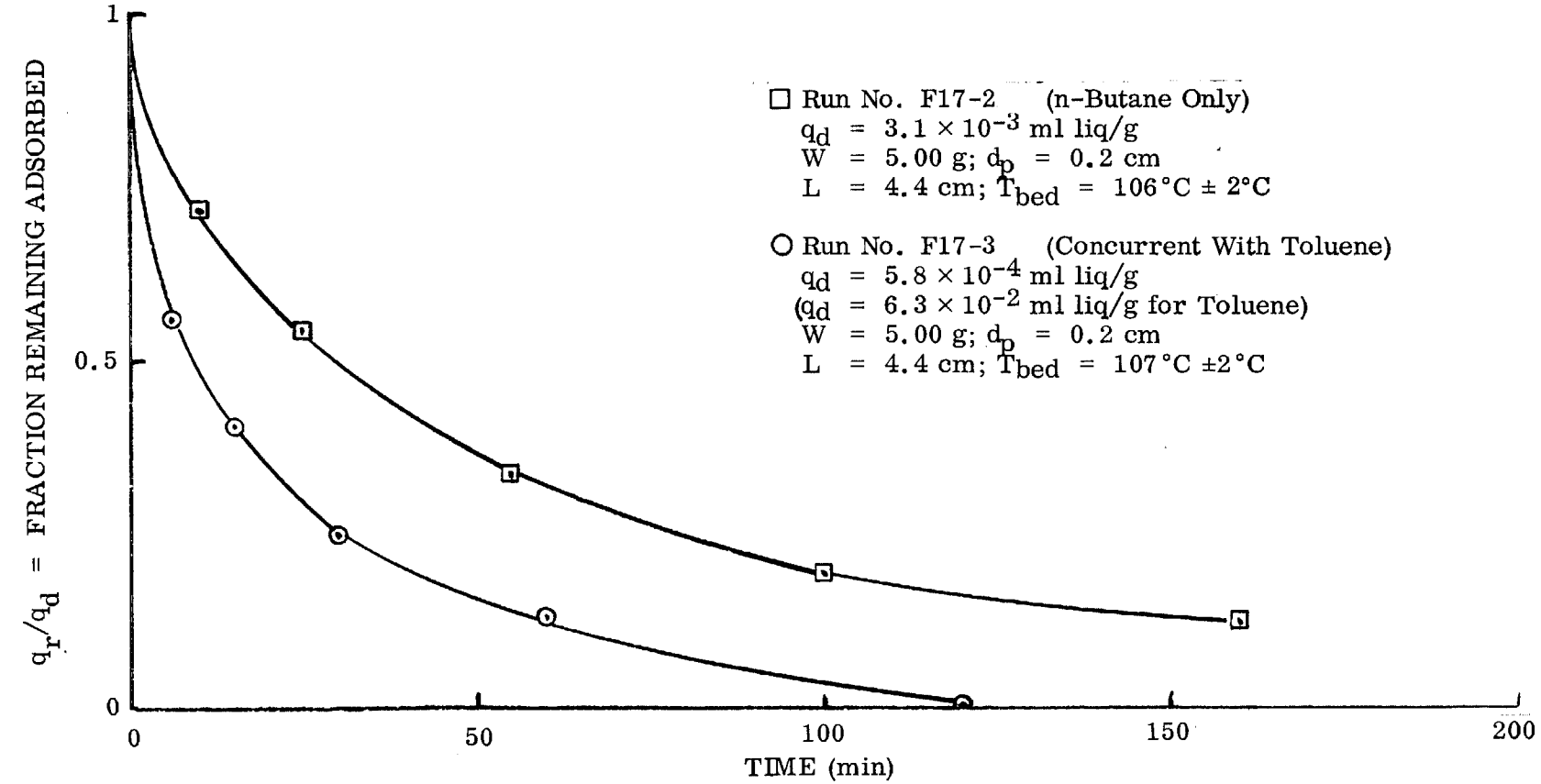

Fig. 7-11 Vacuum Desorption of n-Butane From a Packed Bed of BD Activated Carbon

The presence of n-butane did not hinder the adsorption of toluene in run F17-3. The same amount of toluene was adsorbed in runs F17-1 and -3, and the desorption of toluene was not affected by the presence of n-butane (see Fig. 7-12). Indications are that each component is desorbed independently.

7.3.3 Three Components: Freon-12, n-Butane, and Toluene at 67 °C

The vacuum desorption rate of a ternary mixture of Freon-12, n-butane, and toluene from a bed of BD charcoal has been measured at 67 °C. This temperature was chosen because at higher temperature the adsorption of Freon-12 and of n-butane at MAC becomes negligibly small (due to blockage by toluene) while at lower temperatures the rate of toluene desorption becomes too slow to measure in any convenient experimental time. At 67 °C the rate of Freon-12 desorption was too fast to measure (time for 50% desorption was less than 1 min), while the half-times for n-butane and toluene were 6 min and 4200 min, respectively (see Fig. 7-13 and 7-14). These values are in agreement with the theory presented earlier, although agreement is less exact than found in other runs.

7.4 DETERMINATION OF D_K, KNUDSEN DIFFUSIVITY, BY MEASURING PUMPING SPEED THROUGH A PACKED BED

7.4.1 Experimental Procedure

To determine the diffusion coefficient of n-butane through a packed bed of charcoal, two experimental procedures were available:

(1) Since butane is adsorbed on charcoal, in order to measure D_K directly for butane, the charcoal bed would have to be discarded and a nonadsorbing bed (say, quartz chip) of equal mesh size would have to be substituted.

(2) If the charcoal bed were used, then a nonadsorbed gas (helium) would have to be used. The diffusion coefficient for butane in the bed could then be calculated (from the helium value), since Knudsen diffusion depends only on the inverse square root of mass when converting from one gas to another.

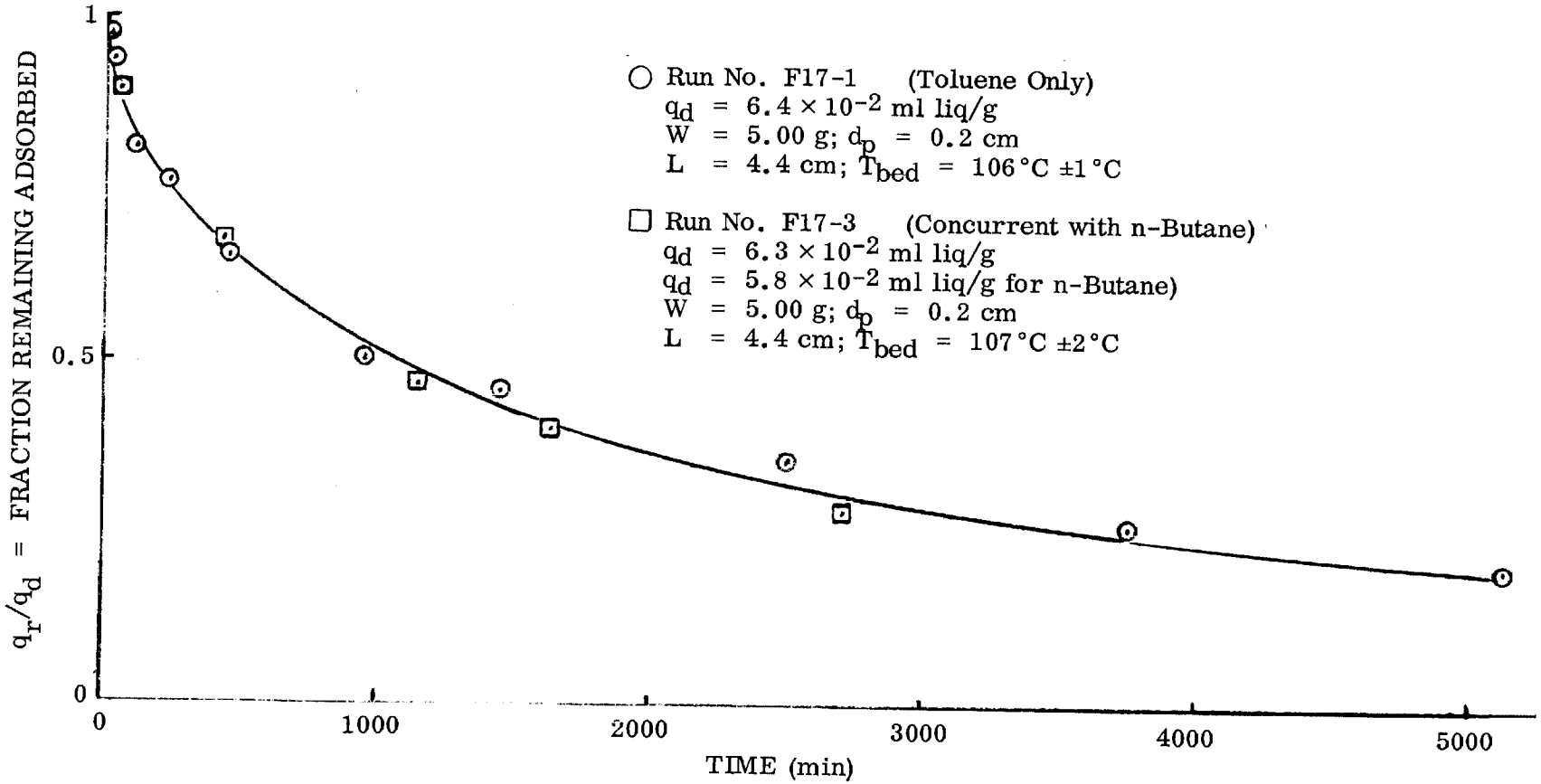

Fig. 7-12 Vacuum Desorption of Toluene From a Packed Bed of BD Activated Carbon

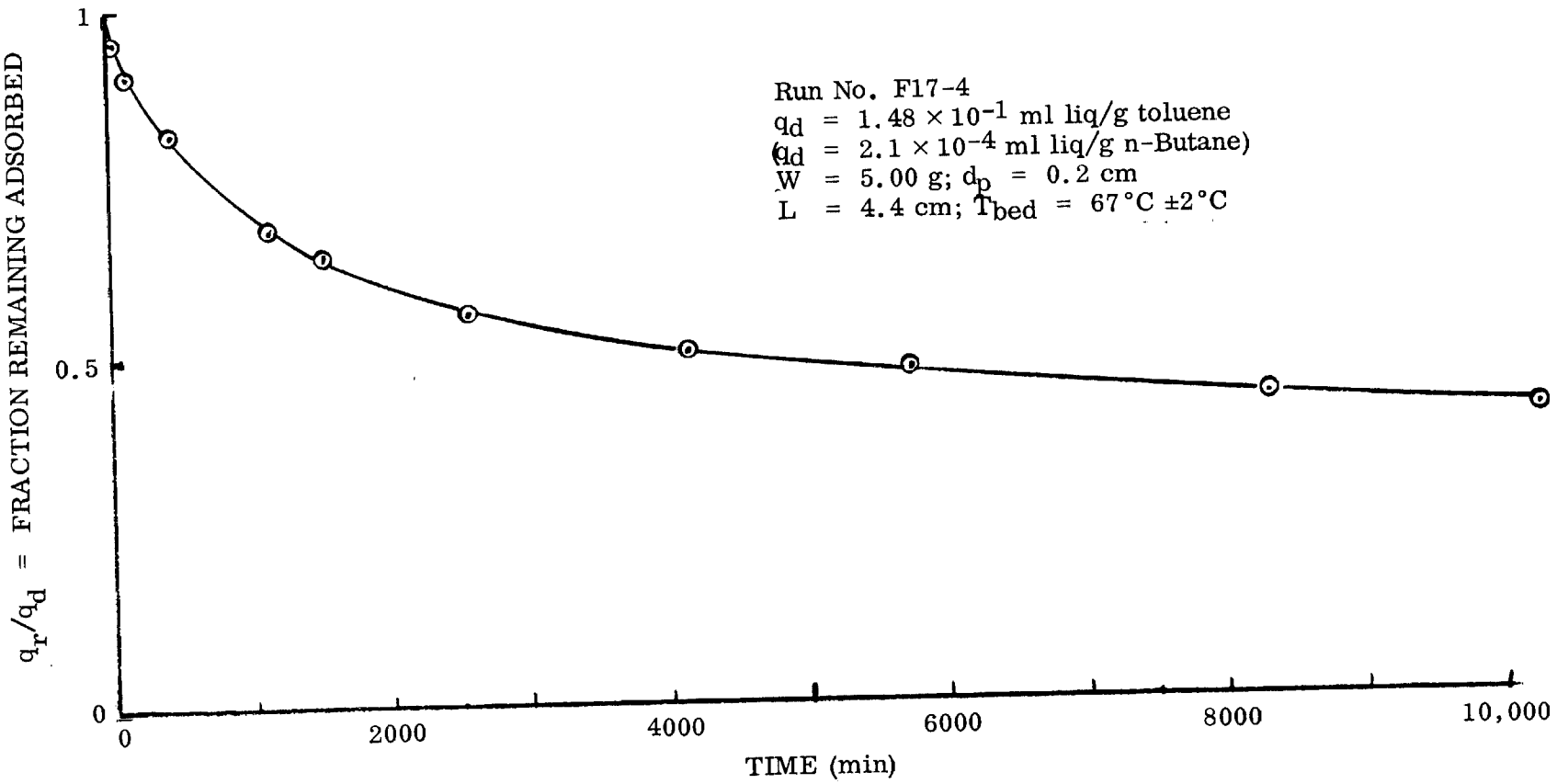

Fig. 7-13 Vacuum Desorption of Toluene From a Packed Bed of BD Activated Carbon During Concurrent Desorption of n-Butane

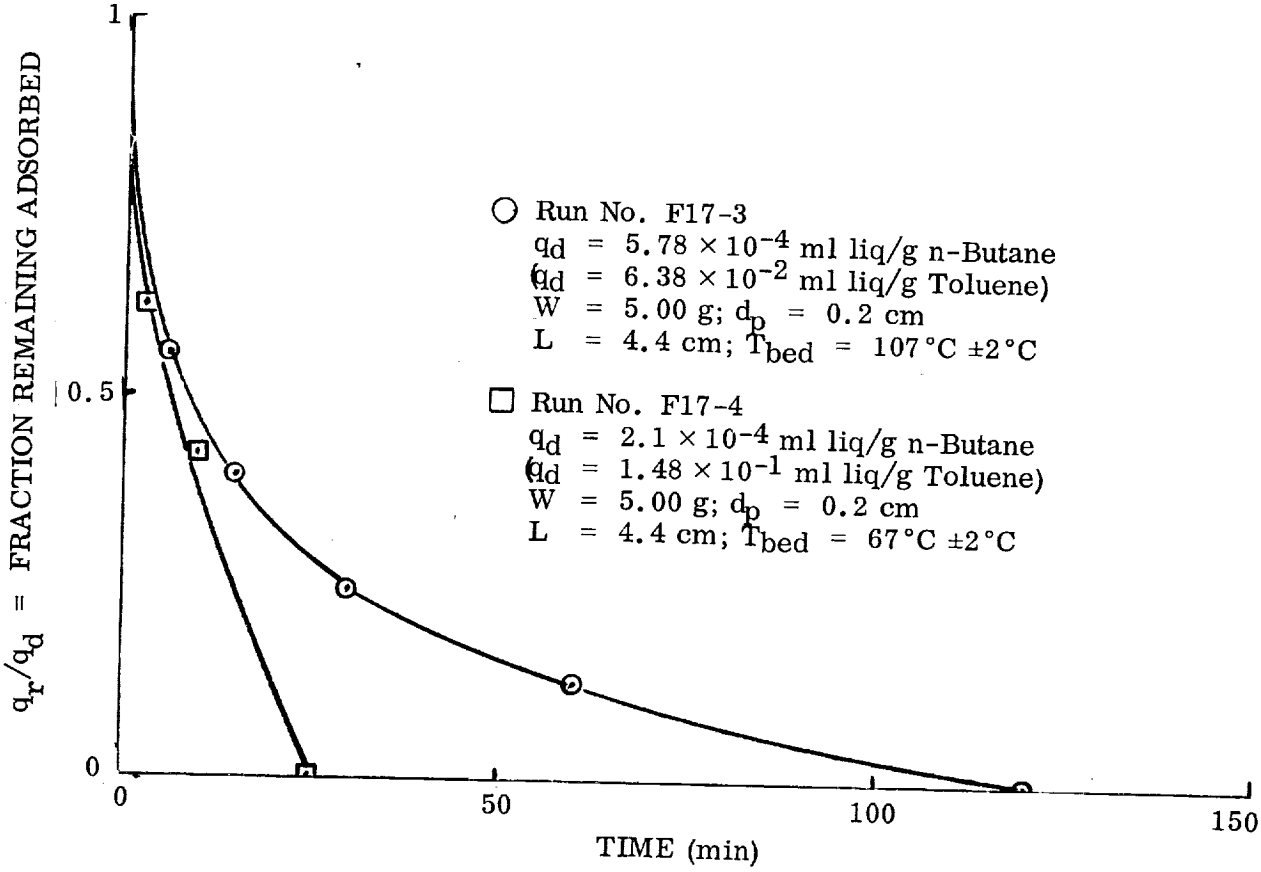

Fig. 7-14 Vacuum Desorption of n-Butane From a Packed Bed of BD Activated Carbon During Concurrent Desorption of Toluene

Since it appeared important to use exactly the same bed for the pumping experiments as for the desorption experiments, it was decided to use alternative (2), above: i.e., to use the same charcoal beds as were used in the butane desorption experiments and to use helium, and as a double check, nitrogen. To obtain an evacuation time constant of reasonable magnitude, a 5-liter bulb was added at the end of the adsorption bed furthest from the vacuum pumps (see Fig. 7-15).

In a typical experiment the charcoal bed is pumped to hard vacuum. The bed and 5-liter volume are isolated from the pumps and filled with helium to a pressure in the micron (10^{-3} torr) range. The main valve between bed and pumps is then opened and the decrease in pressure upstream of the bed is recorded as a function of time. Typical data are shown in Fig. 7-16.

Experiments were carried out with helium at two temperatures (25 and 300°C), for two particle sizes (0.20 and 0.05 cm) and for two bed lengths (4.4 and 8.0 cm). The nitrogen data are shown in Fig. 7-17. Pressures were measured with a Hastings DV-6 vacuum gage which was calibrated with a Datametrics Barocel pressure transducer. After correction with the pressure transducer, plots of log p versus time were linear over almost the whole pressure range (see Fig. 7-16 and 7-17). Above 10^{-3} torr, some curvature of the plots would be expected due to the onset of viscous flow, but this is not observed in the present data. As expected from theory, the runs at higher temperatures are slower than those at room temperature (i.e., $t_{1/2}$ is larger), since the 5-liter volume is kept at room temperature. When proper correction for this is made, the measured diffusion coefficients are proportional to the square root of temperature, as predicted by theory.

7.4.2 Theory and Results

At pressures in the micron range, gases will flow through packed beds by Knudsen flow, which is identical to Knudsen diffusion. By measuring the pumping speed through a packed bed, D_K may be measured directly. If a large volume, V, is connected to

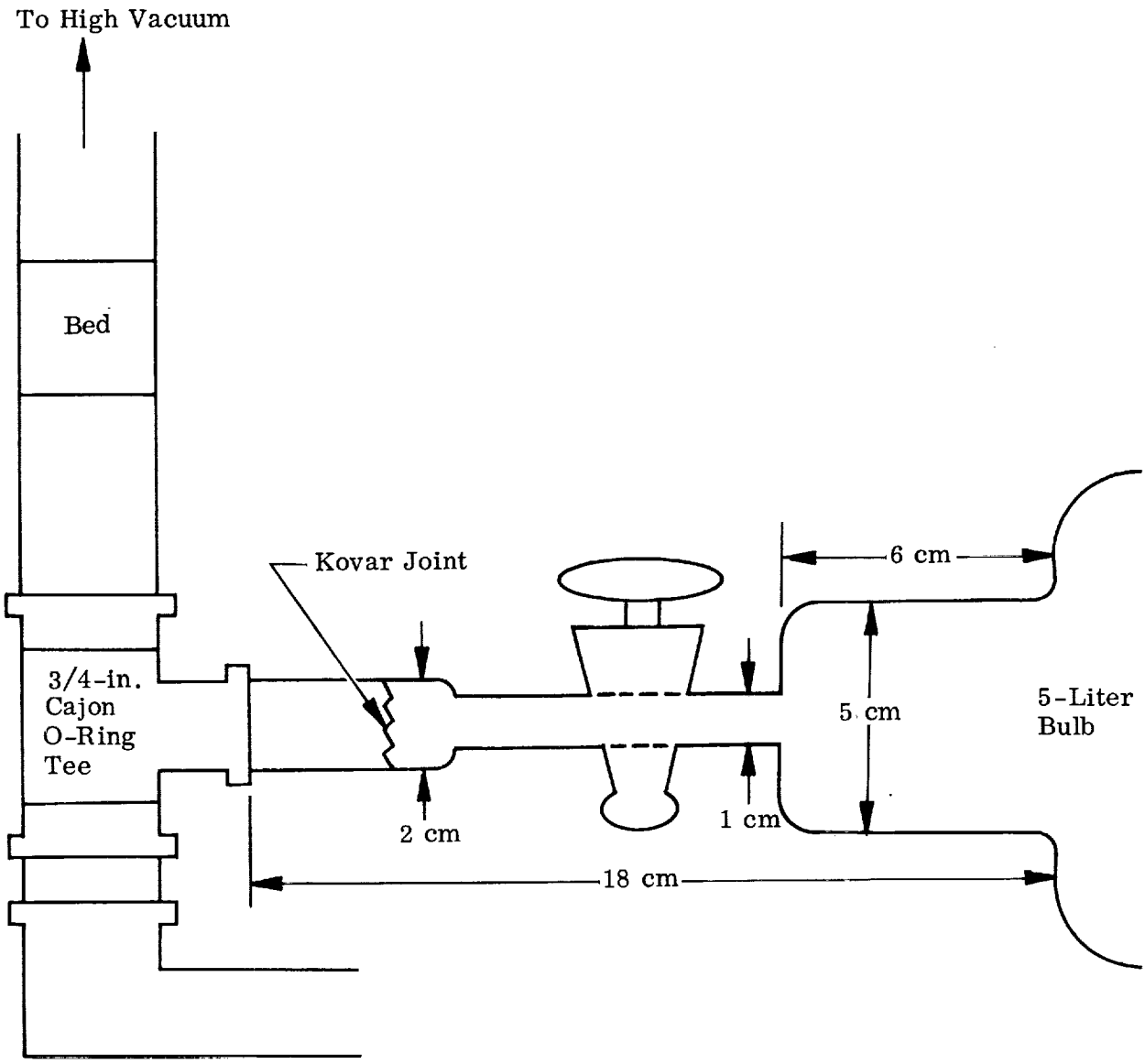

Fig. 7-15 Connection of Ballast Bulb to Inlet of Bed

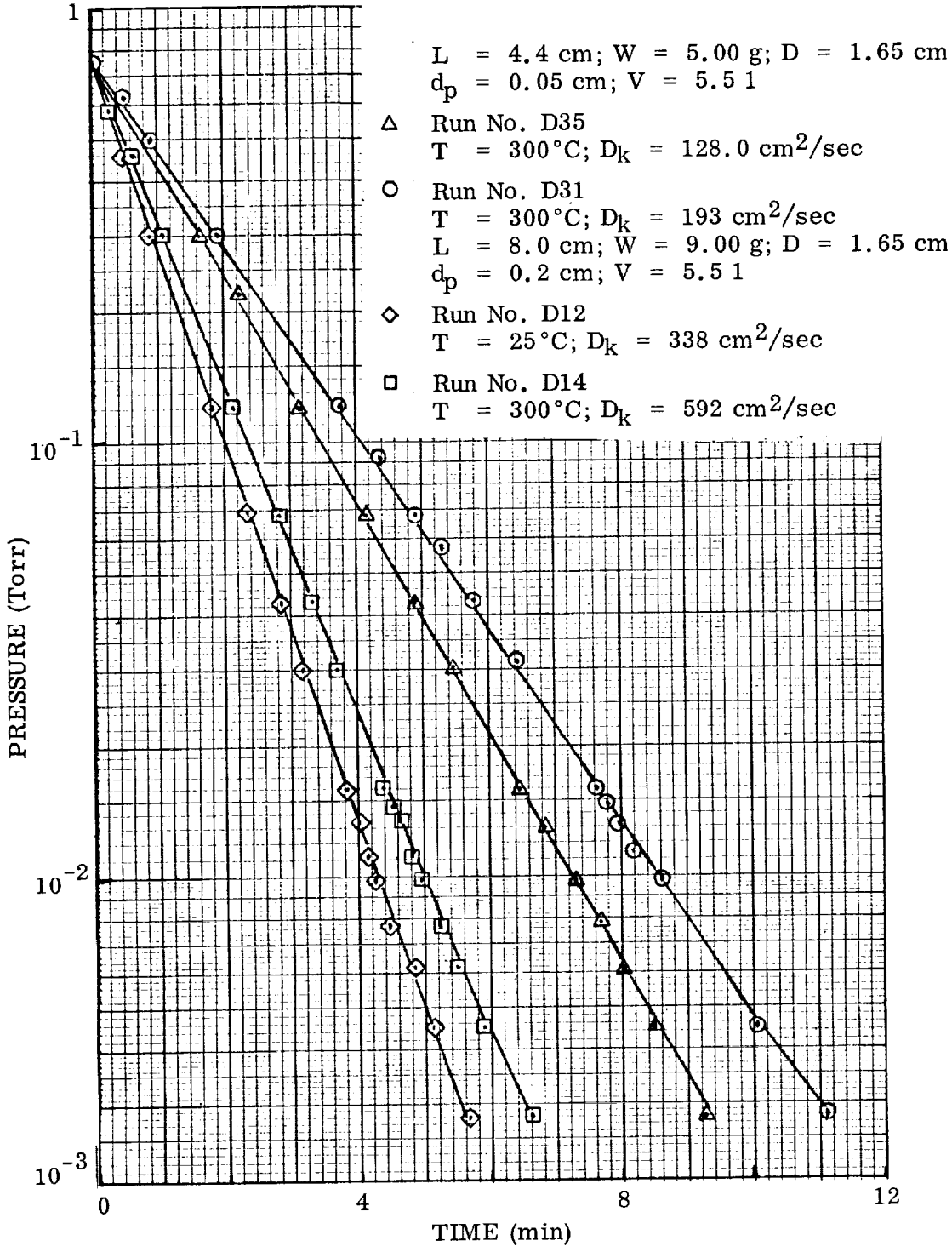

Fig. 7-16 Diffusion Studies of Helium Through Packed Beds of BD Activated Carbon

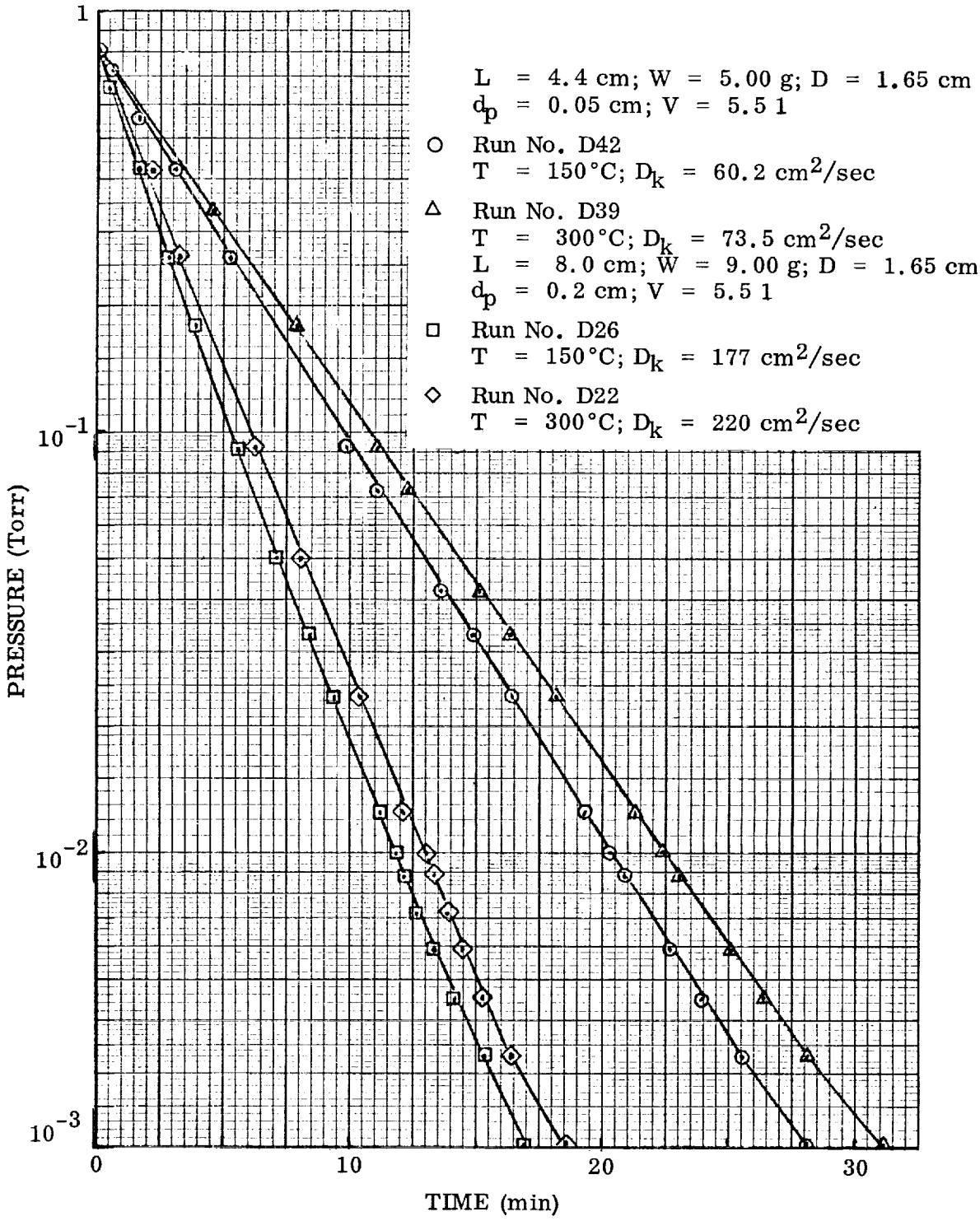

Fig. 7-17 Diffusion Studies of Nitrogen Through Packed Beds of BD Activated Carbon

a fast vacuum pump by a packed bed of length, L, with cross-sectional area, A, then the rate of evacuation of the volume, V, is given by

$$- V \frac{dc}{dt} = AD_K \frac{c}{L} \tag{7.2}$$

where c is the concentration of gas in the large volume. The left side of Eq. 7.2 is the rate of loss of molecules from V, and the right side is the rate of flow of molecules through the bed by Knudsen flow. It is assumed that the pumps are fast enough so that the downstream pressure is effectively zero (i.e., much less than the upstream pressure). Thus, the concentration gradient in the bed, $\Delta c/\Delta x$, is assumed linear and equal to c/L which c is the upstream concentration in the volume V. It is assumed in Eq. 7.2 that the pressure is low enough so that Knudsen and not streamline flow occurs in the bed.

It follows immediately from Eq. 7.2 that the time constant from evacuation of the large volume is

$$\tau = \frac{VL}{AD_K} \tag{7.3}$$

The half-time for evacuation is ln 2 times this, or

$$t_{1/2} = 0.693 \frac{VL}{AD_K} \tag{7.4}$$

Thus, D_K may be computed from Eq. 7.4, so that

$$D_K = 0.693 \frac{VL}{At_{1/2}} \tag{7.5}$$

From the linear plots of Fig. 7-16 and 7-17, half-times were taken and diffusion coefficients were calculated from the above equation. The results are collected in Table 7-2. The data are correlated by calculating a "tortuosity factor," γ_i, from each D_K, defined by the equation (see section 7.5)

$$D_K = \frac{\epsilon}{\gamma_1}(9.7 \times 10^3)\sqrt{\frac{T}{M}}\frac{d_p}{2} \tag{7.6}$$

where the term in parentheses is the Knudsen diffusion coefficient for a cylindrical capillary of diameter d_p. The factor ϵ takes into account that only a fraction ϵ of the bed is open for diffusion, while γ takes into account all other factors.

The tortuosity factors are also shown in Table 7-2. The constancy of γ_i for a given particle size (but changing T and molecular weight) shows that the $(T/M)^{1/2}$ law is obeyed quite accurately. However, the smaller particles have a smaller tortuosity factor (6.3 versus about 9.0) which is hard to explain. This might be due to changing particle shapes as the charcoal is ground smaller (the granules start as quite flat platelike structures before grinding) or to random errors in packing a particular bed. The onset of viscous flow would be in the opposite direction, to make the large particles have an apparent faster pumping speed, and, hence, a lower tortuosity factor, γ_i, than the small particles.

7.5 THEORY AND DISCUSSION OF RATE OF VACUUM DESORPTION FROM A BED

To correlate and predict the experimental results presented in sections 7.1 through 7.4, three theories of bed desorption must be considered. Two of these, fortunately, can be eliminated.

The first and simplest theory is that diffusion of adsorbate through the bed is very fast, so that all granules in the bed are surrounded by high vacuum. All granules would then desorb at the same rate as in the single-particle (microbalance) experiments.

Table 7-2

DIFFUSION PARAMETERS FOR BD CHARCOAL BEDS

	D_K (cm^2/sec)		γ_i	
	d_p = 0.05 cm	d_p = 0.2 cm	d_p = 0.05 cm	d_p = 0.2 cm
Helium, 25°C	128	338	6.24	9.76
300°C	193	592	6.32	8.22
Nitrogen, 25°C (calc.)	49.1	144.5	6.62	8.98
150°C	60.2	177	6.60	9.05
300°C	73.5	220	6.25	8.72
n-Butane, 25°C				
Calc. from He D_K	33.6	88.8	6.25	10.0
Calc. from N_2 D_K	34.1	100	6.55	8.93

The time for half-desorption for the whole bed would then be of the order of seconds, similar to the single-particle experiments. This mechanism may be eliminated immediately since the time for 50% desorption is on the order of days, not seconds. Thus, the rate of diffusion of adsorbate through the bed must be much lower than desorption from a single particle. Two mechanisms of diffusion through the bed must next be considered.

In the Phase 1 Report (Ref. 23) for this contract, it was hypothesized that the main mechanism of transport in the bed was diffusion through the pore structure of the charcoal (see pp. 4-24 through 4-27 of Ref. 23 and also Fig. 7-4 of this report). This hypothesis, however, leads to an incorrect dependence of desorption rate on charcoal granule sizes and so may be discarded. The experimental evidence is clearly that desorption rate is proportional to granule size, whereas a pore diffusion mechanism would predict either no dependence on particle size or inverse dependence. The most likely mechanism of adsorbate flow through the bed appears to be free-molecular Knudsen flow, or diffusion, through the void spaces of the bed, since the pressure is so low that the mean free path is larger than the channel dimensions,

which are about the same size as the charcoal granules. (The mean free path of n-butane at 10-micron pressure is about 0.5 cm, which is larger than the granule size used here.) If it is assumed, then, that Knudsen gas flow in the intergranular spaces is the main mechanism of butane transport in the bed, then the equation of diffusion accompanied by desorption to be solved is

$$D_K \frac{\partial^2 c}{\partial x^2} = \frac{\partial S}{\partial t} \tag{7.7}$$

where

c = gas concentration (mol/cm^3)
S = adsorbed concentration per unit bed volume (mol/cm^3)
x = distance from high-vacuum end of bed (cm)
t = time (sec)
D_K = Knudsen diffusion coefficient in bed as defined by the equation (cm^2/sec)

$$F_x = D_K \frac{\partial c}{\partial x} \tag{7.8}$$

where

F_x = flow rate per unit bed cross section at x (mol/cm^2 sec)

In Eq. 7.7 the term $\partial c/\partial t$ has been neglected, since S is about 10^5 times greater than c. Equation 7.7 is an equation of mass balance which states that the rate at which molecules are added to the flowing stream of adsorbate at a given point in the bed must equal the rate of desorption at this point.

In Appendix Q, it is shown that the solution of Eq. 7.7 gives for the time of half-desorption

$$t_{1/2} = K \frac{L^2}{D_K} \frac{S_o}{c_o} \tag{7.9}$$

where

L = bed length (cm)

D_K = gas-phase diffusion coefficient of adsorbate in the bed voids (cm^2/sec)

S_o = initial adsorbed concentration of adsorbate (mol/cm^3)

c_o = gas-phase concentration of adsorbate in equilibrium with S_o (mol/cm^3)

K = constant of the order of 0.33 which depends on the shape of the adsorption isotherm

A correlation described in Appendix Q for K gives the equation

$$(K)^{-1} = 5.16 - 3.5(NLF) - 1.66(NLF)^{10} \qquad (7.10)$$

where

(NLF) = simple function describing the degree of nonlinearity of the adsorption isotherm

It may be defined as

$$(NLF) = 1 - 2(c/c_o)_{1/2} \qquad (7.11)$$

where

$(c/c_o)_{1/2}$ = value of c/c_o, which makes $S/S_o = 0.50$

To determine $(c/c_o)_{1/2}$, the adsorption isotherm is plotted in reduced units, S/S_o versus c/c_o, where S_o is the initial adsorbed concentration of adsorbate and c_o is the gas-phase concentration in equilibrium with this.

The value of D_K, the free-molecular-flow diffusion coefficient of adsorbate in the bed voids, has been measured experimentally by measuring the pumping speed through the bed (section 7.4) and this gives

$$D_K = \frac{\epsilon}{\gamma_1} (9.7 \times 10^3) \sqrt{\frac{T}{M}} \frac{d_p}{2} \qquad (7.12)$$

where

ϵ = void fraction in the bed
T = temperature (°K)
M = molecular weight (g/mol)
d_p = particle size (cm)
γ_1 = tortuosity factor equal to about 7.0 (see Table 7-2 for details)

Thus, from Eq. 7.9 to 7.12 the time for 50% desorption can be computed for any given adsorbate and at any temperature.

Although Eq. 7.9 gives only the half-time for desorption, the entire course of desorption (i.e., a plot of percent desorbed versus a reduced time parameter, $t/t_{1/2}$) appears to follow the same pattern for both n-butane and toluene. In theory, the shape of this curve should depend somewhat on the shape of the adsorption isotherm, but in practice the shape seems to be similar for butane and toluene and thus one solution to Eq. 7.7 is common for both sorbates. If this is generally true, the common solution which is given in Table 7-3 and plotted in Fig. 7-18 is a general solution.

Table 7-3
PERCENT DESORBED VERSUS REDUCED TIME, $t/t_{1/2}$

% Desorbed	$t/t_{1/2}$
0	0
25	0.25
50	1.0
70	2.7
80	4.0
90	8.0

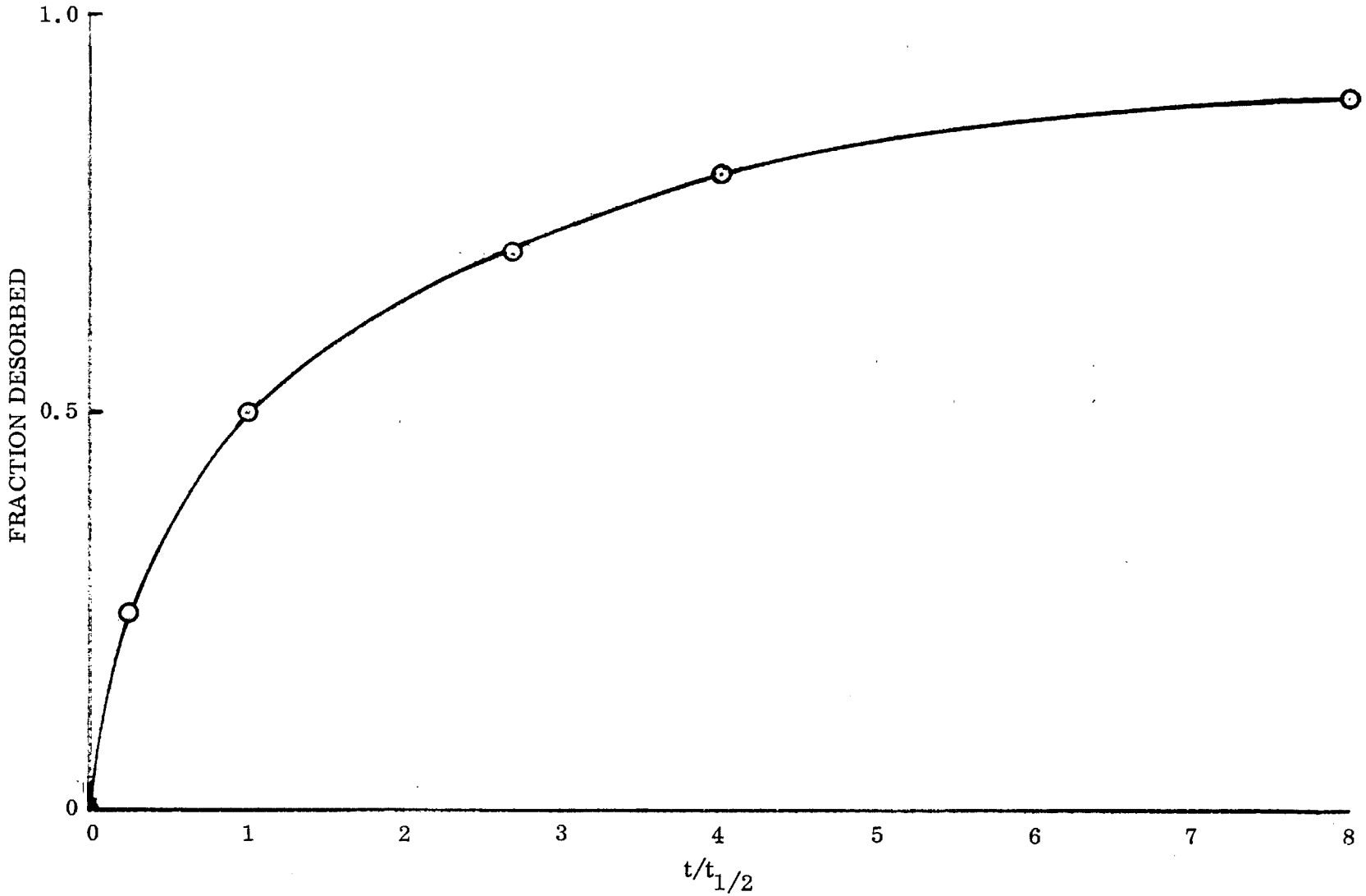

Fig. 7-18 General Solution for Equation 7.7

Thus, from Eq. 7.9 plus Fig. 7-18, the complete course of desorption can be computed. This has been done for curve 2 in Fig. 7-8 which depicts the average desorption rate for three n-butane runs. The tortuosity measured by the helium transport experiment, a K-value of 1/3, and the value of S_o/c_o from the experimental isotherm were used to calculate the half-time. Then the generalized rate curve of Fig. 7-18 was used to calculate the theoretical curve (dotted line in Fig. 7-8). The agreement is well within experimental error for the entire rate curve.

In summary, the preceding theory when applied to the experimental data shows excellent agreement. (The data are summarized in Table 7-1.) The theory correctly predicts that:

(1) Desorption rate should increase with increasing particle size. Thus, the above table shows that 0.20-cm particles desorb much faster than 0.05-cm granules.

(2) The dependence of desorption rate on bed length is correctly predicted as an inverse-square dependence. Compare Run F15-2 with F16-1 in Fig. 7-8.

(3) The absolute values of the times for 50% desorption are predicted almost within the experimental error, the total rate curves are reasonably well reproduced, and the effects of bed length and adsorption capacity are quantitatively predicted from the detailed rate curve from one set of conditions.

Section 8
APPLICATION TO DESIGN PROCEDURE

The ultimate purpose in obtaining the fundamental adsorption information on activated carbon has been to provide the necessary physical-chemical data to form a rational basis for a practical design procedure for sorption filters which can be used to control trace contaminants for extended missions. In this section, the information developed under the current contract will be examined from the design point of view. The purpose is twofold. First, the development of workable design procedures gives a meaningful evaluation of the completeness of current progress in adsorption theory and practice and permits identification of the most critical areas for future research. Second, the development of the design procedures is of intrinsic value for advanced planning and design of future life support systems and as a basis for construction of prototype sorbent filters for engineering evaluation.

The first important question which arises in such a design is that of regenerative versus nonregenerative sorbent systems. Consider, for example, a 9-man, 2-year mission. The nonregenerative design would require either (1) that enough charcoal be launched to last for the 2-year mission or (2) that the charcoal be supplied at intervals, say, every 90 days. In either case, the total amount of charcoal is the same and a crude estimate of the amount can be made without recourse to the specific design. To make such an estimate, it is necessary to assume a reasonable maximum production rate for contaminants. One suggestion for this has been given as 50 g/day nonbiological and 20 g/day biological. For a 2-year mission, this would result in a total contaminant production of 51 Kg (112 lb). Since it may reasonably be expected that the charcoal will adsorb on the average about 1% by weight, then the total charcoal required would be about 5000 Kg (11,000 lb). If the charcoal were replenished on a 90-day basis, the 90-day load would be about 630 Kg (1400 lb).

From such estimates, it is clear that only a regenerative system could be seriously considered. In a regenerative system, there are four general areas of concern: (1) adsorption capacity of the sorbent compared with production rates of trace contaminants, (2) adsorption dynamics, (3) regeneration, and (4) interfacing with the total life support system.

8.1 ADSORPTION DYNAMICS

One complication which is not always recognized in the design of adsorptive removal systems is that adsorption of heavy contaminants even in relatively small concentrations can completely block the adsorption of light contaminants. Thus, if the hydrodynamics of the adsorber are such that the heavy components break through early in the adsorption cycle, then the surface can no longer adsorb lighter components. In fact, the light components which have already been adsorbed begin to desorb as the heavy components break through. Of course, this can happen when the removal efficiency for the heavy components is still favorable for their removal. Thus, it is a requirement of an operable adsorber that the concentration profiles for all the heavy contaminants be sharp enough to leave an appreciable portion of the bed unblocked so that the lighter contaminants can be retained. This is best accomplished through careful design of bed geometry and selection of particle sizes and linear velocities consistent with the bed geometry. In general, this displacement phenomenon requires larger length-to-diameter ratios than have previously been assumed in some designs. This, of course, complicates the selection of a design with a low pressure-drop limitation but suggests substantial benefits in minimizing the total gas flow rate through the adsorber.

A great deal of theoretical work and some experimental work directed toward establishing the theory in various forms has been done on the problem of adsorption dynamics in packed beds by workers in ion exchange, gas chromatography, and chemical reactor design, as well as those primarily interested in adsorption dynamics and equilibria. Robell and Merrill (Ref. 24) have reviewed this work and examined the

various approaches with the objective of recommending procedures which give acceptable engineering predictions of adsorption dynamics. What is suggested is the use of the number of transfer units, N_{TU}, as the figure-of-merit of the adsorption bed and the Peclet number

$$Pe = \frac{d_p u}{D_f} \tag{8.1}$$

where

Pe = Peclet number
d_p = particle diameter (cm)
u = linear velocity (cm/sec)
Df = fluid-phase diffusivity of contaminant (cm^2/sec)

as the system correlation parameter. These have been related via a semiempirical correlation by Vermeulen (Ref. 25), in which the quantity $N_{TU} d_p / bL$ is plotted as a function of the Peclet number on log-log coordinates. A version of this correlation is given in Fig. 8-1, in which the quantities b and L are an isotherm shape factor and the bed length (cm), respectively, while the term D_{pore} represents contaminant diffusivity (cm^2/sec) in the sorbent pores.

In the work of Robell and Merrill (Ref. 24), it is shown that the correlation in Fig. 8-1 is satisfactory for engineering purposes if the number of transfer units is taken as

$$N_{TU} = 4\pi \left(\frac{t_s}{w}\right)^2 \tag{8.2}$$

where

t_s = breakthrough time (sec)
w = breakthrough width (sec)

as shown in Fig. 8-2.

In order for the breakthrough curve to be reasonably sharp (i.e., sharp enough to eliminate poisoning of the sorbent for the lightly adsorbed contaminants), it is necessary to maintain a design such that

$$N_{TU} \geq 100$$

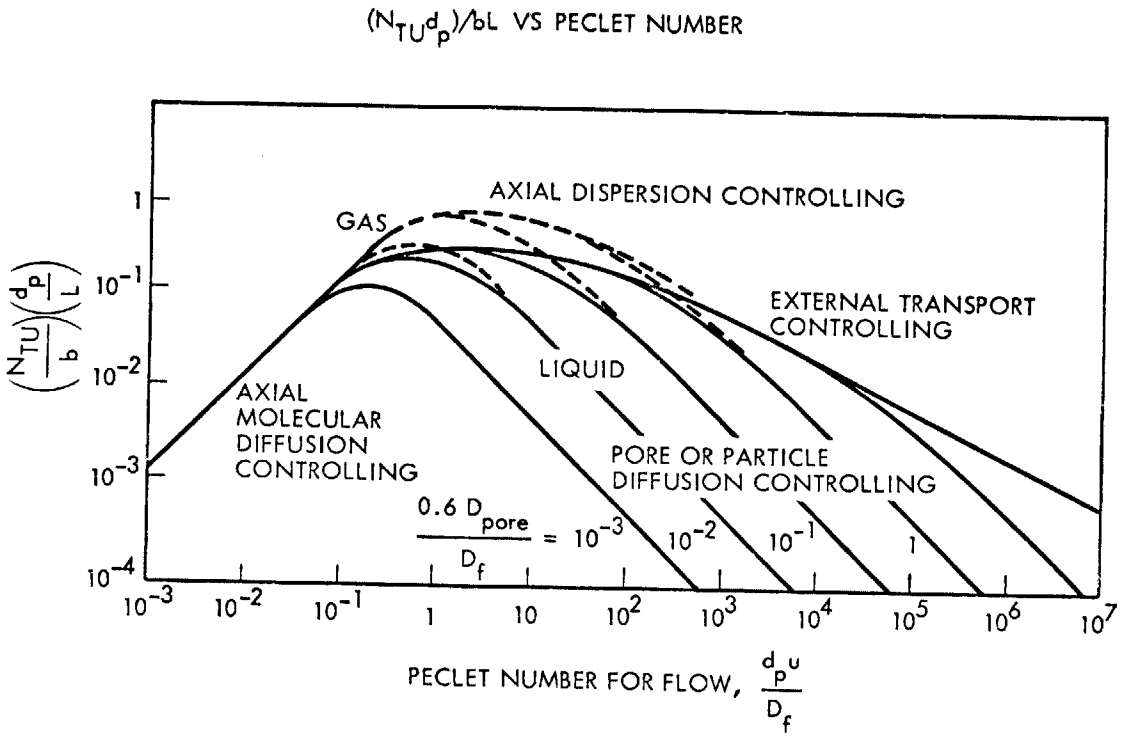

Fig. 8-1 Adsorption Dynamics Correlation

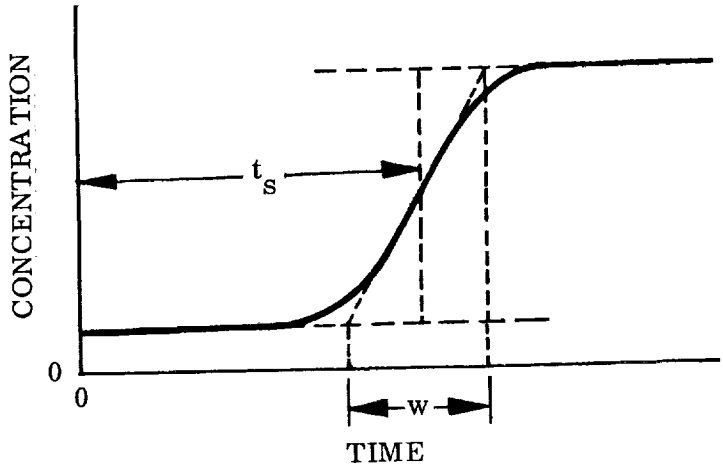

Fig. 8-2 Definition of t_s and w

This can usually be obtained for Peclet numbers between 10^{-1} and 10 where the curve in Fig. 8-1 passes through its maximum. The inequality, Eq. 8-3, then is the first criterion for an acceptable design.

8.2 DESIGN PROCEDURE

A workable design procedure will be described in this section which can be used to give a near-optimum design of a trace contaminant sorbent bed for a large number of trace contaminants. It is essentially the procedure used to produce a design for the NASA/MSC 1973 Basic Subsystems Module (Ref. 26). Because additional information has been obtained since that design, particularly with respect to mixed adsorption and the dynamics of vacuum desorption from sorbent beds, the design approach will be outlined here with attention given to how the newly acquired physical-chemical information should be integrated into the design.

The first step in the design is to define a minimum flow rate for acceptable operation. This is done by writing the mass balance for a contaminant in the cabin:

$$\dot{m} = Fc_c\eta \tag{8.4}$$

where

$\dot{m}$ = production rate of contaminant (mg/sec)

F = volumetric flow rate into the adsorber (l/sec)

c_c = characteristic concentration of contaminant (mg/l)

η = removal efficiency

Using the equation above, the minimum concentrations for a given flow rate can be calculated by assuming $\eta = 1.0$. The minimum flow rate is set by the condition that c_c for all contaminants must be lower than the SMAC value. Violation of this criterion defines flow rate-limited contaminants, and once the minimum flow rate is determined, the cabin concentrations for all the other contaminants may be calculated from Eq. 8.4. From these concentrations, it is possible to calculate the adsorption potential, A, for each of the contaminants.

If the design were to be done by machine calculation, then it would be possible to carry each component (for the BSM design, 150 trace contaminants were considered) individually through the calculation. For a hand-calculated design, it is necessary to make some simplifications at this point for calculational facility.

One such approach used commonly in separation design calculations for complex hydrocarbon mixtures is the definition of a small number of pseudo-components usually grouped according to boiling-point range. In the case of adsorption, a reasonable criterion for grouping would be according to adsorption potential, A. The trace contaminants can be so grouped into 10 or fewer pseudo-components according to their adsorption potential, with appropriately averaged molar volumes, adsorption potentials, boiling points, and molecular weights. Using these pseudo-components in their respective ratios and the generalized potential plot, a relative bed profile can be constructed giving the contaminant concentrations q as a function of bed length L for each pseudo-component, assuming completely sharp breakthrough. (See Fig. 8-3 for the plot derived for the BSM design.) From such a generalized plot, the breakthrough characteristics of any combination of charcoal load and regeneration time could be determined. The arrow on the abscissa in Fig. 8-3 shows the design point selected for the BSM design, with bed length equal to 10^{-1} times the length L_s needed for adsorption of all 10 pseudo-components in a given time.

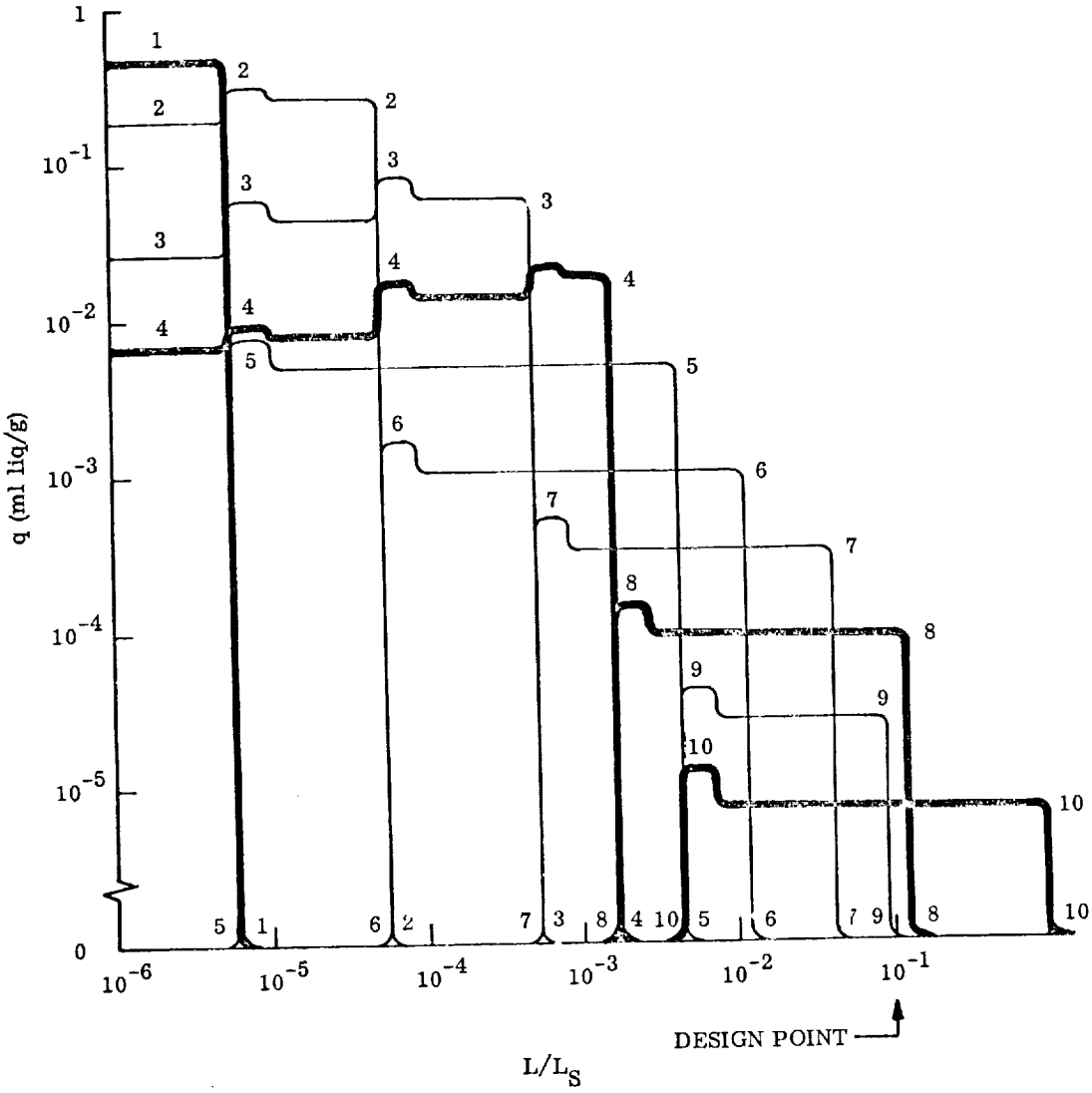

Fig. 8-3 Generalized Bed Profile

Next, a bed geometry consistent with the minimum flow rate and allowable pressure drops is selected to give sharp breakthrough curves (i.e., in accordance with Eq. 8.3). The cycle time is now set by the regeneration which is a function of desorption temperature and bed geometry. Having determined a cycle time, the amount of charcoal is determined from the design point on the generalized concentration profile. Now the selected geometry must be recalculated to be consistent with the charcoal loading, and the procedure iterated to closure. This procedure can be done as a function of desorption temperature to form the basis of an optimization between heating and cooling weight penalties and charcoal loading.

Once the bed has been sized in this way, the actual number of transfer units for each component can be determined and the actual bed profiles calculated using the multicomponent adsorption correlations developed herein (see Section 4). From such a multicomponent bed profile, the actual removal efficiencies for each pseudo-component can be calculated. From these and the design flow rate, the actual cabin concentrations can be estimated. If these are substantially different from those found initially, the whole design procedure must be iterated to closure.

Once the base design is determined in this way, it is possible to complete parametric calculations for interfacing with other modules of the life support system. If such interfacing suggests major changes from the design base case, then a redesign should be completed to the new conditions.

8.3 CRITICAL DESIGN CONTAMINANTS

One of the most enlightening features of design calculations even as crude as those used in BSM design is the identification of the critical design parameters. Specifically, for the BSM design a number of contaminants were identified as possible critical contaminants, i.e., those that might control the system design. The first are those which are flow rate-limited, meaning that the cabin concentration at 100 percent removal efficiency is greater than the MAC value due to the production rate being too high for the given air flow rate. Next are those not removed because

they are too weakly adsorbed or because their production rate is too high for an acceptable design. For the BSM case there were two of the former and a number of the latter.

Flow Rate-Limited Contaminants

Phenol
Pyruvic Acid

Unremoved Contaminants

Acetylene	Nitrogen Dioxide
Carbon Monoxide	Formaldehyde
"Freon-23"	Chlorine
Hydrogen	Hydrogen Chloride
Methane	Hydrogen Sulfide
Nitrous Oxide	Nitric Oxide
Sulfur Dioxide	Ammonia

Usually, the charcoal filter is integrated with some kind of catalytic oxidizer and basic absorber (e.g., lithium hydroxide). Under such circumstances, only ammonia would not be removed by the total system. Thus, the production of ammonia which is mostly biological must either be substantially curtailed, controlled at the source, or removed in some other way than by sorption.

Furthermore, the BSM design has identified those contaminants which break through near the design point. They are:

Acetaldehyde	"Freon-23"
Acetonitrile	"Freon-125"
Acrolein	Methylacetylene
Carbon Disulfide	Methyl Alcohol
Carbonyl Sulfide	Methylhydrazine
Chlorofluoromethane	Methyl Mercaptan
Chloropropane	Nitrogen Tetroxide
Ethane	Propylene
"Freon-21"	Vinyl Chloride

The production rates and allowable concentrations of these contaminants dominate the design. Effort directed toward more careful definition of both of these for these contaminants will result directly in more reliable design.

Under this contract and previous NASA contracts, this laboratory has investigated nearly half of these critical components. Nevertheless, it would be well worth the effort to study this group in more detail, particularly with respect to the blockage effects for mixed adsorption. Also, no work has yet been done to identify those contaminants which are the critical ones for vacuum desorption and such work is essential because of the controlling nature of the pump-out times.

Section 9
ADSORPTION FROM HUMID AIR

All the experiments covered thus far in this report have dealt with adsorption of pure contaminants, mixtures of pure contaminants, or contaminants in dry air (50% oxygen). In actual spacecraft operation, however, water vapor is always present in significant quantities. In order to complete an accurate study of adsorption processes in spacecraft applications, it is of extreme importance to know the effects of water vapor upon the adsorption of contaminants. Only with such knowledge will it be possible to decide upon the optimum location of the sorbent bed in the spacecraft air purification cycle.

To this end, a series of experiments has been performed with two typical contaminant types, one polar and one nonpolar, and at various relative humidities.

9.1 EXPERIMENTAL TECHNIQUE AND RESULTS

The flow system described in Sections 2 and 3 was modified to include a gas-stream humidifier. Several methods of humidification were considered, and it was concluded that an efficient and convenient design was one in which the gas is passed through two water bubblers connected in series (see Fig. 9-1).

The following matters were next dealt with:

(1) Determination of a desirable method for attaining various partial pressures of water effluent from the bubblers
(2) Consideration of the fact that one of the contaminant gases proposed (ethanol) is quite soluble in water

It was decided to introduce the ethanol into the gas stream after humidification.

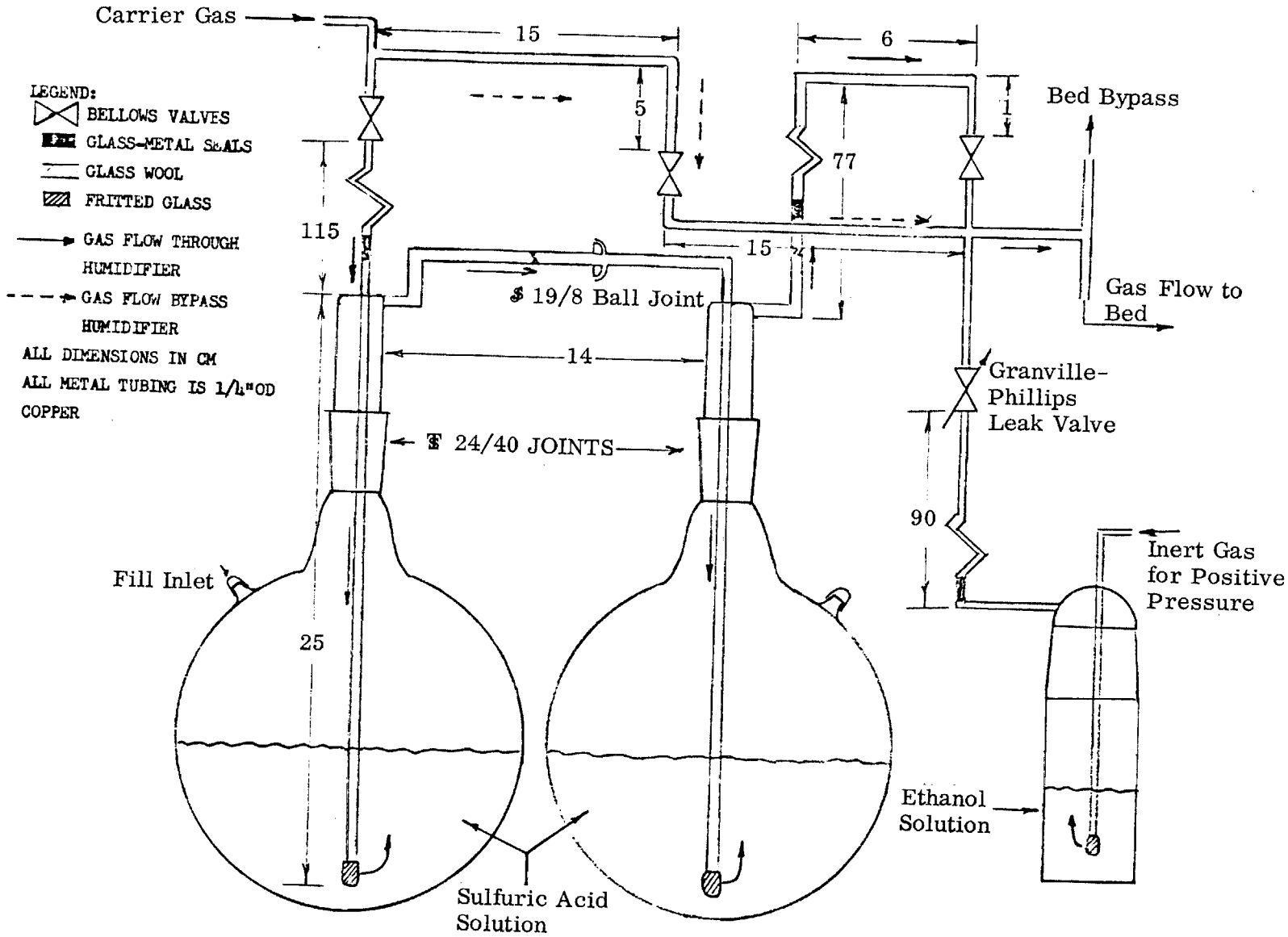

Fig. 9-1 Flow System Humidifier

9.1.1 Design and Fabrication

The humidifier system was designed and built as shown in Fig. 9-1. The two humidifier flasks and the ethanol solution flask were immersed in a constant-temperature water bath at 25 ± 0.02°C.

9.1.2 Method of Establishing Relative Humidity

Two possible methods were considered. One was to lower the temperature of the water reservoirs and thereby decrease the equilibrium vapor pressure of water. The main difficulty with this procedure was that, since the flow runs in general were quite long, it would have been difficult to maintain accurately a constant subambient temperature of, say, 10°C. The second method, which was the one adopted, was based on the fact that the addition of concentrated sulfuric acid to water could be used to establish any desired partial vapor pressure. A summary of pertinent data is given in Table 9-1.

Table 9-1

SUMMARY OF DATA USED TO ESTABLISH DESIRED HUMIDITIES

Percent Relative Humidity at 25°C	p_{H_2O} (torr)	Weight Percent H_2SO_4 (Ref. 27)	Weight H_2SO_4 Used (Ref. 28) (g/l)
100	24.0	0.0	0.0
95	22.8	10.0	106.6
70	16.8	31.5	387.8
45	10.8	46.0	624.2

One problem with this technique was that there was a continuous depletion of water, lost by evaporation into the gas stream. As water was removed, the concentration of sulfuric acid increased and the partial pressure of water decreased. This problem

was solved by choosing an initial volume large enough so that the loss of small amounts of water did not significantly affect the diluted acid composition. In the present case, it was estimated that a volume of 1 liter would experience a loss of water of 0.1%/hr during an average run.

To verify the predicted partial pressures, the system described above was pumped until pressure readings downstream from the second bulb were constant. This pressure was then taken as the partial water vapor pressure at the temperature of the bath surrounding the bulbs.

In the flow experiments described in Sections 2 and 3, premixed gases containing 50% oxygen and 50% nitrogen and one or more trace contaminants at or near their MAC levels were used. In the experiments described here, contaminant introduction had to be modified due to solubility considerations. It was found from the literature that the solubility of n-butane in water is 0.025 ml/ml H_2O (Ref. 29). Calculations indicated that a 1-liter charge of water solution would be saturated with n-butane from the premixed cylinder in approximately 2 hr at the flow rates anticipated. Equilibrium in this manner was performed before diverting the gas through the sorbent bed.

In the case of ethanol as a contaminant, a premixed gas could not be used due to the mutual solubility of ethanol and water. To circumvent the problem of solubility, the system was designed so that the gas stream not containing ethanol was saturated to the desired humidity. Then ethanol vapor was introduced into the gas stream through a Granville-Phillips leak valve to the desired contaminant concentration (see Fig. 9-1).

Using the above-described flow system modifications, the humid air experiments were accomplished. The results are summarized in Table 9-2.

Table 9-2

SUMMARY OF ADSORPTION DATA FOR n-BUTANE, ETHANOL, AND WATER ON BD ACTIVATED CARBON

Run No.	Species	Equilibrium Concentration c_{eq} (ppm)	Equilibrium Pressure p (torr)	Vapor Pressure p^o (torr)	Amount Adsorbed q_a (ml liq/g)	Amount Flow Desorbed q_{df} (ml liq/g)	Adsorption Potential A (mol °K/ml liq)	Temperature T (°C)
F18-1	$n\text{-}C_4H_{10}$	26.4	21.2	25.2	1.9×10^{-3}	1.3×10^{-3}	16.1	26
	H_2O					$\sim 3 \times 10^{-1}$	1.19	
F19-1	$n\text{-}C_4H_{10}$	24.0	21.2	28.3	1.14×10^{-3}	9.8×10^{-4}	16.5	28
	H_2O				3.58×10^{-1}		2.01	
F19-2	C_2H_5OH	60.0	0	19.6	1.1×10^{-2}	1.2×10^{-2}	23.5	66
	H_2O						∞	
F19-3	C_2H_5OH	35.5	0	25.2	2.55×10^{-2}	2.2×10^{-2}	17.5	26
	H_2O						∞	
F19-4	$n\text{-}C_4H_{10}$	25.5	21.2	17.9	9.26×10^{-3}	9.75×10^{-2}	20.4	64
	H_2O				None detected		16.7	
F19-5	C_2H_5OH	20.0	21.2	26.7	5.56×10^{-3}	6.47×10^{-3}	19.1	27
	H_2O						1.6	
F19-6	C_2H_5OH	28.0	21.2	19.6	2.0×10^{-3}	1.7×10^{-3}	25.2	66
	H_2O				None detected		17.5	
F19-7	$n\text{-}C_4H_{10}$	25.6	15.0	26.7	7.43×10^{-3}	7.34×10^{-3}	16.5	27
	H_2O						4.0	
F19-8	$n\text{-}C_4H_{10}$	25.8	15.0	18.7	8.41×10^{-3}	8.70×10^{-3}	20.1	65
	H_2O				None detected		19.8	
F19-9	C_2H_5OH	27.0	15.0	26.7	1.32×10^{-2}	1.46×10^{-2}	18.6	27
	H_2O						4.0	
F19-10	C_2H_5OH	16.2	15.0	19.6	1.39×10^{-3}	2.16×10^{-3}	26.4	66
	H_2O						20.1	
F19-11	$n\text{-}C_4H_{10}$	25.1	10.0	25.2	2.50×10^{-2}	2.58×10^{-2}	16.5	26
	H_2O						6.4	
F19-12	$n\text{-}C_4H_{10}$	26.2	10.0	20.5	8.12×10^{-3}	1.08×10^{-2}	20.3	67
	H_2O						23.7	
F19-13	C_2H_5OH	~ 24	10.0	25.2	1.8×10^{-2}		18.5	26
	H_2O						6.4	
F19-14	C_2H_5OH	20.5	10.0	19.6	2.6×10^{-3}		25.9	66
	H_2O						23.3	

9.2 DISCUSSION

Study of the Table 9-3 and comparison with previous data taken under dry conditions reveal the important role of relative humidity in causing blockage. Some typical values of reduction in contaminant adsorption capacity due to the presence of water vapor are shown in Table 9-3.

Table 9-3

CONTAMINANT BLOCKAGE DUE TO WATER VAPOR

Run No.	Contaminant	Temp. (°C)	Concentration (ppm)	Relative Humidity at 25°C	Blockage (%)
F19-11	n-Butane	26	25	42	28
F19-7	n-Butane	27	26	63	79
F18-1	n-Butane	26	26	89	95
F19-12	n-Butane	67	26	42	0
F19-8	n-Butane	65	26	63	0
F19-4	n-Butane	64	26	89	0
F19-13	Ethanol	26	24	42	5
F19-9	Ethanol	27	27	63	30
F19-5	Ethanol	27	20	89	65
F19-14	Ethanol	66	20	42	56
F19-10	Ethanol	66	16	63	73
F19-6	Ethanol	66	28	89	71

An overwhelming influence of relative humidity is evident, and clearly there is an urgent need to predict such blockage phenomena as part of any realistic design procedure. To accomplish such prediction, use is made of the modified potential theory as expressed in Eq. 4.50,

$$A_T = A + \frac{T}{V_m} \log X_1 \qquad (4.50)$$

Values of A are shown in Table 9-2, along with adsorbed quantities of n-butane and ethanol. It was not possible in these mixed adsorption experiments to measure precisely the amount of water actually adsorbed because of limitations in the detection system used. The adsorption isotherm for water on BD has been measured gravimetrically, however (see Fig. 2-11), and it will be assumed that the amount of water adsorbed is not affected by the presence of the solute (i.e., n-butane and ethanol). This assumption is likely to be inappropriate only at very high values of X_i. Thus, it is possible to calculate the mole fraction,

$$X_1 = \frac{q_s}{q_s + \left(\frac{V_{ms}}{V_{mw}}\right) q_w} \tag{9.1}$$

where

q_s = amount of solute adsorbed, obtained from humid air adsorption
q_w = amount of water adsorbed, obtained from pure water isotherm
V_{ms} = molar volume of solute
V_{mw} = molar volume of water

and

$$q_T = q_s + q_w \tag{9.2}$$

If this model for unmixed adsorption is valid, then it may be expected that a plot of q_T from Eq. 9.2 versus A_T from Eq. 4.50 will closely fit the generalized potential plot. Data from such calculations are summarized in Table 9-4 and plotted in Fig. 9-2. The line in Fig. 9-2 is the generalized potential plot and the data are in excellent agreement except at the highest values of q_T where it is likely that q_w is somewhat less than the value obtained from the pure water isotherm. The uncorrected adsorption potential is plotted in Fig. 9-3 to show the great improvement obtained in using the modified A as in Fig. 9-2. Thus, it is possible to estimate humid air adsorption from the generalized potential plot and the water isotherm. Because this has been

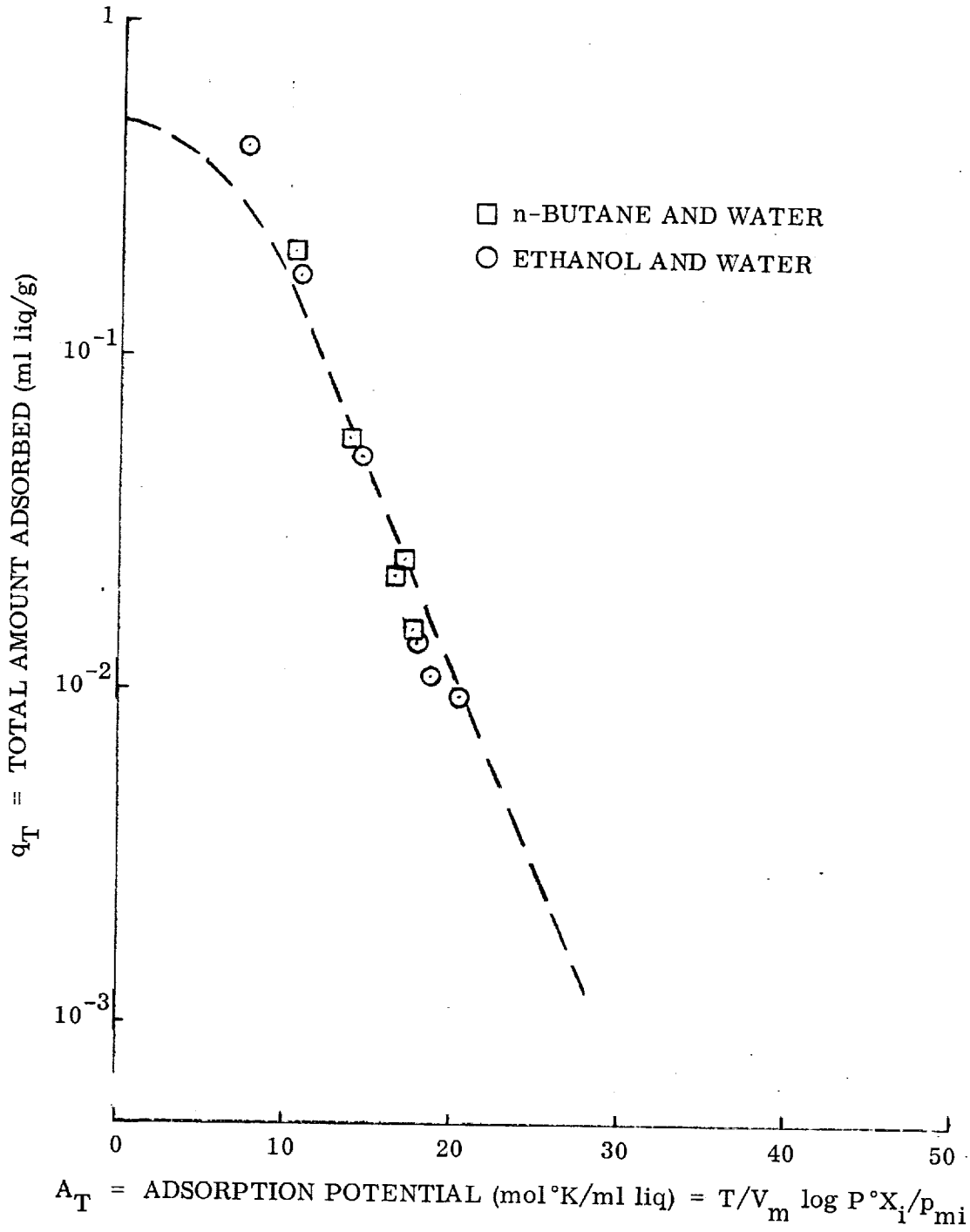

Fig. 9-2 Potential Plot for Adsorption From Dry and Humid Gas Mixtures on BD Activated Carbon

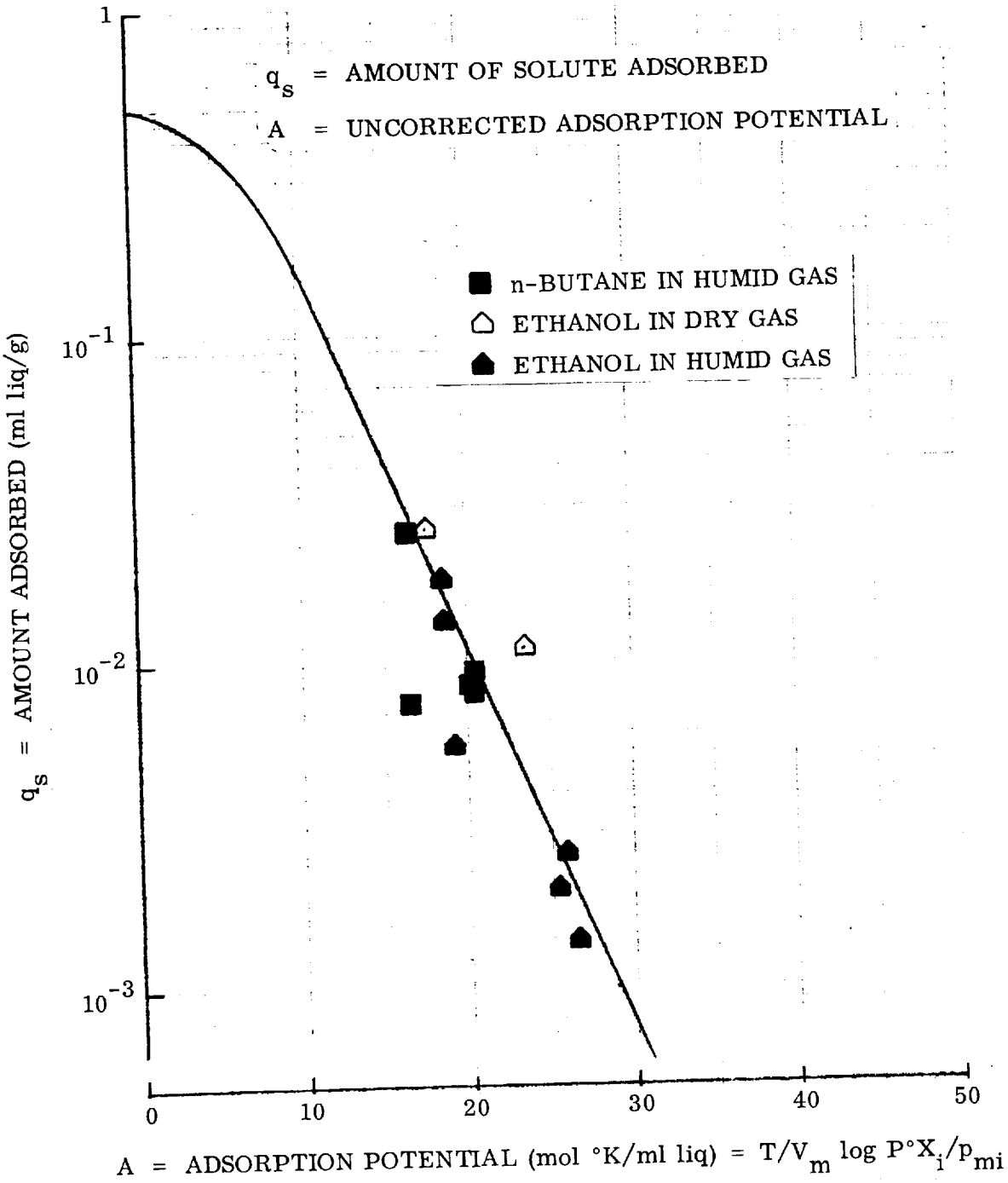

Fig. 9-3 Potential Plot for Adsorption From Dry and Humid Gas Mixtures on BD Activated Carbon

Table 9-4

MODIFIED POTENTIAL-THEORY QUANTITIES FOR HUMID ADSORPTION EXPERIMENTS

Solute	q_s	q_w	q_T	X	A_T	A	Run No.
n-Butane	9.3×10^{-3}	1.5×10^{-2}	2.44×10^{-2}	1.04×10^{-1}	17.0	20.4	F19-4
n-Butane	8.12×10^{-3}	7.0×10^{-3}	1.51×10^{-2}	1.78×10^{-1}	17.7	20.3	F19-12
n-Butane	8.41×10^{-3}	1.4×10^{-2}	2.2×10^{-2}	1.01×10^{-1}	16.5	20.1	F19-8
n-Butane	2.5×10^{-2}	3.2×10^{-2}	5.7×10^{-2}	1.28×10^{-1}	13.7	16.5	F19-11
n-Butane	7.43×10^{-3}	2.0×10^{-1}	2.07×10^{-1}	6.88×10^{-3}	10.3	16.5	F19-7
Ethanol	2.6×10^{-3}	7.0×10^{-3}	9.6×10^{-3}	9.7×10^{-2}	20.4	25.9	F19-14
Ethanol	1.39×10^{-3}	1.0×10^{-2}	1.1×10^{-2}	3.87×10^{-2}	18.7	26.4	F19-10
Ethanol	2.0×10^{-3}	1.2×10^{-2}	1.4×10^{-2}	0.61×10^{-2}	17.9	25.2	F19-6
Ethanol	1.8×10^{-2}	3.2×10^{-2}	5.0×10^{-1}	1.41×10^{-1}	14.4	18.5	F19-13
Ethanol	1.32×10^{-2}	1.6×10^{-1}	1.73×10^{-1}	2.34×10^{-2}	10.7	18.6	F19-9
Ethanol	5.56×10^{-3}	4.2×10^{-1}	4.26×10^{-1}	3.81×10^{-3}	7.4	19.1	F19-5

successful for n-butane, a nonpolar molecule, and ethanol, a polar molecule which might even exhibit hydrogen bonding with water, it is presumed that it may be applied generally.

Section 10
CONCLUSIONS AND RECOMMENDATIONS

10.1 CONCLUSIONS

- A successful correlation for the estimation of sorptive capacity has been determined. This correlation, which has been extended to adsorption potential theory parameters, applies to both pure and mixed contaminants, under both dry and humid conditions, and at various temperatures. The capacity correlation is a vital design tool needed to assess the effect of different operating conditions on equilibrium performance.

- The rate of vacuum desorption from single sorbent particles and from sorbent beds has been characterized. Mechanisms and theories proposed have been experimentally proven to be adequate to describe the phenomena over the ranges tested.

  It has been shown in single-particle studies that the rate-determining step is desorption from the external particle surface. Thus, the rate is inversely proportional to the particle diameter.

  For vacuum desorption from sorbent beds, the rate-determining step is Knudsen diffusion through interparticle voids. The Knudsen diffusivity has been experimentally measured. Although the single-particle studies showed that smaller particles desorb faster, the theory correctly predicts the surprising result that the opposite is true for beds: beds composed of larger particles desorb faster than those containing smaller particles. The desorption rate dependency on bed geometry, adsorption isotherm, and initial gas-phase concentration is also contained in the theory, and the theoretical predictions agree with experimental measurements.

  Neither experimental vacuum desorption rate data nor theoretical descriptions were available prior to this contract. In the course of this work, substantial information on both fronts has been generated, sufficiently to begin design work on a prototype unit.

- The information gained on this program was instrumental in enabling the development of a quantitative design methodology for vacuum-regenerative sorbent systems. This design procedure is the first one known to consider realistically the phenomenon of adsorbate interference.

10.2 RECOMMENDATIONS

- Further adsorption capacity measurements with contaminant mixtures are recommended in order to provide further confirmation of the generality of the modified adsorption potential theory.
- The design, construction, operation, and test of a prototype regenerative sorption system is recommended.
- Implicit in a design procedure, the following steps should be done after theoretical determination of the "key components" (those contaminants which limit the design): For the key components only, (1) obtain accurate production rates, and (2) verify experimentally the capacity and the kinetics.
- Existing sorbent system designs should be updated, based on the advances reported here. A computer program for the design procedure should be developed as part of this task.
- The successful correlation of sorption capacities under humid conditions indicates the theory may be applicable to waste-water purification by adsorption. Appropriate tests should be performed.
- Efforts to establish more carefully the production rates of the design-controlling contaminants should be initiated. In such tests, some attempts should be made to evaluate the attenuation of the rates with times of the order of mission times. The effect of temperature on contaminant production rates from materials within the spacecabin should also be investigated.

Appendix A

SAMPLE CALCULATIONS FOR FLOW EXPERIMENTS

A.1 TYPICAL CONDITIONS DURING CALIBRATION

(a) Flow rate = 250 ml RTP/min

(b) P_{system} = 0.5 atm

(c) Sample loop volume (Beckman Valve) = 2.0 ml

(d) Range × attenuation of the electrometer = 10 × 8

(e) Contaminant peak area for 2.0 ml volume at 0.5 atm total pressure = 2.5 mV-sec as determined by the disk integrator

(f) Electrometer transconductance = 4 picocoulombs/mV-sec (= 4 nmho)

(g) Premixed gas contaminant concentration = 50 ppm

A.2 SAMPLE CALCULATIONS OF DETECTOR OUTPUT

$$\text{Detector output} = \frac{2.5 \text{ mV-sec} \times 10 \times 8 \times 4 \text{ pC/mV-sec}}{0.5 \text{ atm} \times 2 \text{ ml}}$$

$$= \frac{800 \text{ pC}}{\text{ml RTP}}$$

The total response of the detector to 50 ppm contaminant is thus 800 pC/ml RTP which is the response to a known amount of contaminant equal to 5×10^{-5} ml RTP.

A.3 SAMPLE CALCULATIONS OF EFFLUENT CONCENTRATION

P_{system} = 0.5 atm
Loop volume = 2.0 ml
Range × attenuation = 10 × 2

Peak area = 1.5 mV-sec

$$\text{Detector response (for unknown conc.)} = \frac{1.5 \text{ mV-sec} \times 10 \times 2 \times 4\text{pC/mV-sec}}{0.5 \text{ atm} \times 2 \text{ ml}}$$

$$= 120 \text{ pC/ml RTP}$$

Comparison of unknown to known detector response

$$\text{Unknown Concentration} = \frac{\text{unknown response}}{\text{known response}} \times \text{standard concentration}$$

$$= \frac{120}{800} \times 50 \text{ ppm}$$

$$= 7.5 \text{ ppm}$$

A.4 SAMPLE CALCULATION OF AMOUNT ADSORBED, q_a

A typical breakthrough curve for propylene at C_{eff} = 15 ppm

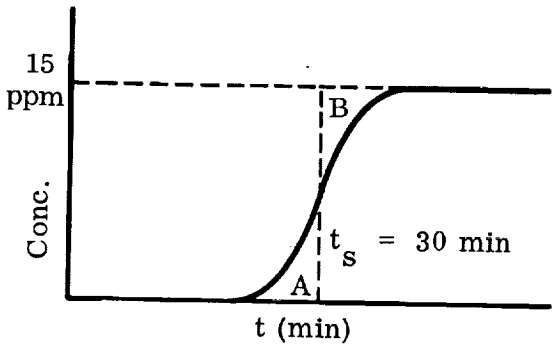

The parameters established from the breakthrough curve are:

(1) C_{eff} = 15 ppm
(2) t_s = 30 min (t_s = time such that area A = area B)
(3) Flow = 500 ml RTP/min

(4) P_{bed} = 0.52 atm (see below for calculation)

Parameters established from other sources:

(1) Weight of bed: W = 0.500 g

(2) Molar volume of the liquid at its normal boiling point: V_m = 66.6 ml liq/mol

(3) Gas constant at RTP = 24 400 ml RTP/mol

$$q_a = \frac{\frac{C_{eff}\,(ppm)}{10^6} \times t_s\,(min) \times V_m \left(\frac{ml\ liq}{mol}\right) \times flow \left(\frac{ml\ RTP}{min}\right)}{W(g) \times gas\ const. \left(\frac{ml\ RTP}{mol}\right)}$$

$$= \frac{15 \times 30 \times 66.6 \times 500 \times 10^{-6}}{0.500 \times 24\,400}$$

$$= 4.92 \times 10^{-3} \frac{ml\ liq}{g\ (sorbent)}$$

Since there was a pressure drop across the bed, an estimate was made of the pressure in the middle of the bed. A typical calculation is given:

P_1 = pressure upstream of bed

P_2 = pressure downstream from bed

ΔP_3 = pressure drop across quartz chips (const.)

P_4 = pressure in the middle of the bed

$$P_4 = P_2 + \frac{(P_1 - \Delta P_3) - P_2}{2}$$

P_1 = 427 torr

P_2 = 380 torr

ΔP_3 = 17 torr (predetermined value)

$$P_4 = 380 + \frac{(427 - 17) - 380}{2}$$

$$= 395 \text{ torr} = \frac{395}{760} = 0.52 \text{ atm}$$

A.5 SAMPLE CALCULATION OF THE ADSORPTION POTENTIAL, A

Typical calculation of the A-value for propylene at 15 ppm and room temperature

$$A = \frac{T\ (°K)}{V_m\ (\text{ml liq/mol})} \log_{10} \frac{P°}{p}$$

where

$P°$ = vapor pressure of the pure contaminant at T°K = 11.2 atm @ 298°K

p = partial pressure of the contaminant in the system = $C_{inlet} \times P_{system}$

$$A = \frac{298°K}{66.6\ \text{ml liq/mol}} \log_{10} \frac{11.2\ \text{atm}}{(15/10^6) \times 0.52\ \text{atm}}$$

$$= 4.47 \frac{\text{mol °K}}{\text{ml liq}} \log 1.45 \times 10^6$$

$$= 27.52 \frac{\text{mol °K}}{\text{ml liq}}$$

Appendix B

SAMPLE WEIGHT AND PRESSURE RECORDS FROM GRAVIMETRIC EXPERIMENTS

A sample of a weight record from typical gravimetric experiments, M20-65 and 66, is presented in Fig. B-1. This is a portion of a strip-chart recording of the electrical output of the electrobalance unit referred to in section 2.1.2. On it are included electrobalance settings, temperature, and other pertinent notes concerning the nature of the experiment.

A sample total and partial pressure record for the same experiments is given in Fig. B-2, which is the recording from a two-pen strip-chart recorder attached to both the total pressure (Barocel) gage and the partial pressure (QRGA) gage described in section 3.1.2. Total pressure may be read directly from the recording as indicated, while partial pressure of each contaminant may be calculated from the mass spectrometer peaks on the chart. Normally, this was only estimated to ensure that the more strongly adsorbed contaminant was not being displaced by the second, less strongly adsorbed one. The calculation is similar to that described in section 5.2.2, except that the peak M/e = 91 was used for toluene, and the ratio S_{43}/S_{91} was taken to be 0.9. Partial pressure of toluene would then be given by the relation

$$p_t = 0.9 \frac{h_{91}}{h_{43}} P \qquad \text{(B.1)}$$

where

p_t = toluene partial pressure (torr)

h_{91}, h_{43} = peak heights for M/e = 91 and 43, respectively (pA)

P = total pressure (Barocel reading) (torr)

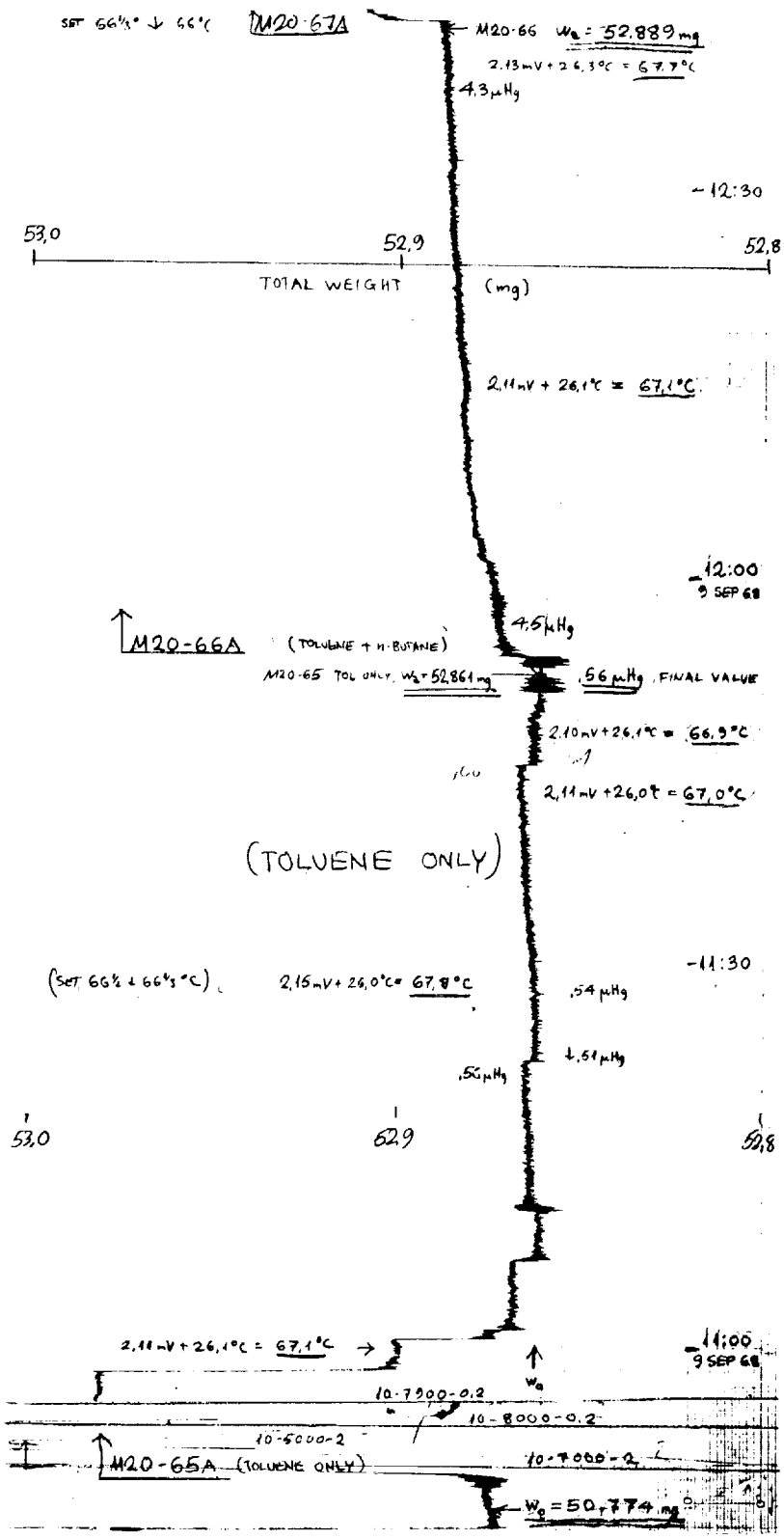

Fig. B-1 Weight Record for Run No. M20-65 and M20-66

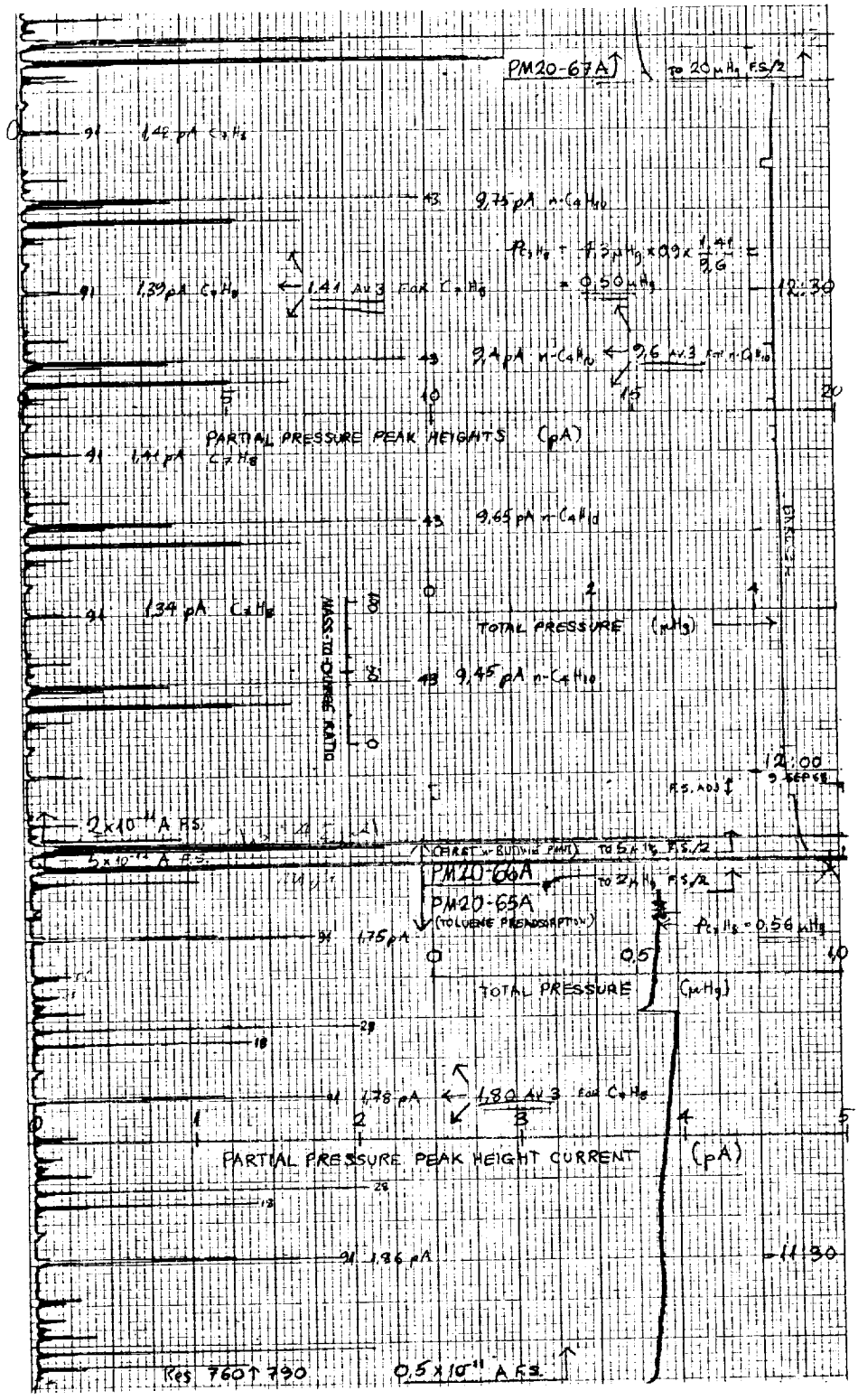

Fig. B-2 Pressure Record for Run No. M20-65 and M20-66

Appendix C

FLOW SYSTEM EXPERIMENTAL SUMMARY

Run No.	Temp. T (°C)	Sorbent	Contaminant	Concentration C_{off} (ppm)	Partial Pressure p (torr)	Total Pressure p (atm)	Adsorption Potential A (mol °K/ml liq/g)	Amount Adsorbed q_{de} (ml liq/g)	Amount Adsorbed q_{de} (ml STP/g)	Vacuum Desorption Time t_d (min)	Amount Flow Desorbed q_{df} (ml liq/g)	Amount Otherwise Removed $q_{de} - q_{df}$ (ml liq/g)	Purpose of Experiment	Remarks
F1-1	24	16 × 20 BD	C_2H_4										System check	
F2-1	24	16 × 20 BD	C_2H_4	60	2.28×10^{-2}	0.5	38.1	8.28×10^{-5}	3.75×10^{-2}	–	8.52×10^{-5}		Reproducibility	
-2	24	16 × 20 BD	C_2H_4	57	2.16×10^{-2}	.5	38.2	7.84×10^{-5}	3.55×10^{-2}	–	7.64×10^{-5}		Reproducibility	
-3	24	16 × 20 BD	C_2H_4	58	2.21×10^{-2}	.5	38.2	7.80×10^{-5}	3.53×10^{-2}	–	7.64×10^{-5}		Reproducibility	
-4	24	16 × 20 BD	C_2H_4	57	2.16×10^{-2}	.5	38.2	7.83×10^{-5}	3.55×10^{-2}	–	–		Reproducibility	
-5	24	16 × 20 BD	C_2H_4	51	1.89×10^{-2}	.5	38.5	8.21×10^{-5}	3.73×10^{-2}	–	8.65×10^{-5}		Reproducibility	
F3-1	24	16 × 20 13X	C_2H_4	67	2.25×10^{-2}	0.5	37.4	2.47×10^{-4}	1.12×10^{-1}	–	–		Different sorbent	
-2	24	16 × 20 13X	C_2H_4	80	3.06×10^{-2}	.5	37.35	2.48×10^{-4}	1.13×10^{-1}	–	–		Different sorbent	
F4-1	25	30 × 40 BD	C_3H_8	–	–	–	–	–	–	–	–	q_{de}	Vacuum desorption system check	
F5-1	25	30 × 40 BD	C_3H_8	34.2	1.38×10^{-2}	0.53	22.7	4.12×10^{-3}	1.24×10^{0}	8	3.91×10^{-3}	0.21×10^{-3}	Desorption rate study	
-2	25	30 × 40 BD	C_3H_8	34.0	1.29×10^{-2}	.50	22.9	3.79×10^{-3}	1.14×10^{0}	50	3.23×10^{-3}	0.56×10^{-3}	Desorption rate study	
-3	25	30 × 40 BD	C_3H_8	35.4	1.35×10^{-2}	.50	22.8	3.67×10^{-3}	1.10×10^{0}	115	2.85×10^{-3}	0.82×10^{-3}	Desorption rate study	
-4	25	30 × 40 BD	C_3H_8	32.1	1.22×10^{-2}	.50	23.0	3.41×10^{-3}	1.02×10^{0}	–	3.58×10^{-3}	–	Desorption rate study	
-5	25	30 × 40 BD	C_3H_8	33.9	1.26×10^{-2}	.50	22.8	3.60×10^{-3}	1.08×10^{0}	360	2.26×10^{-3}	1.34×10^{-3}	Desorption rate study	
-6	25	30 × 40 BD	C_3H_8	33.4	1.27×10^{-2}	.50	22.9	3.49×10^{-3}	1.05×10^{0}	1 000	0.90×10^{-3}	2.59×10^{-3}	Desorption rate study	
-7	25	30 × 40 BD	C_3H_8	34.0	1.32×10^{-2}	.51		–	–					
F6-1	25	30 × 40 BD	(1) C_3H_6	21.0	8.45×10^{-3}	0.53	26.8	1.96×10^{-3}	6.60×10^{-3}	1 000	0	1.96×10^{-3}	Concurrent adsorption of two	
			(2) $CH_2 = CCl_2$	18.3	7.37×10^{-3}	.53	18.4	3.61×10^{-2}	1.01×10^{1}		3.4×10^{-2}	0.2×10^{-2}	Contaminants; also vacuum	
-2	46	30 × 40 BD	(1) C_3H_8	20.2	8.28×10^{-3}	.54	29.8	5.9×10^{-4}	1.98×10^{-1}	1 136	0	5.9×10^{-4}	Desorption of two contaminants	LN trap failure at $t_d < 1\,000$ min
			(2) $CH_2 = CCl_2$	25.8	1.06×10^{-2}	.54	20.4	2.47×10^{-2}	7.98×10^{0}		1.30×10^{-2}	1.17×10^{-2}		
F7-1	102	30 × 40 BD	(1) $CH_2 = CCl_2$	–	–	–	–	–	–	–				
			(2) $C_6H_5CH_3$	–	–		–	–	–	–				
-2	102	30 × 40 BD	(1) $CH_2 = CCl_2$	25.1	1.01×10^{-3}	0.53	27.0	2.20×10^{-3}	6.20×10^{-1}	–	0	–	Displacement of $CH_2 = CCl_2$ by $C_6H_5CH_3$ after t = 91 min	3-day wait between adsorption and desorption steps
			(2) $C_6H_5CH_3$	29.5	1.19×10^{-2}	.53	15.0	5.9×10^{-2}	1.12×10^{1}	–	4.0×10^{-2}			
-3	102	30 × 40 BD	(1) $C_6H_5CH_3$	24.8	9.80×10^{-3}	.52	15.2	5.2×10^{-4}	9.85×10^{0}	–	>1.9 × 10^{-2}		Blockage of $CH_2 = CCl_2$ by $C_6H_5CH_3$ after t = 1016 min	
			(2) $CH_2 = CCl_2$	25.2	9.95×10^{-3}	.52	27.1	2.0×10^{-4}	5.61×10^{-2}	–	4.6×10^{-4}		Reproducibility check	
-4	102	30 × 40 BD	$CH_2 = CCl_2$	25.2	9.97×10^{-3}	.52	26.8	2.66×10^{-4}	7.45×10^{-2}	–	2.43×10^{-3}		Repeat of F7-2	10% discrepancy
-5	101	30 × 40 BD	(1) $CH_2 = CCl_2$	20.5	8.1 × 10^{-3}	.52	27.3	1.89×10^{-3}	5.30×10^{-1}	–	2.4×10^{-4}			
			(2) $C_6H_5CH_3$	–	–	–	–	–	–	–	6.1×10^{-2}			
-6	102	30 × 40 BD	$C_6H_5CH_3$	–	–	–	–	–	–	–				
-7	102	30 × 40 BD	(1) $C_6H_5CH_3$	6.1	2.55×10^{-3}	.55	18.9	2.15×10^{-2}	4.06×10^{0}	–			Blockage of $CH_2 = CCl_2$ by low concentration of $C_6H_5CH_3$	
			(2) $CH_2 = CCl_2$	23.5	9.8×10^{-3}	.55	27.0	1.6×10^{-4}	4.09×10^{-2}	–	$<10^{-4}$			

Run No.	Temp. T (°C)	Sorbent	Contaminant	Concentration C_{eff} (ppm)	Partial Pressure p (torr)	Total Pressure P (atm)	Adsorption Potential A (mol °K/ml liq)	Amount Adsorbed q_g (ml liq/g)	Amount Adsorbed q_g (ml STP/g)	Vacuum Desorption Time t_d (min)	Amount Flow Desorbed q_{df} (ml liq/g)	Amount Otherwise Removed $q_g - q_{df}$ (ml liq/g)	Purpose of Experiment	Remarks
F8-1		30 × 40 BD												
F9-1	25	30 × 40 BD	(1) $n\text{-}C_4H_{10}$	20.4	7.9×10^{-3}	0.51	16.6	3.4×10^{-2}	7.9×10^{0}	4 305	1.4×10^{-2}	2.0×10^{-2}	Desorption rate study and blockage of C_3H_6 by $n\text{-}C_4H_{10}$	
			(2) C_3H_6	.54	2.09×10^{-4}	.51	34.0	1.67×10^{-5}	5.62×10^{-3}		0			
-2	25	30 × 40 BD	(1) $n\text{-}C_4H_{10}$	1.08	4.52×10^{-4}	.55	20.4	8.0×10^{-3}	1.86×10^{0}	5 760	4.5×10^{-2}	3.5×10^{-2}	Desorption rate study and blockage of C_3H_6 by low conc. $n\text{-}C_4H_{10}$	
			(2) C_3H_6	13.2	5.51×10^{-3}	.55	27.6	1.03×10^{-3}	3.47×10^{-1}		0			
-3	27	30 × 40 BD	C_3H_6	13.0	5.43×10^{-3}	.55	27.8	1.18×10^{-3}	3.97×10^{-1}	80	5.9×10^{-4}	5.9×10^{-4}	Adsorption of C_3H_6 and desorption rate study	(Single desorption point)
-4	25	30 × 40 BD	$n\text{-}C_4H_{10}$	–	–	–	–	–	–					
F10-1	25	30 × 40 BD	$n\text{-}C_4H_{10}$	–	–	–	–	–	–					Bed used for MS experiments
F11-1	24	30 × 40 BD	$n\text{-}C_4H_{10}$	21.4	9.02×10^{-3}	0.56	16.4	2.98×10^{-2}	6.91×10^{0}	6 431	1.01×10^{-2}	1.97×10^{-2}	Desorption rate study	
-2	25	30 × 40 BD	$n\text{-}C_4H_{10}$	17.8	7.45×10^{-3}	.55	16.7	2.41×10^{-2}	5.59×10^{0}	1 050	1.86×10^{-2}	0.55×10^{-2}	Desorption rate study	
-3	25	30 × 40 BD	$n\text{-}C_4H_{10}$	18.5	7.74×10^{-3}	.55	16.6	2.62×10^{-2}	6.08×10^{0}	16 767	0.33×10^{-2}	2.29×10^{-2}	Desorption rate study	
-4	27	30 × 40 BD	(1) $n\text{-}C_4H_{10}$	0.9	3.8×10^{-4}	.55	20.9	5.7×10^{-3}	6.32×10^{0}	–	5.3×10^{-3}	–	Blockage of high conc. C_3H_6 by	
			(2) C_3H_6	1580	6.61×10^{-1}	.55	18.5	4.0×10^{-2}	1.35×10^{1}	–	3.8×10^{-2}	–	low conc. $n\text{-}C_4H_{10}$	
-5	27	30 × 40 BD	C_3H_6	1600	6.33×10^{-1}	.52	18.6	4.5×10^{-2}	1.51×10^{1}	–	4.6×10^{-2}	–	Adsorption of C_3H_6	
-6	25	30 × 40 BD	(1) C_3H_6	13.2	5.32×10^{-3}	.53	27.8	1.35×10^{-3}	4.54×10^{-1}	–	4.5×10^{-4}	9.0×10^{-4}	Displacement of C_3H_6 by $n\text{-}C_4H_{10}$	$q_{displaced} = 1.17 \times 10^{-3}$ ml liq/g
			(2) $n\text{-}C_4H_{10}$	20.2	8.13×10^{-3}	.53	16.55	2.71×10^{-2}	6.30×10^{0}	–	2.81×10^{-2}	–		
-7	25	30 × 40 BD	(1) $n\text{-}C_4H_{10}$	19.5	8.00×10^{-3}	.54	16.6	2.58×10^{-2}	6.00×10^{0}	–	–	–	Blockage of C_3H_6 by $n\text{-}C_4H_{10}$	
			(2) C_3H_6	13.4	5.50×10^{-3}	.54	27.8	4.13×10^{-4}	1.39×10^{-1}	–	–	–		
F12-1	25	30 × 40 BD	(1) C_3H_6	13.8	5.35×10^{-3}	0.51	27.8	1.49×10^{-3}	5.01×10^{-1}	–	1.52×10^{-2}	–	Blockage of C_2H_4 by C_3H_6	
			(2) C_2H_4	27.2	1.05×10^{-2}	.51	40.3	4.97×10^{-5}	2.25×10^{-2}	–	4.12×10^{-2}	–		
-2	25	30 × 40 BD	C_2H_4	26.2	9.95×10^{-3}	.50	40.3	4.88×10^{-5}	2.22×10^{-2}	–	4.64×10^{-5}	–	Adsorption of C_2H_4	
F13-1	25	8 × 12 BD	$n\text{-}C_4H_{10}$	19.5	8.15×10^{-3}	0.55	16.2	2.63×10^{-2}	6.11×10^{0}	–	–		Desorption Rate Study	Bed leak
-2	25	8 × 12 BD	$n\text{-}C_4H_{10}$	25.0	1.00×10^{-2}	.53	16.3	3.53×10^{-2}	8.20×10^{0}	4 560	3.3×10^{-3}	–	Desorption Rate Study	
F14-1	25	8 × 12 BD	$n\text{-}C_4H_{10}$	25.3	1.00×10^{-2}	0.52	16.4	3.28×10^{-2}	7.62×10^{0}	4 320	2.5×10^{-2}	3.6×10^{-2}	Desorption Rate Study	Quartz chips in bed
F15-1	25	8 × 12 BD	$n\text{-}C_4H_{10}$	25.3	1.01×10^{-2}	0.52	16.3	3.40×10^{-2}	7.90×10^{0}	5 750	2.9×10^{-2}	3.5×10^{-2}	Desorption Rate Study	Confirms F13-2 data
-2	24	8 × 12 BD	$n\text{-}C_4H_{10}$	26.4	1.05×10^{-2}	.52	16.2	3.56×10^{-2}	8.26×10^{0}	5 580	2.9×10^{-3}	3.6×10^{-2}	Desorption Rate Study	Confirms F13-2 data
-3	105	8 × 12 BD	$n\text{-}C_4H_{10}$	27.0	1.05×10^{-2}	.51	24.2	1.05×10^{-3}	2.44×10^{-1}	11 250	–	1.2×10^{-3}	Desorption Rate Study	Bed problem
F16-1	25	8 × 12 BD	$n\text{-}C_4H_{10}$	26.5	1.03×10^{-2}	0.51	16.2	3.64×10^{-2}	8.45×10^{0}	10 200	5.1×10^{-3}	3.6×10^{-2}	Desorption Rate Study	Long bed (9 g)

Run No.	Temp. T (°C)	Sorbent	Contaminant	Concentration C_{eff} (ppm)	Partial Pressure p (torr)	Total Pressure P (atm)	Adsorption Potential A (mol °K/ml liq)	Amount Adsorbed q_a (ml liq/g)	Amount Adsorbed q_a (ml STP/g)	Vacuum Desorption Time t_d (min)	Amount Flow Desorbed q_{df} (ml liq/g)	Amount Otherwise Removed $q_a - q_{df}$ (ml liq/g)	Purpose of Experiment	Remarks
F17-1	107	8 × 12 BD	C_7H_8	27.3	1.05×10^{-2}	0.51	15.0	5.8×10^{-2}	1.10×10^{1}	2 800	1.8×10^{-2}	6.4×10^{-2}	Desorption Rate Study	
-2	107		$n\text{-}C_4H_{10}$	27.0	1.04×10^{-2}	.51	24.2	2.17×10^{-3}	5.04×10^{-1}	1 000	0	3.1×10^{-3}	Desorption Rate Study	
-3	107	8 × 12 BD	(1) $n\text{-}C_4H_{10}$	26.9	1.04×10^{-2}	.51	24.8	1.82×10^{-3}	4.23×10^{-1}	5 250	0	5.8×10^{-4}	Desorption Rate Study	Displacement and vacuum desorption of two contaminants
			(2) C_7H_8	26.8	1.04×10^{-2}	.51	15.4	5.98×10^{-2}	1.13×10^{1}	5 250	1.1×10^{-2}	5.2×10^{-2}	Desorption Rate Study	
-4	67	8 × 12 BD	(1) C_7H_8	26.5	1.01×10^{-2}	.50	12.2	1.9×10^{-2}	3.7×10^{-1}	10 250	5.2×10^{-2}	9.0×10^{-2}	Desorption Rate Study	Blockage and vacuum desorption of three contaminants
			(2) $n\text{-}C_4H_{10}$	46.0	1.75×10^{-2}	.50	19.5	3.98×10^{-4}	9.24×10^{-2}	10 250	0	2.1×10^{-4}	Desorption Rate Study	
			(3) CCl_2F_2	38.5	1.46×10^{-2}	.50	25.0	9.5×10^{-5}	2.63×10^{-2}	10 250	0	9.5×10^{-5}	Desorption Rate Study	
F18-1	28	30 × 40 BD	(1) $n\text{-}C_4H_{10}$	26.4	1.16×10^{-2}	0.58	16.1	1.9×10^{-3}	4.4×10^{-1}	–	1.3×10^{-3}		Blockage of $n\text{-}C_4H_{10}$ by concurrent adsorption of H_2O	
			(2) H_2O		2.12×10^{1}		1.19				ca.3 $\times 10^{-1}$			
F19-1	28	30 × 40 BD	(1) H_2O		2.12×10^{1}	0.505	2.01	3.58×10^{2}	4.27×10^{2}	–			Blockage of $n\text{-}C_4H_{10}$ by preadsorbed H_2O	
			(2) $n\text{-}C_4H_{10}$	24.0	9.12×10^{-3}	.50	16.5	1.14×10^{-3}	2.65×10^{-1}		9.8×10^{-4}			
-2	66	30 × 40 BD	C_2H_5OH	60	2.3×10^{-2}	.506	23.5	1.1×10^{-2}	4.0×10^{0}	–	1.2×10^{-2}		Adsorption of C_2H_5OH at 66 °C	
-3	26	30 × 40 BD	C_2H_5OH	35.5	1.34×10^{-2}	.497	17.5	2.55×10^{-2}	9.2×10^{0}	–			Adsorption of C_2H_5OH at 26 °C	
-4	64	30 × 40 BD	(1) $n\text{-}C_4H_{10}$	25.5	1.00×10^{-2}	.514	20.4	9.26×10^{-3}	2.06×10^{0}	–	2.2×10^{-2}		Blockage of $n\text{-}C_4H_{10}$ by concurrent adsorption of H_2O	
			(2) H_2O		2.12×10^{1}		16.7	None Detected		–	2.2×10^{-2}			
-5	27	30 × 40 BD	(1) C_2H_5OH	20	7.6×10^{-2}	.502	19.1	5.56×10^{-3}	2.01×10^{0}	–	9.75×10^{-3}		Blockage of C_2H_5OH by concurrent adsorption of H_2O	
			(2) H_2O		2.12×10^{1}		1.6							
-6	66	30 × 40 BD	(1) C_2H_5OH	28	1.06×10^{-2}	.50	25.2	2.0×10^{-3}	7.2×10^{-1}	–	6.47×10^{-3}		Blockage of C_2H_5OH by concurrent adsorption of H_2O	
			(2) H_2O		2.12×10^{1}		17.5	None Detected						
-7	27	30 × 40 BD	(1) $n\text{-}C_4H_{10}$	25.6	9.7×10^{-3}	.50	16.5	7.43×10^{-3}	1.73×10^{0}	–	1.7×10^{-3}		Blockage of $n\text{-}C_4H_{10}$ by concurrent adsorption of H_2O	
			(2) H_2O		1.50×10^{1}		4.0							
-8	65	30 × 40 BD	(1) $n\text{-}C_4H_{10}$	25.8	1.00×10^{-2}	.508	20.1	8.41×10^{-3}	1.96×10^{0}	–	7.34×10^{-3}		Blockage of $n\text{-}C_4H_{10}$ by concurrent adsorption of H_2O	
			(2) H_2O		1.50×10^{1}		19.8	None Detected		–				
-9	27	30 × 40 BD	(1) C_2H_5OH	27.0	1.03×10^{-2}	.501	18.6	1.32×10^{-2}	4.77×10^{0}	–	8.70×10^{-3}		Blockage of C_2H_5OH by concurrent adsorption of H_2O	
			(2) H_2O		1.50×10^{-1}		4.0							
-10	66	30 × 40 BD	(1) C_2H_5OH	16.2	6.2×10^{-3}	.505	26.4	1.39×10^{-3}	5.0×10^{-1}	–	1.46×10^{-2}		Blockage of C_2H_5OH by concurrent adsorption of H_2O	
			(2) H_2O		1.50×10^{1}		20.1							
-11	26	30 × 40 BD	(1) $n\text{-}C_4H_{10}$	25.1	9.4×10^{-3}	.49	16.5	2.50×10^{-2}	5.81×10^{0}	–	2.16×10^{-3}		Blockage of $n\text{-}C_4H_{10}$ by concurrent adsorption of H_2O	
			(2) H_2O		1.00×10^{1}		6.4							
-12	67	30 × 40 BD	(1) $n\text{-}C_4H_{10}$	26.2	1.00×10^{-2}	.50	20.3	8.12×10^{-3}	1.89×10^{0}	–	2.58×10^{-2}		Blockage of $n\text{-}C_4H_{10}$ by concurrent adsorption of H_2O	
			(2) H_2O		1.00×10^{1}		23.7							
-13	26	30 × 40 BD	(1) C_2H_5OH	24	9.1×10^{-3}	.50	18.5	1.8×10^{-2}	6.5×10^{0}	–	1.08×10^{-2}		Blockage of C_2H_5OH by concurrent adsorption of H_2O	Desorption aborted – sampling problems
			(2) H_2O		1.00×10^{1}		6.4							
-14	66	30 × 40 BD	(1) C_2H_5OH	20.5	7.8×10^{-3}	.50	25.9	2.6×10^{-3}	9.4×10^{-1}	–	–		Blockage of C_2H_5OH by concurrent adsorption of H_2O	
			(2) H_2O		1.00×10^{1}		23.3							

Run No.	Temp. T (°C)	Sorbent	Initial Weight (Degassed) w^o (g)	Contaminant	Partial Pressure p_a (μHg)	Adsorption Weight Increase ΔW_a (mg)	Adsorption Potential A (mol°K/ml liq)	Amount Adsorbed q_a (ml liq/g)	Desorption Details	Purpose	Remarks
M1-1	27	30 × 40 BD		C_3H_8	26.6					Flow run in O_2 at 0.5 atm	
M2-1	27	30 × 40 BD	50.318	C_3H_8	13.3		23.1	2.30×10^{-3}		Flow run in O_2/N_2 at 0.5 atm	Excessive base line drift
M3-1	27	30 × 40 BD	49.477	–	–	0.339	–			Differential flow runs in O_2/N_2 at 0.5 atm	Excessive base line drift
-2	27	30 × 40 BD	49.091	C_3H_8	13.3	.460	23.1	4.12×10^{-3}			
M4-1 to -3	27	30 × 40 BD		–	–		–	–		Vacuum background wt. increase	~0.3%/hr wt. increase
M5-1	27	50 mg Ta wt.	50.000	None	–		–	–		Instrument drift	+5μg/hr
M6-1, -2	27	30 × 40 BD		C_3H_8	5.5					System Check	Leaky
M7-1	27	30 × 40 BD	51.443	C_3H_8	5.5	0.087	24.7	2.85×10^{-3}	Aluminum pans	Propane adsorption and desorption	
-2			51.337			.118		3.87×10^{-3}			
-3			51.335			.105		3.48×10^{-3}			
-4			51.346			.097		3.18×10^{-3}			Desorption data useless due to strong flow effects
-5			51.352			.094		3.08×10^{-3}			
-6			51.353			.099		3.25×10^{-3}			
-7	27	30 × 40 BD	51.358	C_3H_8	5.5	.096	24.7	2.82×10^{-3}			Av $q_a = 3.22 \times 10^{-3}$ ml liq/g
M8-1	27	30 × 40 BD	50.626	C_3H_8	5.5	0.080	24.7	2.67×10^{-3}	Nickel screen pans on all experiments henceforth	Minimize flow effects on desorption data	Desorption curve appears normal after few seconds
-2			50.633			.081		2.70×10^{-3}			
-3			50.634			.080		2.67×10^{-3}			
-4			50.635			.082		2.73×10^{-3}			
-5			50.641	C_3H_8		.076	24.7	2.53×10^{-3}			Av $q_a = 2.66 \times 10^{-3}$ ml liq/g
-6			50.628	Ar		.012					
-7			50.631			.009					
-8			50.634			.010				Check on magnitude of pressure effects of unadsorbed gas with similar molecular weight	Av $\Delta W_a = 9\mu g$
-9			50.639			.011					
-10			50.642		5.5	.008					
-11 to -25	27	30 × 40 BD	–	Ar	Various	–				Wt. variation with pressure; buoyancy	
M9-1	27	30 × 40 BD	52.08	$C_6H_5CH_3$	7.0	11.02	9.3	2.72×10^{-1}			
-2 to -5	27	30 × 40 BD	–	$C_6H_5CH_3$	–	–	–	–			Leaky manifold – data useless
-6	27	30 × 40 BD	51.63	$C_6H_5CH_3$	3.5	9.61	10.1	1.66×10^{-1}			
-7 to -13	27	30 × 40 BD	–	$C_6H_5CH_3$	–	–	–	–			Leaky manifold – data useless
M10-1	27	30 × 40 BD	–	$C_6H_5CH_3$	–	–	–	–			System leak
-2	27	30 × 40 BD	52.24	$C_6H_5CH_3$	3.5	10.16	10.1	2.50×10^{-1}			
-3, -4	27	30 × 40 BD	–	$C_6H_5CH_3$	–	–	–	–			Microbalance slit out of adj.
M11-1	27	LS2A	50.56	$C_6H_5CH_3$	15	12.46	8.5	3.16×10^{-1}			
-2			50.38		3.5	8.30	10.1	2.12×10^{-1}			
-3			50.38		3.5	8.75	10.1	2.23×10^{-1}			
-4			50.38		3.5	8.83	10.1	2.25×10^{-1}			
-5 to -8			50.38		3.5	9.01	10.1	2.30×10^{-1}		15 min cycles	>50% desorbed
-9 to -14			50.38		–	–	–	–			Manifold leak – data useless
-15, -16			50.38		–	–	–	–			Data not used
-17 to -22	27	LS2A	50.38	$C_6H_5CH_3$	–	–	–	–			Data not used
M12-	87	50 mg Al wts	50.000	$C_6H_5CH_3$	3.5	–	–	–		Adjust furnaces for minimum thermogravimetric effects	
M13-1 to -3	87	30 × 40 BD		$C_6H_5CH_3$	3.5	3.86	15.3	9.9×10^{-2}			(Av ΔW_a and q_a)
-4	27		49.750	n-C_4H_{10}	3.8	1.032	17.0	3.44×10^{-2}			
-5	32.5		49.785		6.8	.847	17.5	2.82×10^{-2}			
-6	52		49.766		6.8	.454	19.4	1.51×10^{-2}			
-7 to -30	27.5		49.758		Various	–	15.6	5.38×10^{-2}	M13-30D = long desorption	27°C isotherm	
-31 to -43	72		49.740		Various	–	–	–		Find T such that q at 200μ = q at 20μ & 27°C	(q & A at p = 20μHg)
-44 to -57	62.7		49.751	n-C_4H_{10}	Various	–	18.9	1.78×10^{-2}	M13-57D = long desorption	62°C isotherm	T too high
-58 to -60	27	30 × 40 BD	49.864	C_3H_6	9.8	–	26.9	3.25×10^{-2}		C_3H_6 adsorption on "dirty" charcoal	(q & A at p = 20μHg)
M14-1 to -3	26	30 × 40 BD	49.396	C_3H_6	9.8	–	26.7	3.89×10^{-3}			No significant difference
-4 to -21	47.0		49.370	n-C_4H_{10}	Various	–	17.3	3.05×10^{-2}	M14-21D = long desorption	C_3H_6 adsorption on fresh charcoal	
-22 to -24	26		49.438	C_3H_6	9.8	–	26.7	3.66×10^{-3}		47°C isotherm	(q & A at p = 20μHg)
-25 to -27	26		49.460	C_3H_6	9.8	–	26.7	4.74×10^{-3}		Repeat M13-58 to -60	No significant difference
-28 to -34	27.5		49.363	n-C_4H_{10}	Various	–	–	–		Repeat M14-1 to -3 after pump oil removal	No significant difference
-35 to -41	62.8		49.376		Various	–	–	–		Brief 27°C isotherm after pump oil removal	No significant difference
-42 to -61	37.0		49.374		Various	–	16.5	3.90×10^{-2}	M14-61D = long desorption	Brief 62°C isotherm after pump oil removal	No significant difference
-62 to -83	77.0		49.335		Various	–	20.2	1.21×10^{-2}	M14-83D = long desorption	37°C isotherm	(q & A at p = 20μHg)
-84 to -86	–		–		–	–	–	–		77°C isotherm	(q & A at p = 20μHg)(sample loss)
-87	46.2		49.231		28	0.983	16.8	3.31×10^{-2}	High chart speed	System check – no data taken	
-88	67.0		49.206		93	.991	16.9	3.34×10^{-2}	High chart speed	Long desorption after isosteric adsorption: variation with temperature	(sample loss)
-89	87.5		49.206		300	.988	16.8	3.33×10^{-2}	High chart speed		(sample loss)
-90	25.6	30 × 40 BD	48.072	n-C_4H_{10}	6.7	.958	16.9	3.30×10^{-2}	High chart speed		(sample loss)

Run No.	Temp. T (°C)	Sorbent	Initial Weight (Degassed) W^o (g)	Contaminant	Partial Pressure Pa (μHg)	Adsorption Weight Increase ΔW_a (mg)	Adsorption Potential A (mol°K/ml liq)	Amount Adsorbed q_a (ml liq/g)	Desorption Details	Purpose	Remarks
M15-1	26.6	8 × 12 BD	50.365	$n-C_4H_{10}$	13.2	1.009	16.1	3.33×10^{-2}	High chart speed	Long desorption after isosteric adsorption: variation with temperature Also variation with particle size from previous group of experiments	
-2	26.2	↓	50.347	↓	14.7	1.010	15.9	3.33×10^{-2}	↓		
-3	86.8		50.331		143	1.005	17.9	3.31×10^{-2}			
-4	67.0		50.285		102	1.002	16.7	3.31×10^{-2}			
-5	46.8		50.300	$n-C_4H_{10}$	48	1.015	16.3	3.35×10^{-2}			
-6	26.4	8 × 12 BD	50.308	C_3H_8	9.6	.102	23.7	3.43×10^{-2}	High chart speed		
M16-1	27.4	30 × 40 BD	49.750	C_3H_8	9.3	0.109	23.8	3.76×10^{-3}	High chart speed	Long desorption after isosteric adsorption: variation with particle size	
-2	27.4	30 × 40 BD	49.759	C_3H_8	8.3	.099	24.1	3.36×10^{-3}	High chart speed		
M17-1	27.3	50 × 70 BD	49.970	$n-C_4H_{10}$	7.6	0.997	16.9	3.31×10^{-2}	High chart speed	Variation with particle size	
M18-1	87.6	16 × 20 BD	50.191	$n-C_4H_{10}$	220	1.004	17.2	3.32×10^{-2}	High chart speed	Long desorption after isosteric adsorption: reproducibility, variation with temperature, and variation with particle size	
-2	87.3		50.182		235	1.001	17.1	3.31×10^{-2}			Huge thermogravimetric effects
-3											
-4	87.3		50.185		220	1.000	17.2	3.31×10^{-2}			
-5	87.7		50.219		9.8	.130	22.3	4.30×10^{-3}			
-6	87.1		50.233		9.5	.133	22.3	4.39×10^{-3}			Data unsatisfactory – huge $\Delta W/\Delta t$
-7											
-8	87.1		50.248		7.5	.130	22.6	4.30×10^{-3}			
-9	86.9		50.245		>430	2.598		8.59×10^{-2}			
-10	87.2		50.233		22	.264	20.9	8.74×10^{-3}			
-11	87.0		50.241		25	.265	20.8	8.78×10^{-3}			
-12	86.8		50.232		25	.264	20.8	8.74×10^{-3}			Data unsatisfactory
-13	28.3		50.326								
-14	26.1		50.273		17.1	1.009	15.7	3.33×10^{-2}			
-15	27.0		50.271		9.6	1.001	16.5	3.30×10^{-2}			Aborted – pan stuck to tube
-16	86.9		50.422		175	1.005	17.6	3.31×10^{-2}			
-17	87		50.389		160	.990		3.26×10^{-2}			First expt w/non-magnetic
-18	87.6		50.065		165	1.000	17.7	3.31×10^{-2}			Long furnaces
-19	87.6		50.023		225	1.000	17.2	3.32×10^{-2}			
-20	87.9		50.029	$n-C_4H_{10}$	200	1.003	17.4	3.32×10^{-2}	↓		
-21	26.9		50.02	$C_6H_5CH_3$	1.0	6.95	11.4	1.78×10^{-1}	High chart speed		Used later data instead
-22 to -24	26.8		50.02		Various	–		–		Isotherm points	
-25	26.9		50.02		5.0	10.31	9.7	2.65×10^{-1}	High chart speed	Long desorption	
-26, -27	28.2				Various	–		–		Calibration of Pirani gage after adj	Not done rigorously for isotherm use
-28 to -34	26.8		50.04		1 to 100	–	Various	–		Isotherm points	First Barocel isotherm data
-35 to -37	26.8		50.00		200 to 1000		Various	–			
-38	66.8		50.05		100	–	9.4	2.69×10^{-1}			
-39 to -41	66.8		49.59		200 to 1000	–	Various				
-42 to -47	66.8		49.65		1 to 50	–	Various	–		Isotherm points	
-48	.8		49.64		91	10.24	9.5	2.64×10^{-1}	High chart speed	Long desorption	
-49 to -52	106.8		49.63		1 to 10	–	Various	–		Isotherm points	
-53 to -59	106.8		49.63		10 to 1000	–	Various	–		Isotherm points	
-60 to -61	106.6		49.63		.070	10.23	9.0	2.64×10^{-1}	High chart speed	Long desorption	
-62 to -68	66.7		49.63		0.08 to 1.14	–	Various	–		Isotherm points	
-69 to -75	27.0		49.69	$C_6H_5CH_3$	0.1 to 1.46	–	↓	–		↓	
-76 to -78	26.8		49.675	$n-C_4H_{10}$	1 to 2.2	–		–			
-79 A/D	26.8		49.675	$n-C_4H_{10}$	30/8.4	–		–			
-80 to -82	26.8		49.679	$n-C_4H_{10}$	7.1 to 1000	–		–			
-83 to -86	106.8		49.66	$C_6H_5CH_3$	0.26 to 20			–			
-87 to -90	106.8	↓	49.668	$n-C_4H_{10}$	1.35 to 1000	–		–			
-91 to -95	106.9	16 × 20 BD	49.692	$n-C_4H_{10}$	0.1 to 300	–	Various	–		Isotherm points	
M19-1 to -4	26.8	30 × 40 BD	50.212	$n-C_4H_{10}$	0.8 to 30	–	Various	–		27°C isotherm points	
-5 to -7	26.8		50.184	$n-C_4H_{10}$	16 to 1000	–	Various	–		27°C isotherm points	
-8 to -9	106.8		50.110	$n-C_4H_{10}$	1.0, 3.0	–	Various	–		107°C isotherm points	
-10 to -15	107		50.105	$n-C_4H_{10}$	1 to 1000	–	Various	–		107°C isotherm points	
-16 to -20	106.6		50.10	$C_6H_5CH_3$	0.2 to 100	–		–		107°C isotherm points	
-21, -22	106.6		50.11	$C_6H_5CH_3$	48 to 1000	–		–		107°C isotherm points	
-23	107		47.350	$n-C_4H_{10}$	20	20	23.0	3.90×10^{-3}	Mass spec analysis	2-component desorption	
				$C_6H_5CH_3$	40 total	3.098 total	–				
-24	27		47.360	$n-C_4H_{10}$	20	1.447	15.5	4.97×10^{-2}	Mass spec analysis	2-component desorption	
				$C_6H_5CH_3$	40 total	11.69 total	–				
-25	27		47.336	$C_6H_5CH_3$	~0.1	1.900	~14	5.15×10^{-2}	Mass spec analysis	2-component desorption	
				$n-C_4H_{10}$	48	3.112 total	–				
-26	26.8		47.338	$n-C_4H_{10}$	9.0	.976	16.6	3.43×10^{-2}		Long desorption, repeat M13-90	
-27	66.8		47.328	$n-C_4H_{10}$	98	.971	16.8	3.41×10^{-2}		Long desorption, repeat M13-88	
-28	107										Aborted
-29	107	↓	47.270	$n-C_4H_{10}$	710	.967	16.8	3.40×10^{-2}		Long desorption	
-30	26.8	30 × 40 BD	47.268	$n-C_4H_{10}$	8.45	.973	16.7	3.42×10^{-2}		Long desorption, repeat M19-26	

Run No.	Temp. T (°C)	Sorbent	Initial Weight (Degassed) W_s^o (g)	Contaminant	Partial Pressure p_a (μHg)	Adsorption Weight Increase ΔW_a (mg)	Adsorption Potential A (mol°K/ml liq)	Amount Adsorbed q_a (ml liq/g)	Desorption Details	Purpose	Remarks
M20-1	27.1	8 × 12 BD	50.618	$C_6H_5CH_3$	0.8	6.588	11.7	1.67×10^{-1}		2-component desorption	
				$n\text{-}C_4H_{10}$	380	1.477	–	4.84×10^{-3}			
-2 to -8	66.9		50.758	CCl_2F_2	0.1 to 1000	–	Various	–		67°C Freon-12 isotherm points	Poor reproducibility
-9 to -12	26.8		50.735		1.1 to 30	–		–		27°C Freon-12 isotherm points	
-13 to -15	26.8		50.752		100 to 725	–		–		27°C Freon-12 isotherm points	
-16, -17	26.8		50.760		50 to 1000	–		–		27°C Freon-12 isotherm points	
-18 A/D	66.8		50.807	CCl_2F_2	1000, 21	–	Various	–		67°C Freon-12 isotherm points	Poor reproducibility
-19	26.8		50.819	$C_6H_5CH_3$	<0.1	1.043	>14	2.64×10^{-2}		Toluene preadsorption – blockage of n-butane adsorption isotherm	Mass spec analysis shows Freon-12 contamination
-20, -21	26.7		50.819	$n\text{-}C_4H_{10}$	1.5, 5.8	–	Various	–		Toluene preadsorption – blockage of n-butane adsorption isotherm	Mass spec analysis shows no displacement of toluene
-22	26.8		50.710	$C_6H_5CH_3$	<0.1	1.044	>17	2.64×10^{-2}		Toluene preadsorption – blockage of n-butane adsorption isotherm	Mass spec analysis shows no displacement of toluene
-23 to -30	26.8		50.710	$n\text{-}C_4H_{10}$	0.9 to 983	–	Various	–		Few 27°C isotherm points	
-32	66.8		50.709	$C_6H_5CH_{10}$	~.08	1.043	~18	2.64×10^{-2}		Toluene preadsorption	Aborted – mass spec failure (mass spec not used)
-32 to -38	66.8		50.709	$n\text{-}C_4H_{10}$	2.9 to 1000	–	Various	–		Toluene preadsorption – blockage of n-butane adsorption isotherm	
-39 to -41	26.8		50.707	$n\text{-}C_4H_{10}$	2.6 to 453	–	Various	–		Toluene preadsorption – blockage of n-butane adsorption isotherm	Mass spec analysis shows large displacement of toluene
-42	26.8		50.707	$C_6H_5CH_3$	6.8	10.432	9.3	2.64×10^{-1}		67°C n-butane isotherm points	
-43	27.0		50.732	$C_6H_5CH_3$	7.2	10.416	9.3	2.64×10^{-1}		Toluene preadsorption – blockage of n-butane adsorption isotherm	Mass spec analysis shows no displacement of toluene
-44 to -49	26.8		50.732	$n\text{-}C_4H_{10}$	22.2 to 997	–	Various	–		Toluene preadsorption – blockage of n-butane adsorption isotherm	Mass spec analysis shows negligible displacement of toluene
-50	66.8		50.703	$C_6H_5CH_3$	91	10.424	9.5	2.64×10^{-1}		27°C n-butane isotherm points	
-51 to -56	66.8		50.703	$n\text{-}C_4H_{10}$	10.5 to 914	–	Various	–		27°C n-butane isotherm points	
-57 to -64	66.8		50.708	$n\text{-}C_4H_{10}$	0.73 to 980	–	Various	–		67°C n-butane isotherm points	
-65	66.8		50.774	$C_6H_5CH_{10}$	0.55	2.087	16.2	5.28×10^{-2}			
-66 to -73	66.8		50.774	$n\text{-}C_4H_{10}$	3.75 to 992	–	Various	–			
-74	26.8		50.768	$C_6H_5CH_{10}$	<.01	2.089	16.0	5.28×10^{-2}			
-75 to -81	26.8		50.768	$n\text{-}C_4H_{10}$	1.8 to 985	–	Various	–			
-82, -83	26.8		50.707	$n\text{-}C_4H_{10}$	0.64, 1.20	–	Various	–			
-84 to -90	26.8		50.739	$n\text{-}C_4H_{10}$	5.9 to 2×10^4	–	Various	–			
-91 to -95	66.8	8 × 12 BD	50.718	$n\text{-}C_4H_{10}$	199 to 2×10^4	–	Various	–			
M21-1	27	50 mg Ta wt	50.014	$n\text{-}C_4H_{10}$	10	-0.002				"Blank" run in n-butane	Negligible weight change
-2			50.014		100	- .001				"Blank" run in n-butane	
-3			50.014		1 000	.000				"Blank" run in n-butane	
-4			50.014		10 000	+ .004				"Blank" run in n-butane	
-5			50.012	C_2H_5OH	10	- .003				"Blank" run in ethanol	
-6			50.012		100	- .001				"Blank" run in ethanol	
-7			50.012		1 000	- .001				"Blank" run in ethanol	
-8			50.012		10 000	.000				"Blank" run in ethanol	
-9			–	$C_6H_5CH_3$						Mass spec ionization cross-section determinations	Negligible weight change
-10			–	$n\text{-}C_4H_{10}$							
-11			–	$C_6H_5CH_3$							
-12			–	$n\text{-}C_4H_{10}$							
-13			–	C_2H_5OH							
-14			–	C_2H_5OH							
-15			–	C_2H_5OH							
M22-1	21.8	30 × 40 BD	50.862	H_2O	5 000	0.853	9.34	1.75×10^{-2}		22°C water isotherm point	
-2			50.862		10 000	4.121	4.60	8.46×10^{-2}			
-3, -4			50.70		–						
-5			50.70		15 000	21.29	1.84	4.37×10^{-1}			Aborted – insufficient time
-6			50.70		20 000	27.82	0.05	5.71×10^{-1}		22°C water isotherm point	
-7	31.8	30 × 40 BD	51.05	H_2O	5 000	0.58	13.8	1.19×10^{-1}		32°C water isotherm point	
-8			51.05		10 000	1.17	8.90	2.39×10^{-2}		32°C water isotherm point	
-9			51.05		15 000	2.63	6.05	5.38×10^{-2}		32°C water isotherm point	
-10			51.05		20 000	9.16	4.02	1.87×10^{-1}		32°C water isotherm point	
-11	66.8	30 × 40 BD	50.993	H_2O	5 000	0.259	29.1	5.31×10^{-3}		67°C water isotherm point	
-12			50.993		10 000	.345	23.7	7.02×10^{-3}			
-13			50.993		15 000	.427	20.5	8.76×10^{-3}			
-14			50.993		20 000	.497	18.2	1.02×10^{-2}			
-15			50.993		25 000	.595	16.5	1.22×10^{-2}			
-16	46.8	30 × 40 BD	51.10	H_2O	5 000	0.36	21.7	7.3×10^{-3}		67°C water isotherm point	
-17			51.10		10 000	.535	16.2	1.10×10^{-2}		47°C water isotherm point	
-18			51.10		15 000	.725	13.1	1.48×10^{-2}		47°C water isotherm point	
-19			51.10		20 000	1.025	10.8	2.10×10^{-2}		47°C water isotherm point	
-20			51.10							47°C water isotherm point	Aborted – pressure won't go above 20 torr

Appendix E

SUMMARY OF ISOTHERM POINTS FROM DESORPTION RUNS ON GRAVIMETRIC SYSTEM

Table E-1

SUMMARY OF ISOTHERM POINTS FROM DESORPTION RUNS ON GRAVIMETRIC SYSTEM – n-BUTANE

Run No.	Particle Diameter		Temperature (°K)	Equilibrium Pressure		Amount Adsorbed		Adsorption Potential (mol °K/ml liq)
	(mm)	(°C)		Pirani (torr)	Actual (torr)	(ml STP/g)	(ml liq/g)	
M14-87	0.5	46	319	0.102	0.128[a]	7.70	3.37×10^{-2}	16.8
M14-88	0.5	67	340	.297	.093	7.76	3.34×10^{-2}	16.9
M14-89	0.5	87	360	.585	.30	7.75	3.33×10^{-2}	16.8
M14-90	0.5	26	299	.019	.0067[b]	7.68	3.31×10^{-2}	16.9
M15-1	2.0	27	300	0.0345	0.0132[b]	7.73	3.33×10^{-2}	16.1
M15-2	2.0	26	299	.0385	.0147	7.74	3.33×10^{-2}	15.9
M15-3	2.0	87	360	.550	.143	7.70	3.31×10^{-2}	17.9
M15-4	2.0	67	340	.385	.102	7.69	3.31×10^{-2}	16.7
M15-5	2.0	47	320	.165	.048	7.78	3.34×10^{-2}	16.3
M17-1	0.25	27	300	0.0225	0.0076[b]	7.70	3.31×10^{-2}	16.9
M18-1	1.0	88	361	0.90	0.220[c]	7.71	3.32×10^{-2}	17.2
M18-2	1.0	87	360	.95	.235	7.70	3.31×10^{-2}	17.1
M18-4	1.0	87	360	.90	.220	7.69	3.30×10^{-2}	17.2
M18-5	1.0	88	361	.026	.0098	1.00	4.30×10^{-3}	22.3
M18-6	1.0	87	360	.025	.0095	1.02	4.39×10^{-3}	22.3
M18-8	1.0	87	360	.020	.0075	1.00	4.30×10^{-3}	22.6
M18-9	1.0	87	360	2		19.97		
M18-10	1.0	87	360	.085	.022	2.03	8.72×10^{-3}	20.9
M18-11	1.0	87	360	.095	.025	2.04	8.75×10^{-3}	20.8
M18-12	1.0	87	360	.095	.025	2.03	8.74×10^{-3}	20.8
M18-14	1.0	26	299	.0445	.0171	7.74	3.33×10^{-2}	15.7
M18-15	1.0	27	300	.0255	.0096	7.68	3.30×10^{-2}	16.5
M18-16	1.0	87	360	.70	.175	7.70	3.31×10^{-2}	17.6
M18-18	1.0	88	361	.65	.165	7.70	3.31×10^{-2}	17.7
M18-19	1.0	88	361	.90	.225	7.71	3.32×10^{-2}	17.2
M18-20	1.0	88	361	.80	.20	7.73	3.33×10^{-2}	17.4
M19-23	0.5	107	380	–	0.020[d]	0.905	3.90×10^{-3}	23.0
M19-24	0.5	27	300	–	.020	11.53	4.97×10^{-2}	15.5
M19-26	0.5	27	300	–	.0090	7.96	3.42×10^{-2}	16.6
M19-27	0.5	67	340	–	.098	7.92	3.41×10^{-2}	16.8
M19-29	0.5	107	380	–	.710	7.89	3.39×10^{-2}	16.8
M19-30	0.5	27	300	–	.00845	7.94	3.41×10^{-2}	16.7

(a) McLeod gage reading.
(b) From calibration versus McLeod gage.
(c) From calibration versus Barocel.
(d) Barocel reading.

Table E-2

SUMMARY OF ISOTHERM POINTS FROM DESORPTION RUNS ON GRAVIMETRIC SYSTEM – TOLUENE

Run No.	Particle Diameter (mm)	Temperature		Equilibrium Pressure		Amount Adsorbed		Adsorption Potential (mol °K/ml liq)
		(°C)	(°K)	Pirani (torr)	Actual (torr)	(ml STP/g)	(ml liq/g)	
M9-1	0.5	27	300	0.0020	0.0074[a]	51.6	2.72×10^{-1}	9.2
M10-2	0.5	27	300	0.0010	0.0035[a]	47.2	2.50×10^{-1}	9.6
M13-1	0.5	87	360	0.0010	0.0035[a]	18.7	9.9×10^{-2}	14.8
M13-2	0.5	87	360	.0010	.0035[a]	19.0	1.00×10^{-1}	14.8
M13-3	0.5	87	360	.0010	.0035[a]	18.7	9.9×10^{-2}	14.8
M18-21	1.0	27	300	0.0028	0.0010[a]	33.8	1.78×10^{-1}	11.4
M18-25	1.0	27	300	.014	.0050	50.1	2.65×10^{-1}	9.7
M18-48	1.0	67	340	–	.091[b]	50.1	2.65×10^{-1}	9.5
M18-60	1.0	107	380	–	1.070	50.1	2.65×10^{-1}	9.0
M19-25	0.5	27	300	–	0.0001[b]	0.75	5.15×10^{-2}	14
M20-1	2.0	27	300	–	0.0008[b]	31.6	1.67×10^{-1}	11.7
M20-19	2.0	27	300	–	.0001	5.00	2.62×10^{-2}	14
M20-22	2.0	27	300	–	.00001	5.01	2.64×10^{-2}	17
M20-31	2.0	67	340	–	.00008	5.01	2.64×10^{-2}	18
M20-42	2.0	27	300	–	.0068	50.1	2.64×10^{-1}	9.3
M20-43	2.0	27	300	–	.0072	50.0	2.63×10^{-1}	9.3
M20-50	2.0	67	340	–	.091	50.1	2.64×10^{-1}	9.5
M20-65	2.0	67	340	–	.00055	10.0	5.28×10^{-2}	16.2
M20-74	2.0	27	300	–	.0001	10.0	5.28×10^{-2}	16.0

(a) From calibration versus Barocel.
(b) Barcel reading.

Table E-3

SUMMARY OF ISOTHERM POINTS FROM DESORPTION RUNS ON GRAVIMETRIC SYSTEM – PROPANE

Run No.	Particle Diameter (mm)	Temperature		Equilibrium Pressure		Amount Adsorbed		Adsorption Potential (mol°K/ml liq)
		(°C)	(°K)	Pirani (torr)	Actual (torr)	(ml STP/g)	(ml liq/g)	
M2-1	0.5	27	300	–	0.0133[a]	0.69	2.30×10^{-3}	23.1
M3-1,-2	0.5	27	300	–	0.0133[a]	1.24	4.12×10^{-3}	23.1
M7-1	0.5	27	300	0.0133	0.0055[b]	0.86	2.85×10^{-3}	24.7
M7-2	0.5	27	300	.0133	.0055[b]	1.16	3.87×10^{-3}	24.7
M7-3	0.5	27	300	.0133	.0055[b]	1.05	3.48×10^{-3}	24.7
M7-4	0.5	27	300	.0133	.0055[b]	.96	3.18×10^{-3}	24.7
M7-5	0.5	27	300	.0133	.0055[b]	.93	3.08×10^{-3}	24.7
M7-6	0.5	27	300	.0133	.0055[b]	.98	3.25×10^{-3}	24.7
M7-7	0.5	27	300	.0133	.0055[b]	.85	2.82×10^{-3}	24.7
M8-1	0.5	27	300	0.0133	0.0055[b]	0.80	2.67×10^{-3}	24.7
M8-2	0.5	27	300	.0133	.0055[b]	.81	2.70×10^{-3}	24.7
M8-3	0.5	27	300	.0133	.0055[b]	.80	2.67×10^{-3}	24.7
M8-4	0.5	27	300	.0133	.0055[b]	.82	2.73×10^{-3}	24.7
M8-5	0.5	27	300	.0133	.0055[b]	.76	2.53×10^{-3}	24.7
M15-6	2.0	27	300	0.023	0.0096[b]	1.03	3.43×10^{-3}	23.7
M16-1	0.5	27	300	0.0225	0.0093[b]	1.11	3.70×10^{-3}	23.8
M16-2	0.5	28	301	.020	.0083	1.01	3.36×10^{-3}	24.1

(a) Based on analyzed concentration in premixed gas from Matheson.
(b) From calibration versus Barocel.

Appendix F

ADSORPTION ISOTHERM DATA FROM FLOW EXPERIMENTS

Run No.	Sorbent	Contaminant	Temperature T (°C)	Partial Pressure p (torr)	Amount Adsorbed		Adsorption Potential A (mol °K/ml liq)
					q_a (ml STP/g)	q_a (ml liq/g)	
F2-1	16 × 20BD	C_2H_4	24	2.28×10^{-2}	3.75×10^{-2}	8.28×10^{-5}	38.1
-2	16 × 20BD	C_2H_4	24	2.16×10^{-2}	3.55×10^{-2}	7.84×10^{-5}	38.2
-3	16 × 20BD	C_2H_4	24	2.21×10^{-2}	3.53×10^{-2}	7.80×10^{-5}	38.2
-4	16 × 20BD	C_2H_4	24	2.16×10^{-2}	3.55×10^{-2}	7.83×10^{-5}	38.2
-5	16 × 20BD	C_2H_4	24	1.89×10^{-2}	3.73×10^{-2}	8.21×10^{-5}	38.5
F3-1	16 × 20 13X	C_2H_4	24	2.25×10^{-2}	1.12×10^{-1}	2.47×10^{-4}	37.4
-2	16 × 20 13X	C_2H_4	24	3.06×10^{-2}	1.13×10^{-1}	2.48×10^{-4}	37.4
F5-1	30 × 40BD	C_3H_8	25	1.38×10^{-2}	1.24×10^{0}	4.12×10^{-3}	22.7
-2	30 × 40BD	C_3H_8	25	1.29×10^{-2}	1.14×10^{0}	3.79×10^{-3}	22.9
-3	30 × 40BD	C_3H_8	25	1.35×10^{-2}	1.10×10^{0}	3.67×10^{-3}	22.8
-4	30 × 40BD	C_3H_8	25	1.22×10^{-2}	1.02×10^{0}	3.41×10^{-3}	23.0
-5	30 × 40BD	C_3H_8	25	1.26×10^{-2}	1.08×10^{0}	3.60×10^{-3}	22.8
-6	30 × 40BD	C_3H_8	25	1.27×10^{-2}	1.05×10^{0}	3.49×10^{-3}	22.9
F6-1	30 × 40BD	C_3H_6	25	8.45×10^{-3}	6.6×10^{-1}	1.96×10^{-3}	26.8
-2	30 × 40BD	C_3H_6	46	8.28×10^{-3}	1.98×10^{-1}	5.9×10^{-4}	29.8
F7-2	30 × 40BD	CH_3CCl_3	102	1.01×10^{-2}	6.16×10^{-1}	2.20×10^{-3}	27.0
-3	30 × 40BD	C_7H_8	102	9.80×10^{-3}	9.85×10^{1}	5.2×10^{-2}	15.2
-4	30 × 40BD	CH_3CCl_3	102	9.97×10^{-3}	7.45×10^{-2}	2.66×10^{-4}	26.8
-5	30 × 40BD	CH_3CCl_3	101	8.1×10^{-3}	5.3×10^{-1}	1.89×10^{-3}	27.3
-7	30 × 40BD	C_7H_8	102	2.55×10^{-3}	4.06×10^{0}	2.15×10^{-2}	16.9
F9-1	30 × 40BD	n-C_4H_{10}	25	7.9×10^{-3}	7.88×10^{0}	3.4×10^{-2}	16.6
-2	30 × 40BD	n-C_4H_{10}	25	4.52×10^{-4}	1.86×10^{0}	8.0×10^{-3}	20.4
-3	30 × 40BD	C_3H_6	27	5.43×10^{-3}	3.97×10^{-1}	1.18×10^{-3}	27.8
F11-1	30 × 40BD	n-C_4H_{10}	24	9.02×10^{-3}	6.91×10^{0}	2.98×10^{-2}	16.4
-2	30 × 40BD	n-C_4H_{10}	25	7.45×10^{-3}	5.59×10^{0}	2.41×10^{-2}	16.7
-3	30 × 40BD	n-C_4H_{10}	25	7.74×10^{-3}	6.08×10^{0}	2.62×10^{-2}	16.6
-4	30 × 40BD	n-C_4H_{10}	27	3.76×10^{-4}	1.32×10^{0}	5.7×10^{-3}	20.9
-5	30 × 40BD	C_3H_6	25	6.33×10^{-1}	1.51×10^{1}	4.5×10^{-2}	18.6
-6	30 × 40BD	C_3H_6	25	5.32×10^{-3}	4.54×10^{-1}	1.35×10^{-3}	27.8
-7	30 × 40BD	n-C_4H_{10}	25	8.00×10^{-3}	6.00×10^{1}	2.58×10^{-2}	16.6
F12-1	30 × 40BD	C_3H_6	25	5.35×10^{-3}	5.01×10^{-1}	1.49×10^{-3}	27.8
-2	30 × 40BD	C_2H_4	25	9.95×10^{-3}	2.22×10^{-2}	4.88×10^{-5}	40.3
F13-1	8 × 12BD	n-C_4H_{10}	25	8.15×10^{-3}	6.11×10^{0}	2.63×10^{-2}	16.2
-2	8 × 12BD	n-C_4H_{10}	25	1.0×10^{-2}	8.20×10^{0}	3.53×10^{-2}	16.3
F14-1	8 × 12BD	n-C_4H_{10}	25	1.0×10^{-2}	7.62×10^{0}	3.28×10^{-2}	16.4
F15-1	8 × 12BD	n-C_4H_{10}	25	1.01×10^{-2}	7.90×10^{0}	3.40×10^{-2}	16.3
-2	8 × 12BD	n-C_4H_{10}	25	1.05×10^{-2}	8.26×10^{0}	3.56×10^{-2}	16.2
-3	8 × 12BD	n-C_4H_{10}	105	1.05×10^{-2}	2.44×10^{-1}	1.05×10^{-3}	24.2
F16-1	8 × 12BD	n-C_4H_{10}	25	1.03×10^{-2}	8.45×10^{0}	3.64×10^{-2}	16.2
F17-1	8 × 12BD	C_7H_8	107	1.05×10^{-2}	1.10×10^{-1}	5.8×10^{-2}	15.0
-2	8 × 12BD	n-C_4H_{10}	107	1.04×10^{-2}	5.04×10^{-1}	2.17×10^{-3}	24.2
-4	8 × 12BD	C_7H_8	67	1.05×10^{-2}	3.68×10^{-1}	1.94×10^{-1}	12.2

Appendix G

DATA FOR HIGH-PRESSURE VOLUMETRIC ADSORPTION EXPERIMENTS WITH n-BUTANE ON 30 × 40 BD ACTIVATED CARBON

Table G-1

HIGH-PRESSURE VOLUMETRIC-SYSTEM n-BUTANE ISOTHERM DATA FOR 30 × 40 BD ACTIVATED CARBON

Run No.	Temperature (°C)	Temperature (°K)	Equilibrium Pressure (torr)	Amount Adsorbed (ml STP/g)
V1-1	0.0	273.2	32.9	91.8
V1-2			96.9	103.0
V1-3			108.4	104.2
V1-4			127.3	105.8
V1-5			142.4	107.2
V1-6			157.5	108.5
V1-7			178.4	109.3
V2-1	0.0	273.2	1.1	32.5
V2-2			3.3	63.8
V2-3			11.0	81.9
V2-4			20.1	88.9
V2-5			26.8	92.4
V2-6			32.5	94.8
V2-7			40.0	96.1
V3-1	21.5	294.7	11.0	69.2
V3-2			44.1	86.4
V3-3			56.8	89.0
V3-4			68.5	90.9
V3-5			78.0	93.6
V3-6			88.1	95.1
V3-7			98.2	96.0
V3-8			109.7	99.7
V4-1	21.5	294.7	1.4	34.4
V4-2			5.9	60.9
V4-3			15.2	72.4
V4-4			22.5	78.0
V4-5			28.0	80.8
V4-6			37.1	83.6
V4-7			47.8	86.4
V4-8			61.4	89.1
V5-1	51.0	324.2	4.0	36.6
V5-2			10.7	48.7
V5-3			15.9	54.5
V5-4			25.8	60.2
V5-5			35.5	64.2
V5-6			53.9	70.2
V5-7			74.9	74.4
V5-8			99.5	78.5
V5-9			126.0	80.2
V5-10			155.0	83.7
V5-11			176.5	84.7

Table G-2

SELECTED POTENTIAL-PLOT

Run No.	Temperature (°C)	Temperature (°K)	Equilibrium Pressure (atm)	Adsorption Potential (mol°K/ml liq)	Amount Adsorbed (ml liq/g)
V1-7	0.0	273.2	0.235	1.82	4.70×10^{-1}
V2-1			.0015	8.1	1.40×10^{-1}
V2-2			.0045	7.03	2.74×10^{-1}
V3-8	21.5	294.7	0.144	3.60	4.29×10^{-1}
V4-1			.0017	9.4	1.48×10^{-1}
V4-2			.0078	7.5	2.62×10^{-1}
V5-1	51.0	324.2	0.0053	10.1	1.57×10^{-1}
V5-3			.0209	8.04	2.35×10^{-1}
V5-11			.232	4.52	3.64×10^{-1}

Appendix H

EQUATIONS PERTAINING TO MASS SPECTROMETER SAMPLING TECHNIQUE FOR GRAVIMETRIC EXPERIMENTS

The mass spectrometer section of the gravimetric system pictured in Fig. 2-4 and referred to in Section 3.1.2 may be represented by the line drawing in Fig. H-1. In this figure, the following symbols are used to represent system parameters:

V_1	= volume of the microbalance jar section	(ℓ)
V_2	= volume of mass spectrometer section	(ℓ)
V_3	= volume of getter-ion pump section	(ℓ)
p_1	= partial pressure of a particular species in microbalance jar section	(torr)
p_2	= partial pressure of a particular species in mass spectrometer section	(torr)
p_3	= partial pressure of a particular species in getter-ion pump section	(torr)
Q_1	= throughput of a particular species past the limiting conductance between microbalance jar and mass spectrometer sections	(torr-ℓ/sec)
Q_2	= throughput of a particular species past the limiting conductance between mass spectrometer and getter-ion pump sections	(torr-ℓ/sec)
F_1	= limiting conductance for a particular species between microbalance jar and mass spectrometer sections	(ℓ/sec)
F_2	= limiting conductance for a particular species between mass spectrometer and getter-ion pump sections	(ℓ/sec)
S	= pumping speed of getter-ion pump for a particular species	(ℓ/sec)
τ	= response time of mass spectrometer in sampling from microbalance jar section	(sec)

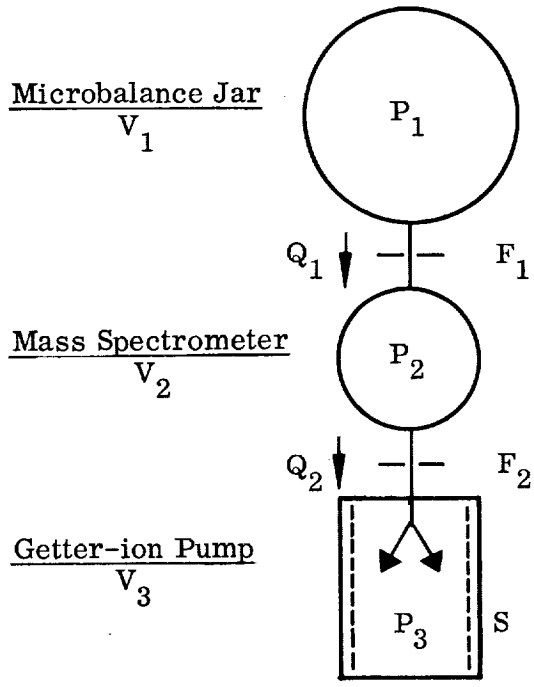

Fig. H-1 Mass Spectrometer Sampling System for Gravimetric Experiments

The throughput past F_1 equals that past F_2 and is equal to pumping speed times pressure in the getter-ion pump:

$$Q_1 = Q_2 = Sp_3 \tag{H. 1}$$

Since conductance may be defined (Dushman, Ref. 2, p. 82) as throughput divided by pressure drop, the following equations hold:

$$Q_1 = F_1 (p_1 - p_2) \tag{H. 2}$$

$$Q_2 = F_2 (p_2 - p_3) \tag{H. 3}$$

Substituting Eq. H.2 and H.3 into Eq. H.7 , one obtains, respectively.

$$F_1 p_1 - F_1 p_2 = S p_3 \tag{H. 4}$$

and

$$F_2 p_2 = (S + F_2)\, p_3 \tag{H. 5}$$

If Eq. H.4 is multiplied by $(S + F_2)/S$,

$$\frac{S + F_2}{S} F_1 p_1 - \frac{S + F_2}{S} F_1 p_2 = (S + F_2)\, p_3 \tag{H. 6}$$

Subtracting Eq. H.6 from Eq. H.4 , one obtains

$$\left[\left(1 + \frac{F_2}{S}\right) F_1 + F_2\right] p_2 = \left(1 + \frac{F_2}{S}\right) F_1 p_1 \tag{H. 7}$$

If Eq. H.7 is divided by the large term on the left-hand side,

$$p_2 = \frac{\left(1 + \frac{F_2}{S}\right) F_1}{\left(1 + \frac{F_2}{S}\right) F_1 + F_2} p_1 \qquad \text{(H. 8)}$$

If the limiting conductance F_2 is significantly lower than the pumping speed S for the species in question, Eq. (H. 8) simplifies to

$$p_2 = \frac{F_1}{F_1 + F_2} p_1 \qquad \text{(H. 9)}$$

Since factors affecting the values of conductance for each species would be the same for both F_1 and F_2, these factors would cancel in Eq. H.9. Thus, partial pressure in the mass spectrometer is dependent only on the partial pressure in the microbalance jar and on the physical dimensions of the limiting conductances F_1 and F_2. This means that no species discrimination will occur as long as the limiting conductance F_2 is much less than the pumping speed S for the species in question.

Response time of the mass spectrometer section may also be determined from the above parameters. If response time is defined as the sampling (mass spectrometer section) volume times pressure divided by the throughput.

$$\tau = \frac{V_2 p_2}{Q} \qquad \text{(H. 10)}$$

Substituting Eq. H.2 in the above equation one obtains

$$\tau = \frac{V_2 p_2}{F_1 (p_1 - p_2)} \qquad \text{(H. 11)}$$

If Eq. H.9 is then substituted into the above equation,

$$\tau = \frac{V_2 \dfrac{\left(1+\dfrac{F_2}{S}\right) F_1}{\left(1+\dfrac{F_2}{S}\right) F_1 + F_2}}{F_1 \left[p_1 \dfrac{\left(1+\dfrac{F_2}{S}\right) F_1}{\left(1+\dfrac{F_2}{S}\right) F_1 + F_2} p_1 \right]} \qquad \text{(H. 12)}$$

which simplifies to

$$\tau = \frac{V_2}{F_2} \left(1 + \frac{F_2}{S}\right) \qquad \text{(H. 13)}$$

Again, if the limiting conductance F_2 is much smaller than the pumping speed S, the above equation simplifies to

$$\tau = \frac{V_2}{F_2} \qquad \text{(H. 14)}$$

For the system described in Section 3.1.2, in which the mass spectrometer section volume V_2 is less than 300 ml and the limiting conductance F_2 is 1.5 1/sec, the response time τ is less than $0.3/1.5 = 0.2$ sec.

Appendix I

CALCULATION OF THERMODYNAMIC QUANTITIES USED IN DISCUSSION IN SECTION 4.2

Calculations of thermodynamic properties of n-butane and toluene from Eq. 4.35 and 4.40 are shown in Tables I-1 and I-2, respectively. The term ϕ in Eq. 4.35 may be defined (see Eq. 4.33) by

$$\phi = R/m \tag{I.1}$$

where

R = gas constant 1.987 (cal/mol°K)

m = slope of the tangent to the potential-plot curve (ml liq/mol°K)

The isosteric heat of adsorption calculated here is defined by Eq. 4.35. The values for the heat of vaporization, ΔH_v, used in these calculations are 5.5 kcal/mol for n-butane and 9.1 kcal/mol for toluene.

Table I-1

CALCULATION OF THERMODYNAMIC QUANTITIES FOR n-BUTANE ADSORPTION AT 300°K BASED ON THE POTENTIAL-PLOT CORRELATION (Fig. 4-2)

Adsorption pressure, p (torr)	1.3×10^{-3}	1.7×10^{-2}	8.8×10^{-2}	1.3×10^{0}
Amount adsorbed, q (ml liq/g)	1.0×10^{-2}	1.0×10^{-1}	1.7×10^{-1}	3.5×10^{-1}
Intercept at A = 0 of tangent to potential-plot curve at q , q° (ml liq/g)	8.8×10^{0}	3.0×10^{0}	1.7×10^{0}	1.06×10^{0}
q/q°	1.14×10^{-3}	3.33×10^{-2}	1.0×10^{-1}	3.30×10^{-1}
ln (q/q°)	-6.78	-3.40	-2.30	-1.11
1/slope of tangent to potential-plot curve at q , 1/m (mol°K/ml liq)	-7.1	-8.6	-9.5	-14.2
$(V_m R/m)$ ln (q/q°) (kcal/mol)	9.2	5.6	4.2	3.0
Isosteric heat of adsorption, $(q_{st})_{th}$ (kcal/mol)	14.7	11.1	9.7	8.5
Fractional coverage, θ	1.81×10^{-2}	1.81×10^{-1}	3.1×10^{-1}	6.3×10^{-1}
Entropy of adsorption, $(q_{st})_{th}/T$ (cal/mol°K)	49.0	37.0	32.3	28.3
-R ln θ (cal/mol°K)	9.66	3.395	2.32	0.92
Adsorption pressure, p (atm)	1.7×10^{-6}	2.2×10^{-5}	1.16×10^{-4}	1.7×10^{-3}
-R ln p (cal/mol°K)	26.4	21.3	18.0	12.7
Theoretical adsorption entropy, $-\Delta S_a$ (cal/mol°K)	53.0	41.6	37.2	30.5

Table I-2

CALCULATION OF THERMODYNAMIC QUANTITIES FOR TOLUENE ADSORPTION AT 300°K BASED ON THE POTENTIAL-PLOT CORRELATION (Fig. 4-3)

Adsorption pressure, p (torr)	–	ca. 1×10^{-5}	3.5×10^{-4}	4.5×10^{-2}
Amount adsorbed, q (ml liq/g)	1.83×10^{-2}	4.98×10^{-2}	1.35×10^{-1}	3.68×10^{-1}
Intercept at A = 0 of tangent to potential-plot curve at q, q° (ml liq/g)	4.90×10^{0}	4.0×10^{0}	2.0×10^{0}	1.0×10^{0}
q/q°	3.74×10^{-3}	1.24×10^{-2}	6.75×10^{-2}	3.68×10^{-1}
ln (q/q°)	-5.59	-4.38	-2.69	-1.00
1/slope of tangent to potential-plot curve at q, 1/m (mol°K/ml liq)	-8.54	-8.90	-10.9	-16.5
$(V_m R/m)$ ln (q/q°) (kcal/mol)	11.20	9.17	6.90	3.88
Isosteric heat of adsorption, $(q_{st})_{th}$(kcal/mol)	20.3	18.3	16.0	13.0
Fractional coverage, θ	3.17×10^{-2}	8.63×10^{-2}	2.34×10^{-1}	6.38×10^{-1}
Entropy of adsorption, $(q_{st})_{th}/T$ (cal/mol°K)	67.7	61.0	53.3	43.3
-R ln θ (cal/mol°K)	6.85	4.87	2.88	0.89
Adsorption pressure, p (atm)	–	ca. 1.3×10^{-8}	4.6×10^{-7}	5.9×10^{-5}
-R ln P (cal/mol°K)	–	ca. 36.0	29.0	19.4
Theoretical adsorption entropy, $-\Delta S_a$ (cal/mol°K)	–	58.0	49.0	37.3

Appendix J

DERIVATION OF EQUATION 4.45

In this section Eq. 4.45 is derived by a kinetic argument, and it is shown that the Langmuir theory of mixed adsorption and the Freundlich theory of mixed adsorption (as derived by Glueckauf, Ref. 20) are special cases of this equation.

The following simple kinetic argument leads to Eq. 4.45:

Consider an adsorbing surface covered to a fraction θ_1 by component 1 and to θ_2 by component 2, with equilibrium gas phase pressures p_1 and p_2. For each component at equilibrium, the rate of evaporation must equal the rate of adsorption. The rate of adsorption is set equal to the collision rate times a sticking coefficient:

$$dq/dt = \left(p_1/\sqrt{2\pi mkT}\right)\alpha \qquad \text{(J. 1)}$$

where

q	= amount adsorbed	(molecule/cm^2)
t	= time	(sec)
p	= pressure	(dyne/cm^2)
m	= molecular mass	(g/molecule)
k	= Boltzmann constant = 1.380×10^{-16}	(erg/molecule°K)
T	= temperature	(°K)
α	= sticking coefficient	

The rate of desorption is set equal to a frequency factor k_o times an Arrhenius activation energy term times the fraction of surface covered:

$$-dq/dt = k_o \exp\left[-\frac{Q(\theta_T)}{RT}\right]\theta_1 \qquad \text{(J. 2)}$$

where

$Q(\theta_T)$ = molar heat of adsorption at total coverage = θ_T (Kcal/mol)

θ_1 = fraction of surface covered by component 1

Equating these rates gives a Langmuir-type equation:

$$\frac{\alpha p_{m1}}{\sqrt{2\pi\, mkT}} = k_o \exp\left[-\frac{Q(\theta_T)}{RT}\right]\theta_T \qquad (J.3)$$

where the subscript "m" on p_{m1} denotes that it is the equilibrium pressure in a mixture.

There are several assumptions in Eq. J.3. $Q(\theta_T)$ is written to indicate that the heat of adsorption of component 1 depends only on the total surface coverage $\theta_T = \theta_1 + \theta_2$. We picture here a heat of adsorption which decreases with surface coverage and depends only on the total amount adsorbed, roughly independent of the composition of the adsorbed layer. Tacitly a uniform surface is also assumed since the rate of evaporation is taken to be proportional to θ_1 and not to a sum over a distribution of heterogeneous sites.

Equation J.3 applies to adsorption from a mixture. For adsorption from the pure component 1 the pressure of pure component 1, p_{o1}, which gives exactly the same total surface coverage θ_T will be given by an analogous equation,

$$\frac{p_{o1}}{\sqrt{2\pi\, mkT}} = k_o \exp\left[-\frac{Q(\theta_T)}{RT}\right]\theta_T \qquad (J.4)$$

where we assume that α and k_o are roughly the same for a surface covered by pure component 1 as for the mixture. In Eq. J.4 the subscript "o" denotes a pure component.

Now, dividing Eq. J.3 by Eq. J.4 gives immediately

$$\frac{p_{m1}}{p_{o1}} = \frac{\theta_1}{\theta_T} \tag{J.5}$$

Since θ_1/θ_T is the mole fraction of component 1 in the adsorbed mixtures (assuming equal areas per molecule), then rearrangement of Eq. J.5 gives

$$p_{m1} = X_1 p_{o1} \tag{J.6}$$

which is the desired equation.

To show that the above equation holds for mixed Langmuir adsorption it is to be noted that the normal Langmuir equation for a single gas,

$$\theta = \frac{a p_1}{1 + a p_1} \tag{J.7}$$

may be rewritten

$$p = \frac{1}{a} \frac{\theta}{1 - \theta} \tag{J.8}$$

Thus, the pressure of the pure gas required to give a particular adsorption θ_T is

$$p_{o1}(\theta_T) = \frac{1}{a} \frac{\theta_T}{1 - \theta_T} \tag{J.9}$$

Here "a" is the ratio of rate constants for adsorption to those for desorption in the original Langmuir derivation.

Now for mixed adsorption it is basic to the Langmuir theory that the pressure of component 1 necessary to give an adsorption θ_1 in the presence of an adsorption θ_2 of the second component is

$$p_{m1} = \frac{1}{a} \frac{\theta_1}{1 - \theta_1 - \theta_2} = \frac{1}{a} \frac{\theta_1}{1 - \theta_T} \tag{J.10}$$

where

$$\theta_T = \theta_1 + \theta_2$$

Now if Eq. J.9 for the pure component 1 is multiplied by $X_1 = \theta_1/(\theta_1 + \theta_2) = \theta_1/\theta_T$, there results

$$X_1 p_{o1}(\theta_T) = \frac{1}{a} \frac{\theta_1}{1 - \theta_T} \tag{J.11}$$

Equating the left sides of Eq. J.11 and J.12 gives

$$p_{m1} = X_1 p_{o1}(\theta_T) \tag{J.12}$$

which is the desired equation (Eq. 4.45).

We next consider Glueckauf's equation for mixed Freundlich-type adsorption on a heterogeneous surface:

$$\log \frac{p_{m1}}{X_1} = \frac{1}{m} \log (\theta_1 + \theta_2) - \text{const.} \tag{J.13}$$

which is Eq. 26, page 382 of Young and Crowell (Ref. 14). Here m is the Freundlich exponent, which both gases presumably obey.

Equation J.13 can be rewritten

$$p_{ml} = X_1 A(\theta_1 + \theta_2)^{1/m} \qquad \text{(J.14)}$$

But $A(\theta_1 + \theta_2)^{1/m}$ is exactly $p_{o1}(\theta_T)$, the equilibrium pressure the pure gas would exert as a coverage of $\theta_T = \theta_1 + \theta_2$, so Eq. J.14 is simply a special case of Eq. J.12 (4.45) adapted for the Freundlich isotherm.

Thus, Eq. 4.45 appears to be a rather general equation which fits a number of diverse models for mixed adsorption.

Appendix K
DETAILS OF DATA OBTAINED WITH THE VOLUMETRIC DESORPTION APPARATUS

Data on n-butane desorption rate from BD charcola at 26°C have been summarized in Section 1.1. Some details are presented here. The data from some thirty determinations are shown in Table K-1. Each run is designated by a symbol such as A-49, in which the letter designates a certain sample of charcoal. With a given letter (say A) a change in number refers to a major change in treatment of that sample, usually a repeated bakeout under high vacuum.

All data for a given sample of carbon and a given initial loading show excellent agreement with second order desorption kinetics. The most extensive data are found in run A-49 in which seven points were obtained (including the first point of A-51). All seven points, when plotted as inverse of fraction left vs. time lie on a straight line going through the correct intercept at zero time. The point is 75.6 percent desorbed is a bit low, but experimental error in reading the Pirani scale at this high pressure is large. In some cases (e.g., D-72 and E-79) only one point at a given loading was taken, since second order seemed well established. In these cases the time for half desorption (used in Fig. 5.3.1-1) was read from a linear second order plot going through the one experimental point and through the correct intercept.

Calibration of Pirani Gage. The Pirani gage was calibrated for n-butane using a McLeod gage. The Pirani scale reading had to be divided by 3.33 to give the true butane pressure. The calibration was checked almost every day.

Adsorption Isotherm. Each time butane was admitted to freshly baked charcoal, a point on the adsorption isotherm was measured. Just as for the rate data, for a given sample of charcoal these data were reproducible, but had a scatter for different samples of charcoal. In particular both samples of 0.1-cm particles adsorbed more strongly

Table K-1

SUMMARY OF DATA FOR n-BUTANE DESORPTION AT 26°C IN VOLUMETRIC APPARATUS

Run No.	Mesh Size (US No.)	Weight (mg)	Bakeout Temp. (°C)	q_o (ml STP/g)	Description Time (min)	Percent Desorbed	Remarks
A-49	16 × 20 (0.1 cm)	10.0	300	6.62	2.04	42.8	
					2.04	42.8	
					6.10	66.0	
					1.03	30.4	
					11.0	75.6	
					4.85	61.3	Low pump speed
A-51	16 × 20	10.0	300	6.62	$\Delta t = 1.0$	30.4	Interrupted experiment
					$\Delta t = 1.0$	17.2	
					$\Delta t = 1.0$	10.8	
					$\Delta t = 1.07$	9.0	
					$\Delta t = 1.33$	7.4	
				Total	5.4	74.8	
A-54	16 × 20	10.0	250	7.10	6.04	65.0	Rebaked
B-63	8 × 12 (0.2 cm)	10.5	300	5.77	6.0	76	
					3.0	61	
					1.5	45	
					0.75	30	
B-63a	8 × 12	10.5	300	5.70	1.5	42	Rebaked
					4.5	68	
C-66	8 × 12	20.0	250	3.36	3.0	33	
					6.0	50	
					12.0	67	
C-69	8 × 12	20.0	400	6.48	2.5	40	Rebaked
				6.48	3.75	47	
				3.35	6.0	50	Low pump speed
D-72	8 × 12	19.0	300	3.38	6.0	44	
				9.48	1.0	28	
				6.52	4.0	42	
E-79	16 × 20	20.0	300	8.47	1.5	47	
				4.54	3.0	51	

than both samples of 0.2-cm particles, so that at a given loading the equilibrium pressure was about a factor of two lower for the smaller particles. This odd phenomenon has also been observed on the microbalance. These data also check with the microbalance data in that, between 3 and 30 μHg pressure, the observed isotherm is linear on a log-log plot (Freundich isotherm) with a slope of 0.5. However, the absolute pressures are a factor of about two higher in the present work (even for 0.1-cm particles) than in the earlier microbalance data (Fig. 2-8). This is most likely due to calibration errors in one or both researches, the McLeod Gage used in the present work being of unknown accuracy.

Interrupted Experiment. In run A-51 an interrupted experiment was performed, to compare with the continuous data of A-49. In A-51 desorption was carried out for 1-minute intervals separated by 10-minute waiting periods. The desorbed butane was accumulated in the cold trap and was never readmitted to the charcoal. The total desorption time for A-51 is, thus, the sum of the individual desorption times, and the total percent desorbed is the sum of the percents desorbed in each increment. The interrupted experiment was somewhat faster than the continuous experiment, especially at high percentages desorbed. Thus, in 5.4 minutes charcoal in the interrupted experiment desorbed 74.8 percent while it took 11.0 minutes to desorb this percent in the continuous experiment. This result is unexpected, since neither pore diffusion effects nor adiabatic cooling effects are to be expected at room temperature. Experimental checks are surely in order, and the proposed experiments with a thermocouple imbedded in a charcoal granule may shed further light on this problem.

Appendix L
DETERMINATION OF DESORPTION RATE ORDER

Many desorption rates have been found to follow kinetics analogous to those of chemical reactions in which the rate of the reaction is proportional to a function of the concentration of a single reactant. Thus, the rate expression for desorption can be written:

$$-dq/dt = kq^n \tag{L.1}$$

where q = amount remaining adsorbed
t = time
k = rate constant
n = rate order.

This rearranges to $$-q^{-n}dq = k\,dt\,, \tag{L.2}$$

which integrates to $$q^{1-n}/(n-1) = kt + c \quad (\text{if } n \neq 1).\ (c = \text{constant}) \tag{L.3}$$

Setting boundary conditions, $$q = q^\circ \quad \text{at} \quad t = 0\,,$$

$$q^{1-n}/(n-1) = kt + q^{\circ\,1-n}/(n-1)\,. \tag{L.4}$$

A characteristic time, τ, may be defined such that,

$$q_{t+\tau} = aq_t \qquad (0 < a < 1)\,. \tag{L.5}$$

For instance, if the characteristic time were defined with $a = 1/2$, it would then be the half-life of the desorption. Since most desorption data cover a fairly limited range of relative amounts remaining adsorbed, usually from 10 to 100 percent, using the half-life would yield only three or four points for the following analysis. A better choice would be $a = 10^{-0.1} = 0.7943$ which would give 10 points per decade.

Then, at some time $= t + \tau$,

$$(aq)^{1-n}/(n - 1) = k(t + \tau) + q^{\circ 1-n}/(n - 1). \qquad (L.6)$$

Subtracting Eq. (L.1) $\qquad (a^{1-n} - 1)q^{1-n}/(n - 1) = k\tau. \qquad (L.7)$

Then, $\qquad \log (a^{1-n} - 1) + (1 - n) \log q - \log (n - 1) = \log k + \log \tau. \qquad (L.8)$

Differentiating: $\qquad (1 - n)d \log q = d \log \tau. \qquad (L.9)$

Thus, the slope of a plot of $\log \tau$ vs. $\log q$, would have a slope $= (1 - n)$. (For the special case of $n = 1$, it can be easily shown that τ is independent of q, so that the slope would equal zero, which is still $n - 1$.)

Further information can be gained from the above plot since, at $\tau = 1$ ($\log \tau = 0$), Eq. (L.8) becomes

$$\log k = \log (a^{1-n} - 1) + (1 - n) \log q' - \log (n - 1). \qquad (L.10)$$

The rate constant may be estimated by the above equation, which rearranges to:

$$k = (a^{1-n} - 1)q'^{1-n}/(n - 1) \qquad (L.11)$$

where n = rate order

q' = intercept, $\tau = 1$ ($\log \tau = 0$).

Alternatively, at $q = 1$ ($\log q = 0$), Eq. L.8 becomes

$$\log k = \log (a^{1-n} - 1) - \log \tau' - \log (n - 1), \qquad (L.12)$$

which on rearrangement yields

$$k = (a^{1-n} - 1)/(n - 1)\tau' \qquad (L.13)$$

where

τ' = intercept at $q = 1$ ($\log q = 0$).

For a series of desorptions of slightly varying order, it would be necessary to approximate the slope of a single order for each set of data points, in order to determine the rate constants in this manner. Thus, the method is somewhat less precise than that of making a plot according to the applicable rate equation.

The method of making such a rate order-determining plot is as follows. Values of a^{-b}, with b varying from 0 to a number sufficiently high such that $a^{-b} = 0.1$ are determined, preferably from mathematical tables. The value of amount adsorbed at or very close to the beginning of the desorption is multiplied by each value of a^{-b}, giving various amounts remaining adsorbed that differ by a factor of a. The calculation of amount adsorbed is reversed so that the weight increase, and thus the total weight, of the desorption sample is known for each value of a^{-b}. The time required to reach each of these successively smaller weights is then determined directly from sample weight recordings. (If the desorption is measured by other than a gravimetric method, some analogous method of determining each successive desorption time must be used.) Next, the difference between each successive desorption time is determined. This difference, τ, is plotted on log-log paper against the amount remaining adsorbed just prior to the beginning of each time period. The slope of the plot = 1 - n; the intercept at $\tau = 1$ ($\log \tau = 0$) = $\log q'$ at $\tau = 1$. The rate order = n. Substitution of n and $\log q'$ at $\tau = 1$ in Eq. L.11 then yields the rate constant.

Appendix M
KINETIC THEORY OF VACUUM DESORPTION

In this section a more detailed kinetic picture of the theory is developed, taking into account explicitly the shape of the adsorption isotherm and the pumping speed.

There are clearly three rate processes which determine the overall rate of desorption from a single particle: 1) rate of diffusion of an adsorbed molecule in the pore structure to the particle surface, 2) rate of the actual desorption step from the adsorbent surface into the gas phase, and 3) pumping speed.

Diffusion within the pore structure can be either Knudsen gas diffusion in the small pores or surface migration of the adsorbed molecule along the pore wall.

M.1 CASE I: GAS DIFFUSION IN PORES

Diffusion of gas within the pore structure when accompanied by adsorption is ruled by the equation (for spherical granules):

$$D\left[\frac{\partial^2 c}{\partial r^2} + \frac{2}{r}\frac{\partial c}{\partial r}\right] = \frac{\partial c}{\partial t} + \frac{\partial S}{\partial t} \qquad \text{(M. 1)}$$

where c and S are the gas-phase and adsorbed-phase concentration, respectively, D is the diffusion coefficient and r is the radial distance from the center of the granule. Since S is enormously greater than c for a good adsorbent, the term $\partial c/\partial t$ can be dropped from Eq. M.1 . Since there are two unknowns (c and S), a

second equation is necessary and this is the equation of adsorption kinetics on the pore wall:

$$\frac{\partial S}{\partial t} = k_A c \left(1 - \frac{S}{S_1}\right) - k_E S \qquad \text{(M. 2)}$$

where Langmuir type kinetics have been assumed, k_A and k_E are rate constants for adsorption and desorption, and S_1 is the adsorbed concentration at one monolayer.

Equations M. 1 and M. 2 are to be solved for boundary conditions determined by the pumping speed. Before investigating this, however, it is noted that if adsorption is very fast, then adsorption equilibrium can be assumed throughout the granule, so that Eq. M. 2 can be replaced by the equation of the adsorption isotherm:

$$S = f_1(c) \qquad \text{(M.3)}$$

Thus $\partial S/\partial t$ in Eq. M. 1 can be replaced by

$$\frac{\partial S}{\partial t} = \frac{df_1(c)}{dc} \frac{\partial c}{\partial t} \qquad \text{(M.1a)}$$

so that Eq. M.1 becomes:

$$D\left[\frac{\partial^2 c}{\partial r^2} + \frac{2}{r}\frac{\partial c}{\partial r}\right] = \frac{df_1(c)}{dc}\frac{\partial c}{\partial t} \qquad \text{(M.4)}$$

Clearly the derivative df_1/dc depends on the shape of the adsorption isotherm and is just the slope of the isotherm, dS/dc. For example, for the Langmuir isotherm it is easy to show that:

$$\frac{df_1(c)}{dc} = \frac{S_o}{c_o} \frac{R_o}{[R_o + (1 - R_o)c/c_o]} \qquad \text{(M.5)}$$

where S_o is the initial adsorbed concentration in the granule and c_o is the gas phase concentration in equilibrium with it. R_o is a parameter determining the fraction of surface covered before desorption begins. When $R_o = 1$, the surface is only slightly covered, and the isotherm is linear. When $R_o = 0$, the surface is fully covered and the isotherm is very non-linear, i.e., irreversible adsorption). Thus for the Langmuir isotherm, the final diffusion equation to be solved is:

$$D\left(\frac{\partial^2 c}{\partial r^2} + \frac{2}{r}\frac{\partial c}{\partial r}\right) = \frac{S_o}{c_o}\,\frac{R}{R + (1 - R)\,c/c_o}\,\frac{\partial c}{\partial t} \qquad \text{(M.6)}$$

This equation is non-linear, except when $R = 1$, so that numerical integration is necessary.

An alternative form to Eq. M.6 is to eliminate c rather than S in Eq. M.1 using the the adsorption isotherm. Thus if the isotherm is inverted to give c as a function of S:

$$c = f_2(S) \qquad \text{(M.7)}$$

then

$$\frac{\partial c}{\partial r} = \frac{df_2(S)}{dS}\,\frac{\partial S}{\partial r} \qquad \text{(M.8)}$$

and Eq. M.1 may be rewritten as:

$$\frac{1}{r^2}\left[\frac{\partial}{\partial r}\, r^2 D\,\frac{df_2(S)}{dS}\,\frac{\partial S}{\partial r}\right] = \frac{\partial S}{\partial t} \qquad \text{(M.9)}$$

This is exactly equivalent to diffusion of a single component in a medium in which the diffusion coefficient depends on concentration,

$$D_1(c) = D \frac{df_2(S)}{dS} \qquad (M.10)$$

We note that if Eq. M.9 had been written for a plane sheet, rather than a sphere, it would be

$$D \frac{\partial}{\partial X} \left[\frac{df_2(S)}{dS} \frac{\partial S}{\partial x} \right] = \frac{\partial S}{\partial t} \qquad (M.11)$$

The importance of Eq. M.11 is that Crank (Ref. 30, Ch. 12) gives numerical solutions for a number of problems with variable diffusion coefficients. Each of Crank's functions which give this variation may be converted into an equivalent isotherm, and thus much numerical work may be avoided.

The boundary conditions for which Eq. M.4 or M.9 must be solved depend on the pumping speed and warrant some investigation. First of all, if pumping speed were infinitely fast, then the boundary condition would be that at the pellet surface the concentration of gas (and a sorbed phase) is zero. For a finite pumping speed, the boundary condition depends on the particular experimental set-up. A rough and ready intuitive boundary condition would be that the outward flux of gas from the granules equals the pumping speed times the concentration at the surface. This clearly is sort of a steady state approximation which neglects the initial transient fall in pressure when the pumps are first turned on.

A mathematically and experimentally exact solution of this troublesome boundary problem is as follows: Experimentally, the charcoal granule is separated from the pumps by a tube of radius r_1 (r_1 = about 1.8 cm for the microbalance). If at distance

L, from the granules, there is located an ion gage (or other fast response manometer), then at zero time, just before the pumps are turned on, this gage will read c_o, the initial pressure in equilibrium with the adsorbent. The pumps are now turned on and the ion-gage reading is recorded as a function of time, and will rapidly decrease by some law, say,

$$\frac{c - c_f}{c_o - c_f} = e^{-bt} \tag{M.12}$$

where c_f is the ultimate pressure and b is an empirical time constant depending on the pumping speed. We now know empirically the pressure history at this one point in the apparatus. (We note that in Eq. M.12 c refers to the partial pressure of adsorbate, and not to the total pressure including water vapor etc.). To relate this known pressure history at a distance L from the adsorbate to that at the adsorbate one must solve the law of flow in the connecting tube. At low pressure around one micron this will be Knudsen flow (or diffusion), and hence one must solve the diffusion equation in the connecting tube simultaneously with Eq. M.4. That is, the pumping or diffusion equation in the connecting tube is

$$D_K \frac{\partial^2 c}{\partial Z^2} = \frac{\partial c}{\partial t} \tag{M.13}$$

where D_K is the Knudsen diffusion coefficient in the tube and Z is distance from the adsorbate. Equation M.13 must be solved with the boundary conditions:

a) At $t = 0$, $c = c_o$ for all Z

b) At $x = L$, c is a known empirical function of time, for example given by Eq. M.12.

c) At $x = 0$ the flux must equal the rate of desorption. The rate of desorption for one granule is the outward flux through the pellet surface,

$$- 4\pi R^2 D \left(\frac{\partial c}{\partial r}\right)_S \tag{M.14}$$

(here R is the granule radius) while the flux through the connecting tube at x = 0 is

$$-\pi r_1^2 D_K \left(\frac{\partial c}{\partial Z}\right)_{x=0} \tag{M.15}$$

so that a boundary condition for both Eq. M.4 and Eq. M.13 is

$$+ N4\pi R^2 \left(\frac{\partial c}{\partial r}\right)_S = \pi r_1^2 D_K \left(\frac{\partial c}{\partial Z}\right)_{x=0} \tag{M.16}$$

where N is the number of adsorbent granules used in this experiment.

Thus the exact solution of the pumping speed problem is to solve Eq. M.4 and Eq. M.13 simultaneously with Eq. M.16 as a common boundary condition. This is likely quite possible but it is probably not necessary for a very good approximation, due to the very small time constant involved in Eq. M.13. The time constant for Eq. M.13 is clearly L^2/D_K, where L is the connecting tube length and D_K is the Knudsen diffusion coefficient in the connecting tube. For microbalance, the connecting tube is about 35 cm long and about 3.5 cm in diameter. The Knudsen diffusion coefficient in a tube of this size is

$$D_K = 9.7 \times 10^3 \times r_1 \sqrt{\frac{T}{M}} = 3.8 \times 10^4 \tag{M.17}$$

Thus the time constant L^2/D is about 3×10^{-2} seconds. This means that the gas in the connecting tube will adjust very rapidly to changing concentrations at the boundaries of the tube providing the time constant of these changes is long compared to 3×10^{-2} seconds. Since the time constant for desorption rate is roughly a thousand times slower, the connecting tube will be in a pseudo-steady state with a linear concentration gradient. This linear gradient will be

$$-\frac{\partial c}{\partial Z} = \frac{c_S - c_f}{L} \tag{M.18}$$

where c_S is the concentration at the pellet surface (Z = O) and c_f is the concentration at the end nearest the pumps (Z = L). Putting Eq. M.18 into M.17 gives the desorption rate:

$$\frac{-d(S/S_o)}{dt} = \frac{\pi r_1^2 D_K}{L}(c_S - c_f) \qquad \text{(M.19)}$$

The multiplying factor

$$\frac{\pi r_1^2 D_K}{L} \qquad \text{(M.20)}$$

is exactly the pumping speed of the connecting tube of length L. Thus Eq. M.19 is the theoretical justification for the intuitive guess mentioned earlier, i.e. that a practical boundary condition might be to equate the rate of desorption to the pumping speed times concentration at the pellet surface.

Thus the theoretical rate of desorption including pumping speed effects can be carried through in either of two stages of approximations: a) the rigorous method of solving Eq. M.4 and Eq. M.13 simultaneously, which will include all transient pumping effects, or b) using Eq. M.19 as the external boundary condition for the pellet, which will neglect the initial transient pumping effects at the very start of the experiment.

A third and most practical method of analyzing for effects of pumping speed is to test a given experiment after it has been performed. Since the rate of desorption is measured in the experiment, this empirical quantity can be put into Eq. M.19 and the concentration at the pellet surface can be computed, since c_S is the only unknown in Eq. M.19. For the pumping speed to be great enough so that it does not affect the

desorption rate, the computed value of c_s must be much less than the gas concentration in equilibrium with the granule at this stage of desorption. Using Eq. M.19, this criterion works out to be

$$\frac{S_p}{-d(S/S_o)/dt} \gg \frac{1}{1 - \frac{p_f}{p_e}} \qquad \text{(M.21)}$$

where

S_p = pumping speed of the connecting tube (cm^3/sec)

p_e = gas pressure which is in equilibrium with the adsorbent at this stage of desorption (atm)

p_f = pressure at a distance L from the absorbent (atm)

Equation M.21 is rapid and easy to apply to a given run. Because desorption rates are fast, it turns out that very large pumping speeds are necessary to measure the true rate of adsorption. This will be discussed later.

To summarize: For the case of gas phase diffusion being the main method of transport in the pores, and for a system with very fast pumping speed, desorption rate should be ruled by Eq. M.4 or M.9 solved with the boundary condition $c = O$ at the granule surface. Whether or not pumping speed is fast enough to make this the experimentally determined rate should be tested by using Eq. M.21.

M.2 CASE II: ADSORBED PHASE DIFFUSION IN PORES

Before discussing solutions of Eq. M.4, the second case for which diffusion in the adsorbed phase is the main mechanism of flow within the granule is considered. Here

the gas phase in the pores is neglected, and in an elementary theory diffusion within the granule would be ruled by the simple diffusion equation:

$$D_S\left(\frac{\partial^2 S}{\partial r^2} + \frac{2}{r}\frac{\partial S}{\partial r}\right) = \frac{\partial S}{\partial t} \qquad \text{(M. 22)}$$

solved with the boundary condition that the diffusive flux at the surface must equal the rate of desorption from the surface or:

$$- D\left(\frac{\partial S}{\partial r}\right)_S = k_E N_S^n - k_A c_S \qquad \text{(M. 23)}$$

where Freundlich desorption kinetics have been assumed for the actual surface desorption step. In Eq. M. 23 N_S is the number of molecules adsorbed per unit surface at the external surface and c_S is the gas phase concentration at the external surface. For very fast pumping speed, c_S is zero, so the last term in Eq. M. 23 may be dropped.

There are however problems connected with Eq. M. 22, for nonlinear isotherms. Equation M. 22 assumes that the adsorbed phase diffusion rate should be proportional to the adsorbed concentration gradient. This is likely a poor assumption in general, since diffusion rates for "imperfect systems" should be proportional to the gradient in free energy or activity. Since this quantity is measured by the pressure of gas $c_e(S)$ in equilibrium with the absorbed concentration S, it appears more reasonable to use the basic flux equation than the diffusion rate across a plane:

$$D_1 \frac{\partial c_e}{\partial r} \qquad \text{(M. 24)}$$

rather than

$$D_S \frac{\partial S}{\partial x} \qquad \text{(M. 25)}$$

If Eq. M.24 rather than Eq. M.25 is used, and if c_e is given by some adsorption isotherm, Eq. M.7, then the diffusion equation to be solved for adsorbed-phase diffusion would be exactly Eq. M.9 with a changed meaning of the diffusion coefficient. In Eq. M.9 it is the Knudsen gas diffusion coefficient, while in the version of Eq. M.9 modified for adsorbed phase diffusion it is defined by Eq. M.24.

Thus, although the diffusion equations for gas diffusion in the pores and for adsorbed phase diffusion are mathematically similar there are three important differences: a) for gas phase diffusion the diffusion coefficient D is the Knudsen diffusion coefficient which is proportional to pore radius. For adsorbed phase diffusion the coefficient D_1 (or D_S) is for two-dimensional migration along the surface, and hence will vary roughly inversely with the pore radius, since the surface area available for two-dimensional migration will vary inversely with pore radius. Thus we expect adsorbed phase (surface) diffusion to be important in very small pores such as those found in charcoal. b) Although the equations are formally similar, the boundary conditions are quite different, since for adsorbed phase diffusion desorption occurs only at the granule surface while for gas phase diffusion it can occur from the internal pore walls throughout the whole granule. Thus when diffusion is very fast compared to desorption rate, for the surface diffusion case the rate becomes equal to the rate of desorption from the external surface only, while in the other case it becomes equal to the desorption rate from the whole internal surface. In particular when adsorbed phase diffusion is very fast, the adsorbed concentration will be uniform throughout the pore structure, and equal to the average concentration $\bar{S}$ within the granule so that the rate of desorption for a single granule becomes, from Eq. M.23,

$$4\pi R^2 \left(k_E N_S^n - k_A c_S\right) \tag{M.26}$$

The adsorption rate constant per unit surface, k_A, may be eliminated in favor of $c_e(\bar{S})$, the gas concentration in equilibrium with $\bar{S}$, so that Eq. M.26 becomes:

$$\text{Rate of Desorption from one granule} = 4\pi R^2 k_E N_S^n \left(1 - \frac{c_S}{c_e(\bar{S})}\right) \tag{M.27}$$

When gas-phase pore diffusion is very fast, the external surface ($4\pi R^2$) in Eq. M.27 is replaced by the total internal surface of the granule

$$\text{Rate of Desorption from one granule} = \frac{4\pi}{3} R^3 \rho_p S_g k_E N_S^n \left(1 - \frac{c_S}{c_e(\bar{S})}\right) \qquad \text{(M.28)}$$

where

ρ_p = particle density
S_g = internal surface area

M.3 SOLUTIONS FOR RATE OF DESORPTION

In this section equations for the absolute rate of desorption will be collected, for the various rate-determining cases. Particular attention will be paid to the dependence of rate on particle size and on temperature. Freundlich kinetics and isotherms will be assumed.

M.3.1 Pumping Speed Limiting

The simplest case is when pumping speed is limiting. Here, by assumption, the desorption rate from the granule is faster than pumping speed, so that each granule is surrounded by its equilibrium gas pressure. Hence, the rate of desorption is the rate at which gas at this pressure is pumped away. For granules containing a concentration, S , of adsorbate, this is, in moles per second,

$$-\frac{dN}{dt} = (S_p)\, c_e(S) \qquad \text{(M.29)}$$

where

S_p = pumping speed (l/sec)
$c_e(S)$ = equilibrium concentration of gas (mol/l)

The number of moles, N, of adsorbate in the charcoal is the volume of activated carbon pellets used times the concentration S, or

$$N = \frac{W}{\rho_p} S \tag{M.30}$$

where w = weight of activated carbon used (g).

Substituting Eq. M.30 into Eq. M.29 gives

$$- \frac{dS}{dt} = \frac{\rho_p}{W} (S_p)\, c_e(S) \tag{M.31}$$

If $c_e(S)$ is given by the Freundlich isotherm, $c_e = kS^n$, or its equivalent c_e

$$c_e/c_o = (S/S_o)^n \tag{M.32}$$

(S_o, c_o are initial concentrations), then substituting Eq. M.32 in Eq. M.31 gives

$$- \frac{d(S/S_o)}{dt} = \left[\frac{\rho_p}{W} (S_p) \left(\frac{c_o}{S_o} \right) \right] \left(\frac{S}{S_o} \right)^n \tag{M.33}$$

Here S/S_o is clearly the fraction remaining. Hence when pumping speed is limiting, the kinetics of desorption are n^{th} order, where n is the exponent in the Freundlich isotherm, and the effective time constant is

$$\tau_{1/2} = \left(\frac{W}{\rho_p} S_o \right) \Big/ (S_p)\, c_o \tag{M.34}$$

This expression is simply equivalent to the number of moles initially adsorbed divided by the number of moles pumped away per second at the initial equilibrium pressure. Clearly the adsorption rate depends on the number of particles (i.e., the weight of carbon) used. (This emphasizes the intuitively obvious criterion that for absorption rate to be independent of pumping speed, the time constant for desorption must be independent of the number of particles used.) The apparent activation energy when pumping speed is limiting will be the heat of adsorption, since at constant initial loading, S_o, the quantity, c_o, in Eq. M.32 must have this exponential increase with temperature in order to obey the usual Clausius-Clapeyron relation used for determining the isosteric heat of adsorption.

M.3.2 Rate Limited by Desorption from External Surface Fed by Fast Surface Migration From Interior

The second simplest case is that of Eq. M.31, which gives $-dN/dt$, the number of molecules per second for one pellet for the above case. Since $N = (4/3\ \pi R^3)S$ and since $S = \rho_p S_g N_S$,

$$-\frac{dS/S_o}{dt} = \frac{3k_E N_o^{n-1}}{\rho_p S_g R}\left(\frac{S}{S_o}\right)^n \qquad (M.35)$$

where N_o is the value of N_S in equilibrium with S_o. Because according to the Freundlich isotherm

$$k_E N_o^n = k_A c_o \qquad (M.36)$$

Eq. M.34 may be rewritten:

$$-\frac{dS/S_o}{dt} = \frac{3k_A}{R}\frac{c_o}{S_o}\left(\frac{S}{S_o}\right)^n \qquad (M.37)$$

where k_A is the rate constant for adsorption per unit surface.

Equation M.35 (or M.37) predicts a rate varying inversely with particle size and with an activation energy equal to the heat of adsorption.

M.3.3 Pore Diffusion Rate Controlling.

For the case of pore diffusion rate controlling Eq. M.4 or Eq. M.9 must be solved with the boundary condition $c = S = O$ at the external surface. (It is assumed that Eq. M.9 holds for both gas diffusion and surface migration, so that we will not distinguish between these mechanisms in this section.) A considerable amount of information can be deduced without even solving the equations, as follows. Both Eq. M.9 and M.4 involve the derivatives which are the slope of the isotherm or the slope of the inverted isotherm. Because we are only concerned with that portion of the isotherm up to c_o (the initial equilibrium gas concentration) it is convenient to write the isotherm in reduced form.

$$\frac{S}{S_o} = f_3(c/c_o) \tag{M.38}$$

where $f_3(c/c_o)$ is some simple function such as $(c/c_o)^{1/2}$ for the Freundlich isotherm. The function $f_3(c/c_o)$ clearly must equal zero when $c/c_o = 0$, and must equal unity when $c/c_o = 1$. When the slope of the unreduced isotherm dS/dc is taken to insert, say, in Eq. M.4, it will always have the form of Eq. M.5 such that

$$dS/dc = \frac{S_o}{c_o} \times \text{a function of } c/c_o \tag{M.39}$$

It follows that for any given adsorption isotherm, the diffusion equation (Eq. M.5 or M.9) can be written in reduced form, involving only c/c_o and its derivatives, plus a

single reduced-time parameter,

$$\tau = \frac{D}{R^2}\left(\frac{c_o}{S_o}\right)t \qquad \text{(M.40)}$$

The fraction desorbed as a function of time will depend only on this parameter, but will be a different function of this parameter for each shape of adsorption isotherm. It follows immediately that the time constant (say the time to reach 50% desorption) will be proportional to the square of the particle size, and that for gas diffusion at least, the activation energy will be the heat of desorption, by the usual Clausius-Clapeyron argument concerning the ratio c_o/S_o. It may be noted that the effective value of the diffusion coefficient, according to Eq. M.40 is lowered by the huge factor of c_o/S_o (about 10^4 to 10^5 for a good absorbent) since 10^4 to 10^5 more molecules must diffuse out than in the absence of adsorption. (It may be further noted that if, for the surface migration case, Eq. M.22 is used then this huge factor does not arise, but if Eq. M.22 is used for non-linear isotherms, then D_S will be so concentration and temperature dependent as to be useless.)

In summary, the essential purpose of detailed solution will be to obtain absolute plots of the fraction desorbed vs. the parameter τ of Eq. M.39. Detailed solutions are available for the following isotherms:

M.3.3.1 Linear Isotherm: For the linear isotherm (i.e., R = 1 in Eq. M.6) the resulting equation is linear and has the classical solution given by Crank (Ref. 30, p. 90, Fig. 6.4, curve marked "Zero"). Crank plots the fraction desorbed vs. the square root of a parameter which is identical with our τ, but in his nomenclature lacks the c_o/S_o factor. Crank's "a" is our radius of the sphere, R. Rate of desorption is almost linear with $\sqrt{\tau}$ up to 50% desorption and then bends over. The value of τ at 50% desorption is $(0.175)^2 = 0.0306$ so that the time for half desorption (sec) is:

$$t_{1/2} = 0.0306\,\frac{R^2}{D}\,\frac{S_o}{c_o} \qquad \text{(M.41)}$$

Although recently Eq. M.4 has been numerically solved for adsorption for the Langmuir isotherm (see Weisz, Ref. 31; also, see Hall, Ref. 32), no solutions for desorption for the Langmuir isotherm seem to exist. (For nonlinear isotherms, the results for adsorption are not applicable to desorption, due to the changed boundary conditions which do not transform into the other problem.) The only other known solutions applicable to desorption appear to be those given by Crank (Ref. 30) for the problem of diffusion coefficients which depend on concentration, which may be transformed into the present problem.

Crank (Ref. 30, ch. 9 and 12) gives solutions for the boundary conditions of desorption of the equation;

$$D_o \frac{\partial}{\partial x}\left[f_4\left(\frac{S}{S_o}\right)\frac{\partial S}{\partial x}\right] = \frac{\partial S}{\partial t} \qquad \text{(M.42)}$$

which is for desorption from a plane sheet or slab in which the diffusion coefficient depends on concentration through the function, $f_4(S/S_o)$. Crank gives solutions for various elementry forms of the function, $f_4(S/S_o)$, such as $\exp(kS/S_o)$. To apply to the present problem it is first necessary to find out what isotherms the function f_4 corresponds to, and secondly to convert to the geometry of desorption from a sphere. The first problem can be solved exactly and the second to a high degree of approximation.

The first problem is exactly solved by the theorem:

To each Crank function, $f_4(S/S_o)$, there corresponds a reduced inverted isotherm:

$$\frac{c}{c_o} = \frac{\int_o^y f_4(y)\,dy}{\int_o^1 f_4(y)\,dy} \qquad \text{(M.43)}$$

where $y = S/S_o$. The reduced inverted isotherm, Eq. M.43, has the correct properties that $c/c_o = 0$ where $S/S_o = 0$, and that $c/c_o = 1$ when $S/S_o = 1$. Furthermore, c/c_o has the important property that

$$\frac{\partial\, c/c_o}{\partial\, S/S_o} = \frac{f_4\,(S/S_o)}{\int_o^1 f_4(y)\,dy} \qquad (M.44)$$

or

$$\frac{dc}{dS} = \frac{c_o}{S_o}\,\frac{f_4\,(S/S_o)}{\int_o^1 f_4(y)\,dy}$$

If Eq. M.44 is now inserted into Eq. M.11 [remembering that $f_2(S)$ in Eq. M.11 equals c in Eq. M.44, because of Eq. M.7], then it follows that

$$\left[D\,\frac{c_o}{S_o}\,\frac{1}{\int_o^1 f_4(y)\,dy}\right]\frac{\partial}{\partial x}\left[f_4\,(S/S_o)\,\frac{\partial S}{\partial x}\right] = \frac{\partial S}{\partial t} \qquad (M.45)$$

Comparing Eq. M.45 with Eq. M.42 shows that the solution for desorption from a plane sheet using the (inverted) isotherm, Eg. M.43, is exactly the same as Crank's solution for the function, f_4, providing that for Crank's D_o there is substituted

$$D_o = D\,\frac{c_o}{S_o}\,\frac{1}{\int_o^1 f_4(y)\,dy} \qquad (M.46)$$

We now apply Eq. M.43 and Eq. M.46 to some results of Crank.

M.3.3.2 Logarithmic Isotherm

A function, $f_4(S/S_o)$, for which Crank gives solutions of Eq. M.40 is

$$f_4 (S/S_o) = \exp (k\, S/S_o) \tag{M.47}$$

According to Eq. M.43, the inverted isoterm this corresponds to is

$$c/c_o = \frac{\exp (k\, S/S_o) - 1}{\exp (k) - 1} \tag{M.48}$$

Solving this for S/S_o gives

$$S/S_o = \frac{1}{k} \log [1 + (\exp k - 1)\, C/C_o] \tag{M.49}$$

which may be called the logarithmic isotherm for present purposes.

Crank (Ref. 30, p. 279, Fig. 12.17) gives solutions for two values of k ($k = \ln 25 = 3.22$ and $k = \ln 10 = 2.303$) plotted as fraction desorbed vs.

$$\left(\frac{D_o t}{\ell^2}\right)^{1/2} \tag{M.50}$$

where ℓ is the half thickness of the slab. Since for this case the integral in Eq. M.46 is

$$\frac{1}{k} (\exp k - 1) \tag{M.51}$$

then Crank's parameter corresponds to plotting fraction desorbed vs.

$$\left[D \frac{c_o}{S_o} \frac{k}{(\exp k - 1)} \frac{t}{\ell^2} \right]^{1/2} \qquad \text{(M.52)}$$

Thus, for the two adsorption isotherms defined by Eq. M.48 (or M.49) with $k = 3.22$ and 2.30, we have solutions for fraction desorbed as a function of the parameter given by Eq. M.52, but for a slab of thickness, 2ℓ, not for a sphere of radius, R.

To deduce the time to desorb from a sphere from the time to desorb from a plane sheet or slab, we introduce the following approximate theorem: If a fraction, F_1, is desorbed from a plane sheet in time, t_1, then in the same time, t, it will desorb from a sphere a fraction, F_2, given by

$$F_2 = 1 - (1 - F_1)^3 \qquad \text{(M.53)}$$

This approximate theorem is based on the geometry of a sphere and the physical fact that the time to diffuse a distance, x, does not depend on the shape of the granule. Thus, if molecules diffuse a radial distance of 20% into a sphere, they have occupied 50% of the volume. Equation M.53 is simply a geometrical illustration that for equal diffusion distances (which should occur in equal times) the fractional volumes outside these distances are given by Eq. M.53. For the only case available, namely the linear isotherm, Eq. M.53 is accurate to a few percent. That is, the rate of diffusion into or out of a sphere can be calculated to a few percent from the rate into a slab by Eq. M.53, as is seen by comparing Fig. 4.6 with Fig. 6.4 of Crank (Ref. 30).

For the moment we are interested in only one main number from Eq. M.53, namely that when 50% is desorbed from a sphere only 20.5% is desorbed from a slab. From Crank's data when 20.5% is desorbed from the slab, this $\sqrt{\tau}$ is 0.080 and 0.11, for $k = 3.22$ and $k = 2.303$, respectively. Hence, for a sphere, when 50% is desorbed, τ is the square of these quantities or 6.4×10^{-3} and 1.21×10^{-2}. Since τ is defined by the bracket of Eq. M.50, we have the relation

$$t_{1/2} = \tau_{1/2} \frac{\exp k - 1}{k} \frac{R^2}{D} \frac{S_o}{c_o} \qquad \text{(M.54)}$$

where $t_{1/2}$ is the time for 50% desorption from a sphere, and $\tau_{1/2}$ is the value of Crank's parameter at 20.5% desorption from a slab. When $k = \ln 25 = 3.22$, then $(\exp k - 1)/k = 7.46$, and $\tau_{1/2} = 6.4 \times 10^{-3}$. So for $k = 3.22$:

$$t_{1/2} = 4.77 \times 10^{-2} \left[\frac{R^2}{D} \frac{S_o}{c_o}\right] \qquad \text{(M.55)}$$

When $k = \ln 10 = 2.303$, then $(\exp k - 1)/k$ equals 3.91 and:

$$t_{1/2} = 4.73 \times 10^{-2} \left[\frac{R^2}{D} \frac{S_o}{c_o}\right] \qquad \text{(M.56)}$$

Equations M.40, M.55, and M.56 now all give the half-desorption times for three different adsorption isotherms. It is seen that as the isotherm gets more non-linear the time for half-desorption gets longer, since the numerical coefficients in front of the three equations increase with degree of non-linearity.

So far we have not discussed the shape of the curve, percent desorbed vs. time, since interest has been focussed on the absolute value of the half-desorption times as a function of the important parameters. We are now in a position to make our important deduction concerning the shape of this curve: All of Crank's curves for percent desorbed from a slab vs. $\sqrt{\tau}$ are linear up to 50% or so desorbed, independent of the shape of the adsorption isotherm. This is a basic characteristic of diffusion into a slab. Referring to Eq. M.53, this means that

$$F_1 = At^{1/2} \qquad \text{(M.57)}$$

where A = the desorption curve shape parameter,

holds up to $F_1 = 0.50$ or so, so that

$$F_2 = \text{fraction desorbed from a sphere}$$

$$= 1 - (1 - At^{1/2})^3 \qquad \text{(M.58)}$$

should hold up to very high percentages desorbed from a sphere. Thus the simple deduction can be made that if pore diffusion rate is ruling, the fraction F_2 desorbed from a spherical granule should be ruled by:

$$F_2 = 1 - \left(1 - At^{1/2}\right)^3 \qquad \text{(M.59)}$$

from zero to 80 or more percent desorbed. Equation M.59 is very easy to test experimentally. It may be rearranged to give:

$$1 - (1 - F_2)^{1/3} = At^{1/2} \qquad \text{(M.60)}$$

so that a plot of $\log [1 - (1 - F_2)^{1/3}]$ vs. $\log t$ should be a straight line of slope 0.50. In preliminary plots this law seems to hold very well, especially at the lower temperatures. At the highest temperatures the slope tends to be less than 0.50. It should not be minimized that the desorption curves which are of complex shape can be fitted by a single parameter A in Eq. M.60.

Appendix N
DERIVATION OF EQUATION 6.9

In this section Eq. 6.9 is derived from first principles. The rate of desorption from a single granule (assumed spherical) may be formulated as follows: If the concentration of adsorbate in the granule is S , then the total number of moles in one granule is the volume of the granule times S or

$$n = \frac{\pi d_p^3}{6} S \qquad (N.1)$$

where

n	= number of moles in one granule	(mol)
d_p	= granule diameter	(cm)
S	= concentration of adsorbate in the granule	(mol/cm^3)

The rate of desorption is clearly the time derivative of this, obtained by writing $-dS/dt$ for S in the above expression.

If the rate of desorption equals the rate of evaporation from the external granule surface, then this rate is the external surface area (πd_p^2) times the rate per unit area. The rate equation is thus

$$-\frac{\pi d_p^3}{6}\frac{dS}{dt} = \pi d_p^2 r_A \qquad (N.2)$$

where

r_A	= desorption rate per unit area	(mol/cm^2-sec)
t	= time	(sec)

When the granule is in adsorption equilibrium, the rate of adsorption per unit area is the rate that molecules strike the surface times a sticking coefficient, α, or

$$r_A = \frac{\bar{v}}{4} c_e(S)\ \alpha \qquad (N.3)$$

where

$c_e(S)$ = vapor concentration in equilibrium with the adsorbed concentration S (mol/cm^3)

$\bar{v}$ = average molecular velocity (cm/sec)

At equilibrium the rate of adsorption equals the rate of desorption. It is now assumed that the rate of desorption into high vacuum is the same as the rate in the presence of the equilibrium vapor (i.e., that the presence of a low pressure of vapor does not affect the rate that molecules leave the surface). Thus, Eq. N.3 is inserted for the bracket of Eq. N.2. This gives

$$-\frac{dS}{dt} = \frac{3}{2}\frac{1}{d_p}\bar{v}\ \alpha c_e(S) \qquad (N.4)$$

If S is now eliminated in favor of the more practical variable, q (whose units are ml STP/g), and if $c_e(S)$ is eliminated in favor of the more practical variable of pressure in torr, then Eq. 6.9 immediately results.

Langmuir (cf. Dushman, Ref. 21, p. 18) has used a similar argument to estimate the vapor pressure of metals from the rate of evaporation of hot wires. Here the argument is inverted, so that the rate of evaporation may be estimated from the equilibrium pressure.

Appendix O
CALIBRATION OF MANOMETER SYSTEM

The manometer system, shown in Fig. O-1 and Fig. 7-2, was used in the vacuum desorption system (see section 7.2.1). The desorbed material, collected in the main traps, was transferred through stopcock No. 3 and condensed with liquid nitrogen in the collecting tube (see Fig. O-1). The stopcock was then closed, and the condensed material expanded in the volume V_2. This procedure demands an accurate value for volume V_2 so calculations can be made in regard to the amount desorbed.

The calibration of the manometer volumes was performed on sides A and B to obtain accurate volumes (see Fig. O-1).

The calibration procedure was as follows:

(1) The calibrated volume was mounted and evacuated through stopcock No. 2 on a calibrated volumetric system.
(2) After evacuation, n-butane gas was admitted into the volumetric system and the calibrated volume. The total pressure was read on a Wallace and Tiernan FA-145 gage.
(3) Stopcock No. 2 was then closed and the calibrated volume was transferred to the manometer system as shown in Fig. O-1.
(4) The manometer system up to stopcock No. 2 was evacuated through the main vacuum system and isolated through stopcock No. 3.
(5) Collecting tube A was immersed in liquid nitrogen and stopcock No. 2 was opened.
(6) All of the n-butane in the calibrated volume was condensed in the collecting tube and stopcock No. 3 was closed.
(7) The liquid-nitrogen trap was removed and the system allowed to come to equilibrium at room temperature.
(8) The pressure of the closed system was read with the mercury manometer.

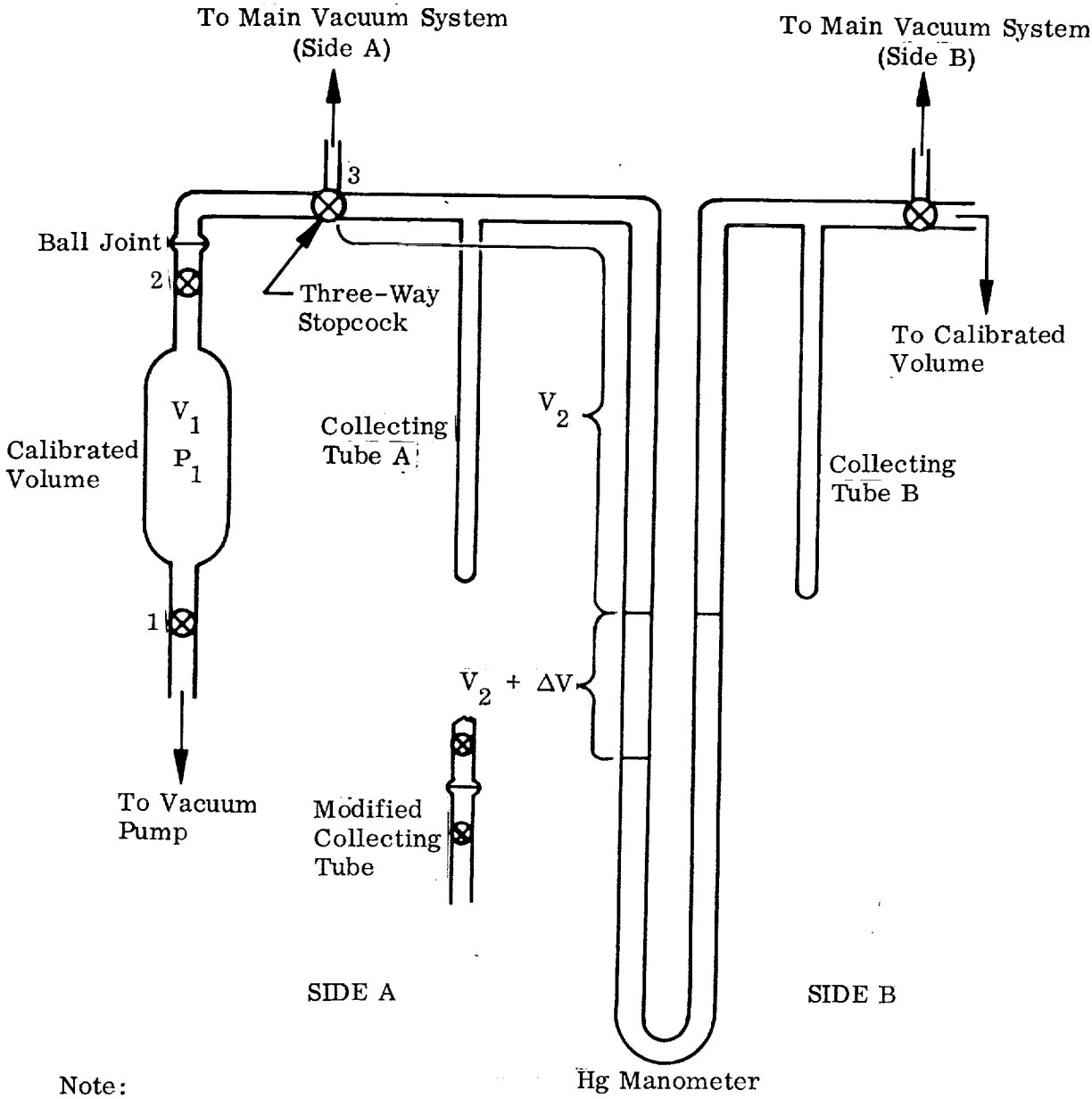

Note:
Not to scale.
Manometer and collecting tube made from 4 mm ID precision glass tubing.
⊗ = high vacuum glass stopcocks.

Fig. O-1 Manometer System for the High Vacuum Desorption System

Since the total volume of the system varied depending on the total pressure, it was useful to use the "zero-point" volume. This is the volume of the system when both sides of the mercury column are equal as would be the case when both sides are under vacuum or exposed to the atmosphere.

(9) Given the pressure in the closed manometer system, the volume can be calculated from the simple (PV) gas law relationship. Finally, a ΔV is subtracted from the calculated volume (see Fig. O-1) to obtain the "zero-point" volume.

(10) The same procedure of calibration was used on both sides of the manometer system.

For Run No. F17-1 and thereafter there was a modification of the manometer system. Two microstopcocks were glass-blown into the collecting tube with a ball joint in between. (See Fig. O-1.) This allowed one to collect all the sample in the lower part of the tube and then disconnect the section for weighing on a balance.

Appendix P
SAMPLE CALCULATION OF VACUUM DESORPTION DATA

As described in previous sections, the desorbed contaminant was collected in a liquid nitrogen trap (see section 7.2.1). At various times t the trap was isolated and the condensed material was transferred to the manometer system (see Fig. O-1, Appendix O). Using n-butane as an example, the following calculation was performed to determine the amount of material desorbed in time, t .

$$q_{de} = V_m \frac{P(V + \Delta V)}{RT \times 760\ W}$$

where

q_{de}	=	amount of n-butane desorbed in time, t	(ml liq)
V_m	=	molar volume for n-butane = 96.4	(ml liq/mol)
P	=	pressure in the manometer system	(torr)
V	=	"zero-point" volume	(ml)
ΔV	=	added volume due to manometer depression due to pressure P . Calculated from tube dimensions	(ml)
R	=	gas constant = 83.0	(ml atm/mol°K)
T	=	manometer system temperature	(°K)
W	=	weight of activated carbon in bed	(g)

For example, if the total manometer pressure is 300 torr (manometer depression = 15 cm), the zero-point volume is 10.95 ml, and the temperature is 297.2°K, then

$$\Delta V = \pi (0.2)^2(15) = 1.884 \text{ ml (tube ID = 0.4 cm)}$$

$$V + \Delta V = 10.95 + 1.88 = 12.83 \text{ ml}$$

$$q_{de} = (96.4 \text{ ml liq/mol}) \frac{(12.83 \text{ ml})(300 \text{ torr})}{(83.0 \text{ ml-atm/mol°K})(297.2°K)(760 \text{ torr/atm})(1.00 \text{ g})}$$

$$= \frac{(96.4)(12.83)(300) \text{ ml liq/g}}{(83.0)(297.2)(760)(1.00)}$$

$$q_{de} = 1.98 \times 10^{-2} \text{ ml liq/g}$$

The same calculation is made for all samples taken at various times t , therefore, the total amount vacuum desorbed is

$$q_{de}^{total} = \sum_{t=1} q_{de}$$

The total amount of n-butane desorbed from the bed is

$$q_d = q_{de}^{total} + q_{df}$$

where

q_{df} . = amount desorbed by flow desorption at the conclusion of vacuum desorption (ml liq/g)

Appendix Q
DERIVATION OF SOLUTIONS FOR EQUATION 7.7

In this section solutions of Eq. 7.7 are derived. In particular it is shown that Eq. 7.7 can be converted to a diffusion equation with variable diffusion coefficients which has already been solved by Crank (Ref. 30, Ch. 9 and 12, esp. p. 278 et seq.). Equation 7.7 is first rewritten:

$$D_K \frac{\partial}{\partial x} \frac{\partial c}{\partial x} = \frac{\partial S}{\partial t} \qquad (Q.1)$$

A second equation is clearly needed since the above equation has two dependent variables. Since by hypothesis desorption from a single particle is faster than diffusion through the bed, the bed must be in local adsorption equilibrium. That is, S, the adsorbed concentration, varies through the bed (i.e., is a function of x), but each particle is surrounded by a gas pressure of adsorbate which is equilibrium with its particular value of S. Thus, the second equation is the equation of the adsorption isotherm, and the isotherm equation may be used to eliminate c from Eq. Q.1 in favor of S. Thus, because the bed is in adsorption equilibrium

$$\frac{\partial c}{\partial x} = \left(\frac{dc}{dS}\right)_e \frac{\partial S}{\partial x} \qquad (Q.2)$$

where $(dc/dS)_e$ is the slope of the inverted adsorption isotherm (c versus S). If the inverted isotherm is written in reduced form,

$$c/c_o = f_1 (S/S_o) \qquad (Q.3)$$

then

$$\left(\frac{\partial c}{\partial S}\right)_e = \frac{c_o}{S_o} f_2 (S/S_o) \qquad (Q.4)$$

where $f_2(S/S_o)$ is the slope of the reduced isotherm, Eq. Q.3. Here S_o is the initial adsorbed concentration in the bed, and c_o is the vapor concentration in equilibrium with S_o.

Substituting Eq. Q.2 and Q.4 into Eq. Q.1 gives

$$D_K \frac{c_o}{S_o} \frac{\partial}{\partial x} \left[f_2(S/S_o) \frac{\partial S}{\partial x} \right] = \frac{\partial S}{\partial t} \qquad (Q.5)$$

Equation Q.5 may be written in reduced form:

$$\frac{\partial}{\partial Z} \left[f_2(y) \frac{\partial y}{\partial Z} \right] = \frac{\partial y}{\partial \tau_1} \qquad (Q.6)$$

where $y = S/S_o$, $Z = x/L$, L = bed length, and τ_1, a reduced time parameter, is defined by

$$\tau_1 = \frac{D_K}{L^2} \frac{c_o}{S_o} t \qquad (Q.7)$$

Now Eq. Q.5 (or Eq. Q.6) is exactly the equation for diffusion without adsorption for the case when the diffusion coefficient varies with concentration. (see Crank, Ref. 30, loc. cit., Eq. 9.5). Since in general the adsorption isotherm is non-linear, the above equations are non-linear, and numerical integration is necessary. However, Crank has carried out the necessary tedious numerical work for a variety of f_2-functions. For Crank the f_2-function describes how the diffusion coefficient varies with

concentration. For the present work it is the slope of an adsorption isotherm. Thus, to every f_2-function for which Crank derives solutions there corresponds for the present problem an adsorption isotherm which can be derived by integration of Crank's f_2-function. The exact relationship between the reduced isotherm and the f_2-function is:

$$\frac{c}{c_o} = \frac{\int_o^y f_2(y)\, dy}{\int_o^1 f_2(y)\, dy} \qquad (Q.8)$$

where $y = S/S_o$. Thus, the slope of the reduced isotherm (Eq. Q.8) is proportional to $f_2(y)$, and the integral in the denominator is a normalizing factor so that c/c_o is unity when S/S_o is unity. Thus, to get exact analogy with Crank's solution, his D_o (the diffusion coefficient at zero concentration) must be replaced for the present desorption case by an effective diffusion coefficient,

$$D_o = D_K \frac{c_o}{S_o} \frac{1}{\int_o^1 f_2(y)\, dy} \qquad (Q.9)$$

To illustrate a particular example in detail, one f_2-function used by Crank (Ref. 30, Fig. 12-17) is

$$f_2(S/S_o) = \exp k\, S/S_o \qquad (Q.10)$$

(i.e., for his case the diffusion coefficient increases exponentially with concentration). For the present case this corresponds to the isotherm (obtained by putting Eq. Q.10 into Eq. Q.8),

$$c/c_o = \frac{\exp k\, S/S_o - 1}{\exp k - 1} \qquad (Q.11)$$

Crank gives his solutions in the form of plots of percent desorbed versus a reduced time parameter which for present purposes (using Eq. Q.9) is

$$\tau^{1/2} = \left[D \frac{c_o}{S_o} \frac{1}{L^2} \frac{kt}{(\exp k - 1)} \right]^{1/2} \qquad \text{(Q. 12)}$$

Thus, from Fig. 12-17 of Crank it may be read that, when 50% is desorbed from the bed (for the case k = 3.219), the value of the reduced $\tau^{1/2}$ is 0.223. Hence, the value of τ is the square of this, or 0.0497, at 50% desorption. Putting these values (τ = 0.0497 and k = 3.219) into Eq. Q. 12 gives

$$0.0497 = D \frac{c_o}{S_o} \frac{1}{L^2} \frac{3.219}{24} t_{1/2} \qquad \text{(Q. 13)}$$

where $t_{1/2}$ is the actual time for 50% desorption (not the reduced time). Solving Eq. Q. 13 for $t_{1/2}$ gives

$$t_{1/2} = 0.373 \frac{L^2}{D_K} \frac{S_o}{c_o} \qquad \text{(Q. 14)}$$

Now, the time for 50% desorption for other-shaped isotherms will differ from Eq. Q. 14 only in the numerical factor, which has been called K in Eq. 7.9 of section 7.5. In each case this numerical factor, K , will be a number read from Crank's curves times a normalization factor obtained by integrating the f_2-function.

Thus, for each f_2-function used by Crank, K was computed and also the adsorption isotherm was calculated and plotted from Eq. Q. 8. To correlate K as a function of isotherm shape, the simple non-linear function (NLF) of Eq. 7.11 was calculated for each isotherm, and K was plotted as a function of this. The resulting curve was then found to be fitted by Eq. 7.10 to a good degree of accuracy.

Thus, from Eq. 7.9, 7.10 and 7.11 the time for 50% desorption for any-shaped isotherm can be calculated.

REFERENCES

1. M. Polányi, "Über die Adsorption vom Standpunkt des dritten Wärmesatzes," Verh. Deut. Physik. Ges. 16, 1012–6 (1914)

2. M. Polányi, "Adsorption von Gasen (Dämpfen) durch ein festes nichtflüchtiges Adsorbens," Verh. Deut. Physik. Ges. 18, 55–80 (1916)

3. M. Polányi, "Neueres über Adsorption und Ursache der Adsorptionskräfte," Z. Elektrochem. 26, 370 – 4 (1920)

4. W. K. Lewis et al., "Adsorption Equilibria. Hydrocarbon Gas Mixtures," Ind. Eng. Chem. 42, 1319 – 26 (1950)

5. R. Grant, M. Manes, S. Smith, "Adsorption of Normal Paraffins and Sulfur Compounds on Activated Carbon," A. I. Ch. E. J. 8, 403–6 (1962)

6. A. J. Robell, F. G. Borgardt, and E. V. Ballou, "Gaseous Contaminant Removal by Adsorption," Chem. Eng. Prog. Symp. Ser. No. 63, 76–80 (1966)

7. T. L. Hill, "Statistical Mechanics of Multimolecular Adsorption. IV. The Statistical Analog of the BET Constant $a_1 b_2/b_1 a_2$. Hindered Rotation of a Symmetrical Diatomic Molecule Near a Surface," J. Chem. Phys. 16, 181–89 (1948)

8. A. J. Robell, E. V. Ballou, and F. G. Borgardt, "Basic Studies of Gas-Solid Interactions III.," LMSC Report No. 6-75-65-22 (30 Apr 1965)

9. R. T. Davis et al., "Adsorption of Gases on Surfaces of Powders and Metal Foils," J. Phys. Colloid Chem. 51, 1232–48 (1947)

10. P. H. Emmett and M. Cines, "Surface Area Measurements on Metal Spheres and Carbon Blacks," J. Phys. Colloid Chem. 51, 1329–41 (1947)

11. S. Brunauer, The Adsorption of Gases and Vapors, Princeton Univ. Press, 1945

12. G. Halsey and H. S. Taylor, "The Adsorption of Hydrogen on Tungsten Powders," J. Chem. Phys. 15, 624–30 (1947)

13. S. Ross and J. P. Olivier, On Physical Adsorption, Interscience, New York 1964

14. D. M. Young and A. D. Crowell, Physical Adsorption of Gases, Butterworths, London, 1962

15. J. H. de Boer and S. Kruyer, "Entropy and Mobility of Adsorbed Molecules IV. Aliphatic Hydrocarbons on Charcoal," Proc. Kon. Ned. Akad. Wetenschap. 56B, 415–26 (1953)

16. J. H. de Boer and S. Kruyer, "Entropy and Mobility of Adsorbed Molecules I. Procedure; Atomic Gases on Charcoal," Proc. Kon. Ned. Akad. Wetenschap. 55B, 451–63 (1952)

17. A. L. Myers and J. M. Prausnitz, "Thermodynamics of Mixed-Gas Adsorption," A. I. Ch. E. J. 11, 121–7 (1965)

18. R. J. Grant and M. Manes, "Adsorption of Binary Hydrocarbon Gas Mixtures on Activated Carbon," Ind. Eng. Chem. Fund. 5, 490–8 (1966)

19. A. W. Loven et al., in J. Makowski et al., "Collective Protection Against CB Agents," Eighth Progress Report on Contract No. DA 18-035-AMC-279(A), AiResearch Mfg. Co. Report No. CB-1008 (Feb 1966)

20. E. Glueckauf, "Theory of Chromatography. Part 9. The 'Theoretical Plate' Concept in Column Separations," Trans. Farad. Soc. 51, 34–44 (1955)

21. S. Dushman, Scientific Foundations of Vacuum Technique, Wiley, New York, 1966

22. G. Wyllie, "Evaporation and Surface Structure of Liquids," Proc. Roy. Soc. A197, 383–95 (1949)

23. A. J. Robell, C. R. Arnold, and G. J. Kersels, "Adsorption of Trace Contaminants and Regeneration of Sorbents," LMSC Report No. L-62-67-1 (20 Apr 1967)

24. A. J. Robell and R. P. Merrill, "Gaseous Contaminant Removal by Adsorption: II. Adsorption Dynamics in Fixed Beds," A. I. Ch. E. Symp. Ser. (in press)

25. T. Vermeulen and G. Klein, Section 16 in Chemical Engineer's Handbook, 4. ed., R. Perry et al., ed., McGraw-Hill (1963)

26. A. J. Robell, R. P. Merrill, and C. R. Arnold, "Activated Charcoal Air Filter System for the NASA 1973 Basic Subsystem Module," LMSC Report No. 6-78-68-21 (Jun 1968)

27. J. Timmermans, The Physico-Chemical Constants of Binary Systems in Concentrated Solutions, v. 4, Interscience, New York, 1960

28. Handbook of Chemistry and Physics, 43. ed., Chemical Rubber Publishing Co., 1962

29. H. Stephen and T. Stephen, eds., Solubilities of Inorganic and Organic Compounds, v. 1, part 1, Macmillan, New York, 1963

30. J. Crank, The Mathematics of Diffusion, Oxford, London, 1956

31. P. B. Weisz, "Sorption-Diffusion in Heterogeneous Systems. Part 1. – General Sorption Behaviour and Criteria," Trans. Farad. Soc. 63, 1801–23 (1967)

32. K. R. Hall et al., "Pore- and Solid-Diffusion Kinetics in Fixed-Bed Adsorption under Constant-Pattern Conditions," Ind. Eng. Chem. Fund. 5, 212–23 (1966)